

# UNCLASSIFIED

AD NUMBER
AD879285
NEW LIMITATION CHANGE
TO Approved for public release, distribution unlimited
FROM Distribution authorized to U.S. Gov't. agencies and their contractors; Critical Technology; 30 JUN 1970. Other requests shall be referred to Office of Naval Research, Aeronautics Programs, ATTN: Code 461, Arlington, VA 22217.
AUTHORITY
29 Aug 1973, ST-A per ONR ltr

THIS PAGE IS UNCLASSIFIED

AD879285

FILE COPY

TR-170-1

ADAPTIVE CONTROL AND GUIDANCE  
FOR TACTICAL MISSILES

VOLUME II. PARTS III AND IV  
ADAPTIVE CONTROL APPLICATIONS AND GUIDANCE

30 June 1970



6 JACOB WAY/READING, MASSACHUSETTS 01867 (617) 944-6850

12

519

TR-170-1

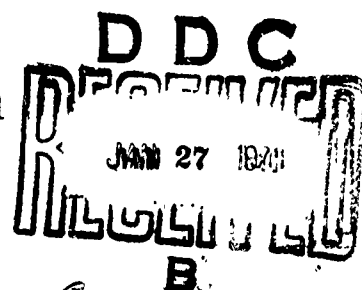
ADAPTIVE CONTROL AND GUIDANCE  
FOR TACTICAL MISSILES

VOLUME II: PARTS III AND IV  
ADAPTIVE CONTROL APPLICATIONS AND GUIDANCE

30 June 1970

Prepared for the  
OFFICE OF NAVAL RESEARCH  
AERONAUTICS PROGRAMS, CODE 461  
DEPARTMENT OF THE NAVY  
ARLINGTON, VIRGINIA 22217

Under  
Contract Number N00014-69-C-0391



Prepared by:

Charles F. Price

Approved by:

Arthur A. Sutherland, Jr.  
Arthur Gelb

This document is subject to special export controls and each transmittal to foreign governments or foreign nationals may be made only with prior approval of the Office of Naval Research, Code 461. Reproduction in whole or in part is permitted for any purpose of the United States Government.

Copyright © 1970  
by  
THE ANALYTIC SCIENCES CORPORATION  
6 Jacob Way  
Reading, Massachusetts

## FOREWORD

The underlying purpose of this report is to present an objective evaluation of several techniques for adaptively controlling and guiding tactical missiles. Because design trade-offs always exist between performance and control system complexity, there is probably no one control method that is preferable for all applications. Consequently, in this work no single method is advocated as the panacea for all missile design problems. Instead the discussion emphasizes distinguishing characteristics of each technique so the reader can judge which is most suitable for his own situation.

A by-product of this research effort is an organized, unified discussion of many technical aspects of adaptive control which have heretofore been available only in isolated papers. New research results produced by this investigation are also included. Therefore, although this study has been performed primarily for tactical missile applications, the material collected here should also be of interest to those working in other areas where adaptive control methods are needed.

The authors are grateful for the encouragement and support provided by Mr. David Siegel of the Office of Naval Research and Mr. Paul Blatt of the Air Force Flight Dynamics Laboratory. Acknowledgement is also made to Professor Richard V. Monopoli of the University of Massachusetts for his contributions relative to Liapunov design techniques. Helpful assistance was provided in several technical areas by Professor John J. Deyst, Jr. of the Massachusetts Institute of Technology and by Dr. Joseph J. Budelis. Appreciation is also expressed to Professor Wallace E. VanderVelde of the Massachusetts Institute of Technology for his helpful review of portions of the document.



### ABSTRACT

The fields of adaptive control and guidance are searched for techniques that can be beneficially applied to the design of guidance systems for tactical missiles. A large number of existing adaptive control techniques are investigated and new methods which are suited to the needs of missile control systems, are proposed. The feasibility of promising autopilot design procedures is demonstrated through computer simulations, using realistic time-varying airframe dynamics. Guidance techniques for tactical missiles are also reviewed and a number of steering laws, derived from optimal control theory, are evaluated. Quantitative comparisons are made between different guidance laws on the basis of intercept accuracy and control effort expended.

The report is published in two volumes containing four basic parts -- Introduction (which includes the summary and conclusions for the entire report), Adaptive Control Theory, Adaptive Control Applications, and Guidance. The first two parts constitute Volume I and the remainder together with several appendices compose Volume II.

## TABLE OF CONTENTS

	<u>Page No.</u>
FOREWORD	iii
ABSTRACT	v

### VOLUME I: PART I

#### INTRODUCTION

1.	OVERVIEW	1-1
	1.1 Background and Objectives	1-1
	1.2 Summary	1-2
	1.2.1 Tactical Missile Operational Requirements	1-3
	1.2.2 Adaptive Control	1-6
	1.2.3 Guidance	1-13
	1.3 Conclusions	1-14
	1.3.1 Control	1-14
	1.3.2 Guidance	1-17
	1.3.3 Areas for Additional Research	1-19
	1.4 Reading Guide	1-21
2.	DEFINITIONS AND CONCEPTS	2-1
	2.1 Guidance and Control: Definitions	2-1
	2.2 Adaptive Control System: A Definition	2-4
	2.3 Types of Adaptive Control Systems	2-6
	2.3.1 Parameter Adaptive Control Systems (PACS)	2-7
	2.3.2 Learning Control System (LCS)	2-14
	2.3.3 Adaptive Insensitive Control Systems (AICS)	2-18
	2.3.4 Summary	2-20
3.	APPLICATION OF ADAPTIVE METHODS TO GUIDANCE AND CONTROL OF TACTICAL MISSILES	3-1
	3.1 Factors Affecting Design of Guidance and Control Systems	3-1
	3.1.1 Target Dependent Design Considerations	3-2

TABLE OF CONTENTS (Continued)

	<u>Page No.</u>
3.1.2 Weapon System Dependent Design Considerations	3-8
3.1.3 Adaptive Design Considerations	3-18
3.1.4 Summary	3-24
3.2 Tactical Missions Requiring an Adaptive Guidance and Control System	3-25
3.2.1 Air Targets	3-25
3.2.2 Ground Target: Stand-off Missile	3-27
3.2.3 Summary	3-28

VOLUME I: PART II

ADAPTIVE CONTROL THEORY

4. PARAMETER ADAPTIVE CONTROL SYSTEMS WITH IMPLICIT PLANT IDENTIFICATION	4-1
4.1 Error Signals in Adaptive Systems	4-1
4.1.1 The Output Error	4-2
4.1.2 Reference Model State Independent Error Signals	4-4
4.2 Gradient Methods for Adaptive Control	4-8
4.2.1 The M.I.T. Gradient Rule	4-13
4.2.2 A Discrete Form of the M.I.T. Rule	4-23
4.2.3 A Relay Form of the M.I.T. Rule	4-26
4.2.4 A Simplified Gradient Technique	4-28
4.2.5 Parameter-Perturbation Gradient Techniques	4-36
4.2.6 Performance of Gradient Methods	4-44
4.2.7 Decoupled Gradient Adaptation Algorithms	4-59
4.3 Accelerated Gradient Parameter Adjustment Methods	4-62
4.4 Liapunov Design Methods	4-69
4.4.1 Design Principles	4-70
4.4.2 Adaptation Rate for Liapunov Methods	4-81
4.4.3 A Synthesis Procedure Applicable for Missile Control	4-87
4.4.4 Theoretical Limitations of Liapunov Techniques	4-97

TABLE OF CONTENTS (Continued)

	<u>Page No.</u>
4.5 Dither-Adaptive Systems	4-100
4.5.1 Background	4-100
4.5.2 Principles of Operation	4-101
4.6 Summary and Conclusions	4-113
4.6.1 Summary	4-113
4.6.2 Conclusions	4-115
 5. PARAMETER ADAPTIVE CONTROL SYSTEMS WITH EXPLICIT PLANT IDENTIFICATION	 5-1
5.1 Introduction	5-1
5.2 Open Loop Adaptive Methods	5-4
5.3 Model Following Adaptive Control	5-6
5.4 Adaptive Optimal Control	5-14
5.4.1 Adaptive Optimal Regulator	5-15
5.4.2 Adaptive Optimal Model Following Systems	5-21
5.4.3 Transformation of Variables	5-30
5.4.4 Other Optimization Methods	5-35
5.5 Summary and Conclusions	5-37
 6. PARAMETER ESTIMATION	 6-1
6.1 Problem Formulation	6-1
6.2 Equation Coefficient Identification	6-4
6.2.1 Deterministic Equation Coefficient Identification	6-5
6.2.2 Stochastic Equation Coefficient Identification	6-10
6.3 Basic Parameter Estimation and Function Generation	6-19
6.4 Combined Identification and Adaptive Control	6-23
6.5 Summary and Conclusions	6-24
 7. LOW SENSITIVITY CONTROL SYSTEMS	 7-1
7.1 Complex Plane Methods	7-2
7.1.1 Frequency Domain Compensation Techniques	7-2
7.1.2 State Variable Feedback	7-7
7.1.3 Closed Loop Pole Sensitivity	7-14
7.1.4 Summary of Complex Plane Methods	7-15
7.2 Time Domain Sensitivity Functions	7-16
7.3 Minimax Design	7-19
7.4 Liapunov Design Methods	7-22

TABLE OF CONTENTS (Continued)

	<u>Page No.</u>
7.5 Bistable Controllers	7-35
7.6 Summary and Conclusions	7-38
REFERENCES	R-1
DISTRIBUTION LIST	

---

VOLUME II: PART III

ADAPTIVE CONTROL APPLICATIONS

8.	APPLICATIONS: PARAMETER ADAPTIVE CONTROL SYSTEMS WITH IMPLICIT PLANT IDENTIFICATION	8-1
8.1	Design Considerations	8-1
8.1.1	Airframe Dynamics	8-1
8.1.2	Performance Criteria	8-8
8.2	Application of the Accelerated Gradient Method	8-13
8.2.1	Design Procedure: General Considerations	8-13
8.2.2	A Pitch Rate Autopilot	8-19
8.2.3	A Normal Acceleration Autopilot	8-37
8.2.4	An Adaptive Reference Model	8-48
8.3	Application of Liapunov Design Techniques	8-55
8.3.1	Design Procedure	8-55
8.3.2	Selection of Parameters	8-59
8.3.3	Performance Evaluation	8-60
8.3.4	An Adaptive Reference Model	8-66
8.4	Summary and Conclusions	8-67
8.4.1	Summary	8-67
8.4.2	Conclusions	8-68
9.	APPLICATIONS: PARAMETER ADAPTIVE CONTROL SYSTEMS WITH EXPLICIT PLANT IDENTIFICATION	9-1
9.1	Pole Assignment	9-3
9.2	The Adaptive Optimal Regulator	9-8

TABLE OF CONTENTS (Continued)

	<u>Page No.</u>
9.2.1 Design of a Third Order Adaptive Optimal Regulator	9-9
9.2.2 Design of a Third Order Adaptive Suboptimal Regulator	9-15
9.3 Adaptive Optimal Model Following Systems	9-18
9.4 Response Comparisons	9-24
9.5 Rapidly Varying Plant Parameters	9-34
9.6 Summary and Conclusions	9-37
10. APPLICATIONS: LOW SENSITIVITY CONTROL SYSTEMS	10-1
10.1 Design Procedure	10-1
10.2 Selection of Parameters	10-8
10.3 Performance Evaluation	10-9
10.4 Summary and Conclusions	10-13

VOLUME II: PART IV

GUIDANCE

11. GUIDANCE SYSTEMS FOR TACTICAL MISSILES	11-1
11.1 Guidance Equations	11-2
11.2 Homing Guidance Techniques	11-5
11.2.1 Classical Homing Guidance Techniques	11-5
11.2.2 Adaptive Optimal Guidance	11-14
11.3 Steering Law Performance Analysis	11-23
11.3.1 Terminal Miss Sensitivity to Initial Conditions	11-25
11.3.2 Control Effort Sensitivity to Initial Conditions	11-33
11.3.3 Steering Law Evaluation	11-43
11.3.4 Terminal Miss Sensitivity to Measurement Bias Errors	11-51
11.3.5 Summary	11-54
11.4 A Coupled Guidance-Autopilot Steering Law	11-56

TABLE OF CONTENTS (Concluded)

	<u>Page No.</u>
11.4.1 Problem Formulation	11-57
11.4.2 Performance Analysis	11-63
11.5 Summary and Conclusions	11-75
APPENDICES	
A LINEAR DYNAMICAL SYSTEMS	A-1
B OPTIMAL CONTROL OF LINEAR SYSTEMS	B-1
C AN ANALYSIS OF THE M.I.T. GRADIENT METHOD	C-1
D STABILITY THEORY	D-1
E A LOCAL STABILITY THEOREM FOR ADAPTIVE SYSTEMS	E-1
F THE STEADY-STATE MATRIX RICCATI EQUATION	F-1
G ADJOINT THEORY FOR LINEAR SYSTEMS	G-1
H TRAJECTORY DATA	H-1
REFERENCES	R-1
DISTRIBUTION LIST	

LIST OF FIGURES

<u>Figure No.</u>		<u>Page No.</u>
8.1-1	Geometrical Definitions of Pitch Plane State Variables	8-4
8.1-2	Input-Output Relations for Autopilot Design Problem	8-6
8.1-3	Pitch Rate and Normal Acceleration Step Responses for Two Flight Conditions	8-11
8.1-4	Illustration of the Effect of a Pitch Rate Adaptive Autopilot on Normal Acceleration Response	8-12
8.2-1	Locus of the Closed Loop Poles for the Adaptive Control System With No Adaptive Loop Compensation ( $G_c(s) = 1$ )	8-23
8.2-2	Locus of the Closed Loop Poles for the Adaptive Control System With Adaptive Loop Compensation ( $G_c(s) = s+6.0$ )	8-23
8.2-3	An Accelerated Gradient Controller for a Pitch Rate Autopilot	8-25
8.2-4	Step Responses of a Gradient-Adaptive Controller for a Pitch Rate Autopilot	8-29
8.2-5	Step Responses of an Accelerated Gradient Adaptive Controller for a Pitch Rate Autopilot	8-30
8.2-6	Pitch Rate Responses for an Adaptive Pitch Rate Autopilot With Different Levels of Input Commands	8-32
8.2-7	Normal Acceleration Responses for an Adaptive Pitch Rate Autopilot With Different Levels of Input Commands	8-33
8.2-8	Pitch Rate Response With Time-Varying Airframe Parameter Parameters	8-35
8.2-9	Pitch Rate Responses With Rapid Airframe Parameter Variations That Lead to Autopilot Instability	8-36
8.2-10	Root Locus of the Closed Loop Adaptive Control System for Positive $k_e$ With No Adaptive Loop Compensation ( $G_c(s)=1$ )	8-42
8.2-11	Root Locus of the Closed Loop Adaptive System for Positive $k_e$ With Negative Gain Compensation ( $G_c(s) = -1$ )	8-43
8.2-12	An Accelerated Gradient Controller for a Normal Acceleration Autopilot	8-45



LIST OF FIGURES (Continued)

<u>Figure No.</u>		<u>Page No.</u>
8.2-13	Root Locus of $T_e(s)$ for Positive $k_e$ With $G_c(s)$ Given by Eq. (8.2-43)	8-46
8.2-14	Step Response of Adaptive Normal Acceleration Autopilot Using the Accelerated Gradient Method	8-47
8.2-15	An Accelerated Gradient Controller for a Pitch Rate Autopilot With an Adaptive Reference Model	8-51
8.2-16	Autopilot Responses for a System Using an Adaptive Reference Model: Adaptive Control Loop Disconnected	8-53
8.2-17	Autopilot Responses for a System Using an Adaptive Reference Model: Adaptive Control Loop Connected	8-54
8.3-1	Airframe and Input-Output Relations for an Adaptive Control System	8-56
8.3-2	Liapunov Design Technique Applied to a Second Order Airframe	8-61
8.3-3	Step Response of Control System in Fig. 8.3-2 for a Constant Plant, With ( $\lambda^{-1} = 5.5$ ) and Without ( $\lambda^{-1} = 0$ ) Adaptation	8-62
8.3-4	Pitch Rate Response of Reference Model and Pitch Rate Error Signal for the Liapunov Design in Fig. 8.3-2	8-63
8.3-5	Pitch Rate Error Signal With $\sigma = 0$	8-64
8.3-6	Pitch Rate Error Signal With Actuator Lag	8-65
8.3-7	Pitch Rate Response for Rapid Airframe Parameter Variations	8-65
8.3-8	Liapunov Design Technique Applied to a Second Order Airframe With an Adaptive Reference Model	8-66
9.1-1	Structure of a Missile Adaptive Controller With Explicit Plant Identification	9-2
9.1-2	Adaptive Linear Feedback Controller	9-2
9.1-3	Value of the Real Part of the Most Significant Closed Loop Pole: Pole Assignment Technique	9-6

LIST OF FIGURES (Continued)

<u>Figure No.</u>		<u>Page No.</u>
9.2-1	Performance Index as a Function of the Number of Optimal Gain Recalculations: Adaptive Optimal Regulator	9-13
9.2-2	Value of the Real Part of the Most Significant Closed Loop Pole: Optimal Regulator Method	9-14
9.2-3	Comparison of the Values of the Real Part of the Most Significant Closed Loop Pole for the Optimal and Suboptimal Regulator Designs	9-18
9.3-1	Values of the Real Part of the Most Significant Closed Loop Pole: Optimal Model Following System	9-22
9.4-1	Magnitude Profile of Commanded Acceleration	9-25
9.4-2	Autopilot Response Histories Along a Simulated Missile Trajectory for Three Adaptive Control Systems Using Explicit Plant Identification	9-26/9-27/9-28/9-29/9-30
9.5-1	Response Characteristics While Airframe Parameters are Varying Rapidly: Autopilot Designed Using Pole Assignment Technique With Adaptive Closed Loop Poles	9-36
10.1-1	Plant-Reference Model Input-Output Relations for a Low Sensitivity Control System	10-2
10.1-2	Mechanization of Insensitive Controller Based on Liapunov Design Procedure	10-7
10.1-3	Alternative Representation for Fig. 10.1-2	10-8
10.3-1	Step Response for the Pitch Rate Autopilot With a Time-Invariant Plant	10-10
10.3-2	Step Response for the Pitch Rate Autopilot With a Time-Varying Plant	10-11
10.3-3	Autopilot Response for the Pitch Rate Autopilot With a Time-Invariant Plant and Constant Drive Level D	10-12
10.4-1	Adaptive Reference Model Configuration	10-14
11.1-1	Definitions of Guidance Variables	11-3
11.2-1	Pursuit Guidance Trajectory	11-9

LIST OF FIGURES (Continued)

<u>Figure No.</u>		<u>Page No.</u>
11.2-2	Beam Rider Guidance Trajectory	11-10
11.2-3	Proportional Guidance	11-12
11.2-4	Relative Coordinate System in Proportional Guidance	11-13
11.3-1	Normalized Miss Distance for an Initial Cross-Track Velocity: Optimal Steering Law, $a_{c1}(t)$	11-29
11.3-2	Normalized Miss Distance for an Initial Cross-Track Velocity: Suboptimal Steering Laws, $a_{c2}(t)$ and $a_{c3}(t)$	11-29
11.3-3	Normalized Miss Distance Caused by Target Acceleration: Optimal Steering Law, $a_{c1}(t)$	11-30
11.3-4	Normalized Miss Distance Caused by Target Acceleration: Suboptimal Steering Law, $a_{c2}(t)$	11-30
11.3-5	Normalized Miss Distance Caused by Target Acceleration: Suboptimal Steering Law, $a_{c3}(t)$	11-31
11.3-6	Normalized Miss Distance Caused by Initial Line-of-Sight Rate: Optimal Steering Law, $a_{c1}(t)$	11-31
11.3-7	Normalized Miss Distance Caused by Initial Line-of-Sight Rate: Suboptimal Steering Laws, $a_{c2}(t)$ and $a_{c3}(t)$	11-32
11.3-8	Root Normalized Effort Caused by Initial Cross-Track Velocity or Initial Line-of-Sight Rate: Optimal Steering Law, $a_{c1}(t)$	11-36
11.3-9	Root Normalized Effort Caused by Initial Cross-Track Velocity or Initial Line-of-Sight Rate: Suboptimal Steering Laws, $a_{c2}(t)$ and $a_{c3}(t)$	11-36
11.3-10	Root Normalized Effort Caused by Target Acceleration: Optimal Steering Law, $a_{c1}(t)$	11-37
11.3-11	Root Normalized Effort Caused by Target Acceleration: Suboptimal Steering Law, $a_{c3}(t)$	11-37
11.3-12	Root Normalized Effort Caused by Target Acceleration: Suboptimal Steering Law, $a_{c2}(t)$	11-38
11.3-13	Autopilot Block Diagram	11-40

LIST OF FIGURES (Continued)

<u>Figure No.</u>		<u>Page No.</u>
11.3-14	Root Normalized Effort Versus Normalized Terminal Miss Caused by an Initial Cross-Track Velocity	11-45
11.3-15	Root Normalized Effort Versus Peak Normalized Miss Produced by Target Acceleration	11-49
11.3-16	Normalized Miss Distance Caused by Target Acceleration Measurement Bias Error: Optimal Steering Law, $a_{c1}(t)$	11-52
11.3-17	Normalized Miss Distance Caused by Target Acceleration Measurement Bias Error: Suboptimal Steering Law, $a_{c2}(t)$	11-52
11.3-18	Peak Normalized Miss, Produced by Target Acceleration Measurement Bias Error, Versus Peak Normalized Miss Caused by Target Acceleration	11-54
11.4-1	A Second Order Autopilot Design for a Suboptimal Steering Law	11-61
11.4-2	Normalized Terminal Miss Distance Produced by an Initial Cross-Track Velocity	11-65
11.4-3	Closed Loop Pole Locations for the Second Order Autopilot and its First Order Approximation	11-67
11.4-4	Root Normalized Effort Caused by an Initial Cross-Track Velocity	11-69
11.4-5	Root Normalized Effort Versus Normalized Terminal Miss Caused by an Initial Cross-Track Velocity	11-70
11.4-6	Comparison of Representative Time Histories for Optimal and Suboptimal Gains	11-73
A-1	Illustration of Continuous Representation of Linear Dynamic Equations	A-2
A-2	Block Diagram Representation of Eq. (A-2)	A-3
A-3	Block Diagram of a Hypothetical Linear Dynamic System	A-4
A-4	Illustration of the Behavior of the State for a First Order Homogeneous System	A-8

PART III  
ADAPTIVE CONTROL APPLICATIONS

## 8. APPLICATIONS: PARAMETER ADAPTIVE CONTROL SYSTEMS WITH IMPLICIT PLANT IDENTIFICATION

In this chapter two adaptive control techniques described in Chapter 4 -- the accelerated gradient and Liapunov design methods -- are considered for tactical missile autopilot design. Our primary goal is to demonstrate the feasibility of these methods in terms of resulting missile performance. The accelerated gradient method is applied to both adaptive pitch rate and normal acceleration autopilots and the Liapunov method is used for pitch rate control.

### 8.1 DESIGN CONSIDERATIONS

In designing any control system, adaptive or not, one begins with a mathematical model for the plant and specified performance criteria. We first discuss these aspects of the problem formulation for tactical missiles.

#### 8.1.1 Airframe Dynamics

The rotational motion of an airframe is generally described in terms of 6 state variables -- three angles and three angular rates. The exact differential equations of motion for these variables are nonlinear and are also coupled to the translational motion of the airframe through such quantities as air speed and altitude which describe the missile's flight condition. As is mentioned in Section 2.1, the coupling between translation and rotation is simplified if the former, being affected primarily by the

relatively long response time of the guidance loop, is regarded as being independent of the autopilot characteristics. Consequently, with respect to the rotational equations of motion, the variables which define the flight condition can be regarded as time-varying quantities that are independent of the missile airframe response characteristics. The dimensionality of the rotational equations is usually reduced by considering them to be separable into three uncoupled motions -- pitch, yaw, and roll -- each of which is controlled separately. In a cruciform missile pitch and yaw dynamics are identical,\* both being used to respond to steering commands, and the function of the roll control system is primarily one of stabilization. After these simplifications there still remain nonlinearities in the dependence of the equations of motion upon angle of attack and control surface deflection angle; linearization is achieved by employing small angle approximations.

In this report we are interested not only in autopilot design, but also in the relationship of the autopilot to the overall performance of the guidance system. The latter is investigated by assuming the missile's translational motion is confined to a single plane, taken to be the pitch plane. Consequently the autopilot governing pitch motion which receives the steering commands is most relevant for this study.

The mathematical model used here to describe pitch motion is for a missile which develops control forces through aerodynamic lift provided by fixed wings or by the missile body, with the aid of tail-mounted control surfaces. This is currently the most common configuration.

---

\* In the discussion that follows the effects of gravity are neglected. However, the text speaks of "pitch" dynamics in the "pitch" plane, recognizing that in a strict sense it is the horizontal plane and yaw dynamics that are described.

The model assumes second order airframe and first order actuator dynamics with equations of motion given by

$$\begin{aligned}\dot{q}(t) &= M_q q(t) + M_\alpha \alpha(t) + M_\delta \delta(t) \\ \dot{\alpha}(t) &= q(t) - L_\alpha \alpha(t) - L_\delta \delta(t) \\ \dot{\delta}(t) &= -\lambda \delta(t) + \lambda u(t) \\ a(t) &= -V [\dot{\alpha}(t) - q(t)]\end{aligned}\tag{8.1-1}$$

where  $M_q$ ,  $M_\alpha$ ,  $M_\delta$ ,  $L_\alpha$ , and  $L_\delta$  are stability derivatives and

$$\begin{aligned}q(t) &= \text{pitch rate} & \alpha(t) &= \text{angle of attack} \\ a(t) &= \text{normal acceleration} & u(t) &= \text{control command} \\ \delta(t) &= \text{control surface deflection} & -\lambda &= \text{actuator pole} \\ V &= \text{air speed}\end{aligned}$$

Refer to Fig. 8.1-1 for a geometrical definition of autopilot state variables. The stability derivatives can be expressed analytically in terms of aerodynamic coefficients, airframe parameters, airspeed, and dynamic pressure by the relations

$$\begin{aligned}M_q &= \frac{\bar{q} S d^2}{2 I_{yy} V} C_{M_q} & M_\alpha &= \frac{\bar{q} S d}{I_{yy}} C_{M_\alpha} \\ M_\delta &= \frac{\bar{q} S d}{I_{yy}} C_{M_\delta} & L_\alpha &= \frac{\bar{q} S}{m V} C_{N_\alpha} \\ L_\delta &= \frac{\bar{q} S}{m V} C_{N_\delta}\end{aligned}\tag{8.1-2}$$



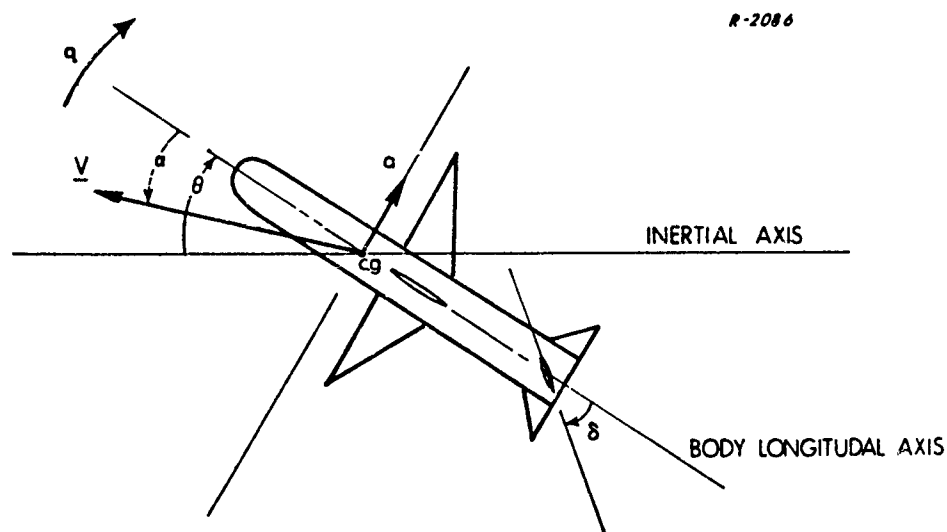


Figure 8.1-1 Geometrical Definitions of Pitch Plane State Variables

where

$\bar{q}$  = dynamic pressure

$I_{yy}$  = moment of inertia about pitch axis

$S$  = lifting surface area

$d$  = characteristic length

$C_{M_q}, C_{M_\alpha}, C_{M_\delta}$  = moment coefficients

$C_{N_\alpha}, C_{N_\delta}$  = normal force coefficients

$m$  = mass

The equations of motion can be expressed in the vector-matrix form

$$\begin{bmatrix} \dot{q}(t) \\ \dot{a}(t) \\ \dot{\delta}(t) \end{bmatrix} = \begin{bmatrix} M_q & \frac{1}{V} \frac{\alpha}{L_\alpha} & M_\delta - \frac{M_\alpha L_\delta}{L_\alpha} \\ V L_\alpha & -L_\alpha & -\lambda V L_\delta \\ 0 & 0 & -\lambda \end{bmatrix} \begin{bmatrix} q(t) \\ a(t) \\ \delta(t) \end{bmatrix} + \begin{bmatrix} 0 \\ \lambda V L_\delta \\ \lambda \end{bmatrix} u(t) \quad (8.1-3)$$

or, in abbreviated notation,

$$\dot{\underline{x}}(t) = A \underline{x}(t) + \underline{b} u(t)$$

$$A \triangleq \begin{bmatrix} a_{11} & a_{12} & a_{13} \\ a_{21} & a_{22} & a_{23} \\ 0 & 0 & a_{33} \end{bmatrix}; \quad \underline{b} \triangleq \begin{bmatrix} 0 \\ b_2 \\ b_3 \end{bmatrix} = \begin{bmatrix} 0 \\ -a_{23} \\ -a_{33} \end{bmatrix} \quad (8.1-4)$$

To design an adaptive autopilot using the techniques suggested in Chapter 4 we augment Eq. (8.1-4) with the equations of motion for a known reference model that has desired output response characteristics. The total system is illustrated in Fig. 8.1-2 and is described by the relations

$$\begin{aligned} \dot{\underline{x}} &= A \underline{x}(t) + \underline{b} u(t) & y(t) &= \underline{c}^T \underline{x}(t) \\ \underline{m}(t) &= H \underline{x}(t) & u(t) &= v(t) - r(t) \\ \dot{\underline{x}}_m(t) &= A_m \underline{x}_m(t) + \underline{b}_m v(t) & y_m(t) &= \underline{c}_m^T \underline{x}_m(t) \\ e(t) &= y(t) - y_m(t) \end{aligned} \quad (8.1-5)$$

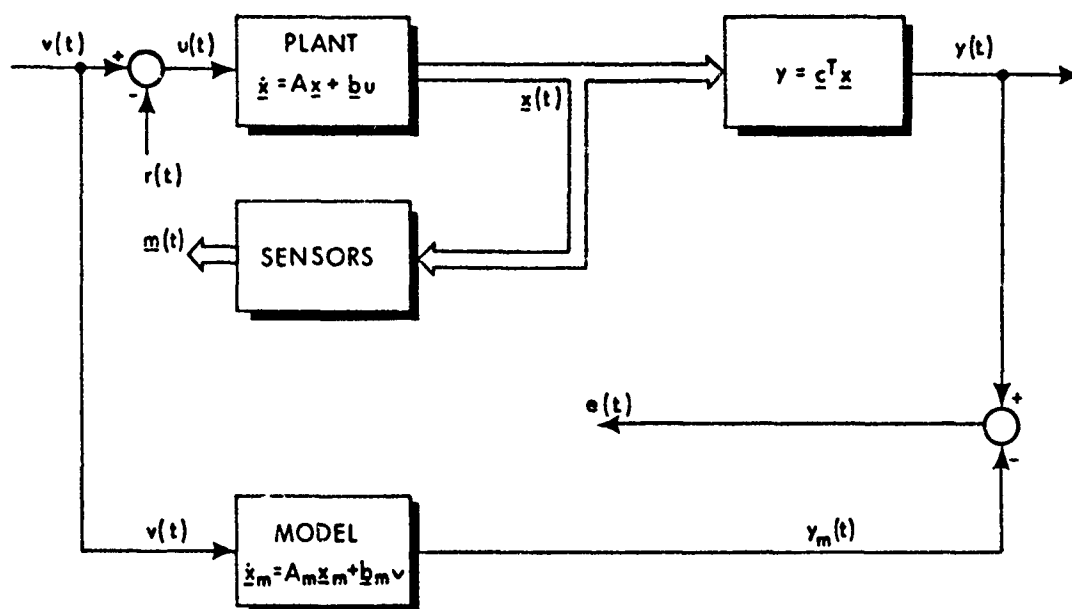


Figure 8.1-2 Input-Output Relations for Autopilot Design Problem

where  $\underline{x}_m(t)$  is the state of the reference model having time-invariant\* dynamics described by  $\underline{A}_m$  and  $\underline{b}_m$ ,  $y(t)$  is the output of the autopilot which is to be compared with the model output  $y_m(t)$ ,  $e(t)$  is the output error signal,  $\underline{m}(t)$  is the set of measurements available for use by the controller,  $v(t)$  is the steering command input, and  $r(t)$  is that portion of the control command which can be specified by the designer. The overall objective is to choose  $r(t)$  so that the output error signal remains small.

Another expression that is useful for describing the airframe dynamics is the input-output transfer function relating  $y(t)$  and  $u(t)$ , given by

$$\frac{Y(s)}{U(s)} = \underline{c}^T (Is - \underline{A})^{-1} \underline{b} \quad (8.1-6)$$

\* In Section 8.2.4 it is demonstrated that an adaptive (time-varying) reference model has advantages for missile control.

where  $Y(s)$  and  $U(s)$  are the Laplace transforms of  $y(t)$  and  $u(t)$  and it is assumed that  $A$  and  $\underline{b}$  are time invariant. For the applications being considered, specific expressions for  $\underline{c}$  are

$$\underline{c}^T = [1 \ 0 \ 0] \Rightarrow y(t) = q(t)$$

$$\underline{c}^T = [0 \ 1 \ 0] \Rightarrow y(t) = a(t) \quad (8.1-7)$$

Substitution of Eqs. (8.1-4) and (8.1-7) into Eq. (8.1-6) produces

$$\begin{aligned} \frac{Q(s)}{U(s)} &= \frac{-(a_{33}a_{13} + a_{12}a_{23}) \left( s - \frac{a_{13}a_{33}a_{22}}{a_{33}a_{13} + a_{12}a_{23}} \right)}{(s+\lambda) \left( s^2 - (a_{11} + a_{22})s + a_{11}a_{22} - a_{12}a_{21} \right)} \\ \frac{A(s)}{U(s)} &= \frac{-a_{23} \left( s^2 - a_{11}s + \frac{a_{21}a_{13}a_{33}}{a_{23}} \right)}{(s+\lambda) \left( s^2 - (a_{11} + a_{22})s + a_{11}a_{22} - a_{12}a_{21} \right)} \end{aligned} \quad (8.1-8)$$

where  $Q(s)$  and  $A(s)$  denote the transforms of  $q(t)$  and  $a(t)$ .

The above mathematical description of the missile airframe omits contributions from structural bending modes and sensor dynamics. This keeps the control system sufficiently simple to permit the scope of this study to include several adaptive techniques, but retains enough detail to permit realistic conclusions about control of the dominant response characteristics. In a complete missile control system design, any high order effects neglected in synthesizing the autopilot should be included in simulation evaluations of performance.

In order to evaluate various control schemes, a set of typical missile dynamics is required for performing computer simulations; it

should include the time-varying character of airframe parameters along the flight path. Two sets of such data are given in Appendix H, representing air-to-surface and surface-to-air types of trajectories.

### 8.1.2 Performance Criteria

In designing an adaptive system care must be exercised in choosing a set of reference model dynamics and an output signal  $y(t)$ . One's first thought may be to designate any conveniently measured state variable as the output variable and select a reference model having natural frequencies such that the model output  $y_m(t)$  has a desirable transient response. Then the controller would be designed to make the error between the output variables small, according to some adaptive procedure. However, if this reasoning is applied too loosely the result can be an adaptive control system with exactly the wrong performance characteristics. This point will be elaborated as we discuss a proper design procedure for the missile application.

From a functional point of view, the missile autopilot exists only to serve the guidance objectives. Consequently performance criteria for the control system should be based upon what is required by the steering commands. In Chapter 11 it is demonstrated that most effective guidance laws use a normal acceleration steering command so that the autopilot output variable of interest is normal acceleration,  $a(t)$  in Eq. (8.1-3). Thus the reference model specifications should be such that the model's normal acceleration  $a_m(t)$  has desired response characteristics to  $v(t)$  and the adaptive controller should attempt to null the error

$$e(t) = a(t) - a_m(t)$$

That is to say, an adaptive normal acceleration autopilot is desired.

For reasons related to the adaptation properties of the system, which are discussed more fully in the sequel, it is sometimes tempting to try achieving acceleration control indirectly by using a state variable other than normal acceleration to define the output of the autopilot. Specifically, we know from Eq. (8.1-1) that constant values of pitch rate, and acceleration are related simply by

$$a = qV \quad (8.1-9)$$

This represents the steady state airframe response to a step input. If an estimate of air speed is available, a constant pitch rate command can be applied which yields the desired constant acceleration after the transient has subsided. Consequently one might consider implementing an adaptive pitch rate autopilot, even though acceleration is the quantity of importance, in the expectation that the acceleration and pitch rate transient responses would have similar response times. Unfortunately, this approach can be incorrect, depending upon the type of missile being employed.

To understand the potential fallacy of the technique described above, one must consider the dynamic relationship between pitch rate and normal acceleration for the particular missile under consideration. If the airframe depends upon aerodynamic forces for developing the lift required to produce normal acceleration, the dependence between  $a(t)$  and  $q(t)$  changes with flight condition (FC). To illustrate this fact consider an airframe modelled by Eq. (8.1-3) and suppose  $u(t)$  is given by

$$u(t) = v(t) - k_1 q(t) - k_2 a(t) - k_3 \dot{a}(t)$$

with the set of constant gains  $k_1$ ,  $k_2$ , and  $k_3$  chosen at different flight conditions so that the resulting system poles have specified values. This can always be done because the system is controllable (Ref. 30). In particular, choose two sets of gains so that the system poles are at  $-40$ ,  $-5 + j5$ ,  $-5 - j5$  in both flight conditions 4 (high altitude) and 6 (low altitude) of Tables H.1 and H.2 and apply a step pitch rate command  $v(t)$  which yields a normal acceleration of  $28.0 \text{ feet/sec}^2$  in the steady state. The resulting step responses are shown in Fig. 8.1-3. Notice that the settling times of the system are about the same for both flight conditions because the system closed loop poles are the same for both cases. However, the overshoot in pitch rate is considerably different in the two cases, that for condition 4 being considerably larger. The physical reason for this behavior is that the missile, being aerodynamically controlled, must develop a larger angle of attack at FC 4 than at FC 6 to achieve the same normal acceleration, primarily because the dynamic pressure is lower. More specifically, in the case illustrated here, the velocities are nearly the same at both flight conditions but the altitudes are considerably different. At the higher altitude (FC 4) the air density is lower so that the lifting surfaces are less effective than at low altitudes; thus a larger angle of attack is required to achieve the same lifting force. This reasoning implies that the pitch rate must have a greater peak value if the settling time is to be the same at both flight conditions.

The above example illustrates that the physics of aerodynamic missile control demands a wide variation in pitch rate transient response as plant dynamics change, if the settling time of the normal acceleration response is to remain constant. Consequently if one should try to obtain uniform pitch rate response, just the opposite result will be achieved; i.e., the acceleration transient response will vary widely over different flight conditions. This behavior is rather simply described analytically with

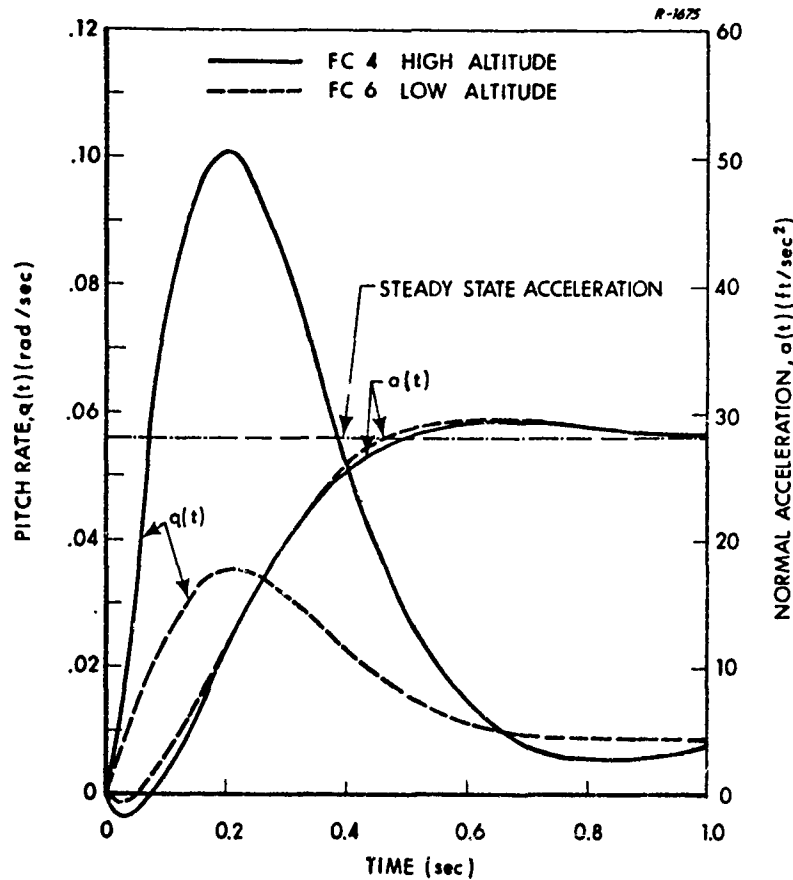


Figure 8.1-3 Pitch Rate and Normal Acceleration Step Responses for Two Flight Conditions

the aid of the diagram in Fig. 8.1-4. Suppose an adaptive autopilot can be designed so that at all flight conditions the pitch rate response to a command input  $v(t)$  is described by a fixed reference model transfer function,  $T_m(s)$ . However, the dynamic relationship between pitch rate and normal acceleration is deduced from Eq. (8.1-8),

$$\frac{A(s)}{Q(s)} = \frac{a_{23} \left( s^2 - a_{11}s + \frac{a_{21}a_{13}a_{33}}{a_{23}} \right)}{(a_{33}a_{13} + a_{12}a_{23}) \left( s - \frac{a_{13}a_{33}a_{22}}{a_{33}a_{13} + a_{12}a_{23}} \right)} \quad (8.1-10)$$



R-3565

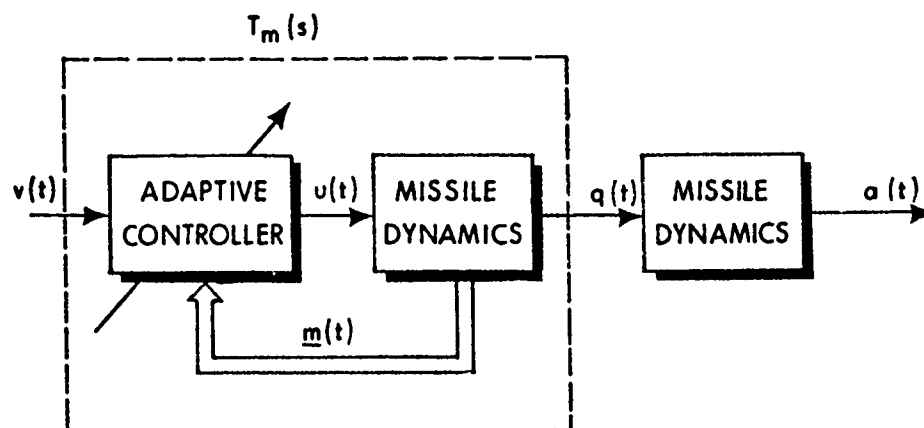


Figure 8.1-4 Illustration of the Effect of a Pitch Rate Adaptive Autopilot on Normal Acceleration Response

Evidently the latter transfer function is unaffected by the adaptive controller and is sensitive to variations in the elements of  $A$  and  $b$  in Eq. (8.1-4). Consequently the acceleration response to the input, given by

$$\frac{A(s)}{V(s)} = T_m(s) \frac{A(s)}{Q(s)} \quad (8.1-11)$$

is also subject to changes in its parameters. The most important effect is the single pole in Eq. (8.1-10) which tends to be smaller in magnitude at high altitudes and/or low air speed (FC 4 in Fig. 8.1-3) than it is at low altitudes and/or high air speed (FC 6 in Fig. 8.1-3). The resulting effect on normal acceleration response is a variation in settling time as flight conditions change; this is demonstrated subsequently in simulation results.

The conclusion is that an adaptive normal acceleration autopilot is required for aerodynamically controlled missiles. When other mechanisms which are independent of aerodynamic forces, such as thrust vectoring, are used for developing control force, it is possible that a pitch rate autopilot will yield satisfactory performance. In any case, the designer must keep in mind that normal acceleration is actually the output variable of interest and ensure that its response characteristics are correct for whatever control scheme is devised.

Many adaptive techniques developed or proposed in the past have been concerned with controlling aircraft airframe pitch rate or roll motion. Little attention has been given to the problem of designing an adaptive normal acceleration autopilot using the methods described in Chapter 4. Both pitch rate and acceleration control of missiles are investigated in subsequent sections.

## 8.2 APPLICATION OF THE ACCELERATED GRADIENT METHOD

Having outlined requirements for autopilots in Section 8.1, we now consider application of a particular adaptive technique, the accelerated gradient method discussed in Section 4.3. In this section the design procedure is explained in detail and simulation results are presented for both pitch rate and normal acceleration autopilots.

### 8.2.1 Design Procedure: General Considerations

The design procedure for an accelerated gradient controller consists of three distinct steps:

- Define the controller structure.
- Derive the simplified gradient adaptation algorithm.
- Introduce linear compensation in the adaptive loop.

The Controller Structure — The equations of motion are given by Eq. (8.1-5) and measurements (or estimates) of the state variables are assumed to be available, i.e.,

$$\underline{m}(t) = \underline{x}(t)$$

The free control variable  $r(t)$  is defined to be

$$r(t) = (1 - k(t)) v(t) + \underline{h}(t)^T \underline{x}(t) \quad (8.2-1)$$

so that the input to the plant,  $u(t)$ , becomes

$$u(t) = k(t) v(t) - \underline{h}(t)^T \underline{x}(t) \quad (8.2-2)$$

where  $k(t)$  and  $\underline{h}(t)$  are adaptive gains. Thus we assume all three state variables -- pitch rate, normal acceleration, and control surface deflection -- are available for feedback control. This particular controller structure is chosen so that any values of the closed loop poles, which are the eigenvalues of the matrix  $(A - \underline{b}\underline{h}^T)$ , can be selected by proper choice of  $\underline{h}$ , given  $A$  and  $\underline{b}$ . The gain  $k(t)$  is introduced to provide independent control over the d-c gain between input and output.

The error signal  $e(t)$  is given by

$$e(t) = \underline{c}^T (\underline{x}(t) - \underline{x}_m(t)) \quad (8.2-3)$$

where

$$\underline{c}^T = \begin{bmatrix} 1 & 0 & 0 \end{bmatrix}; \text{ pitch rate autopilot} \\ \begin{bmatrix} 0 & 1 & 0 \end{bmatrix}; \text{ normal acceleration autopilot} \quad (8.2-4)$$

The detailed simulation of each type of autopilot is considered separately in Sections 8.2.2 and 8.2.3.

The Simplified Gradient Adaptation Algorithm — The adaptive controller for the autopilot is designed by applying techniques suggested in Sections 4.2.4, 4.2.6, and 4.3. The basic adaptation algorithm is chosen using the gradient method described in Section 4.2.4; then linear compensation is added as needed in the adaptive loop to improve the adaptation speed. The relations for the simplified gradient adaptation algorithm are given by Eqs. (4.2-30) and (4.2-37) for the system with adaptive feedback gains  $\underline{h}(t)$ . These are repeated here for convenience in the form

$$\dot{h}_i(t) = \beta'_i \underline{c}^T (\underline{x}(t) - \underline{x}_m(t)) x_i(t) \\ \beta'_i = \beta_i \text{sign} \left[ \underline{c}^T A^{N-1} \underline{b} \right]; \quad i = 1, \dots, n \quad (8.2-5)$$

where  $\beta'_i$  is an adaptation gain whose magnitude  $\beta_i$  is chosen by the designer and whose algebraic sign is specified by the quantity in brackets. The quantity  $N$  is the smallest positive integer such that  $(\underline{c}^T A^{N-1} \underline{b})$  is nonzero.

The autopilot equations of motion are the same form as Eq. (4.2-37) except for the additional adaptive gain  $k(t)$  in Eq. (8.2-2) for which an adjustment algorithm must be provided. This can be obtained from the first expression in Eq. (4.2-27), which holds for any adaptive quantity appearing in the differential equation for  $\underline{x}(t)$ . Thus

$$\dot{\mathbf{k}}(t) = -\beta_k e(t) \mathbf{c}^T \frac{\partial \mathbf{x}(t)^{(N)}}{\partial \mathbf{k}} \quad (8.2-6)$$

where  $\beta_k$  is a positive gain to be chosen by the designer. Evaluating the partial derivative in Eq. (8.2-6), one obtains

$$\frac{\partial \mathbf{x}(t)^{(N)}}{\partial \mathbf{k}} = \mathbf{A}^{N-1} \mathbf{b} v(t) \quad (8.2-7)$$

where  $N$  is the smallest integer greater than or equal to one such that

$$\mathbf{c}^T \mathbf{A}^{N-1} \mathbf{b} \neq 0$$

By analogy with the solutions obtained for the gains  $\beta_i'$ , let

$$\beta_k' \triangleq \beta_k \text{sign} \left[ \mathbf{c}^T \mathbf{A}^{N-1} \mathbf{b} \right] \quad (8.2-8)$$

Now, Eqs. (8.1-5), (8.2-1) through (8.2-3), and (8.2-5) through (8.2-8) are combined to yield the equations of motion of the gradient-adaptive control system;

$$\begin{aligned} \dot{\mathbf{x}}(t) &= (\mathbf{A} - \mathbf{b} \mathbf{h}(t)^T) \mathbf{x}(t) + \mathbf{b} k(t) v(t) \\ \dot{\mathbf{x}}_m(t) &= \mathbf{A}_m \mathbf{x}_m(t) + \mathbf{b}_m v(t) \\ \dot{h}_i(t) &= \beta_i' e(t) x_i(t); \quad i = 1, \dots, n \\ \dot{k}(t) &= -\beta_k' e(t) v(t) \\ e(t) &= \mathbf{c}^T \left[ \mathbf{x}(t) - \mathbf{x}_m(t) \right] \end{aligned} \quad (8.2-9)$$

where  $\underline{c}$  is given by one of the expressions in Eq. (8.2-4), according to which type of autopilot is under consideration.

Adaptive Loop Compensation — Following the procedure suggested in Eq. (4.2-39) of Section 4.2.6, we expand  $\underline{h}(t)$ ,  $\underline{x}(t)$ , and  $\underline{k}(t)$  about nominal values

$$\underline{k}(t) = \underline{k}_0 + \delta \underline{k}(t) \quad \underline{h}(t) = \underline{h}_0 + \delta \underline{h}(t) \quad \underline{x}(t) = \underline{x}_m(t) + \delta \underline{x}(t) \quad (8.2-10)$$

and linearize Eq. (8.2-9). With the nonlinear and forcing terms neglected, the result is

$$\begin{bmatrix} \delta \dot{\underline{x}}(t) \\ \delta \dot{\underline{h}}(t) \\ \delta \dot{\underline{k}}(t) \end{bmatrix} = \begin{bmatrix} \underline{A} - \underline{b} \underline{h}_0^T & -\underline{b} \underline{x}_m(t)^T & \underline{b} \underline{v}(t) \\ \underline{B}' \underline{x}_m(t) \underline{c}^T & [0] & \underline{0} \\ -\beta'_k \underline{v}(t) \underline{c}^T & \underline{0}^T & 0 \end{bmatrix} \begin{bmatrix} \delta \underline{x}(t) \\ \delta \underline{h}(t) \\ \delta \underline{k}(t) \end{bmatrix} \quad (8.2-11)$$

where  $\underline{B}'$  is a diagonal matrix whose diagonal elements are the gains  $\beta'_i$ . Proceeding in exactly the same way used to derive the error expression in Eq. (4.2-48), one obtains

$$\underline{E}(s) = - \left[ \beta'_k \underline{v}^2 + \sum_{i=1}^n \beta'_i \underline{x}_{m_i}^2 \right] \underline{G}_0(s) \underline{E}(s) \frac{1}{s} \quad (8.2-12)$$

where

$$\underline{G}_0(s) = \underline{c}^T (\underline{I}s - \underline{A} + \underline{b} \underline{h}_0^T)^{-1} \underline{b} \quad (8.2-13)$$

and  $v(t)$  and  $\underline{x}_m(t)$  are considered constants. Recall that  $G_o(s)$  is just the transfer function between the output  $y(t)$  and the modified command input  $k(t) v(t)$  with the nominal feedback gains  $\underline{h}_o$  implemented in the controller.

Equation (8.2-12) provides a means for analyzing the stability properties of the gradient-adaptive controller. To improve its convergence properties, we apply the method of Section 4.3 which introduces linear compensation,  $G_{c1}(s)$  and  $G_{c2}(s)$ , into the adaptive loop to obtain an accelerated gradient algorithm. This algorithm is the same as Eq. (4.3-5) with the additions

$$\begin{aligned} p_k(t) &= e_f(t) v(t) & W_k(s) &= G_{c2}(s) P_k(s) \\ \dot{k}(t) &= -\beta'_k w_k(t) \end{aligned} \quad (8.2-14)$$

where  $P_k(s)$  and  $W_k(s)$  denote Laplace transforms of  $p_k(t)$  and  $w_k(t)$ . The new error equation has the form

$$\begin{aligned} E(s) &= -k_e \left[ \frac{G_o(s) G_{c1}(s) G_{c2}(s)}{s} \right] E(s) \\ k_e &\triangleq \beta'_k v^2 + \sum_{i=1}^n \beta'_i x_{m_i}^2 \end{aligned} \quad (8.2-15)$$

The above discussion is largely a brief review of material discussed in Chapter 4 and provides the framework for the particular application described in the next three sections.

### 8.2.2 A Pitch Rate Autopilot

The first application we consider is that of a pitch rate autopilot for the missile dynamics given in Appendix H, Section H.1. For this case we have

$$\underline{c}^T = [1 \ 0 \ 0] \quad (8.2-16)$$

in Eq. (8.2-9).

Before specifying the detailed construction of the controller, the value of  $N$  in Eq. (8.2-5) must first be determined. Referring to Eqs. (8.1-3), (8.1-4), and (8.2-16) it is evident that

$$\begin{aligned} N = 1: \quad \underline{c}^T \underline{b} &= 0 \\ N = 2: \quad \underline{c}^T \underline{A} \underline{b} &= b_2 a_{12} + b_3 a_{13} \end{aligned} \quad (8.2-17)$$

Consequently  $N = 2$  and from the data in Table H.3 it follows that

$$\underline{c}^T \underline{A} \underline{b} < 0$$

for all flight conditions. Therefore Eqs. (8.2-5) and (8.2-8) imply that

$$\begin{aligned} \beta'_i &= -\beta_i; & \beta_i &> 0 \\ \beta'_k &= -\beta_k; & \beta_k &> 0 \end{aligned} \quad (8.2-18)$$

Combining these results with Eqs. (8.2-9), (4.3-5), (8.2-14), and (8.2-16) one obtains the following set of expressions for a pitch rate autopilot:



Accelerated Gradient Adaptive Controller  
for a Pitch Rate Autopilot

$$\begin{aligned}
 \dot{\underline{x}}(t) &= (A - \underline{b}\underline{h}(t)^T) \underline{x}(t) + \underline{b} k(t) v(t) \\
 \dot{\underline{x}}_m(t) &= A_m \underline{x}_m(t) + \underline{b}_m v(t) \\
 e(t) &= x_1(t) - x_{m1}(t) & E_f(s) &= G_{c1}(s) E(s) \\
 p_i(t) &= e_f(t) x_i(t) & p_k(t) &= e_f(t) v(t) \\
 W_i(s) &= G_{c2}(s) P_i(s) & W_k(s) &= G_{c2}(s) P_k(s) \\
 \dot{h}_i(t) &= -g \gamma_i w_i(t) & \dot{k}(t) &= g \gamma_k w_k(t)
 \end{aligned} \tag{8.2-19}$$

where  $i = 1, \dots, n$  and we have made the definitions

$$\begin{aligned}
 \gamma_i &\triangleq \beta_i / g > 0 \\
 \gamma_k &\triangleq \beta_k / g > 0
 \end{aligned} \tag{8.2-20}$$

The positive quantity  $g$  is introduced to provide convenient control over the adaptive loop gain  $k_e$  derived from Eqs. (8.2-15), (8.2-18), and (8.2-20);

$$k_e = -g \left[ \gamma_k v^2 + \sum_{i=1}^n \gamma_i x_{m_i}^2 \right] < 0 \tag{8.2-21}$$

At this stage, the designer's task is divided into four well defined phases:

- Determine the required adaptive loop compensation.
- Select appropriate specifications for the reference model.
- Determine the adaptation gains  $\beta_i$  and  $\beta_k$ ,  $i = 1, \dots, n$ .
- Evaluate performance with simulations.

These steps are completed below, for the specific example represented by the air-to-surface trajectory data in Section H.1.

Adaptive-Loop Compensation — To determine  $G_{c1}(s)$  and  $G_{c2}(s)$ , examine the root locus of the denominator in the transfer function

$$T_e(s) = \frac{1}{s + k_e G_o(s) G_c(s)} \quad G_c(s) \triangleq G_{c1}(s) G_{c2}(s) \quad (8.2-22)$$

associated with Eq. (8.2-15). Recall that  $G_o(s)$  as given by Eq. (8.2-13) is assumed to have poles identical with those of the model (see Eq. (4.2-43)). Its zeros are determined by evaluating the numerator in Eq. (8.2-13). Defining the elements of  $A$  and  $b$  as in Eq. (8.1-4),  $G_o(s)$  is obtained in the form

$$G_o(s) = \frac{g_o (s - z_o)}{(s - p_{m1})(s - p_{m2})(s - p_{m3})}$$

$$g_o = -(a_{33} a_{13} + a_{12} a_{23}) \quad z_o = -a_{13} a_{33} a_{22} / g_o \quad (8.2-23)$$

where  $p_{m1}$ ,  $p_{m2}$ , and  $p_{m3}$  are the specified reference model poles.

Evidently the gain  $g_o$  and zero  $z_o$  of  $G_o(s)$  both depend upon the variable plant parameters and are independent of the feedback gains  $h_o$ . Reference to Table H.3 indicates that  $g_o$  and  $z_o$  are negative for all flight conditions. Substitution of Eq. (8.2-23) into Eq. (8.2-22) produces

$$T_e(s) = \frac{1}{s + \frac{k_e g_o (s - z_o) G_c(s)}{(s - p_{m1})(s - p_{m2})(s - p_{m3})}} \quad (8.2-24)$$

where the product  $(k_e g_o)$  is always positive if  $\gamma_i$  and  $\gamma_k$  in Eq. (8.2-21) are positive.

The reference model poles are chosen so that desirable response characteristics are achieved; for this investigation

$$p_{m_1} = -40.0 \quad p_{m_2} = -5.0 + j5.0 \quad p_{m_3} = -5.0 - j5.0 \quad (8.2-25)$$

providing a time constant on the order of 0.2 sec. Evaluation of  $z_o$  and  $g_o$  for representative flight conditions indicates that their ranges are approximately

$$\begin{aligned} 300 &\leq |g_o| \leq 15,000 \\ 0.04 &\leq |z_o| \leq 1.25 \end{aligned} \quad (8.2-26)$$

Taking  $G_c(s) = 1$  -- corresponding to the gradient controller derived in Eq. (8.2-9) -- the locus of poles of  $T_e(s)$  is shown qualitatively in Fig. 8.2-1. As  $k_e$  increases in magnitude, the complex poles move toward the  $j\omega$  axis, eventually crossing into the right-half-plane causing the system to become unstable. The pole at the origin moves toward the zero of  $G_o(s)$ .

To improve the adaptation speed of the system, compensation should be introduced so that the real parts of the complex poles become more negative as the loop gain is increased. This can be most easily accomplished by specifying

$$G_c(s) = s - z_c \quad z_c < 0 \quad (8.2-27)$$

For this example, we take  $z_c = -6.0 \text{ sec}^{-1}$  and compare the resulting root locus in Fig. 8.2-2 with that in Fig. 8.2-1. Evidently much better

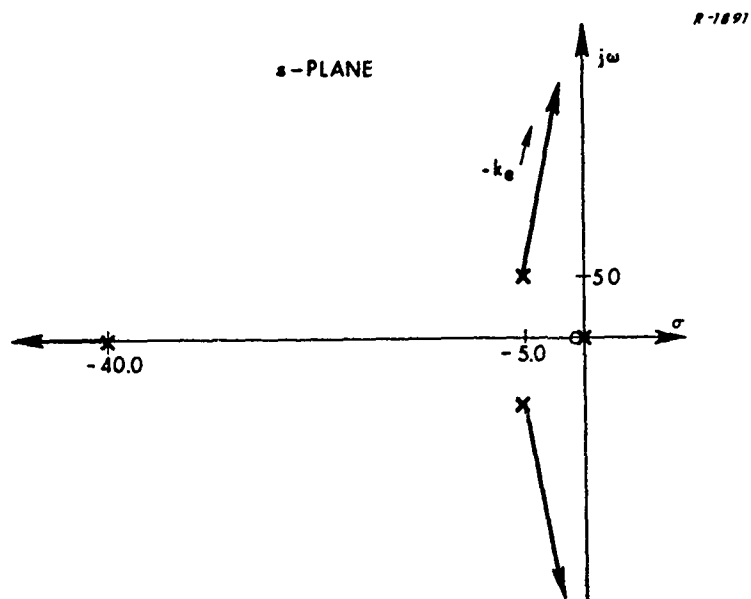


Figure 8.2-1 Locus of the Closed Loop Poles for the Adaptive Control System With No Adaptive Loop Compensation ( $G_c(s) = 1$ )

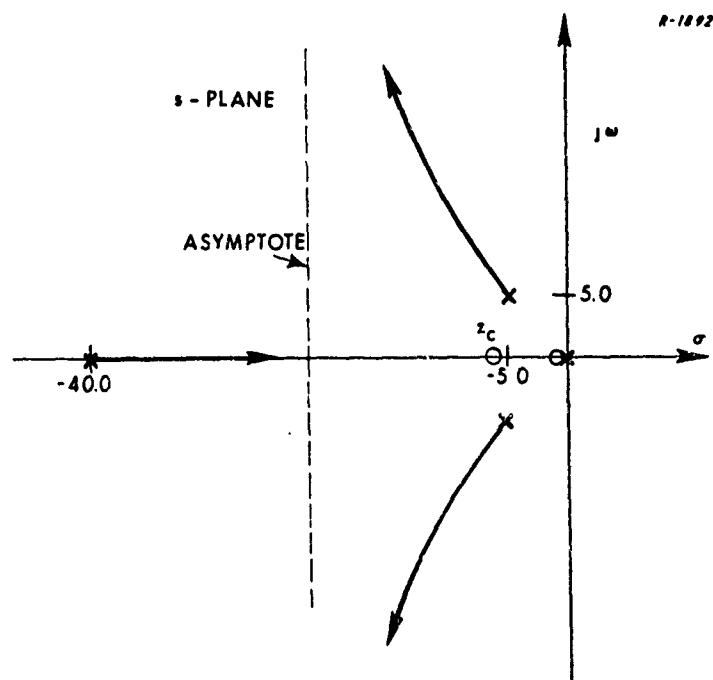


Figure 8.2-2 Locus of the Closed Loop Poles for the Adaptive Control System With Adaptive Loop Compensation ( $G_c(s) = s + 6.0$ )

damping of the complex poles can be achieved as the adaptive loop gain is increased.

In mechanizing Eq. (8.2-27) note that  $G_c(s)$  is not realizable. This difficulty is circumvented by taking  $G_{c1}(s)$  in Eq. (8.2-22) equal to one and

$$G_{c2}(s) = s - z_c$$

Thus from Eq. (8.2-19) we obtain

$$\begin{aligned} H_i(s) &= -g \gamma_i \frac{G_{c2}(s) P_i(s)}{s} \\ K(s) &= g \gamma_k \frac{G_{c2}(s) P_k(s)}{s} \end{aligned} \quad (8.2-28)$$

where  $H_i(s)$  and  $K(s)$  are the Laplace transforms of  $h_i(t)$  and  $k(t)$ . In this manner one is required only to mechanize a realizable transfer function

$$\frac{G_{c2}(s)}{s} = \frac{s - z_c}{s}$$

Recall that the same technique is employed in Example 4.3-1.

From the above discussion we now know the structure of the adaptive control system to within specific values for the adaptation gains and some additional parameters which define the reference model. A block diagram of the system is shown in Fig. 8.2-3. For simulation purposes switches  $S$  are included in the adaptive loop which can be opened to eliminate the integrator by-pass associated with the accelerated

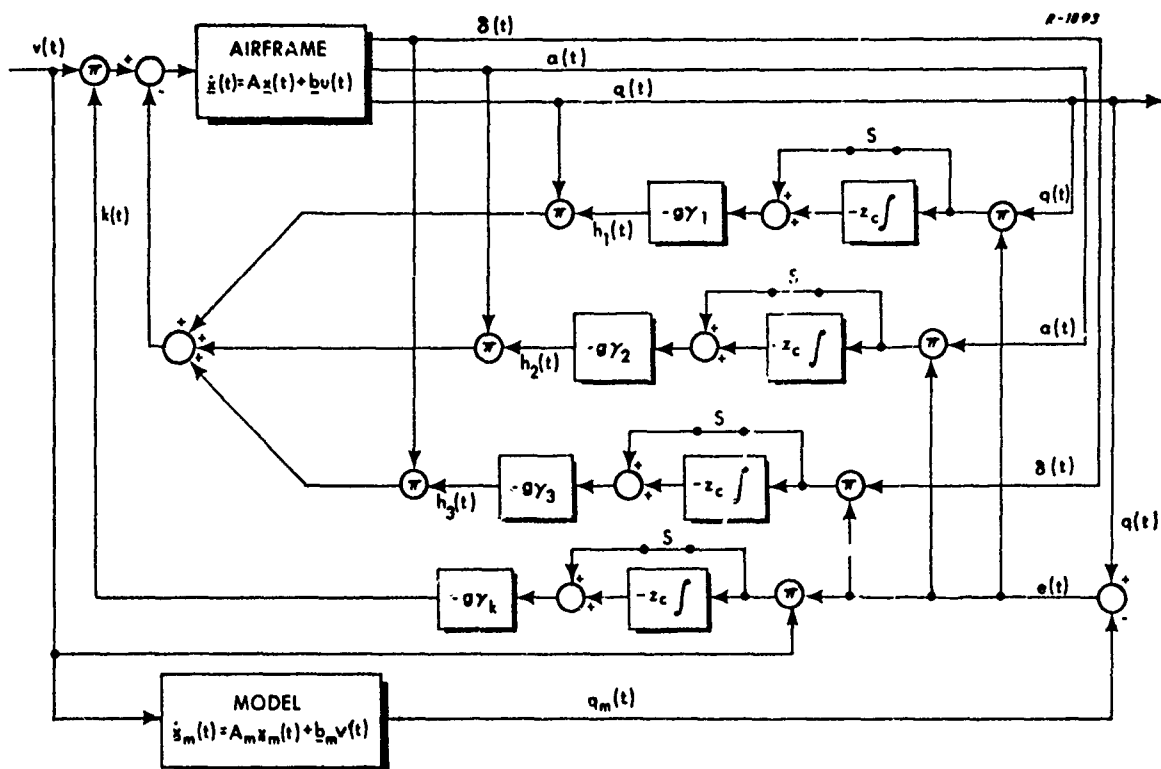


Figure 8.2-3 An Accelerated Gradient Controller for a Pitch Rate Autopilot

gradient algorithm. This permits us to simulate the system behavior both with and without adaptive loop compensation to provide a comparison between conventional gradient and accelerated gradient designs. Of course the switches would not be present in an actual system mechanization.

Reference Model Specifications — The fixed parameters for the reference model are chosen to be identical to those in the actual autopilot at flight condition 6 (see Section H.1) when feedback gains,  $\underline{h}_m$ , are selected so that the system poles match those specified in Eq. (8.2-25) and  $k_m$  is chosen so that the d-c gain between input and output is unity. The rationale for this selection is that the model should be one which not only has satisfactory response characteristics but also is compatible with the

actual airframe. Thus the elements of  $A_m$  and  $b_m$  are determined by requiring

$$\begin{aligned} A_m &= A_6 - b_6 h_m^T \\ b_m &= k_m b_6 \end{aligned} \quad (8.2-29)$$

where  $A_6$  and  $b_6$  are the values of  $A$  and  $b$  at flight condition 6 (see Table H.3). The quantities  $h_m$  and  $k_m$  are determined from the relations

$$\begin{aligned} \text{Det} \left[ Is - A_6 + b_6 h_m^T \right] &= (s+40)(s+5+j5)(s+5-j5) \\ k_6 &= \lim_{s \rightarrow 0} \frac{1}{c^T \left[ Is - A_6 + b_6 h_m^T \right]^{-1} b_6} \end{aligned} \quad (8.2-30)$$

The result of carrying out the above calculations is

$$\begin{aligned} A_m &= \begin{bmatrix} -1.63 & -1.42 \times 10^{-2} & -2.93 \times 10^2 \\ 3.51 \times 10^3 & -1.26 & -3.18 \times 10^4 \\ 0.929 & -3.45 \times 10^{-4} & -47.1 \end{bmatrix} \\ b_m^T &= [ 0.0 \quad -4.47 \times 10^3 \quad -6.61 ] \end{aligned} \quad (8.2-31)$$

In addition some method is required for specifying the initial values of the adaptive gains,  $h(t_0)$  and  $k(t_0)$ . This is accomplished for each simulation by assuming the initial flight condition (i.e., the initial values,  $A_0$  and  $b_0$ , of the airframe parameters) is known, matching the closed loop

system poles to those of the model and requiring the d-c gain to be unity. Following Eq. (8.2-30),  $\underline{h}(t_0)$  and  $k(t_0)$  are obtained from

$$\text{Det} \left[ \text{Is} - \text{A}_0 + \underline{b}_0 \underline{h}(t_0)^T \right] = (s+40)(s+5+j5)(s+5-j5)$$

$$k(t_0) = \lim_{s \rightarrow 0} \frac{1}{\underline{c}^T \left[ \text{Is} - \text{A}_0 + \underline{b}_0 \underline{h}(t_0)^T \right]^{-1} \underline{b}_0} \quad (8.2-32)$$

Determine Adaptation Gains — The adaptation gains  $\beta_i = g\gamma_i$  and  $\beta_k = g\gamma_k$  must be selected to obtain satisfactory adaptation properties. Recall the discussion in Section 4.2.6 suggesting that they be chosen to contribute equally to the adaptive loop gain  $k_e$ . Another important consideration is that the resulting variations in the gains  $\underline{h}_i(t)$  and  $k(t)$  as adaptation proceeds should be "reasonable." A certain amount of personal judgement is involved in this part of the design process and some trial and error experimentation seems unavoidable. For this example suitable values of the quantities  $\gamma_i$  and  $\gamma_k$  are

$$\begin{aligned} \gamma_1 &= 1.0 \times 10^4 & \gamma_2 &= 1.0 \\ \gamma_3 &= 5.0 \times 10^2 & \gamma_k &= 2.0 \times 10^6 \end{aligned} \quad (8.2-33)$$

which size the adaptation gains relative to one another. Simulation results are presented for various values of the parameter  $g$  which adjusts the level of the adaptive loop gain.

Simulation Results and Evaluation — The first thing to be demonstrated is the improvement in adaptation time achieved through the use of



linear compensation in the adaptive loop. To obtain a system configuration equivalent to the gradient-adaptive controller described by Eq. (8.2-9) which has no adaptive loop compensation, the switches S in Fig. 8.2-3 are opened and  $z_c$  is set equal to -1.0. A set of system simulations is performed beginning at flight condition 4,  $t = 23.0$  secs., letting the system parameters vary linearly as prescribed in Eq. (H-2). The system output to a step input command,  $v$ , of .026 rad/sec. is observed for an interval of one second. The outputs of both the model and system are shown in Fig. 8.2-4 for three different values of  $g$ . Notice that increasing the gain does little to reduce the error over the one second interval but the oscillation frequency of the adaptive loop noticeably increases. The latter behavior is qualitatively predicted by the root locus in Fig. 8.2-1.

Now we assess the effect of closing the switch S in Fig. 8.2-3, which mechanizes the accelerated gradient controller. For this case three one-second runs were performed for various values of  $g$  under the same conditions described in the preceding paragraph except that the compensation zero is located at -6.0. The corresponding pitch rate curves are shown in Fig. 8.2-5. Evidently considerable improvement is obtained in adaptation speed when the adaptive loop gain is increased, as predicted in Fig. 8.2-2. There is a slight tendency toward high frequency oscillations as  $g$  gets larger because the complex poles in Fig. 8.2-2 asymptotically approach a line parallel to the  $j\omega$  axis. The accelerated gradient controller performance is evidently superior to that exhibited in Fig. 8.2-4 and seems to be well suited for missile applications where rapidly changing missile parameters require a rapidly adapting autopilot.

Next we demonstrate the effect of variations in input signal level upon adaptation characteristics. From Eq. (8.2-21) one expects the adaptation time to increase as  $v(t)$  is reduced in magnitude because the adaptive

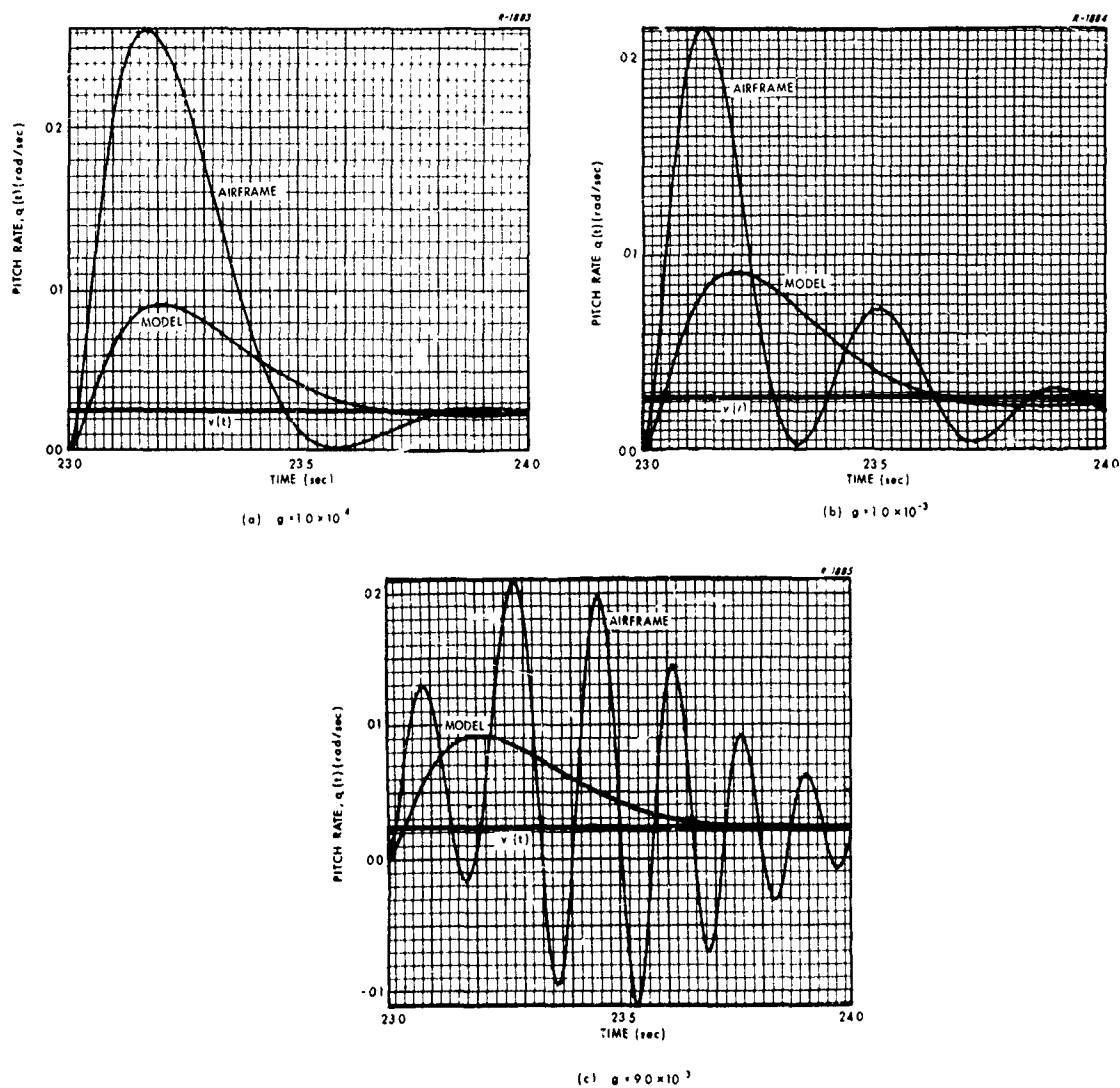


Figure 8.2-4 Step Responses of a Gradient-Adaptive Controller for a Pitch Rate Autopilot

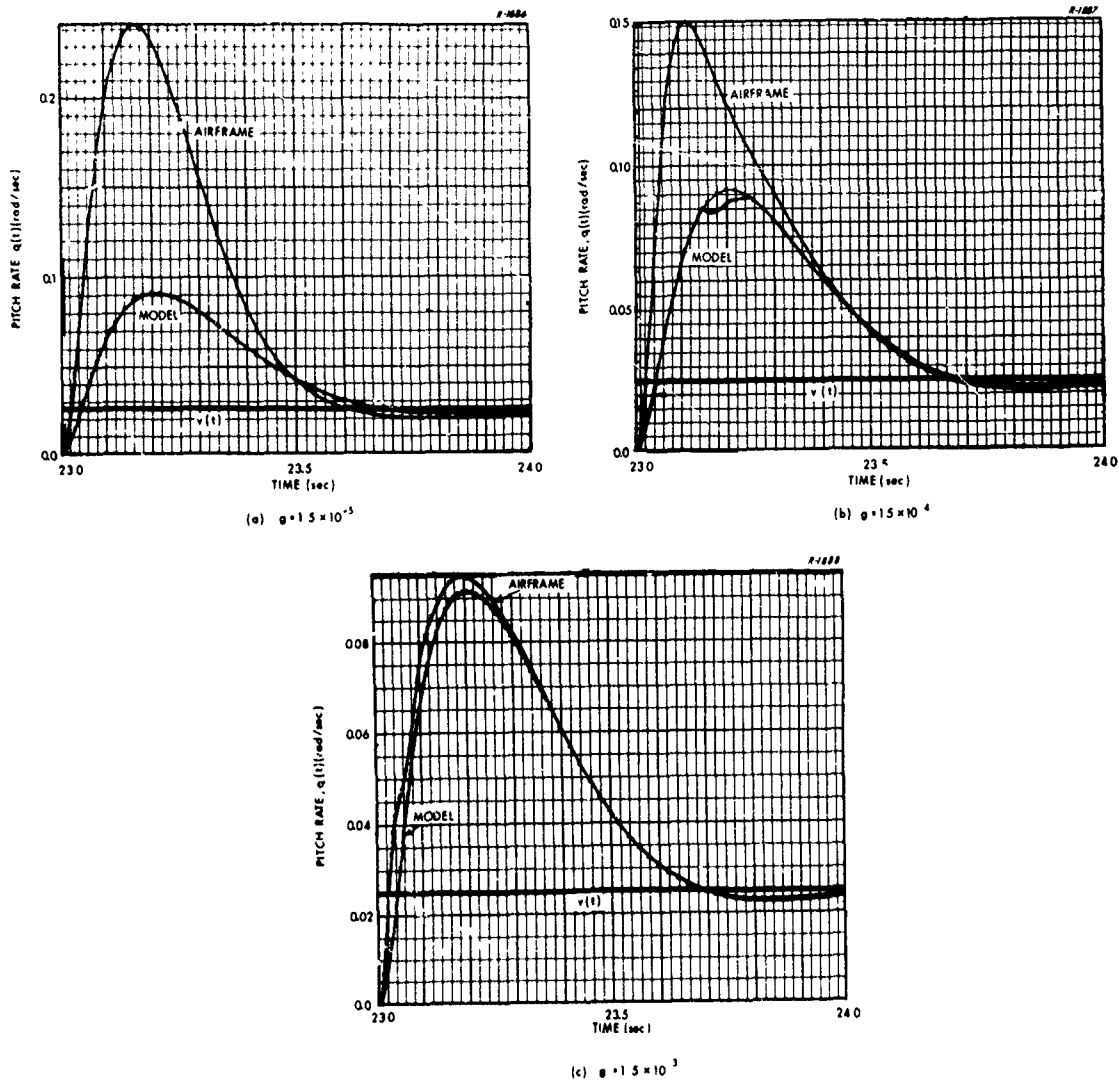


Figure 8.2-5 Step Responses of an Accelerated Gradient Adaptive Controller for a Pitch Rate Autopilot

loop gain  $k_e$  also decreases. This behavior is shown in Fig. 8.2-6. First a simulation is made with

$$|v(t)| = 3.4 \times 10^{-6} \text{ radian/sec} \quad z_c = -6.0$$

$$g = 1.5 \times 10^{-3}$$

The corresponding pitch rates for the reference model and the system are shown in Fig. 8.2-6(a) over a two second period beginning at flight condition 4. The algebraic sign of  $v(t)$  is switched at  $t = 24.0$  to represent changing input commands at one second intervals. Note that almost no adaptation takes place. When the input command level is increased to  $10^{-2}$  rad/sec the adaptive loop gain in Eq. (8.2-21) increases and much better adaptation is observed in Fig. 8.2-6(b). In tactical missiles it is expected that a steering command will be present most of the time while a target is being pursued but its amplitude may fluctuate. To counteract this effect, the gain  $g$  could be adjusted in response to the measured average value of the steering command. For example, let

$$g(t) = \frac{k_g}{\frac{1}{\tau} \int_{t-\tau}^t v(\lambda)^2 d\lambda} \quad (8.2-34)$$

where  $\tau$  is an interval somewhat longer than the model settling time and  $k_g$  is a proportionality constant. The mechanization of Eq. (8.2-34) is known as a signal-adaptive technique because it adapts to changes in input signal characteristics. Thus there can be a need to make adaptive changes in the adaptive loop gain.

Another important fact to be illustrated about adaptive systems is that good adaptation characteristics for one state variable (e. g., pitch

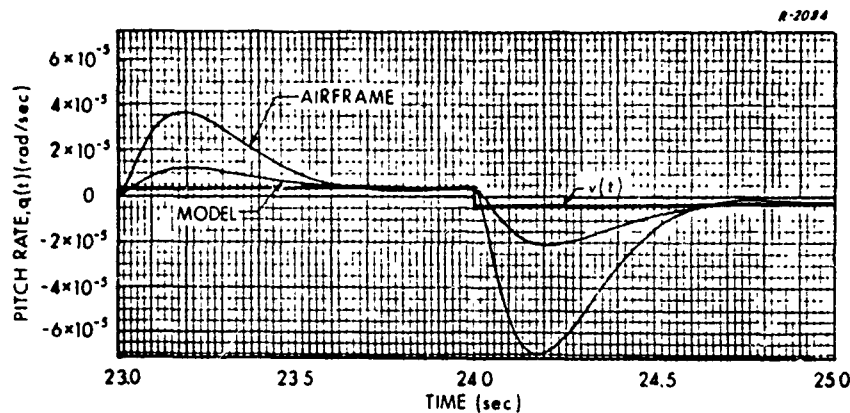
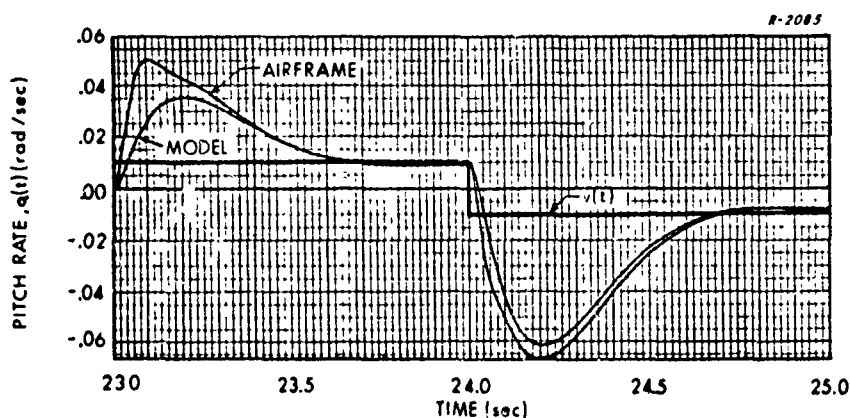
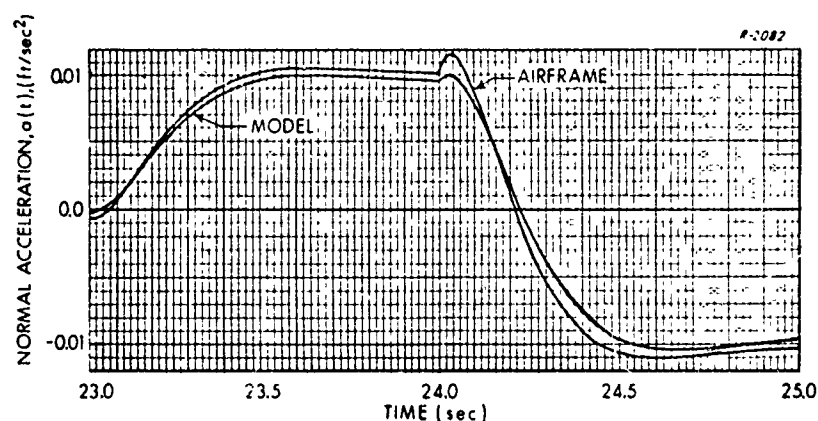
(a)  $|v(t)| = 3.4 \times 10^{-6}$  rad/sec(b)  $|v(t)| = 1.0 \times 10^{-2}$  rad/sec

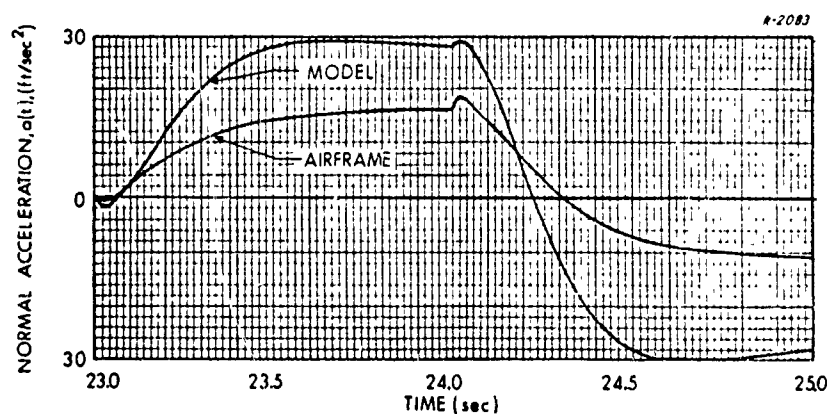
Figure 8.2-6 Pitch Rate Responses for an Adaptive Pitch Rate Autopilot With Different Levels of Input Commands

rate) do not necessarily imply good adaptation for other state variables (e.g., normal acceleration). This point has been emphasized in Section 8.1.2. Suppose the designer is actually interested in the missile's normal acceleration response and desires that the latter should follow the reference model acceleration output for the parameters in Eq. (8.2-31). If he tries to accomplish this goal by designing an adaptive pitch rate autopilot, the resulting normal acceleration response may exhibit exactly the wrong behavior. This claim is verified by examining time histories of normal acceleration corresponding to the simulations performed for

Fig. 8.2-6. In Fig. 8.2-7(a) curves of normal acceleration for both the reference model and the system are shown which are taken from the simulation performed for Fig. 8.2-6(a). Recall that very little adaptation is achieved for pitch rate in this case. However, the acceleration responses are reasonably close together, indicating good autopilot performance with respect to normal acceleration. Figure 8.2-7(b) shows acceleration response curves for the case given in Fig. 8.2-6(b). Now good adaptation is obtained in pitch rate but the system's acceleration response relative to



(a)  $|v(t)| = 3.4 \times 10^{-6} \text{ rad/sec}$



(b)  $|v(t)| = 1.0 \times 10^{-2} \text{ rad/sec}$

Figure 8.2-7 Normal Acceleration Responses for an Adaptive Pitch Rate Autopilot With Different Levels of Input Commands

the model's is poor. The physical reasons for this behavior are discussed in Section 8.1.2; it is characteristic of aerodynamically controlled missiles.

The performance of any adaptive system using implicit plant identification should also be evaluated by simulating a trajectory which passes through several different flight conditions. This will test the ability of the adaptation algorithm to adjust the adaptive gains so that the system output follows the model output as the plant parameters vary with time. For this purpose the air-to-surface missile trajectory was simulated from flight condition 2 at  $t = 6$  seconds through flight condition 4 to  $t = 26$  seconds with linearly varying plant parameters. Because the missile is thrusting during the first part of this segment of the trajectory, plant parameters vary over a wide range, as indicated in Tables H.1 to H.4, and the air-frame is actually exposed to a continuum of changing flight conditions. Note particularly that dynamic pressure changes by a factor of four in the first two seconds. Pitch rate responses are exhibited in Fig. 8.2-8 for two representative sets of three second intervals, one at the beginning and the other at the end of the time period considered. The input command  $v(t)$  is a piecewise constant signal which changes its level at one second intervals, as indicated. These results indicate the ability of the accelerated gradient technique to rapidly adapt to the reference model and maintain a small output error for a wide variation in the missile dynamic characteristics.

Finally, it is important to point out potential disadvantages of this method. The principal defect of the accelerated gradient technique (and any gradient method) is that satisfactory behavior cannot be guaranteed. The root locus in Fig. 8.2-2 is an indication of local stability properties only; nothing can be said about global behavior. Indeed, if plant parameters vary too rapidly and over too great a range, the validity of the

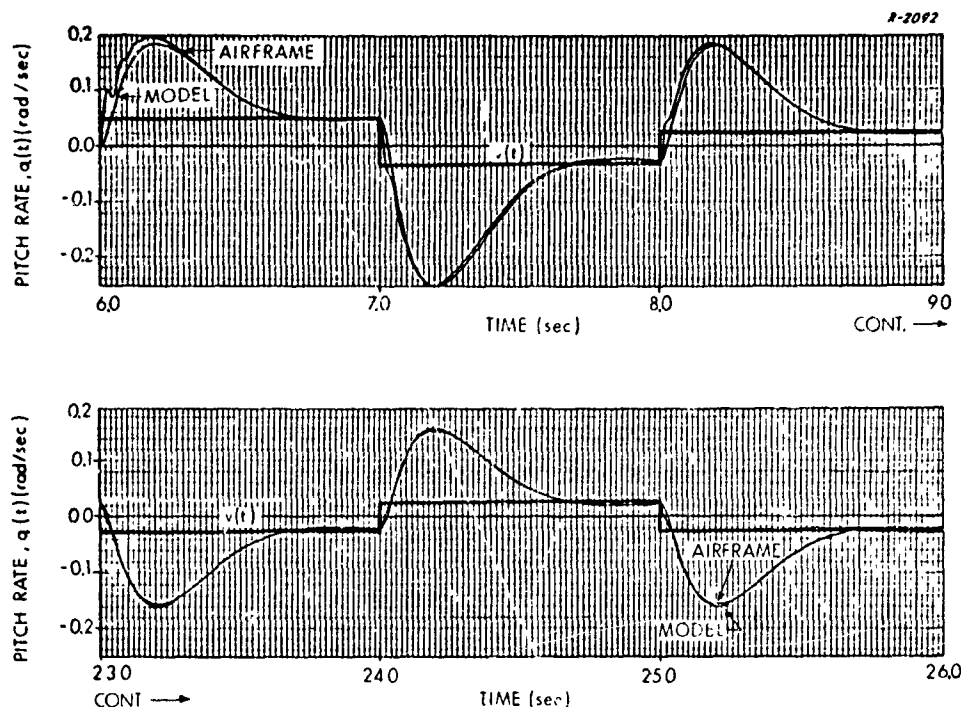


Figure 8.2-8 Pitch Rate Response With Time-Varying Airframe Parameters

gradient arguments used in designing the controller becomes questionable and system instability may result. To illustrate this fact an autopilot simulation was conducted with the autopilot in Fig. 8.2-3 over the first six seconds of the trajectory summarized in Table H.1. From zero to five seconds the airframe parameters are constant with a relatively low dynamic pressure. At time  $t = 5.0$  secs., the engine ignites and delivers a thrust of about 25 g's, causing rapid parameter variations. The resulting behavior of the adaptive control system is illustrated in Fig. 8.2-9. For the first 5 seconds satisfactory adaptive operation is observed, but shortly after the engine ignites the system becomes unstable. This simply emphasizes the fact that the full operating regime and different controller designs (e.g., different forms of  $G_c(s)$  in Eq. (8.2-22)) must be considered when testing an adaptive technique of this type. For example, a



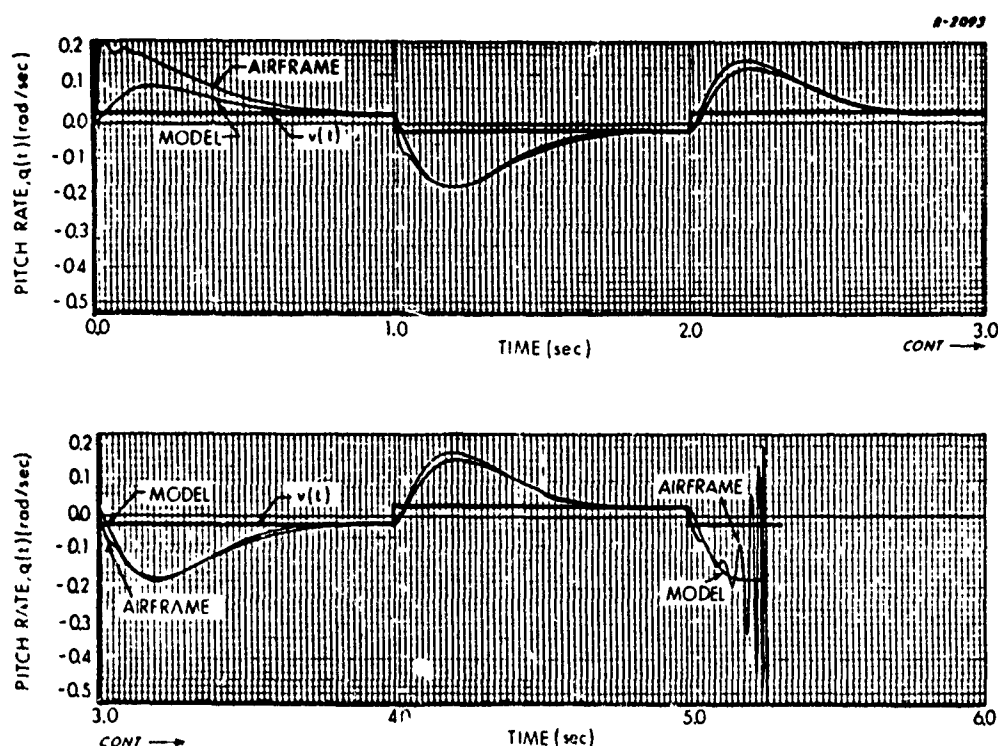


Figure 8.2-9 Pitch Rate Responses With Rapid Airframe Parameter Variations That Lead to Autopilot Instability

modification to the design in Fig. 8.2-3 that might improve the system stability characteristics is the addition of an adaptive filter in the control loop having a set of adaptive gains  $\underline{g}$ . The filter configuration would be chosen such that for each possible set of values of the airframe parameters the autopilot input-output transfer function can be made identical to that of the model for some choice of gains  $\underline{g}$ ,  $\underline{h}$ , and  $\underline{k}$ . Recall that the set of gains --  $\underline{h}$  and  $\underline{k}$  -- provide control over the autopilot closed loop poles and the steady-state gain but not over the closed loop zeros. The investigation of this possibility should be the subject of future study.

The pitch rate autopilot described here serves mainly to demonstrate capabilities and limitations of the accelerated gradient adaptive control technique, especially its improvement over conventional gradient methods. With respect to missile pitch rate control we make the following conclusions on the basis of these simulation results:

- The accelerated gradient technique has the potential to achieve rapid adaptation in the presence of a time-varying plant.
- Extremely rapid parameter variations, such as are encountered while thrusting, can cause instability of gradient-type methods.
- Adaptive pitch rate control does not provide good normal acceleration response for an aerodynamically controlled missile because the dynamic relationship between pitch rate and normal acceleration varies with flight condition.

Evidently the autopilot design in Fig. 8.2-3, based on forcing missile pitch rate to follow that of a fixed reference model, is not practical for adaptively controlling the normal acceleration of missile airframes which depend upon aerodynamic lift to develop control forces. We shall see in Section 8.2.4 that this conclusion can be reversed if an adaptive (time-varying) reference model is permitted.

### 8.2.3 A Normal Acceleration Autopilot

In this section we apply the accelerated gradient method to the problem of designing a normal acceleration autopilot for the airframe data given in Appendix H. The rationale for this objective is that the adaptation

algorithm should be based upon an error signal which directly reflects the difference between the actual and the desired autopilot performance.

Proceeding in the same manner used in Section 8.2.2 we first determine the value of  $N$  in Eq. (8.2-5), noting that

$$\underline{c}^T = [0 \ 1 \ 0]. \quad (8.2-35)$$

Referring to Eqs. (8.1-3), (8.1-4), and (8.2-35) it is determined that when  $N$  is one,

$$\underline{c}^T \underline{b} = b_2$$

Consequently  $N = 1$  and from Table H.3 it follows that  $b_2 > 0$  for all flight conditions. Therefore from Eqs. (8.2-5) and (8.2-8) it follows that

$$\begin{aligned} \beta'_i &= \beta_i \triangleq g\gamma_i & \beta_i &> 0 \\ \beta'_i &= \beta_k \triangleq g\gamma_k & \beta_k &> 0 \end{aligned} \quad (8.2-36)$$

Combining these results with Eqs. (8.2-9), (4.3-5), (8.2-15), and (8.2-35) one obtains the following equations:

Accelerated Gradient Adaptive Controller  
for a Normal Acceleration Autopilot

$$\dot{\underline{x}}(t) = (A - \underline{b}\underline{h}(t)^T) \underline{x}(t) + \underline{b}k(t) v(t)$$

$$\dot{\underline{x}}_{-m}(t) = A_{-m} \underline{x}_{-m}(t) + \underline{b}_{-m} v(t)$$

$$e(t) = x_2(t) - x_{m_2}(t)$$

$$E_f(s) = G_{c_1}(s) E(s)$$

$$p_i(t) = e_f(t) x_i(t); \quad i = 1, \dots, n$$

$$p_k(t) = e_f(t) v(t)$$

$$W_i(s) = G_{c_2}(s) P_i(s); \quad i = 1, \dots, n$$

$$W_k(s) = G_{c_2}(s) P_k(s)$$

$$\dot{h}_i(t) = g\gamma_i w_i(t); \quad i = 1, \dots, n$$

$$\dot{k}(t) = -g\gamma_k w_k(t) \tag{8.2-37}$$

The quantity  $g$  is defined as in Eq. (8.2-21) to provide control over the adaptive loop gain,  $k_e$ , given by Eqs. (8.2-15) and (8.2-36) as

$$k_e = g \left[ \gamma_k v^2 + \sum_{i=1}^n \gamma_i x_{m_i}^2 \right] > 0 \tag{8.2-38}$$

where  $g$ ,  $\gamma_k$ , and  $\gamma_i$  are all positive constants. Now we proceed to complete the four design steps described in Section 8.2.2 -- determine the adaptive loop compensation, select the reference model, determine adaptation gains, and evaluate performance -- using the airframe data given in Section H.1.

Adaptive Loop Compensation — To determine  $G_{c1}(s)$  and  $G_{c2}(s)$ , examine the root locus of the denominator in the transfer function

$$T_e(s) = \frac{1}{s + k_e G_o(s) G_c(s)}$$

$$G_c(s) \triangleq G_{c1}(s) G_{c2}(s) \quad (8.2-39)$$

associated with the error equation in Eq. (8.2-15). Recall that  $G_o(s)$  as given by Eq. (8.2-13) is assumed to have poles identical with those of the model (see Eq. (4.2-43)); its zeros are determined by evaluating the numerator in Eq. (8.2-13). Using  $A$  and  $b$  as defined in Eq. (8.1-4),  $G_o(s)$  is obtained in the form

$$G_o(s) = \frac{g_o (s^2 + a_o s + b_o)}{(s - p_{m1})(s - p_{m2})(s - p_{m3})} \quad b_o = \frac{a_{21} a_{13} a_{33}}{a_{23}}$$

$$g_o = -a_{23} \quad a_o = -a_{11} \quad (8.2-40)$$

where  $p_{m1}$ ,  $p_{m2}$ , and  $p_{m3}$  are the specified reference model poles. The gain  $g_o$  and polynomial coefficients,  $a_o$  and  $b_o$ , all depend upon the variable plant parameters, and are independent of the feedback gains  $h_o$ . Table H.3 indicates that

$$g_o > 0, \quad a_o > 0, \quad b_o < 0$$

and furthermore

$$|b_o| \gg |a_o|$$

Consequently the numerator of  $G_o(s)$  has two zeros,  $z_1$  and  $z_2$ , with values given approximately by

$$z_1, z_2 \cong \pm \sqrt{|b_o|} \quad (8.2-41)$$

and  $T_e(s)$  in Eq. (8.2-39) becomes

$$T_e(s) = \frac{1}{s + \frac{k_e g_o (s-z_1)(s-z_2)}{(s-p_{m_1})(s-p_{m_2})(s-p_{m_3})}} G_c(s) \quad (8.2-42)$$

The reference model poles are assigned the same numerical values as in Eq. (8.2-25), i.e.,

$$p_{m_1} = -40.0 \quad p_{m_2} = -5.0 + j5.0 \quad p_{m_3} = -5.0 - j5.0$$

Evaluation of  $g_o$  and  $b_o$  for representative flight conditions indicates that the ranges of the transfer function gain and zeros are approximately

$$1000 < g_o < 41000$$

$$2.7 < |z_1|, |z_2| < 120$$

Taking  $G_c(s) = 1$  -- corresponding to the gradient controller derived in Eq. (8.2-9) -- the first difficulty with the gradient method is encountered. Because of the right-half-plane zero in the numerator of  $G_o(s)$  (i.e.,  $G_o(s)$  is a nonminimum phase transfer function), the locus of poles of  $T_e(s)$  in Eq. (8.2-42) for  $k_e$  positive and  $g_o$  fixed has one branch entirely in the right-half-plane, as indicated in Fig. 8.2-10. Because the algebraic sign of  $k_e$  is specified to be positive in Eq. (8.2-38) as a result

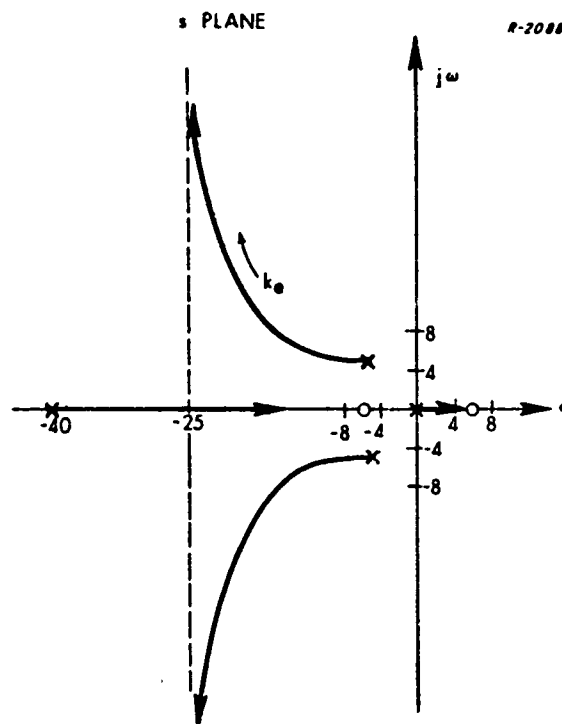


Figure 8.2-10 Root Locus of the Closed Loop Adaptive Control System for Positive  $k_e$  With No Adaptive Loop Compensation ( $G_C(s) = 1$ )

of the design procedure, the gradient-adaptive controller is locally unstable for this application. This is clearly an unacceptable operating condition and is evidence of the fact that the gradient concept for controller design is not always valid.\* The above stability problem can be eliminated by assigning

\* This behavior is attributable to the fact that the expansion in Eq. (4.2-24) used to derive the simplified gradient algorithm provides a poor approximation to the index  $J$  for the purpose of controlling normal acceleration. An analysis reveals that the M.I.T. rule described in Section 4.2.1 is also locally unstable because, in this particular application, the continuous adaptation algorithm is a relatively poor approximation to the ideal gradient technique expressed by Eq. (4.2-10). The possibility of the latter effect is discussed in Appendix C. The conclusion is that neither analog gain adjustment rule described in Section 4.2 behaves as desired for this application. The discrete gain adjustment rule discussed in Section 4.2.2 does not suffer from either of the above noted difficulties; therefore it may be a better method for this application. This point is also mentioned at the end of Section 4.3.

a negative gain to the compensating transfer function, e.g., take  $G_c(s) = -1$ . However, a new complication arises; the root locus shown in Fig. 8.2-11 indicates that the adaptive system becomes unstable for sufficiently high gain. Consequently in order to improve system adaptation time as we did for the pitch rate autopilot, more thought must go into selecting an appropriate form for  $G_c(s)$ .

R-2089

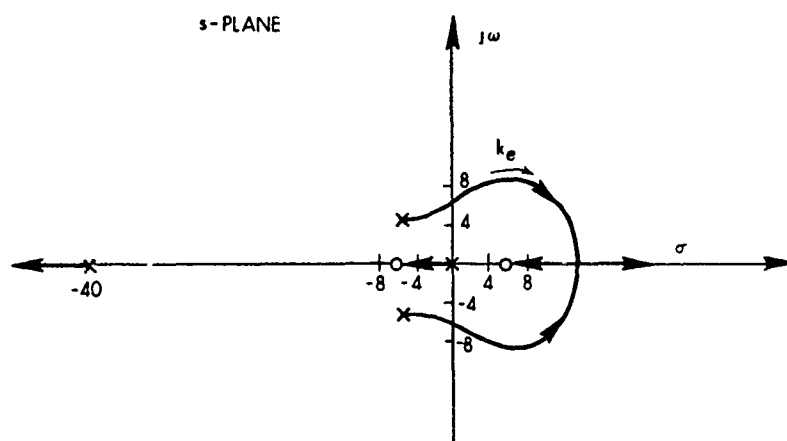


Figure 8.2-11 Root Locus of the Closed Loop Adaptive System for Positive  $k_e$  With Negative Gain Compensation ( $G_c(s) = -1$ )

The fact is that in situations like that described above no form of linear adaptive loop compensation can function to permit a stable system for all positive values of  $k_e$ . The right-half-plane zero will always "attract" one branch of the locus of poles of  $T_e(s)$ . After some experimentation  $G_c(s)$  was chosen to have the form

$$G_c(s) = \frac{-(s-z_{c_1})(s-z_{c_2})(s-z_{c_3})}{(s-p_{c_1})(s-p_{c_2})} \quad (8.2-43)$$



which is divided between  $G_{c_1}(s)$  and  $G_{c_2}(s)$  in Eq. (8.2-39) as follows:

$$G_{c_2}(s) = -\left(s - z_{c_1}\right)$$

$$G_{c_1}(s) = \frac{\left(s - z_{c_2}\right)\left(s - z_{c_3}\right)}{\left(s - p_{c_1}\right)\left(s - p_{c_2}\right)} \quad (8.2-44)$$

The structure of the resulting system is illustrated in Fig. 8.2-12.

Specific values for the parameters in  $G_c(s)$  are:

$$\begin{aligned} z_{c_1} &= -0.5 & p_{c_1} &= -15.0 + j 8.7 \\ z_{c_2} &= -6.0 + j 6.0 & p_{c_2} &= -15.0 - j 8.7 \\ z_{c_3} &= -6.0 - j 6.0 \end{aligned} \quad (8.2-45)$$

The root locus diagram as a function of  $k_e$  for this choice of compensation is shown qualitatively in Fig. 8.2-13. The simulation results discussed below indicate that the restriction on the range of variation of the adaptive loop gain and its sensitivity to airframe parameter variations prevents achieving adaptation characteristics that are as good as those obtained for pitch rate in the preceding section.

Reference Model Specifications — The fixed parameters for the reference model are the same as those used for the pitch rate autopilot. The elements of  $A_m$  and  $b_m$  are given by Eq. (8.2-31). The initial values of the adaptive gains are the solutions to Eq. (8.2-32) perturbed by 10% to provide a significant error signal.

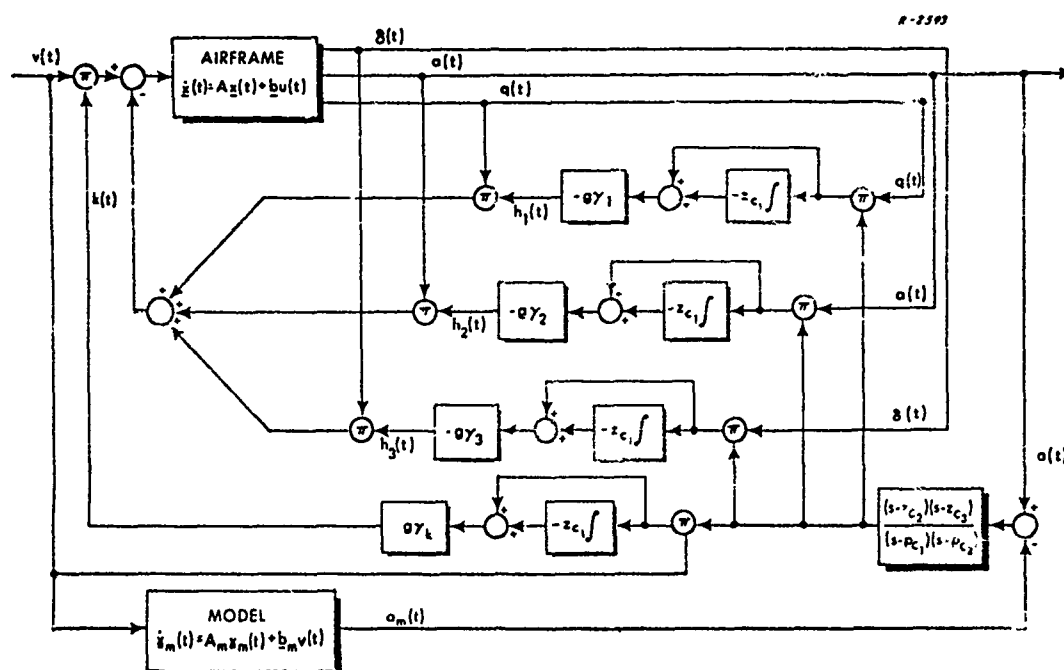


Figure 8.2-12 An Accelerated Gradient Controller for a Normal Acceleration Autopilot

Selections for Adaptation Gains — The adaptation gains  $\beta_i = g\gamma_i$  and  $\beta_k = g\gamma_k$  are selected by the same procedure described for the pitch rate autopilot. The specific values used in this example are

$$\begin{aligned} \gamma_1 &= 7.5 \times 10^4 & \gamma_2 &= 1.0 \\ \gamma_3 &= 5.0 \times 10^4 & \gamma_k &= 0.5 \end{aligned} \quad (8.2-46)$$

Simulation results are presented for various values of the parameter  $g$  which provides control of the adaptive loop gain.

Simulation Results — Graphs of normal acceleration output for both the plant and the reference model are shown in Fig. 8.2-14 for different values of the gain factor  $g$ . The airframe dynamics are constant

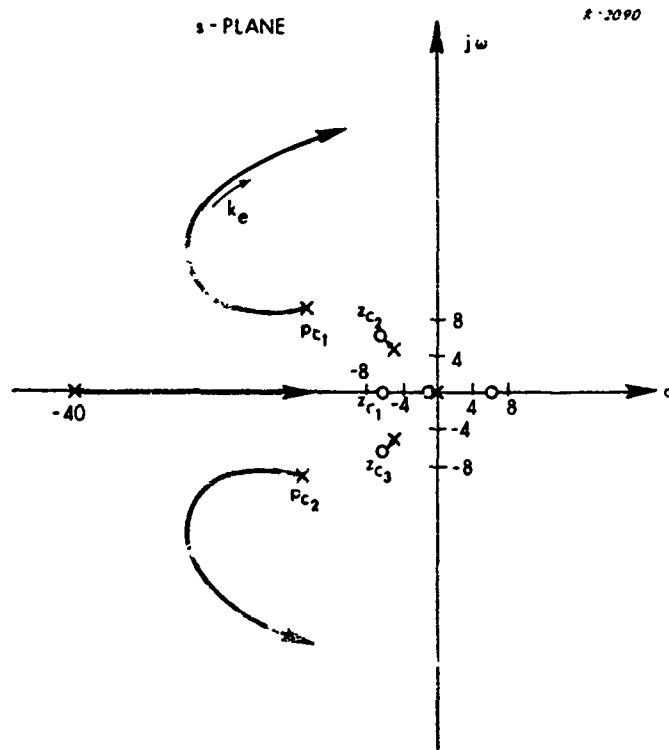


Figure 8.2-13 Root Locus of  $T_e(s)$  for Positive  $k_e$   
With  $G_c(s)$  given by Eq. (8.2-43)

and correspond to flight condition 4 in Table H.1. It is observed that a moderate improvement in adaptation properties over a one-second interval is obtained as  $g$  varies from 0 (no adaptation) to  $3.0 \times 10^{-8}$ . However the results are not so dramatic as those in Fig. 8.2-5 for the pitch rate autopilot. When  $g$  becomes as large as  $1.0 \times 10^{-7}$  (Fig. 8.2-14(d)) the system is unstable, as predicted qualitatively from Fig. 8.2-13. It is also found that the best value of the gain  $g$  for flight condition 4 causes the system to be unstable when the plant dynamics are changed to flight condition 6 in Table H.1, implying that careful tuning of the adaptive loop gain is required as flight conditions vary in order that the system operates satisfactorily. The need to know the flight condition in order to make on-line adjustments to the adaptation algorithm tends to negate the purpose of an adaptive

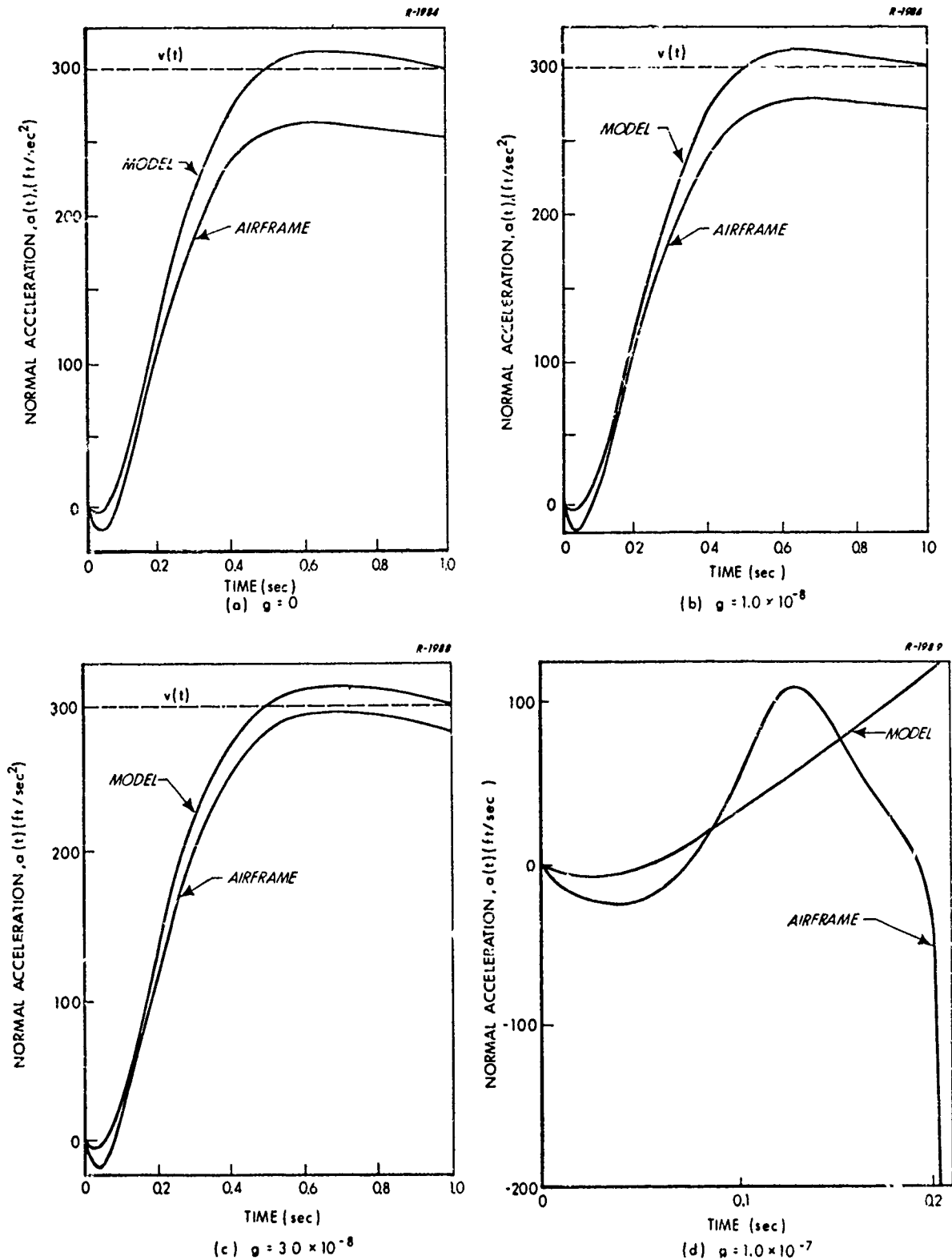


Figure 8.2-14 Step Response of Adaptive Normal Acceleration Autopilot Using the Accelerated Gradient Method

controller having implicit plant identification; namely, it is desired that explicit identification be avoided.

#### 8.2.4 An Adaptive Reference Model

In Sections 8.2.2 and 8.2.3 it is observed that satisfactory adaptive normal acceleration response is difficult to achieve with the accelerated gradient method for the particular missile application we are considering. Good pitch rate adaptation characteristics are obtained in Section 8.2.2 with the pitch rate autopilot; however the corresponding normal acceleration response is sensitive to the missile's flight condition. The latter behavior is explained by the fact that the relationship between the transient dynamics of  $q(t)$  and  $a(t)$  is dependent upon the values of the airframe parameters. Consequently if  $q(t)$  is forced to follow the output of a fixed reference model at all flight conditions, the transient characteristics of  $a(t)$  must necessarily vary. Alternatively in Section 8.2.3 an adaptive normal acceleration autopilot is studied. However, the nonminimum phase character of the airframe input-output transfer function causes the stability properties of the control system to be quite sensitive to flight condition.

To achieve better normal acceleration response from the pitch rate autopilot, one can consider using an adaptive reference model; heretofore the model dynamics have been time-invariant. This suggestion is motivated by the fact that at each flight condition the adaptive controller ideally should have the capability to make the compensated airframe input-output dynamics identical with those of the reference model for some choice of the adaptive gains  $h$  and  $k$ . We have already noted that  $h$  and  $k$  alone do not provide enough freedom to accomplish this. Therefore an alternative reference model is advocated which is obtained by continuously

identifying enough plant parameters and simultaneously changing the corresponding elements in  $\underline{A}_m$  and  $\underline{b}_m$  so that the associated transfer functions satisfy

$$\underline{c}^T \left( \underline{I}s - \underline{A}_m(\hat{\underline{a}}) \right)^{-1} \underline{b}_m(\hat{\underline{a}}) = \underline{c}^T \left( \underline{I}s - \underline{A} + \underline{b}\underline{h}^T \right)^{-1} \underline{b}k \quad (8.2-47)$$

for some values of  $k$  and  $\underline{h}$  at each flight condition. The quantity  $\hat{\underline{a}}$  in Eq. (8.2-47) is the measurement or estimate of the plant parameters required to specify the reference model.

In the applications we have been considering, where full state feedback and control over the d-c gain is assumed, the above procedure is equivalent to requiring the reference model and missile airframe input-output transfer functions to have the same zeros. It is evident from Eqs. (8.1-10) and (8.1-11) that such a procedure applied to a pitch rate autopilot should improve normal acceleration response; the zero of  $T_m(s)$  will be adjusted so that it always approximately cancels the objectionable pole in  $A(s)/Q(s)$ .

System Design — To apply the above idea to a pitch rate autopilot, recall that the input-output transfer function for the airframe has the form (see Eq. (8.1-8))

$$\frac{Q(s)}{U(s)} = \frac{c(s-z)}{s^3 + a_1 s^2 + a_2 s + a_3} \quad (8.2-48)$$

Accordingly, require that the reference model input-output transfer function be

$$\frac{Q_m(s)}{V(s)} = \frac{c_m(s-\hat{z})}{s^3 + a_{m1} s^2 + a_{m2} s + a_{m3}} \quad (8.2-49)$$

where  $\hat{z}$  is an estimate of  $z$  and  $c_m$  satisfies

$$c_m = - \frac{a_{m3}}{\hat{z}} \quad (8.2-50)$$

The coefficients in the denominator of Eq. (8.2-49) are specified by the designer; e.g.,

$$s^3 + a_{m1}s^2 + a_{m2}s + a_{m3} \triangleq (s - p_{m1})(s - p_{m2})(s - p_{m3})$$

and Eq. (8.2-50) provides unity d-c gain between  $V(s)$  and  $Q_m(s)$ .

The adaptive controller is configured almost the same as in Fig. 8.2-3. One exception is that the reference model dynamics are now given by Eq. (8.2-49) which requires an estimate of  $z$ . Also, since we are interested in commanding pitch rate to produce a desired normal acceleration,  $a_c(t)$ , the latter must be scaled using the steady state relation given in Eq. (8.1-9); i.e.,

$$v(t) = a_c(t)/\hat{V}$$

where  $\hat{V}$  is an estimate of the missile's airspeed. This implies that air speed must also be identified. Both of these alterations to Fig. 8.2-3 are indicated in Fig. 8.2-15.

Comparing Eqs. (8.2-48) and (8.1-8) it follows that

$$z = \frac{a_{13}a_{33}a_{22}}{a_{13}a_{33} + a_{12}a_{23}} \quad (8.2-51)$$

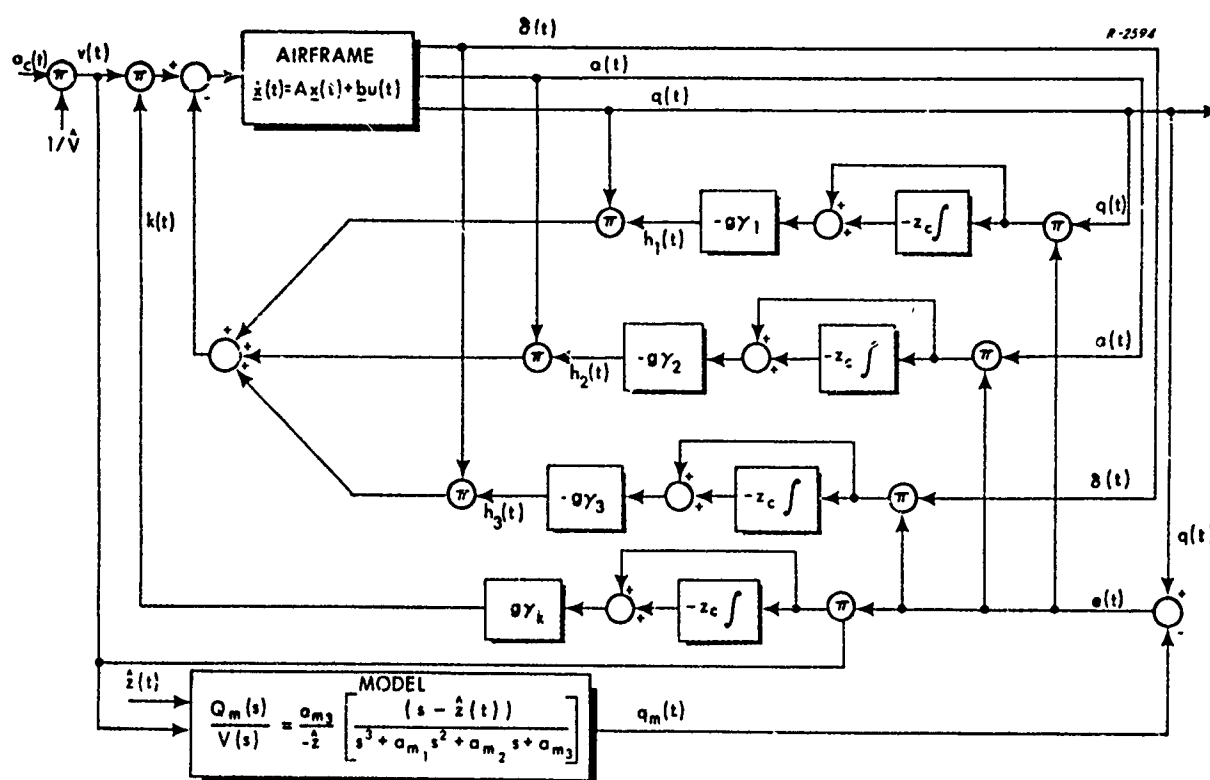


Figure 8.2-15 An Accelerated Gradient Controller for a Pitch Rate Autopilot With an Adaptive Reference Model

The data in Table H.3 indicate that the denominator in Eq. (8.2-50) is dominated by the term  $(a_{13}a_{33})$ ; therefore  $z \approx a_{22}$ . In other words,  $z$  can be approximately identified by estimating only the element  $a_{22}$  in Eqs. (8.1-3) and (8.1-4).

The subject of parameter estimation is discussed in Chapters 5 and 6 where it is postulated that all the parameters of  $A$  and  $b$  in Eq. (8.1-4) are to be identified. When that capability is available, the control methods described in Chapter 5 are better suited for autopilot design. However, here we are suggesting that partial plant identification can be beneficially applied to the accelerated gradient method; this technique may offer advantages in situations where it is easier to obtain a few parameter estimates ( $\hat{z}$  and  $\hat{V}$ ) than it is to identify all the elements of  $A$  and  $b$ .



Simulation Results — The adaptive reference model prescribed by Eqs. (8.2-49) and (8.2-50) was simulated for the accelerated gradient controller described in Section 8.2.2. The estimate of the airframe zero was updated continuously according to

$$\hat{z}(t) = a_{22}(t)$$

All other model parameter values are identical to those used for the simulation associated with Figs. 8.2-6(b) and 8.2-7(b). Recall that the latter demonstrate how good adaptation in pitch rate leads to poor adaptation in normal acceleration when the reference model dynamics are fixed.

Initial values for the adaptive gains are obtained by multiplying the solutions to Eq. (8.2-32) with a scaling factor of 0.70. This is necessary to develop a significant error signal when the adaptive loop is disconnected ( $g = 0$  in Fig. 8.2-15). All other system parameter values are the same as those used for Figs. 8.2-6(b) and 8.2-7(b). Two simulations were performed; one with  $g = 0$  (no adaptation) and one with  $g = 1.5 \times 10^{-3}$ , the latter being the same value used for the above referenced figures. From the response curves displayed in Figs. 8.2-16 and 8.2-17, it is observed that the adaptive reference model enables the accelerated gradient technique to produce the desired adaptive response characteristics in both pitch rate and normal acceleration.

Conclusions — The distinguishing characteristic of the method using an adaptive reference model is that it requires identification of both  $a_{22}$  in Eq. (8.1-4) and the missile airspeed,  $V$ . It is a useful technique for modifying the structure of the accelerated gradient controller described in previous sections so that desired normal acceleration response characteristics can be obtained for the tail-controlled missile in Fig. 8.1-2.

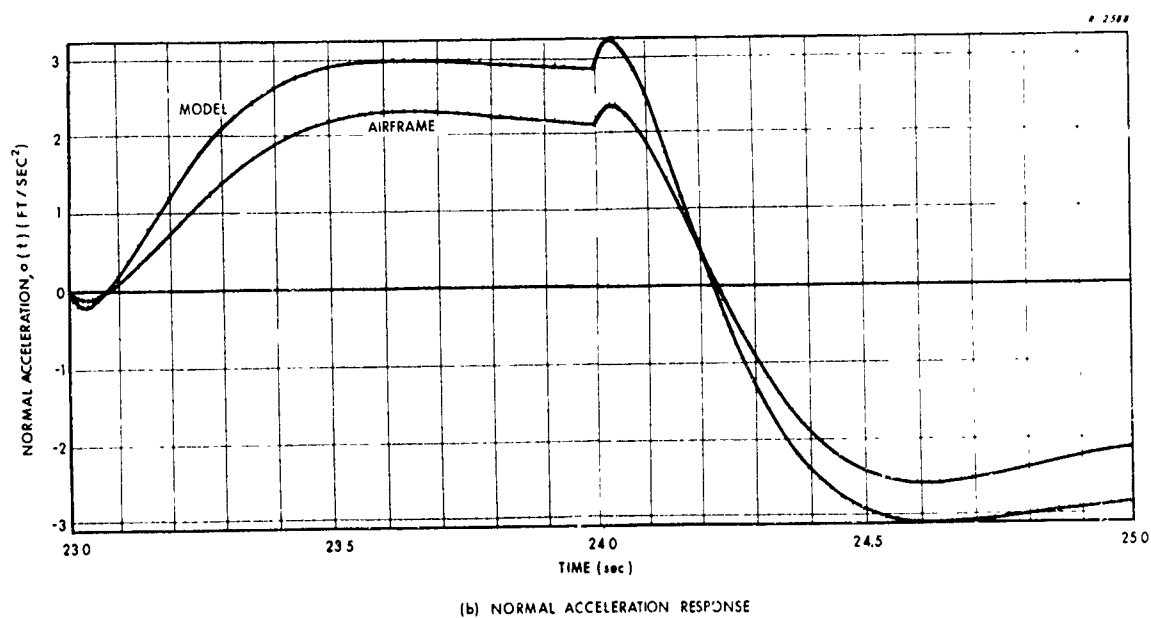
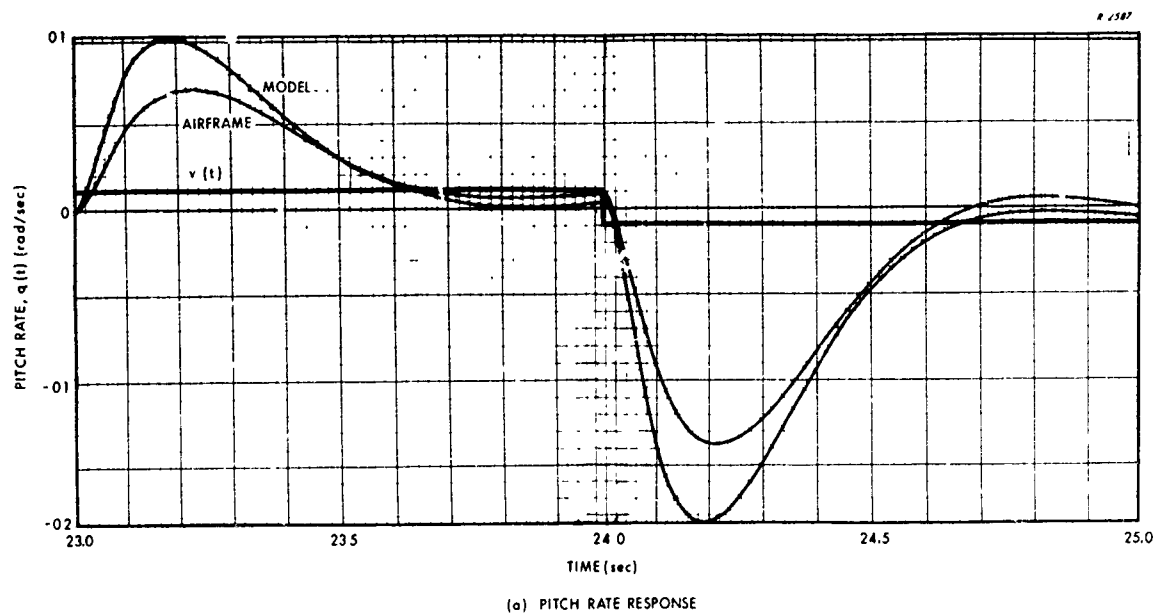


Figure 8.2-16 Autopilot Responses for a System Using an Adaptive Reference Model: Adaptive Control Loop Disconnected

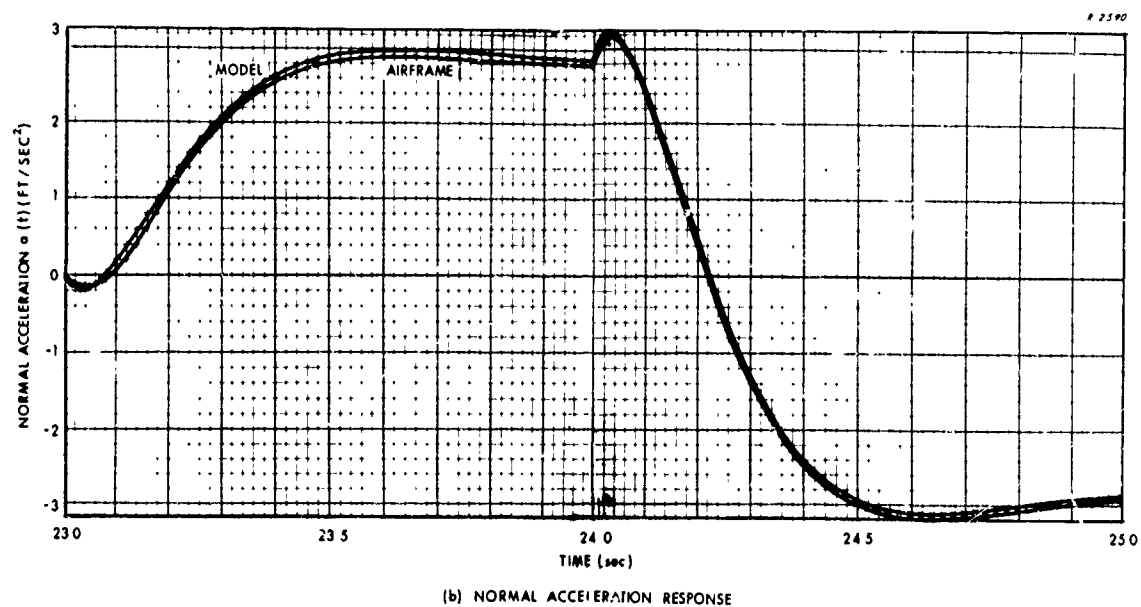
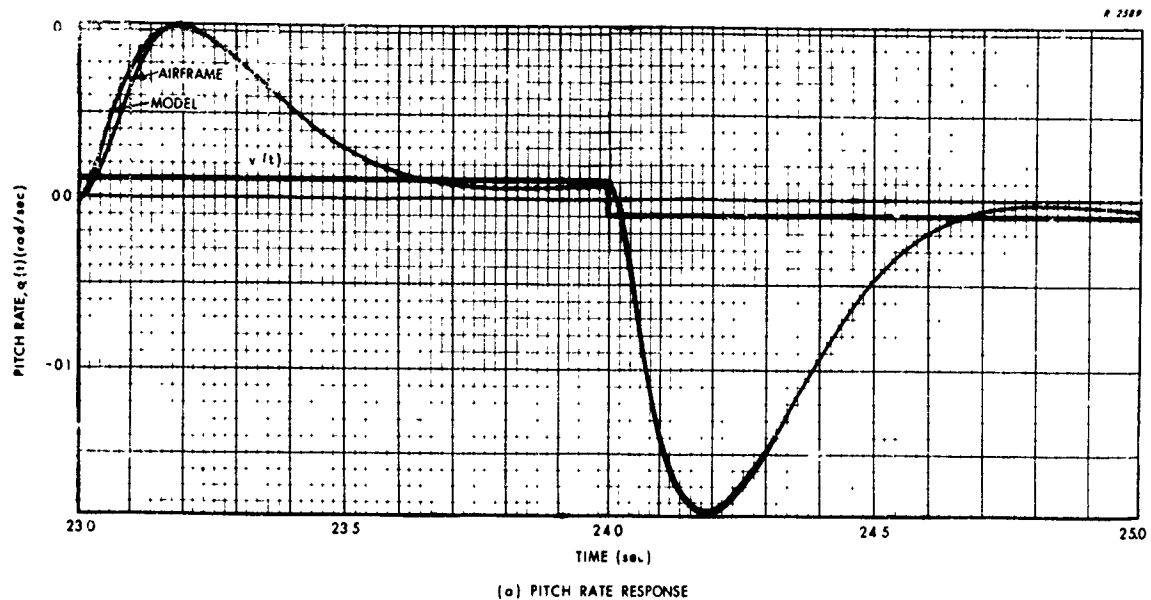


Figure 8.2-17 Autopilot Responses for a System Using an Adaptive Reference Model: Adaptive Control Loop Connected

Although estimates of only two parameters are required, it may be argued that it is almost as easy to identify all the parameters in Eqs. (8.1-4). If so, then one of the adaptive control methods suggested in Chapter 5 may be more appropriate. Further investigation of this question should be pursued to determine whether partial plant identification of the type advocated above has any distinct advantages over complete identification.

### 8.3 APPLICATION OF LIAPUNOV DESIGN TECHNIQUES

In Section 4.4.3 a Liapunov synthesis procedure is described which is suitable for adaptive control of tactical missiles provided the input-output transfer function is minimum phase. The reason for this restriction is discussed in Section 4.4.4. In this section, the method is used for pitch control of a second order airframe with the dynamics of the control surface actuator neglected. The sequential development closely follows Section 4.4.3 to provide a specific illustration of the steps involved. The discussion evolves in three steps -- design procedure, selection of parameters, and performance evaluation. Then a brief discussion is given describing how the adaptive reference model concept introduced in Section 8.2.4 can be used to achieve adaptive control of normal acceleration.

#### 8.3.1 Design Procedure

Let the input-output relations for the autopilot design problem be represented by Fig. 8.3-1, by analogy with Fig. 4.4-3. In Laplace transform notation the equations for the airframe and the reference model are

$$\begin{aligned}(s^2 + bs + a) Y(s) &= k(s - z) U(s) \\ (s^2 + b_m s + a_m) Y_m(s) &= k_m(s - z_m) V(s)\end{aligned}\tag{8.3-1}$$

R-1987

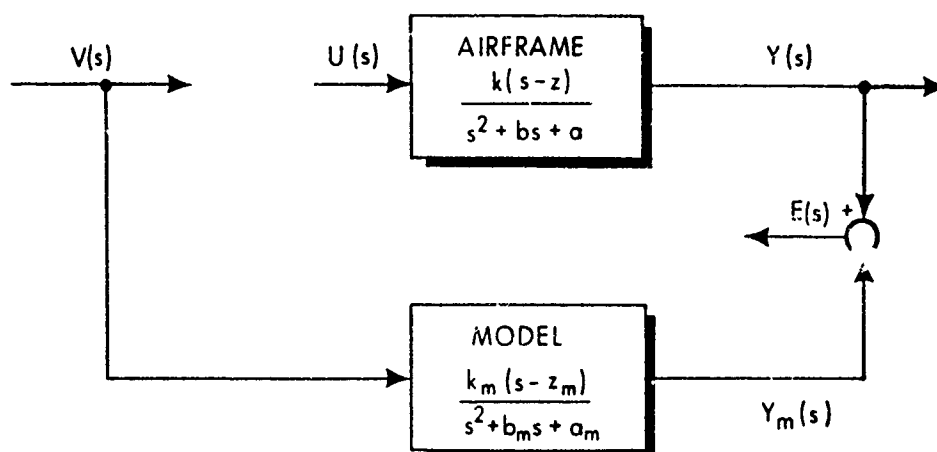


Figure 8.3-1 Airframe and Reference Model Input-Output Relations for an Adaptive Control System

Subtracting these expressions and adding the quantity

$$(s^2 + b_ms + a_m)Y(s)$$

to both sides of the result produces the error equation

$$(s^2 + b_ms + a_m)E(s) = (b_m - b)s + a_m - a)Y(s) + k(s-z)U(s) - k_m(s-z_m)V(s) \quad (8.3-2)$$

which has a form similar to Eq. (4.4-31).

Now divide both sides of Eq. (8.3-2) by the polynomial

$$p_c(s) = s - p_1$$

where  $p_1$  is a negative number whose allowed range of values is to be determined presently. The result after carrying out the required number of steps in dividing by  $p_c(s)$  is

$$\begin{aligned}
 (s + b_m + p_1)E(s) = & - \left[ \frac{a_m + p_1(b_m + p_1)}{s - p_1} \right] E(s) + b_m - b Y(s) \\
 & + \left[ \frac{a_m - a + p_1(b_m - b)}{s - p_1} \right] Y(s) + kU(s) \\
 & + \frac{p_1 - z}{s - p_1} U(s) - \frac{k_m(p_1 - z_m)V(s)}{s - p_1} - k_m V(s) \quad (8.3-3)
 \end{aligned}$$

which has the same form as Eqs. (4.4-32) and (4.4-33). Now for stability of the error signal we require that

$$b_m + p_1 > 0$$

on the left-hand-side of Eq. (8.3-3), or

$$p_1 > -b_m \quad (8.3-4)$$

This provides the condition needed on  $p_c(s)$ .

Referring to the right-hand side of Eq. (8.3-3) define new variables

$$\begin{aligned}
 Y_c(s) &= \frac{Y(s)}{s - p_1} & E_c(s) &= \frac{E(s)}{s - p_1} \\
 U_c(s) &= \frac{U(s)}{s - p_1} & V_c(s) &= \frac{V(s)}{s - p_1}
 \end{aligned} \quad (8.3-5)$$

and vector quantities

$$\underline{\rho} = \begin{bmatrix} b_m - b \\ a_m - a + p_1(b_m - b) \\ p_1 - z \\ k_m(z_m - p_1) \\ -a_m - p_1(b_m + p_1) \end{bmatrix} ; \underline{f}(t) = \begin{bmatrix} y(t) \\ y_c(t) \\ u_c(t) \\ v_c(t) \\ e_c(t) \end{bmatrix} \quad (8.3-6)$$

Rewriting Eq. (8.3-3) in the time domain, with the aid of Eqs. (8.3-5) and (8.3-6), produces a differential equation for the error in the form of Eq. (4.4-42),

$$\dot{e}(t) = -(b_m + p_1) e(t) + \underline{\rho}^T \underline{f}(t) + k u(t) - k_m v(t) \quad (8.3-7)$$

The adaptive controller is derived directly from Eq. (4.4-43). Because Eq. (8.3-7) is a scalar error equation,  $Q$  and  $q$  in Eq. (4.4-43) are also scalars to which we can assign the value one. Also, since  $\Lambda$  is an arbitrary positive definite matrix and  $k$  is unknown, choose the former to be diagonal and replace the latter by its algebraic sign. The application we are considering is the same as in Section 8.2.2 so that  $k$  is the same as  $g_0$  in Eq. (8.2-23), which is a negative quantity for all flight conditions. With these assumptions, the adaptation algorithm becomes

$$\begin{aligned} u(t) &= (-\underline{h}_c(t)^T + \sigma e(t) \begin{bmatrix} \underline{f}(t) \\ \underline{v}(t) \end{bmatrix}^T \Lambda^{-1}) \begin{bmatrix} \underline{f}(t) \\ \underline{v}(t) \end{bmatrix} \\ \dot{\underline{h}}_c(t) &= -\Lambda^{-1} \begin{bmatrix} \underline{f}(t) \\ \underline{v}(t) \end{bmatrix} e(t) \end{aligned} \quad (8.3-8)$$

where the six diagonal elements of  $\Lambda$  and the positive scalar  $\sigma$  remain to be selected.

The implementation of this adaptive system is illustrated in Fig. 8.3-2. To provide a means for exercising control over the total adaptive loop gain, define the  $i^{\text{th}}$  element of  $\Lambda$  to be  $\lambda\lambda_i$  where the quantities  $\lambda_i$  are chosen to achieve the proper relative weighting on the elements of  $\underline{f}(t)$  and  $\underline{v}(t)$  in Eq. (8.3-8) and  $\lambda$  is a scaling factor. The adaptation algorithm is computationally more complex than the accelerated gradient method described in Section 8.2; it requires two additional adaptive gains and mechanization of the filters with transfer function  $1/p_c(s)$ .

To set initial values for the feedback gains  $\underline{h}_c(t)$ , Eq. (4.4-47) is solved for the initial flight condition with the modification,

$$\underline{h}_c = \frac{\eta}{k} \begin{bmatrix} \rho \\ -k_m \end{bmatrix} \quad (8.3-9)$$

The quantity  $\eta$  is a positive factor which permits the adaptive gains to be initially "detuned" from their optimum values. It represents whatever inaccuracy may exist in knowledge of the initial values of the plant parameters.

### 8.3.2 Selection of Parameters

For simulation purposes the airframe dynamics are taken from the trajectory data in Section H.1 with the actuator dynamics neglected. The dynamics of the reference model are taken from flight condition 6 in Table H.3. The controller gains --  $\lambda_i$ ,  $\sigma$  and  $p_i$ ,  $i = 1, \dots, 6$  -- are assigned values



$$\begin{array}{ll} 1/\lambda_1 = 9.0 \times 10^2 & 1/\lambda_2 = 3.0 \times 10^3 \\ 1/\lambda_3 = 3.0 \times 10^5 & 1/\lambda_4 = 2.34 \times 10^4 \\ 1/\lambda_5 = 1.8 \times 10^3 & 1/\lambda_6 = 6.0 \times 10^4 \\ p_1 = 3.0 & \sigma = 0.167 \end{array}$$

The quantity  $\lambda$  is a parameter used to adjust the total effective loop gain.

### 8.3.3 Performance Evaluation

To demonstrate the operation of the system illustrated in Fig. 8.3-2, a simulation was conducted with the plant parameters fixed at the values specified by flight condition 2 in Table H.1 and an adaptive loop gain  $\lambda^{-1} = 5.5$ . The initial values of the adaptive gains  $h_i(t)$  were computed from Eq. (8.3-9) with  $\eta = 0.6$  and a step pitch rate command,  $v = 0.01$  radians/second was applied. In Fig. 8.3-3 the reference model response, the airframe response, and the associated Liapunov function are plotted as a function of time. The airframe response without adaptation ( $\lambda^{-1} = 0$ ) is also shown for comparison. Evidently significant improvement is provided by the adaptive design. Observe that the Liapunov function decreases most rapidly initially, when the error is largest, as expected from Eq. (4.4-45). It should be noted that the large overshoot in the reference model response is required in order to rapidly develop normal acceleration. Thus a pitch rate model is chosen on the basis of the desired normal acceleration response, just as we did in simulations for the accelerated gradient method.

To demonstrate the performance of this system design in the presence of time-varying system dynamics, the trajectory in Section H.1 was simulated over a three second interval beginning at  $t = 7$  seconds,

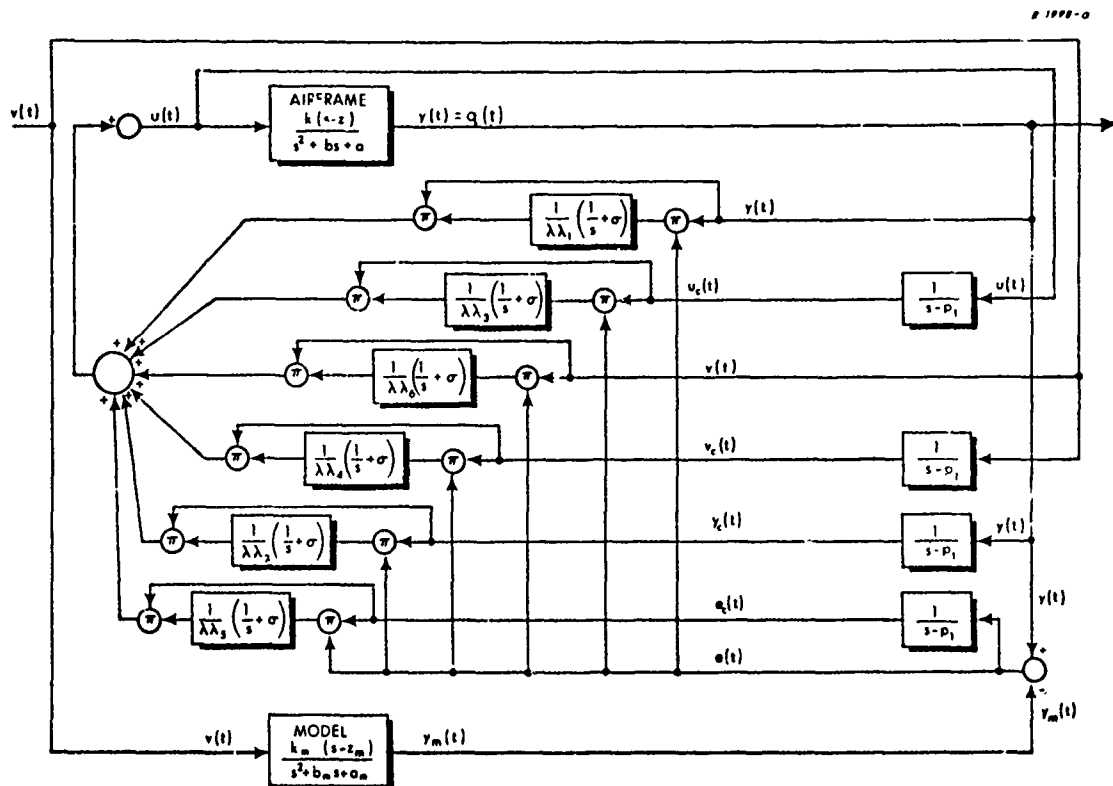


Figure 8.3-2 Liapunov Design Technique Applied to a Second Order Airframe

"half-way" between flight conditions 2 and 3 in Table H.1. This includes a portion of the missile's thrusting period. The initial values of the adaptive gains were calculated according to Eq. (8.3-9) with the detuning factor  $\eta$  equal to 0.75. The response curves are shown in Figs. 8.3-4(a) and (b). The error between the reference model output and the airframe pitch rate is plotted explicitly in Fig. 8.3-4(b) because of its small magnitude relative to the pitch rate. Evidently the control system is able to maintain a very small error level relative to the model response; the performance is somewhat better than that achieved with the accelerated gradient method over the same trajectory (see Fig. 8.2-8 for comparison).

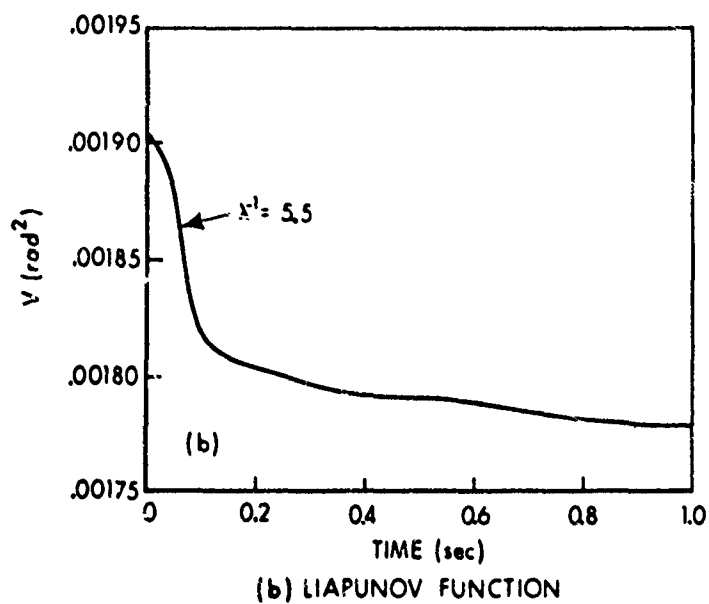
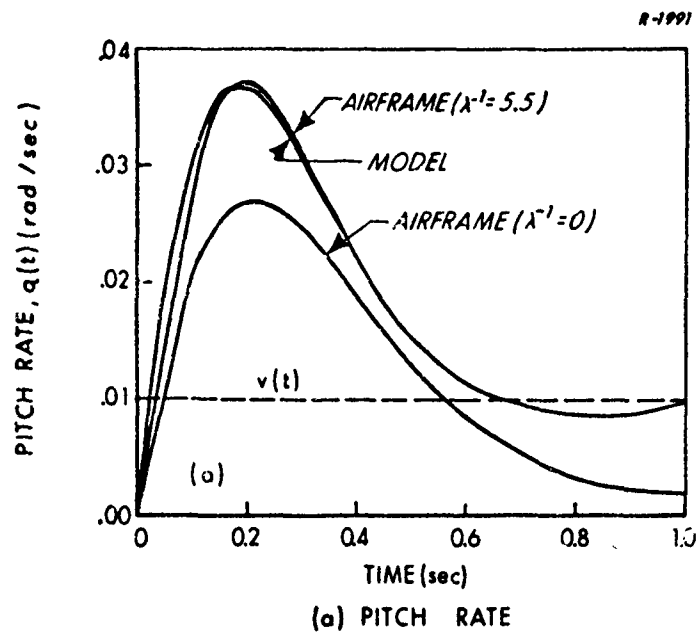


Figure 8.3-3 Step Response of Control System in Fig. 8.3-2 for a Constant Plant, With ( $\lambda^{-1} = 5.5$ ) and Without ( $\lambda^{-1} = 0$ ) Adaptation

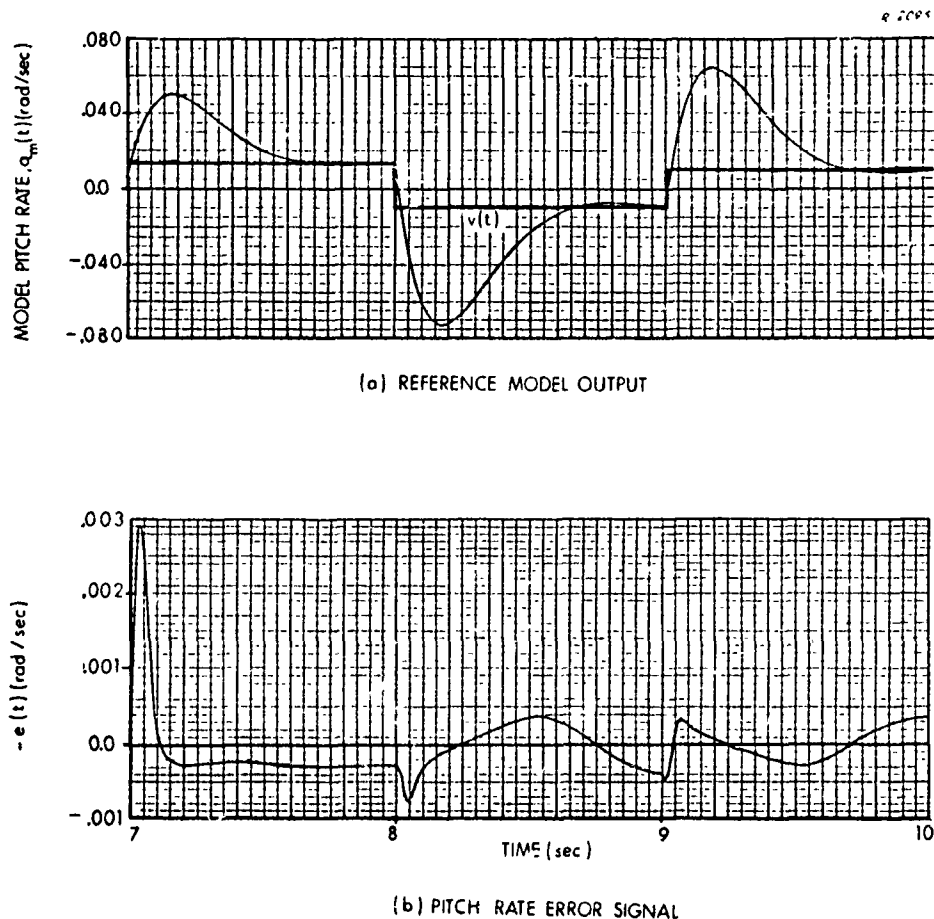


Figure 8.3-4 Pitch Rate Response of Reference Model and Pitch Rate Error Signal for the Liapunov Design in Fig. 8.3-2

In Fig. 8.3-5 the effect of setting the gain  $\sigma$  to zero in Eq. (8.3-8) is demonstrated; this is similar to opening the switch S in Fig. 8.2-3 for the accelerated gradient method. Recall that the term in the expression for the feedback control associated with this gain is designed to improve the adaptation rate of the system. When the simulation of Fig. 8.3-4 was rerun with  $\sigma = 0$ , the resulting error signal shown in Fig. 8.3-5 was significantly larger than that in Fig. 8.3-4(b) indicating that  $\sigma \neq 0$  does improve the system adaptation characteristics.

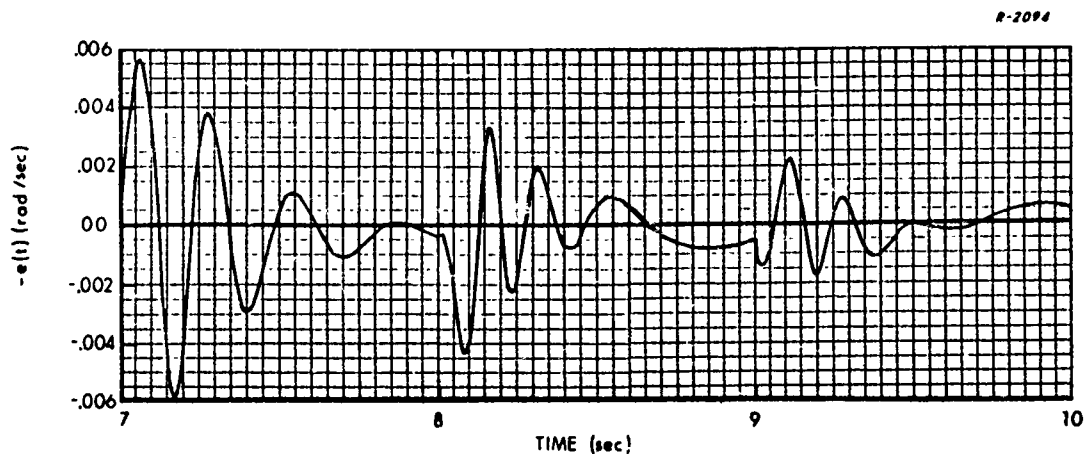


Figure 8.3-5 Pitch Rate Error Signal With  $\sigma = 0$

The controller described above is designed for a second order airframe, neglecting actuator dynamics. To determine the effect of the actuator, a simulation was performed using the same controller as in Fig. 8.3-2 with a first order lag inserted between the input  $u(t)$  and the airframe. The time constant of the lag is 0.02 seconds, taken from the data in Section H.1. The trajectory is the same as for Figs. 8.3-4 and 8.3-5 and the resulting error signal is shown in Fig. 8.3-6. As contrasted with Fig. 8.3-4(b) a relatively large transient error is incurred each time the input signal  $v(t)$  changes sign. However its duration is short -- on the order of 0.2 seconds which is comparable to the reference model response time.

Finally, we wish to demonstrate that the Liapunov technique is capable of providing good adaptive performance over the entire thrusting period of the trajectory in Section H.1. The simulation was performed for a three second interval beginning at 5 seconds with the gain detuning factor  $\eta$  set at 0.9 in Eq. (8.3-9). The pitch rate responses of both the reference model and the airframe are given in Fig. 8.3-7. Again the adaptive controller succeeds in tracking the reference model output very well,

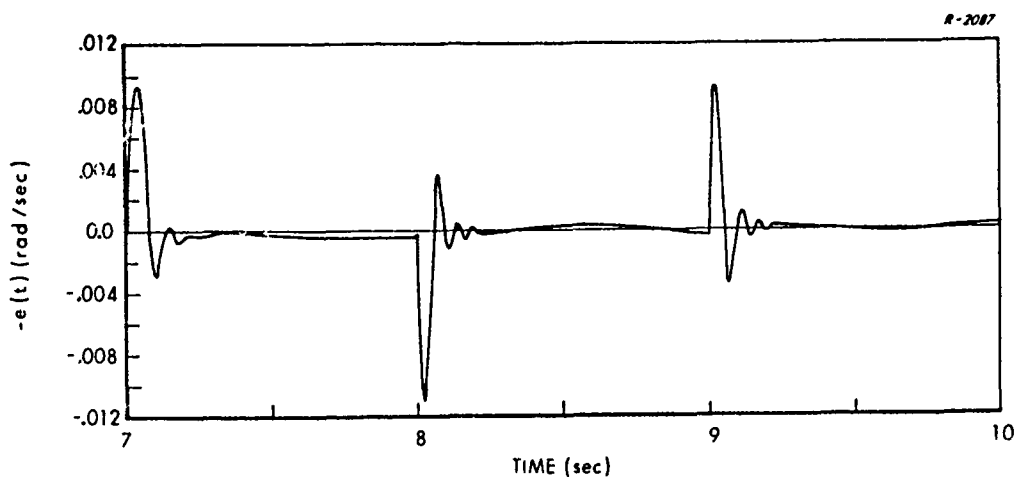


Figure 8.3-6 Pitch Rate Error Signal With Actuator Lag

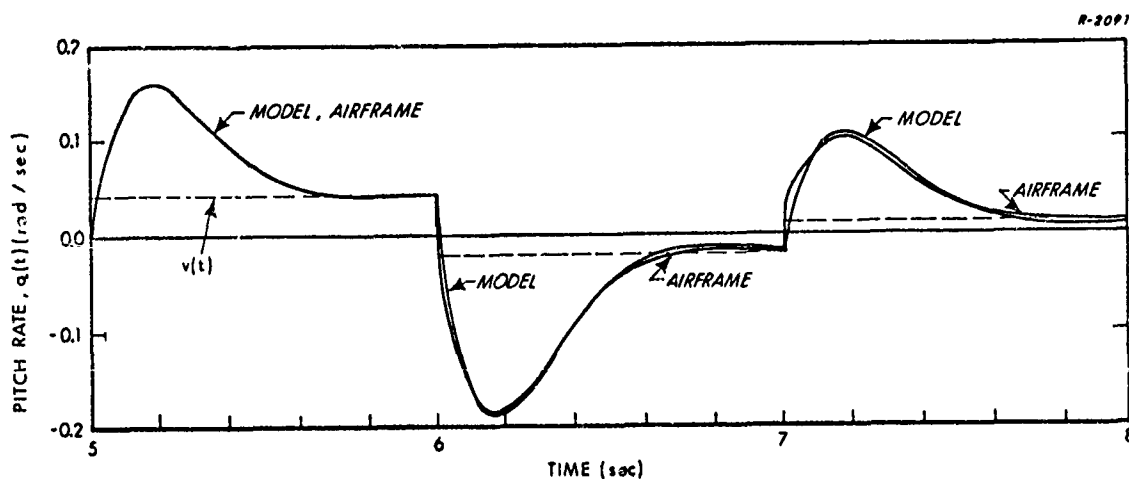


Figure 8.3-7 Pitch Rate Response for Rapid Airframe Parameter Variations

even though plant parameters are varying rapidly. This behavior contrasts favorably with the operation of the accelerated gradient technique in Fig. 8.2-9. However it may be simply a fortuitous circumstance because the theory predicts good operation only when plant parameters are constant.

### 8.3.4 An Adaptive Reference Model

When a partial plant identification capability is available, good adaptive normal acceleration response can probably be achieved if the Liapunov design technique is modified to include an adaptive reference model, just as described for the accelerated gradient method in Section 8.2.4. The use of an adaptive reference model forces the system to respond to input commands in such a fashion that the airframe acceleration output has the desired characteristics. The implementation of this idea is illustrated by the conceptually simple modifications to Fig. 8.3-2 indicated in Fig. 8.3-8. Only estimates of airspeed and the actual airframe zero,  $z$ , are required. No simulations were performed for this design.

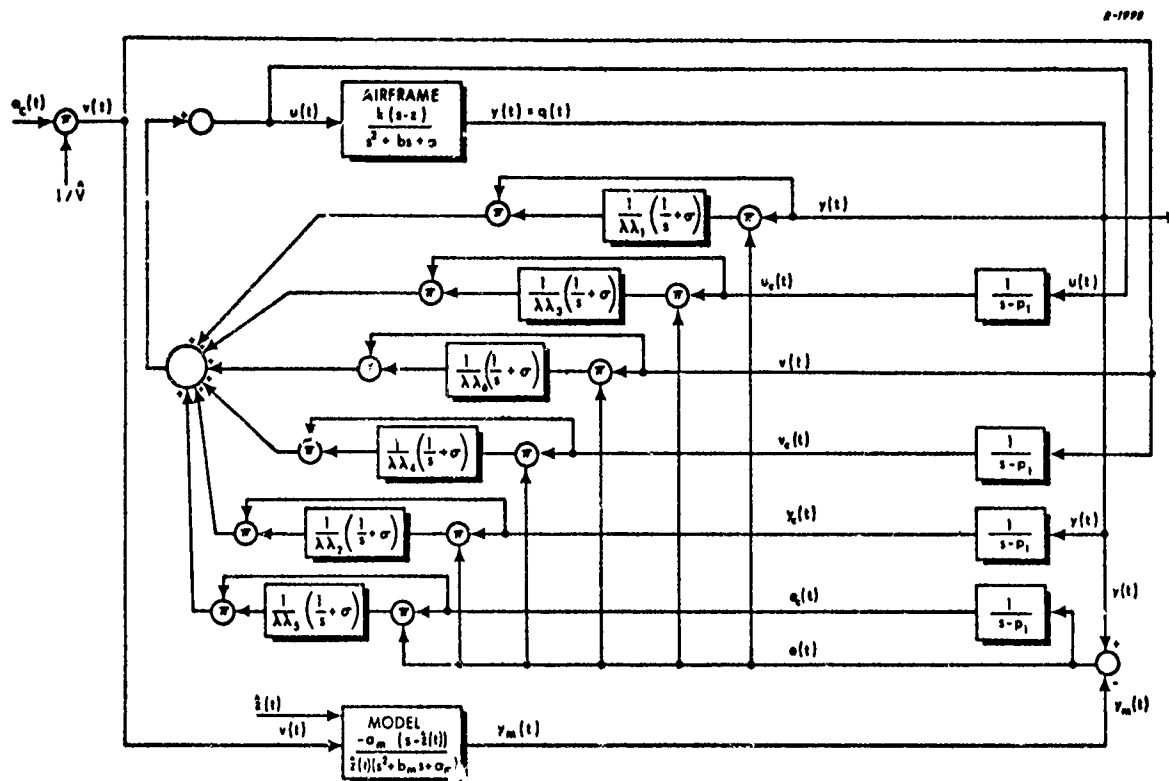


Figure 8.3-8 Liapunov Design Technique Applied to a Second Order Airframe With an Adaptive Reference Model

The same comments made for the accelerated gradient technique concerning the practicality of an adaptive reference model apply to the Liapunov procedure. If it is deemed easier to identify only a few airframe parameters ( $z$  and  $V$ ) instead of the entire plant, the procedure described above may offer computational advantages over the methods described in Chapter 5 which require complete plant identification. Further investigation of the adaptive reference model concept is needed to determine its merits vis a vis complete identification.

## 8.4 SUMMARY AND CONCLUSIONS

### 8.4.1 Summary

The Accelerated Gradient Method — The accelerated gradient method is applied to pitch rate and normal acceleration autopilots in Sections 8.2.2 and 8.2.3. The technique is characterized by a time-invariant reference model and no plant identification capability. The principal observations are that relatively good adaptive pitch rate control can be achieved whereas the normal acceleration autopilot adapts slowly and its stability characteristics are sensitive to flight conditions. The latter behavior is caused by the fact that the airframe input-output transfer function has a right-half-plane zero whose location is a function of flight condition. When a partial plant identification capability is feasible, it is demonstrated in Section 8.2.4 that an adaptive reference model used in conjunction with a pitch rate autopilot can yield good adaptive normal acceleration response.

A specific disadvantage of gradient type methods is that their global stability properties are generally unknown and situations where the



system becomes unstable can occur. A large amount of simulation with some trial and error design may be required to arrive at a satisfactory system configuration

Liapunov Design Method -- The Liapunov design technique is applied to a missile pitch rate autopilot in Section 8.3; as already noted in Section 4.4.4, this method is suited only for controlling minimum phase plants. The controller configuration is characterized by a time-invariant reference model and no plant identification capability. Rapid adaptation characteristics are observed in all simulations performed. However, it should be emphasized that the theory ensures the desired global stability properties only when plant parameters are constant. During periods of rapidly changing flight conditions, there is no guarantee that the system will remain stable. Just as with gradient methods, considerable simulation is required to definitively establish its usefulness for a particular set of circumstances. The results presented here indicate that Liapunov synthesis procedures are feasible and promising for controlling the output of a minimum phase airframe transfer function, i.e., one which has no right-half-plane zeros.

In order to circumvent the restriction to minimum phase plants when an adaptive normal acceleration autopilot is needed for tail-controlled missile, the adaptive reference model concept is suggested in Section 8.3.4. The latter is implemented in the same fashion as described in Section 8.2.4 for the accelerated gradient method.

#### 8.4.2 Conclusions

The simulation results presented in this chapter indicate that both the accelerated gradient and Liapunov design methods are feasible for

adaptive control of a missile airframe, subject to wide parameter variations whose input-output transfer function is minimum phase. The Liapunov design technique achieves somewhat better adaptation characteristics because of the inherent stability properties of the resulting adaptive controller.

Both of the above techniques, as developed in Chapter 4, are not well-suited for controlling normal acceleration in the tail-controlled missile illustrated in Fig. 8.1-1 because of the associated nonminimum phase transfer function. We have pointed out that one way of overcoming this problem is to utilize an adaptive reference model with a pitch rate autopilot; the net effect is to control both pitch rate and normal acceleration. Another possible solution is a change in the airframe design that will eliminate the nonminimum phase characteristic. Some possible methods of accomplishing the latter are outlined below.

The right-half-plane zero in the transfer function between control surface deflection and normal acceleration for the missile in Fig. 8.1-1 occurs because the control surfaces are mounted on the tail, behind the center of gravity. To produce an acceleration in one direction the control surface must deflect at an angle which initially produces an acceleration -- i.e., a force on the control surface -- in the opposite direction.\* The right-half-plane zero can be removed by putting the control surface forward of the missile's center of gravity in a canard configuration (Refs. 129, 130). Although this airframe structure sometimes has certain aerodynamic disadvantages -- e.g., the drag may be excessive and the flow of air over the primary lifting surfaces (wings) can be distorted by the wake of the canard

---

\* See the curves in Fig. 8.2-14 where the acceleration just after  $t = 0$  is in the direction opposite to that commanded.

structure -- it is worthwhile considering for alleviating the problems encountered in normal acceleration control.

Another possible airframe configuration is a form of direct lift control (Refs. 129, 131, 132) provided by a rotatable wing near the center of gravity, in conjunction with tail controls. Many of the problems associated with missile autopilot design are a result of the fact that the airframe must pitch to increase angle of attack to produce aerodynamic lift. The ability of the control surfaces to generate pitching moments varies with flight condition, also causing the airframe response characteristics to vary. This difficulty is largely eliminated if the airframe wings can be rotated with respect to the fuselage in the same fashion as the tail control surface. This provides the capability for rapidly changing the angle of attack (with respect to the wings) so that the missile can quickly develop a lifting force at any flight condition. In this configuration the tail control surface may still be needed to maintain airframe stability.

Finally we note that the need for adaptive control in missile applications arises largely through variations in airframe aerodynamic properties. Therefore the need for an adaptive autopilot may be reduced if a method of control -- such as thrust vectoring<sup>\*</sup> -- is employed which does not depend on aerodynamic forces for developing control moments and maneuvering accelerations.

This chapter has treated a variety of methods associated with implicit plant identification for adaptively controlling a missile airframe. In the next chapter techniques are considered which depend upon explicit plant identification.

---

\* Thrust vectoring refers to a concept where a variable component of the main engine thrust vector normal to the missile's longitudinal axis is used to control airframe pitch motion, and the primary maneuvering force is supplied by the longitudinal component of thrust combined with a large angle of attack.

## 9. APPLICATIONS: PARAMETER ADAPTIVE CONTROL SYSTEMS WITH EXPLICIT PLANT IDENTIFICATION

In Chapter 5 a number of adaptive techniques depending upon explicit identification of plant parameters are reviewed. Three of these -- using pole assignment, optimal regulator, and optimal model following concepts -- are examined here for possible application to tactical missiles. In applying each of these methods, the actuator and airframe are considered to comprise a third order linear system with dynamics as specified in Eqs. (8.1-3) and (8.1-4). A functional block diagram of the adaptive controller is shown in Fig. 9.1-1. The airframe equations of motion are known to within a set of varying parameters,  $\underline{a}$ , that can be accurately estimated by one of the methods discussed in Chapter 6. All state variables -- control surface deflection, normal acceleration, and pitch rate -- are considered available for use in the controller and for providing parameter estimates,  $\hat{\underline{a}}$ .

In all the applications examined here the controller structure is linear, with adaptive gains whose values depend upon the parameter estimates, as indicated in Fig. 9.1-2. The equations of motion have the form

$$\begin{aligned}\dot{\underline{x}}(t) &= \underline{A}(\underline{a}) \underline{x}(t) + \underline{b}(\underline{a}) \left( -\underline{h}(\hat{\underline{a}})^T \underline{x}(t) + k(\hat{\underline{a}}) v(t) \right) \\ y(t) = a(t) &= \underline{c}^T \underline{x}(t); \quad \underline{c}^T = [0 \ 1 \ 0] \quad (9.1-1)\end{aligned}$$

There is one gain associated with each state variable and a fourth is applied at the input to give the proper steady state (d-c) gain between  $v(t)$  and the airframe output. In this chapter we shall think of the output as being normal acceleration, consistent with the steering commands expected from the guidance loop. The only functional difference between each type of adaptive

R-1712

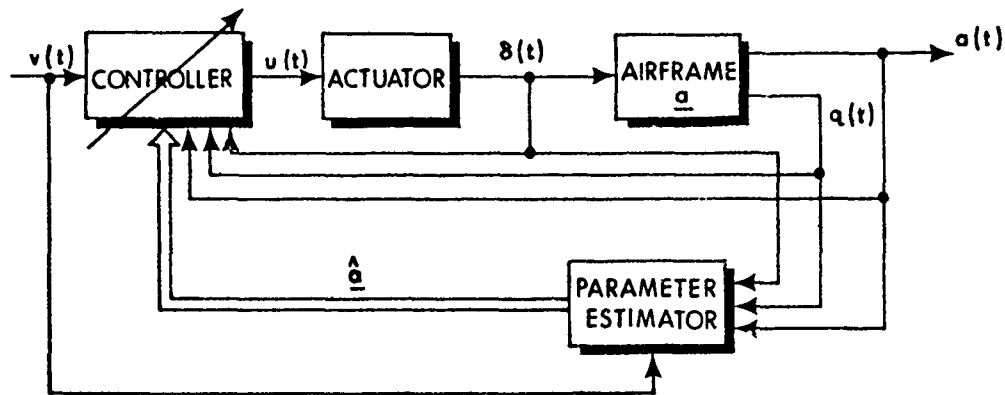


Figure 9.1-1 Structure of a Missile Adaptive Controller With Explicit Plant Identification

R-2621

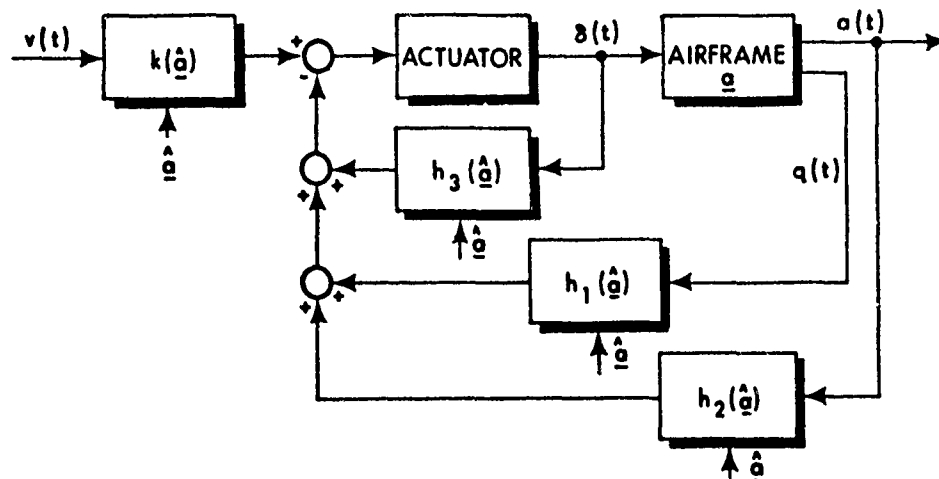


Figure 9.1-2 Adaptive Linear Feedback Controller

system discussed in this chapter is the algorithm used to define the feedback gains in terms of  $\hat{a}$ . The methods are described individually in Sections 9.1, 9.2, and 9.3 and their associated responses to input commands are compared in Section 9.4. Section 9.5 discusses the application of the most promising method, the pole assignment technique, to a missile with rapidly varying parameters such as exist in a dogfight engagement.

## 9.1 POLE ASSIGNMENT

An adaptive procedure for selecting feedback gains to position the closed loop poles for a controllable linear system is described in Section 5.3. The gains are obtained as functions of the parameter estimates  $\hat{\underline{a}}$  by solving Eq. (5.3-7), rewritten here in the form

$$\text{Det} \left[ \text{Is} - \underline{A}(\hat{\underline{a}}) + \underline{b}(\hat{\underline{a}}) \underline{h}^T \right] = s^3 + a_m s^2 + b_m s + c_m \quad (9.1-2)$$

For the missile application  $\underline{A}$  and  $\underline{b}$  are defined in Eq. (8.1-4) and are regarded here as functions of the estimated parameters. The quantities  $a_m$ ,  $b_m$  and  $c_m$  -- are the coefficients of the expanded polynomial on the right hand side of Eq. (5.3-7); i.e.,

$$\begin{aligned} s^3 + a_m s^2 + b_m s + c_m &\triangleq (s - p_{m_1})(s - p_{m_2})(s - p_{m_3}) \\ a_m &= -p_{m_1} - p_{m_2} - p_{m_3} \\ b_m &= p_{m_1} p_{m_2} + p_{m_1} p_{m_3} + p_{m_2} p_{m_3} \\ c_m &= -p_{m_1} p_{m_2} p_{m_3} \end{aligned} \quad (9.1-3)$$

where the quantities,  $p_{m_i}$ , are the desired closed loop poles. Equation (9.1-2) is solved by expanding the determinant and equating like powers of  $s$ . The result is a linear set of equations having a solution given by

$$\underline{h}(\hat{\underline{a}}) = \underline{P}(\hat{\underline{a}})^{-1} \underline{d}(\hat{\underline{a}}) \quad (9.1-4)$$

where

$$\begin{aligned}
 P(\hat{a}) &\triangleq - \begin{bmatrix} 0 & \hat{b}_2 & b_3 \\ -\hat{a}_{13}b_3 & -\hat{a}_{12}\hat{b}_2 & \hat{a}_{11}\hat{b}_2 & (\hat{a}_{11} + \hat{a}_{22})b_3 \\ -\hat{a}_{13}\hat{a}_{22}b_3 & \hat{a}_{13}b_3\hat{a}_{21} & (\hat{a}_{11}\hat{a}_{22} - \hat{a}_{21}\hat{a}_{12})b_3 \end{bmatrix} \\
 d(\hat{a}) &\triangleq \begin{bmatrix} -\hat{a}_{11} & -\hat{a}_{22} & -a_{33} & -a_m \\ -\hat{a}_{11}(\hat{a}_{22} + a_{33}) + \hat{a}_{12}\hat{a}_{21} & -a_{33}\hat{a}_{22} + b_m \\ a_{33}(\hat{a}_{21}\hat{a}_{12} - \hat{a}_{11}\hat{a}_{22}) - c_m \end{bmatrix}
 \end{aligned} \tag{9.1-5}$$

The carat superscript denotes those elements of  $A$  and  $b$  which must be estimated;  $a_{33}$  and  $b_3$  describe the actuator dynamics which are assumed to be known. The gains  $h$  can be updated from Eqs. (9.1-4) and (9.1-5) whenever new parameter estimates are generated.

The d-c gain  $k(\hat{a})$  is determined so that the acceleration output equals the input in the steady state when  $v(t)$  is constant. In other words, setting  $\underline{x}(t)$  equal to zero in Eq. (9.1-1) and solving for  $a(t)$ , we require

$$a(t) = -\underline{c}^T (A - \underline{b}h^T)^{-1} \underline{b}kv = v \tag{9.1-6}$$

Thus the solution for  $k$  becomes

$$k(\hat{a}) = - \frac{1}{\underline{c}^T (A(\hat{a}) - \underline{b}(\hat{a})h(\hat{a})^T)^{-1} \underline{b}(\hat{a})} \tag{9.1-7}$$

Equations (9.1-4) and (9.1-7) together completely specify the adaptive controller.

Application — Using the air-to-surface trajectory data given in Section H.2 of Appendix H, an autopilot control system was simulated. The

airframe dynamics along the trajectory were made time-varying by the linear interpolation procedure described in Section H.1. The values of the assigned poles,  $p_{m_i}$  in Eq. (9.1-3), are

$$\begin{aligned} p_{m_1} &= -60.0 \\ p_{m_2}, p_{m_3} &= -23.0 \pm j 17.6 \end{aligned} \quad (9.1-8)$$

These particular choices provide a comparison with the adaptive optimal controllers discussed later in this chapter.

If the adaptive gains are continuously computed from Eqs. (9.1-3) and (9.1-6), the instantaneous system poles will always be at the values specified by Eq. (9.1-7). However, practically speaking it takes time to obtain parameter estimates and to carry out the calculations needed to determine  $\hat{h}$  and  $\hat{k}$ . In addition, the computation equipment must generally perform other tasks related to guidance and navigation. Consequently it is possible to up-date the adaptive gains only at discrete times separated by intervals of some specified length. During each interval the plant parameters continue to vary and the closed loop system poles depart from the desired values. Therefore one measure of the performance of the system and an indication of how often the gains should be recomputed is provided by a graph showing variations in pole location as a function of time. Fortunately not all of the poles need be examined, only those nearest the imaginary axis contribute significantly to the system response. It is the real part of the latter which is of most interest because it is closely related to the system settling time.

The variation of the real part,  $\sigma$ , of the dominant complex poles of the missile autopilot along the trajectory is shown in Fig. 9.1-3. The



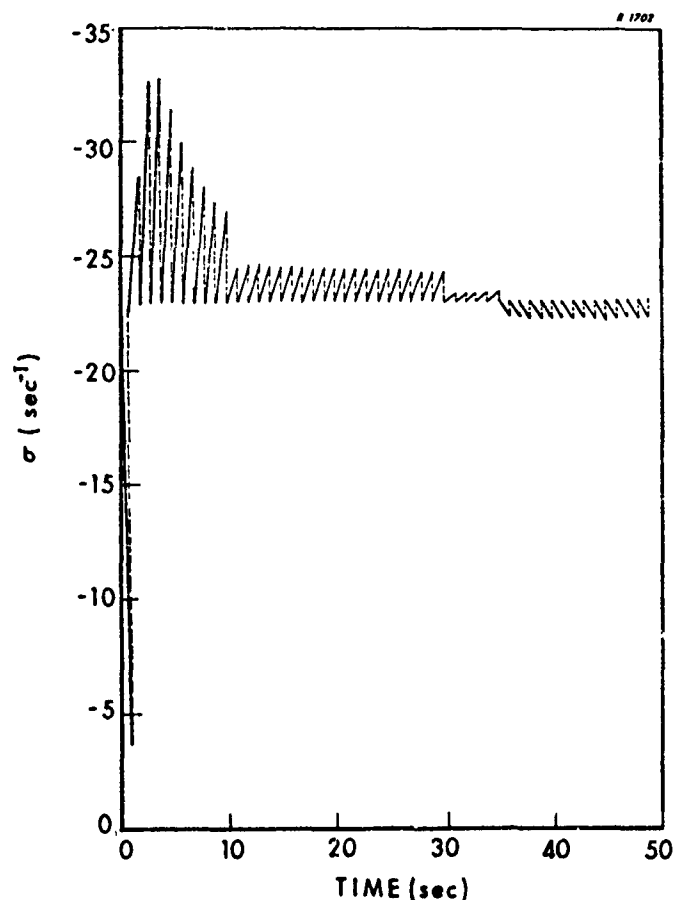


Figure 9.1-3 Value of the Real Part of the Most Significant Closed Loop Pole: Pole Assignment Technique

adaptive gains  $k$  and  $h$  were recomputed every second, resulting in discontinuous changes in  $\sigma$  as indicated by the dashed lines in the figure. Notice the especially rapid changes near the beginning of the trajectory. This behavior is partially caused by the fact that the missile airframe parameters vary most rapidly during the boost phase of the trajectory; also the closed loop poles are most sensitive to changes in plant parameters when the dynamic pressure is low. The latter effect is caused by the fact that the vector  $b$  in Eq. (9.1-2) varies with flight condition. Consequently during those periods of time when the feedback gains  $h$  are constant,

the sensitivity of the closed loop poles to changes in  $\underline{b}$  is partially determined by  $\underline{h}$ . When dynamic pressure is low the magnitude of  $\underline{b}$  tends to be small, requiring large feedback gains to achieve specified closed loop poles; hence the sensitivity to parameter variations tends to be greatest at low dynamic pressure. This is one illustration of a case where feedback can increase system sensitivity to changes in plant dynamics (see the related discussion in Section 7.1). From the trend indicated during the first second of flight it is seen that the autopilot would become temporarily unstable if the gains were updated less frequently. The above observations indicate that the pole assignment technique should yield a satisfactory response time over most of the trajectory provided plant identification is rapidly accomplished. A more definitive judgement about the system's performance can be made from viewing sample autopilot response curves. These are provided in Section 9.4 and are compared with the other adaptive methods being evaluated.

The implementation of the adaptive pole assignment controller is relatively easy to accomplish and is therefore quite competitive with other techniques which require plant identification. The mechanization of Eqs. (9.1-4) and (9.1-5) with a digital computer provides the capability to rapidly update feedback gains.

In this application only one set of closed loop poles is assigned in solving for the feedback gains from Eq. (9.1-4). However different sets of closed loop poles --  $p_{mi}$ ,  $i = 1, \dots, M$  -- could be specified for different ranges of flight conditions. For example, if the autopilot closed loop poles are required to have smaller magnitudes near the beginning of the trajectory than those specified in Eq. (9.1-8), then less frequent gain calculations are needed. This effect is also a result of the fact that the sensitivity of the closed loop poles to changes in parameters is partially determined by the

gains  $\underline{h}$ . The larger are the magnitudes of the elements of  $\underline{h}$ , the greater is the effect of parameter variations. Reducing the magnitude of the desired closed loop poles tends to reduce the level of the gains and thus reduce sensitivity. With this modification to the pole assignment method, Eq. (9.1-4) symbolically becomes

$$\underline{h}(\hat{\underline{a}}, \underline{p}_{m_i}) = \underline{P}(\hat{\underline{a}})^{-1} \underline{d}(\hat{\underline{a}}, \underline{p}_{m_i}) \quad (9.1-9)$$

where both  $\hat{\underline{a}}$  and  $\underline{p}_{m_i}$  change adaptively, the former as new estimates are generated and the latter as flight conditions change. The dependence of the gains on the assigned poles is explicitly provided by Eq. (9.1-3).

The above proposal is another type of adaptive reference model (see Section 8.2-4) where the model specifications (i.e., assigned poles) are adjusted with changes in flight condition so that acceptable system behavior is obtained. It is consistent with the idea that the designer should not expect the control system to produce fixed response characteristics that are unreasonable for some operating conditions.

## 9.2 THE ADAPTIVE OPTIMAL REGULATOR

In contrast with the pole assignment method discussed previously, optimal control techniques achieve a compromise between the objectives of obtaining good response characteristics and maintaining acceptable control levels. In this section the adaptive optimal regulator described in Section 5.4.1 and Appendix B is implemented using trajectory data provided in Section H.2. The term "adaptive" denotes the fact that a method is provided for recomputing optimal feedback gains on-line as new estimates of

plant parameters are obtained. Both optimal and suboptimal designs are considered.

### 9.2.1 Design of a Third Order Adaptive Optimal Regulator

In this section we apply optimal control techniques to design an adaptive autopilot for a tactical missile having a first order actuator and a second order airframe with dynamics specified in Eqs. (8.1-3) and (8.1-4). The problem as outlined in Section 5.4.1 is to assume  $v(t)$  is zero in Eq. (9.1-1) and determine  $u(t)$  in the equations of motion,

$$\dot{\underline{x}}(t) = A\underline{x}(t) + \underline{b}u(t); \quad \underline{x}(t_0) = \underline{x}_0 \quad (9.2-1)$$

such that the performance index

$$J = \int_{t_0}^{\infty} \left[ \underline{x}(t)^T Q \underline{x}(t) + ru(t)^2 \right] dt \quad (9.2-2)$$

is minimized. This problem formulation leads to solutions for the gains  $\underline{h}$  and  $k$  in Eq. (9.1-1) which are given in Eqs. (5.4-4), (5.4-5) and (5.4-8) in terms of the parameter estimates. These expressions are repeated here with  $\hat{\underline{a}}$  substituted for  $\underline{a}_0$ :

$$\underline{h}(\hat{\underline{a}})^T = \frac{1}{r} \underline{b}(\hat{\underline{a}})^T S(\hat{\underline{a}}) \quad (9.2-3)$$

$$-SA(\hat{\underline{a}}) - A(\hat{\underline{a}})^T S + \frac{1}{r} S \underline{b}(\hat{\underline{a}}) \underline{b}(\hat{\underline{a}})^T S - Q = 0. \quad (9.2-4)$$

$$k(\hat{\underline{a}}) = - \frac{1}{\underline{c}^T (A(\hat{\underline{a}}) - \underline{b}(\hat{\underline{a}}) \underline{h}(\hat{\underline{a}})^T)^{-1} \underline{b}(\hat{\underline{a}})} \quad (9.2-5)$$

Recall that each calculation for the gains  $\underline{h}(\hat{\underline{a}})$  in Eq. (9.2-3) requires the matrix  $S(\hat{\underline{a}})$ , which is the solution to the nonlinear steady state Riccati equation in Eq. (9.2-4). This generally must be accomplished by an iterative procedure. One efficient method that is suitable for low order systems is the Newton-Raphson technique discussed in Appendix F. Applied to this problem, an approximate solution for  $S(\hat{\underline{a}})$  is obtained by iteratively solving the linear matrix equations

$$\left(\underline{A} - \frac{1}{r} \underline{b} \underline{b}^T \underline{S}_k\right)^T \underline{S}_{k+1} + \underline{S}_{k+1} \left(\underline{A} - \frac{1}{r} \underline{b} \underline{b}^T \underline{S}_k\right) + \frac{1}{r} \underline{S}_k \underline{b} \underline{b}^T \underline{S}_k + \underline{Q} = 0 \quad (9.2-6)$$

In order that the sequence  $\dots S_0, S_1, \dots$  converges to the proper value, the starting value  $S_0$  is chosen such that the eigenvalues of the matrix

$$\left(\underline{A} - \frac{1}{r} \underline{b} \underline{b}^T \underline{S}_0\right) \quad (9.2-7)$$

all have negative real parts. Enough iterations are performed so that acceptable accuracy in  $S$  is achieved; typically five to ten are required for the simulations described here.

The problem of determining how often to calculate  $\underline{h}(\hat{\underline{a}})$  is more important here than in the pole assignment method because of the increased computational load imposed by the need to determine  $S(\hat{\underline{a}})$ . One method for deciding this question is to evaluate the performance index  $J$  for the representative trajectory as a function of the number,  $N$ , of gain recalculations. Presumably, if  $\underline{h}(\hat{\underline{a}})$  is updated too infrequently, it will differ widely from its optimum value along significant portions of the trajectory because of airframe parameter variations. This fact should be reflected in an increase in  $J$  as  $N$  decreases. Hopefully a computation interval can be found that is

short enough to yield an acceptably small value of  $J$  and yet is long enough with respect to the system response time so the infinite upper limit in the integral of Eq. (9.2-2) remains valid. If this cannot be done, it implies that system parameters are varying too rapidly for adaptive steady state regulator gains to yield an adequate controller design.

The performance evaluation described above was carried out over the same 50 second trajectory used in Section 9.1 by calculating

$$J(N) = \sum_{i=1}^N \int_{t_i}^{t_{i+1}} \left( \underline{x}(t)^T Q \underline{x}(t) + r u_i(t)^2 \right) dt$$

where the times  $t_i$  are equally spaced points at which  $\underline{h}$  is recalculated according to Eq. (9.2-3), using parameter estimates  $\hat{\underline{a}}_i$ . The parameters were assumed to be perfectly estimated in this simulation. The elements of  $A$  and  $\underline{b}$  in Eq. (9.2-1) were taken from Table H.6 with linear interpolation between the given flight conditions. At times  $t_i$ , the following operations were performed:  $A$  and  $\underline{b}$  were updated in Eqs. (9.2-6) and (9.2-7), an approximate solution was obtained for  $S(\hat{\underline{a}}_i)$  by Newton-Raphson iteration, and the adaptive gains were recomputed. Two different values of the weighting matrix  $Q$  were chosen,

$$Q_1 = \begin{bmatrix} 1.0 \times 10^{-3} & 0 & 0 \\ 0 & 2.0 \times 10^{-8} & 0 \\ 0 & 0 & 1 \end{bmatrix}; \quad Q_2 = \begin{bmatrix} 1.0 \times 10^{-2} & 0 & 0 \\ 0 & 2.0 \times 10^{-8} & 0 \\ 0 & 0 & 1 \end{bmatrix} \quad (9.2-8)$$

with a fixed value of  $r$ ,  $r = 1.0$ . The equations of motion were "driven" by taking the input  $v(t)$  as zero and setting the state of the autopilot to a specified value,  $\pm \underline{x}_0$ , at one second intervals, with the sign alternating at

successive intervals. This simulates a situation where the system has been allowed to reach steady state in response to a constant input command and then  $v(t)$  is suddenly changed to zero.

The variation in  $J$  as a function of  $N$  is plotted in Fig. 9.2-1 for both weighting matrices  $Q_1$  and  $Q_2$ . Only integer values of  $N$  have meaning but points are connected by straight lines to indicate trends. The value  $N = 0$  corresponds to no feedback compensation at all, i.e.,  $h = 0$ . The points where  $J$  has the value " $\infty$ " occur when the system becomes unstable, resulting in an essentially "infinite" cost. One conclusion is that too few recalculations, which can result in large departures of the gains from their optimum values as parameters vary, are worse than no feedback ( $h = 0$ ). This sensitivity problem is the same type encountered in the pole assignment technique in the preceding section. With weighting  $Q_2$  the system becomes unstable when  $N$  is too small; the same behavior is observed with the pole assignment technique if the feedback gains are recalculated too infrequently. However, it is clear that the minimum of  $J$  is achieved for all practical purposes when  $N \geq 10$  for both choices of  $Q$ ; this is to be contrasted with the 50 recalculations required to maintain stability in the case illustrated by Fig. 9.1-3.

To compare the pole assignment method and the optimal regulator on the same basis, graphs of the real part of the closed loop airframe poles are shown in Fig. 9.2-2 for the optimal regulator design with  $Q = Q_2$  and  $N = 10$ . This value of the weighting matrix is used throughout our subsequent discussion. The discontinuities in the curve at 5 second intervals are the points at which a new set of optimal gains is computed. In the same figure the curve corresponding to the uncompensated airframe ( $N = 0$ ) is also shown. The horizontal dotted line at the value -23 represents the design value for the adaptive pole assignment system.

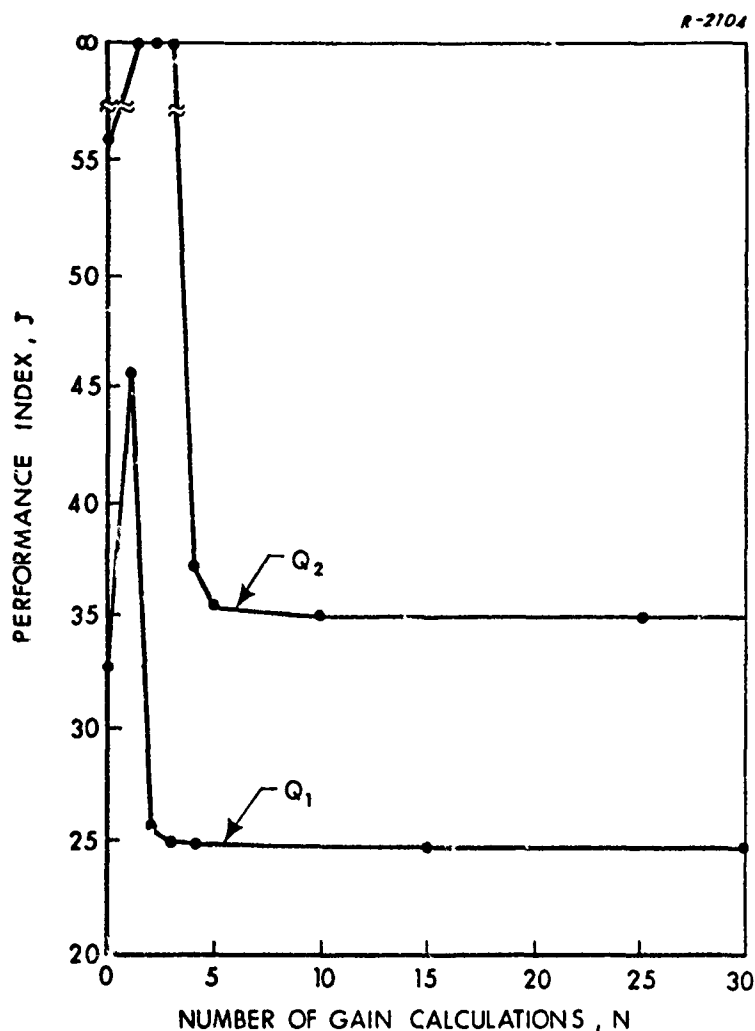


Figure 9.2-1 Performance Index as a Function of the Number of Optimal Gain Recalculations: Adaptive Optimal Regulator

The weighting matrix for the performance index is chosen so that the optimal regulator feedback gains make the closed loop system poles at 25 seconds equal to those specified for the pole assignment method in Eq. (9.1-8). In other words the missile autopilot using the optimal regulator gains has the same dynamics as the adaptive pole assignment system at one instant of time along the missile's trajectory. This provides a basis of comparison for the performance of the two systems. We can suppose



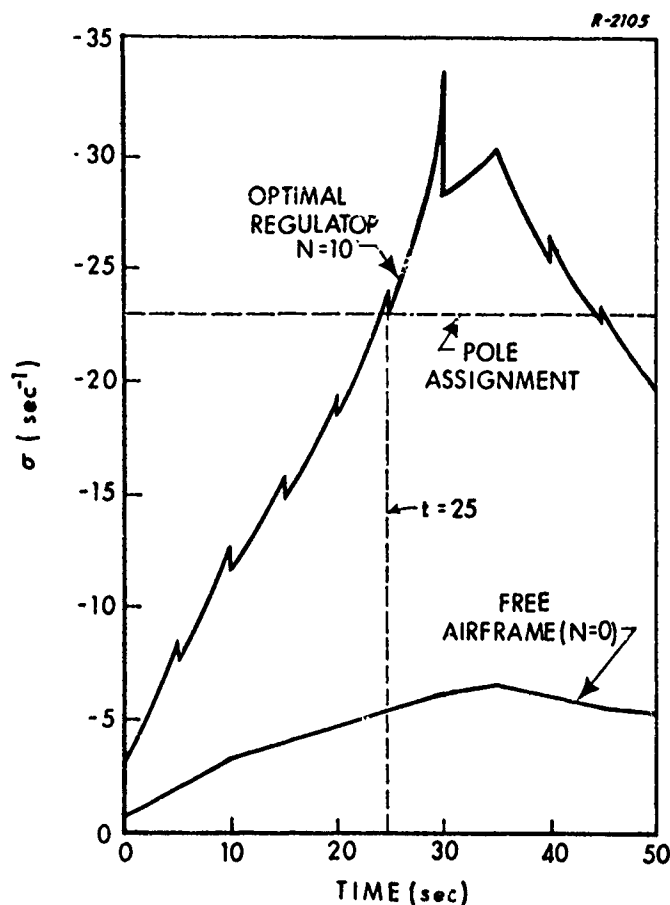


Figure 9.2-2 Value of the Real Part of the Most Significant Closed Loop Pole: Optimal Regulator Method

that ideally the instantaneous system closed loop poles should always have the values specified in Eq. (9.1-8). This can be assured using adaptive pole assignment by recomputing the gains sufficiently often. On the other hand the optimal regulator provides the desired response characteristics at only one instant. At other points on the trajectory, Fig. 9.2-2 indicates a shorter or longer settling time (larger or smaller  $\sigma$ ) depending upon the compromise between response speed and control level dictated by the minimization of the performance index in Eq. (9.2-2). This is exactly the sort of comparison one expects because the pole assignment technique

places no penalty on the control magnitude required to give the desired output performance. These comparisons are also supported by the output response curves presented in Section 9.4.

The main objection to using the optimal regulator design is that one has no direct control over how much the closed loop response characteristics vary as plant parameters change. The designer may be willing to accept some deviation from criteria such as those specified in Eq. (9.1-8), but variations of the kind indicated in Fig. 9.2-2 may be too large -- especially near the beginning of the trajectory. More detailed discussion of this point is given in Section 5.4.1 and Appendix B. Possible alternative methods are provided by the optimal model following systems described in Sections 5.4.2 and 5.4.3 which have the capability for obtaining more uniform output performance characteristics over a range of flight conditions. One of these is examined in Section 9.3.

#### 9.2.2 Design of a Third Order Adaptive Suboptimal Regulator

Many linear optimal control problems suffer from the "curse of dimensionality" in that a large number of variables are required to describe the plant dynamics and considerable computation is required to obtain optimum feedback gains. This is a very important consideration in adaptive systems when the feedback gains must be updated on-line by solving the matrix Riccati equation. To accomplish this task using the Newton-Raphson iteration (Eq.(9.2-6)), the computation time required is proportional to  $n^6$  where  $n$  is the dimension of the state. Hence even a small reduction in the number of state variables can substantially reduce the computational load. Consequently it is desirable to consider suboptimal control laws which neglect some of the state variables. This is often justified in linear systems

when certain open loop poles do not contribute significantly to the open loop response. Such is the case in missiles if dynamics introduced by the flexible airframe, actuator and sensors are negligible compared with those of the airframe's rigid body motion. In this section we evaluate the system design obtained by solving the optimal control problem with the actuator dynamics in Eq. (8.1-3) neglected, and then implementing the resulting feedback gains with the actuator included.

The equations of motion for the second order system corresponding to Eq. (8.1-3) with  $\delta(t)$  regarded as the control variable are

$$\begin{bmatrix} \dot{q}(t) \\ \dot{\alpha}(t) \end{bmatrix} = \begin{bmatrix} M_q & M_\alpha \\ 1 & -L_\alpha \end{bmatrix} \begin{bmatrix} q(t) \\ \alpha(t) \end{bmatrix} + \begin{bmatrix} M_\delta \\ -L_\delta \end{bmatrix} \delta(t) \quad (9.2-9)$$

where  $\alpha(t)$  is the angle to attack. Comparing the third order and second order systems, make the identifications

$$u(t) = \delta(t)$$

$$\alpha(t) = \frac{1}{VL_\alpha} \left( a(t) - VL_\delta \delta(t) \right) \quad (9.2-10)$$

Denoting the diagonal elements of  $Q$  in Eq. (9.2-2) by  $q_{11}$ ,  $q_{22}$  and  $q_{33}$  with off-diagonal terms equal to zero and substituting for  $a(t)$  from Eq. (9.2-10), the performance index  $J$  in Eq. (9.2-2) becomes

$$J = \int_{t_0}^{\infty} \left[ q_{11} q(t)^2 + q_{22} V^2 (L_\alpha \alpha(t) + L_\delta u(t))^2 + (q_{33} + r) u(t)^2 \right] dt \quad (9.2-11)$$

If the optimal feedback gains for minimizing  $J$  in Eq. (9.2-11) for the second order system are  $h'_1$  and  $h'_2$ , the corresponding values of the gains for the third order system illustrated in Fig. 9.1-2 are obtained by setting

$$h'_1 q(t) + h'_2 \alpha(t) = h_1 q(t) + h_2 a(t) + h_3 \delta(t)$$

Substitution for  $\alpha(t)$  from Eq. (9.2-10) into the above expression and equating coefficients of like state variables on each side of the equation produces

$$\begin{aligned} h_1 &= h'_1 & h_2 &= \frac{h'_2}{VL_\alpha} \\ h_3 &= -\frac{h'_2 L_\delta}{L_\alpha} \end{aligned} \quad (9.2-12)$$

Plots of the real part of the dominant pole for both the suboptimal and optimal adaptive systems are shown in Fig. 9.2-3 for two different values of the actuator pole,  $-\lambda$ . In both cases the feedback gains are recalculated at one second intervals ( $N = 50$ ) and with  $Q = Q_2$ . Observe that for  $\lambda$  as large as 200 (actuator time constant  $= 5 \times 10^{-3}$  sec.) there is appreciable deviation in the optimal and suboptimal curves during the later portion of the trajectory, as the system closed loop poles move further into the left-half-plane. The conclusion is that in order for the second order design to be a good approximation to the third order design, the actuator poles must not only be far removed from those of the uncompensated missile airframe, but they should also be some distance from those of the compensated airframe. This condition does not hold for all flight conditions in the system we are considering ( $\lambda = 50$ ); consequently actuator dynamics are not neglected in subsequent sections.

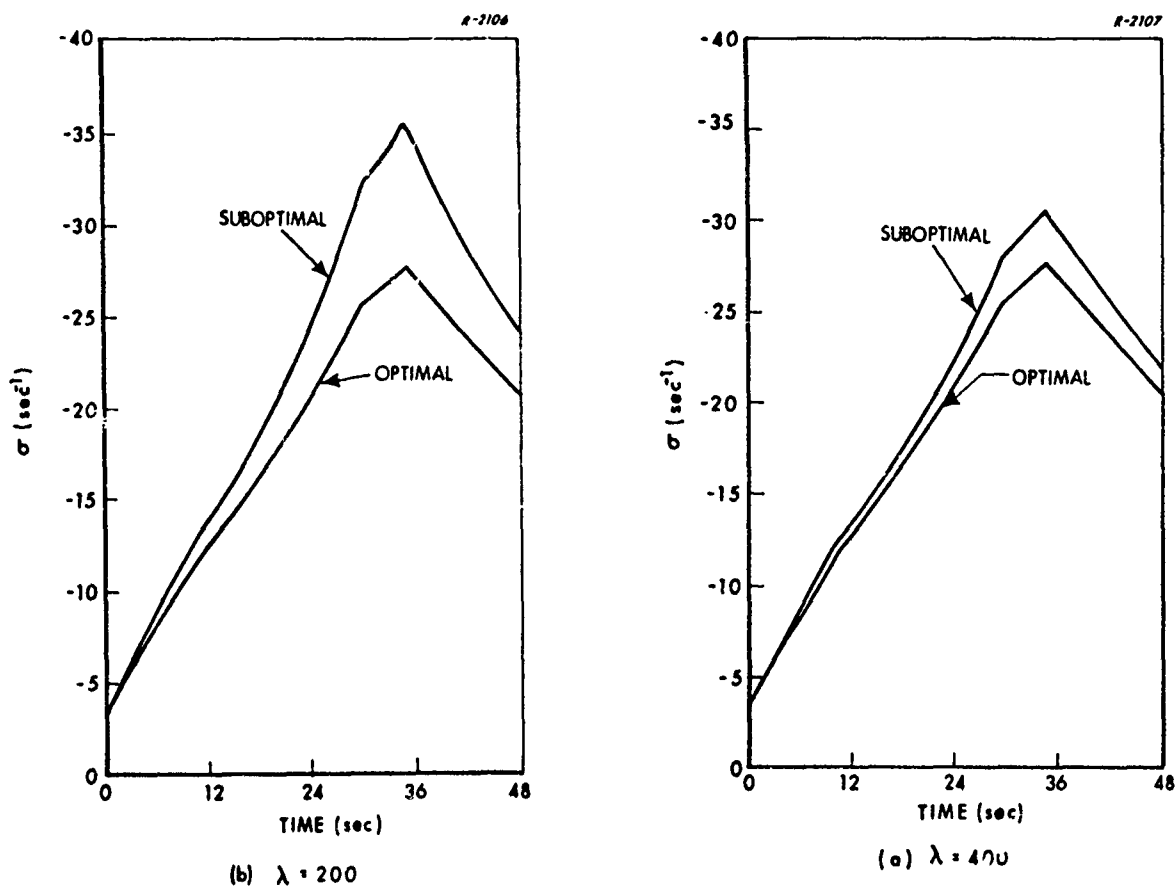


Figure 9.2-3 Comparison of the Values of the Real Part of the Most Significant Closed Loop Pole for the Optimal and Suboptimal Regulator Designs

### 9.3 ADAPTIVE OPTIMAL MODEL FOLLOWING SYSTEMS

In this section we apply the "model-in-the-performance-index" model following control technique described in Section 5.4.2 to a missile autopilot. This method permits adaptive regulation of control system response characteristics along a trajectory by defining a performance criterion in terms of the error between the actual (measured) and the desired airframe dynamic properties. The error signal is given by

$$\underline{\tilde{e}}(t) = (\underline{A}(\hat{\underline{a}}) - \underline{A}_m) \underline{x}(t) + \underline{b}(\hat{\underline{a}}) u(t), \quad (9.3-1)$$

as in Eq. (5.4-13), where the matrix  $\underline{A}_m$  represents the dynamics of a reference model,

$$\dot{\underline{x}}_m(t) = \underline{A}_m \underline{x}_m(t)$$

The objective is to determine  $u(t)$  so that

$$J = \int_{t_0}^{\infty} \left[ \underline{\tilde{e}}(t)^T \underline{Q} \underline{\tilde{e}}(t) + r u(t)^2 \right] dt \quad (9.3-2)$$

is minimized. Again the notation  $\underline{A}(\hat{\underline{a}})$  and  $\underline{b}(\hat{\underline{a}})$  is used to emphasize the dependence of the control upon parameter estimates. This problem formulation leads to solutions for the gains  $\underline{h}$  and  $\underline{k}$  in Eq. (9.1-1) which are given in Eqs. (5.4-14), (5.4-15) and (5.4-8). These expressions are repeated here with  $\hat{\underline{a}}$  substituted for  $\underline{\hat{a}}_0$ :

$$\underline{h}(\hat{\underline{a}})^T = \frac{\underline{b}(\hat{\underline{a}})^T}{\underline{\tilde{r}}(\hat{\underline{a}})} \left[ \underline{\tilde{S}}(\hat{\underline{a}}) + \underline{Q} \underline{\tilde{H}}(\hat{\underline{a}}) \right]$$

$$\underline{\tilde{r}}(\hat{\underline{a}}) \triangleq \underline{b}(\hat{\underline{a}})^T \underline{Q} \underline{b}(\hat{\underline{a}}) + r$$

$$\underline{\tilde{H}}(\hat{\underline{a}}) \triangleq \underline{A}(\hat{\underline{a}}) - \underline{A}_m$$

$$\underline{k}(\hat{\underline{a}}) = - \frac{1}{\underline{c}^T (\underline{A}(\hat{\underline{a}}) - \underline{b}(\hat{\underline{a}}) \underline{h}(\hat{\underline{a}})^T)^{-1} \underline{b}(\hat{\underline{a}})} \quad (9.3-3)$$

where  $\tilde{S}(\hat{a})$  satisfies

$$\begin{aligned} -\tilde{S}\tilde{A}(\hat{a}) - \tilde{A}(\hat{a})^T \tilde{S} + \frac{1}{\tilde{r}(\hat{a})} \tilde{S}\tilde{b}(\hat{a}) \tilde{b}(\hat{a})^T \tilde{S} - \tilde{H}(\hat{a})^T \tilde{Q}(\hat{a}) \tilde{H}(\hat{a}) &= 0 \\ \tilde{A}(\hat{a}) &\triangleq A(\hat{a}) - \frac{1}{\tilde{r}(\hat{a})} \tilde{b}(\hat{a}) \tilde{b}(\hat{a})^T Q \tilde{H}(\hat{a}) \\ \tilde{Q}(\hat{a}) &\triangleq Q - \frac{1}{\tilde{r}(\hat{a})} Q \tilde{b}(\hat{a}) \tilde{b}(\hat{a})^T Q \end{aligned} \quad (9.3-4)$$

Equation (9.3-4) is solved iteratively for  $\tilde{S}(\hat{a})$  using the same Newton-Raphson method described in the preceding section. The response of the airframe tends to be similar to that of the model to the extent that the difference,  $\Delta A$ , between the dynamics of the reference model and the closed loop control system, as expressed by

$$\Delta A \triangleq (A(\hat{a}) - \tilde{b}(\hat{a}) \tilde{h}(\hat{a})^T - A_m), \quad (9.3-5)$$

is made small by the resulting value of  $\tilde{h}$ .

Simulations of this technique were performed with  $A_m$  given by

$$A_m = (A - \tilde{b} \tilde{h}_m^T) \quad (9.3-6)$$

where  $A$  and  $\tilde{b}$  have the values for the trajectory used in Sections 9.1 and 9.2 at time  $t = 25$  seconds and  $\tilde{h}_m$  is the solution to the optimal regulator problem at the same instant with  $Q = Q_2$ . In this way a consistent comparison is made between the model following system and the other control techniques evaluated in this chapter. Numerical values for the model parameters are

$$A_m = \begin{bmatrix} -7.64 & 0.041 & -454.0 \\ -1.51 \times 10^4 & 3.53 & 8.47 \times 10^4 \\ 4.31 & 4.47 \times 10^{-2} & -95.8 \end{bmatrix} \quad (9.3-7)$$

Appropriate weighting constants for the performance index are

$$Q = Q_3 = q \begin{bmatrix} 0.3 & 0 & 0 \\ 0 & 2.0 \times 10^{-7} & 0 \\ 0 & 0 & 1.0 \end{bmatrix}; \quad r = 1.0 \quad (9.3-8)$$

where  $q$  is an adjustable parameter to provide comparative simulation results.

The real part of the most significant pole along the missile trajectory is displayed in Fig. 9.3-1 for three different values of  $q$  and with the feedback gains calculated at one second intervals. The dashed horizontal line at  $\sigma = -23.0$  represents the specifications in Eq. (9.1-8) on which the pole assignment technique was based. Observe that as  $q$  increases, at  $t = 25$  seconds the value of  $\sigma$  for the model following system appears to approach a limit that coincides with both the curve for the optimal regulator and the horizontal dashed line. This behavior is a consequence of the fact that as  $q$  is increased (or alternatively as  $r$  is decreased) the optimal feedback gains  $\underline{h}$  also approach a limit, as discussed in Section 5.4.2. When  $t = 25$  seconds this limit is identical with the feedback gains in the optimal regulator and the pole assignment system because the reference model dynamics defined by Eqs. (9.3-6) and (9.3-7) are identical to those of the optimal regulator at 25 seconds. That is to say,

$$\lim_{q \rightarrow \infty} \Delta A \Big|_{t=25} = 0$$



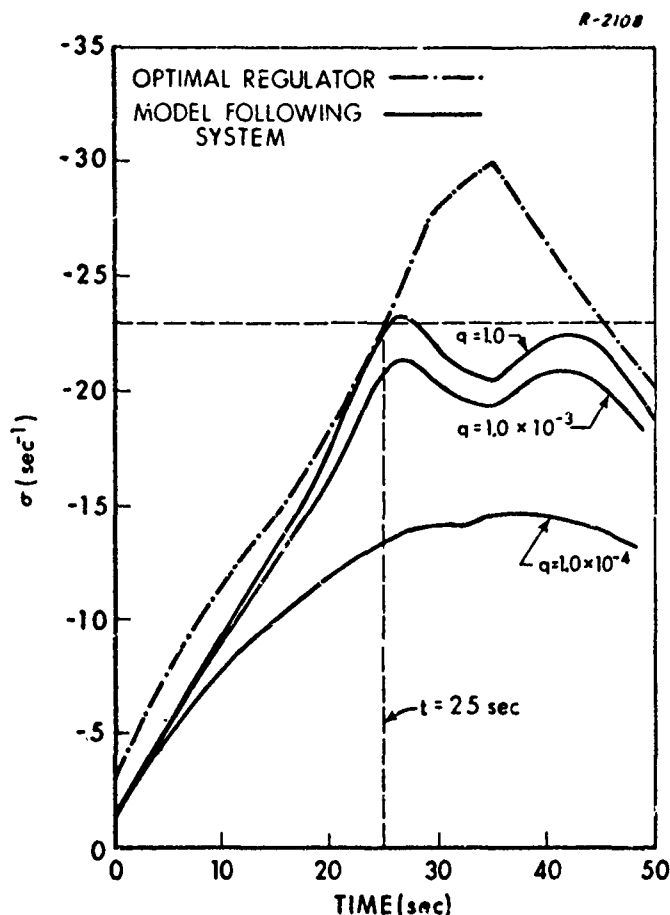


Figure 9.3-1 Values of the Real Part of the Most Significant Closed Loop Pole:  
Optimal Model Following System

where  $\Delta A$  is defined in Eq. (9.3-5). Consequently the model in the performance index (with large  $q$ ), the optimal regulator, and the pole assignment methods all yield the same controller at one point on the trajectory. This property permits a meaningful comparison of the three techniques at other points along the trajectory.

As indicated in Fig. 9.3-1, for a large value of  $q$  the tendency of this control system to conform to the model (in terms of the location of the most significant closed loop pole) is moderately better than the optimal regulator for  $t > 25$  sec and is about the same as the regulator for  $t < 25$  sec.

Deviations from the model are a result of our inability to choose  $\underline{h}(t)$  to make  $\Delta A$  identically zero everywhere on the trajectory. Consequently a compromise between control level and response characteristics is exerted by the optimization criterion, just as in the regulator method.

The primary advantage offered by the model following scheme for this application, relative to the optimal regulator, is a conceptual one. If one deliberately specifies a set of model dynamics  $A_m$  that the compensated airframe can duplicate at one particular flight condition, then an optimal control law which minimizes  $J$  in Eq. (9.3-2) closely approximates the model at that flight condition if the performance index weighting constant  $q$  in Eq. (9.3-8) is sufficiently large. By contrast, it is more difficult to determine what choices of  $Q$  and  $r$  in Eq. (9.2-2) realize specified dynamics at any flight condition. However, this distinction may be somewhat academic from the designer's point of view because the performance indices are chosen "off-line" where there is sufficient time to evaluate different values of  $Q$  and  $r$ .

The computational requirements for this model following system are somewhat greater than for the optimal regulator as indicated by comparing Eqs. (9.3-3) and (9.3-4) with Eqs. (9.2-3) and (9.2-4). This disadvantage weighed against the small improvement obtained in Fig. 9.3-1 indicates that the model-in-the-performance-index technique investigated here is relatively unattractive for controlling longitudinal airframe motion. For other applications where there is more than one plant input variable (e.g., lateral motion control) a better match between system and model dynamics might be achieved over the entire trajectory using the model following method discussed above.

It is noted in Section 5.4.3 that the model-in-the-performance-index method discussed above can be made to yield more uniform

performance by transforming state variables to phase variable canonical form. The resulting adaptive control law requires some additional computation to derive the required transformation matrix. This possibility is not pursued here.

Another type of model following technique considered in Section 5.4 is the "model-in-the-system" approach having the structure indicated in Fig. 5.4-2. It is capable of making the airframe and reference model dynamics approximately identical for a wide range of flight conditions, at the expense of requiring a high gain type feedback structure and more complex computations (see Eqs. (5.4-19) and (5.4-20)). This method is not evaluated here because nearly the same performance characteristics, without the above stated disadvantages, are achievable using the pole assignment method.

#### 9.4 RESPONSE COMPARISONS

From the designer's point of view, the best comparison among different control methods is provided by simulation of the time histories of the control variables and important state variables. This permits one to examine the actual transient characteristics of the system in response to representative input commands, thus obtaining empirical knowledge of such parameters as rise time, overshoot, and settling time.

To perform this type of study, the operation of the three adaptive controllers -- pole assignment, optimal regulator, and model following -- described in the preceding sections was simulated along the surface-to-air trajectory described in Section H.2. Airframe dynamics were varied with time according to the linear interpolation technique described in Section H.1.

The commanded acceleration  $v(t)$  is a piecewise constant function which changes level and alternates its sign at one second intervals according to

$$v(n+1) = -f(n+1) \operatorname{sign} [v(n)]; \quad n = 1, 2, \dots$$

$$v(0) = f(0)$$

where  $f(t)$  is specified graphically in Fig. 9.4-1. The use of acceleration commands that gradually increase in magnitude is reasonable if the missile is launched some distance from a target. The adaptive gains are also updated at one second intervals along the trajectory. Graphs of the corresponding control surface deflection  $\delta(t)$  and normal acceleration  $a(t)$  are shown in Figs. 9.4-2(a) through (e) over selected one second intervals along the trajectory. The magnitude of the control surface deflection is of interest because in practice it usually has an upper bound that cannot be exceeded; furthermore it is an indication of the control level required at the actuator input.

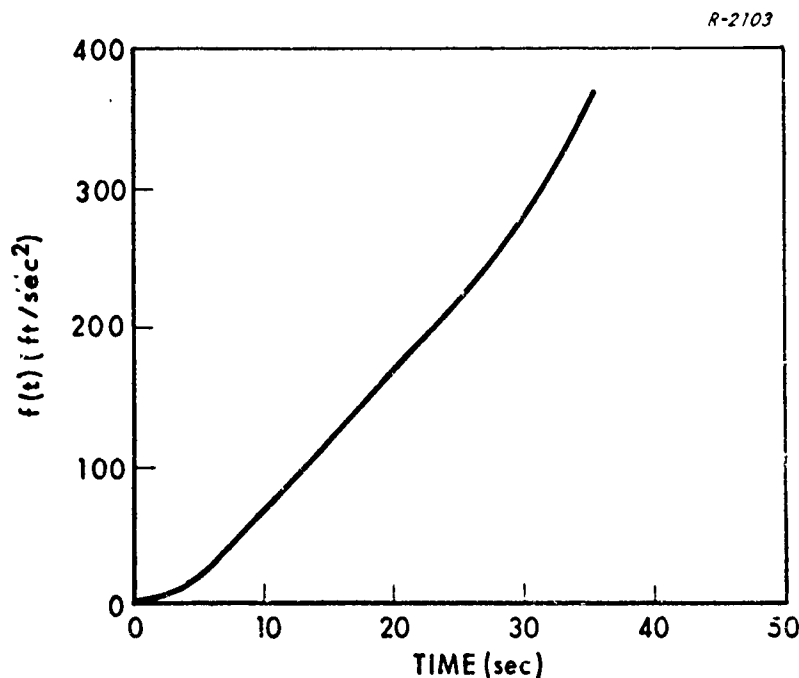


Figure 9.4-1 Magnitude Profile of Commanded Acceleration

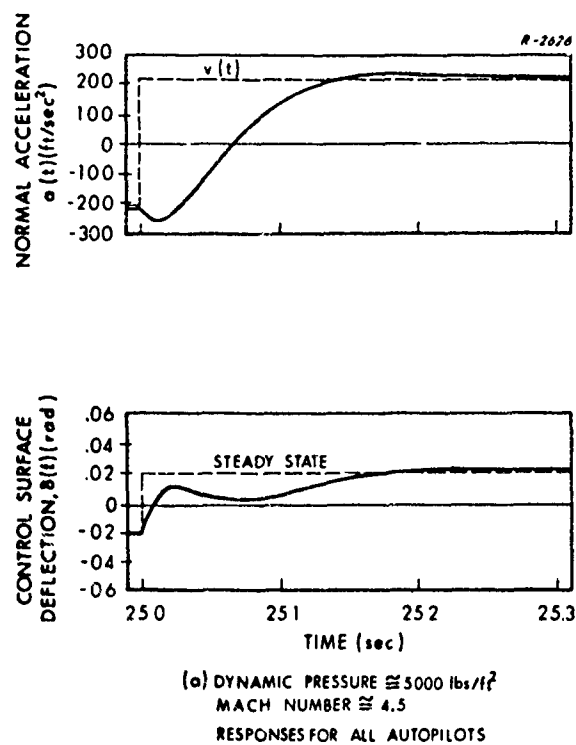
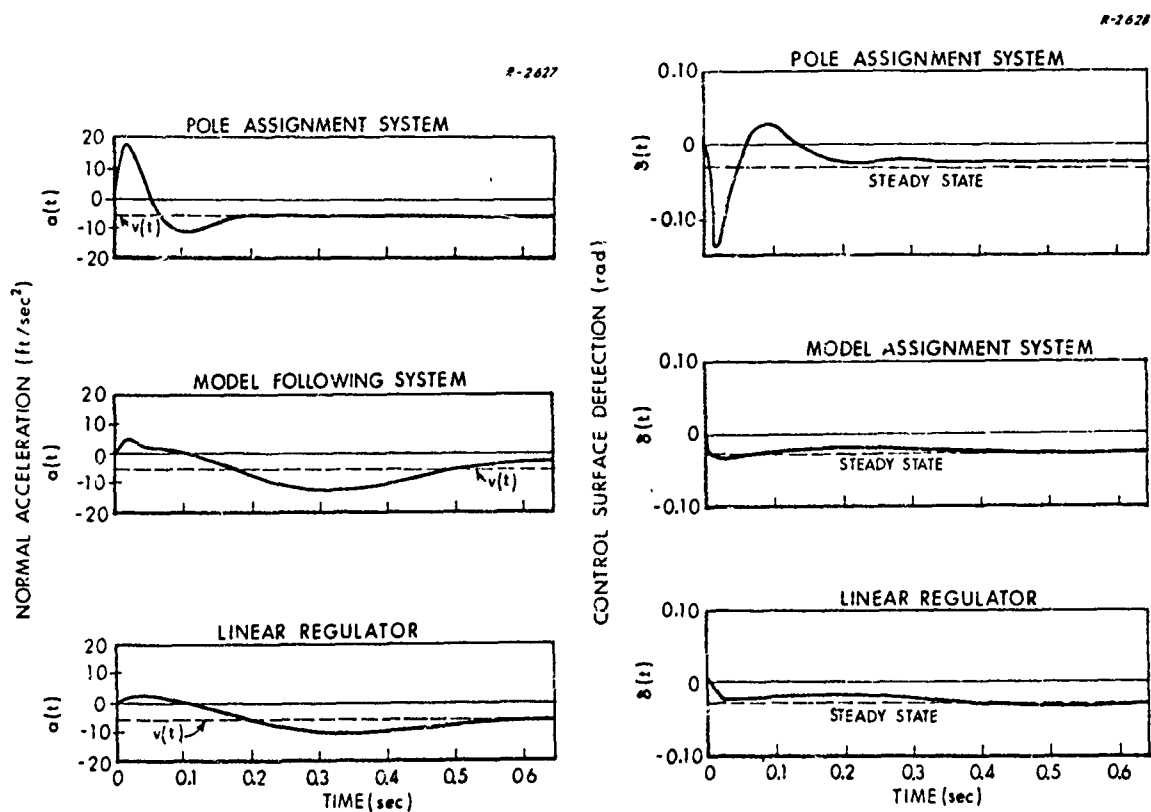


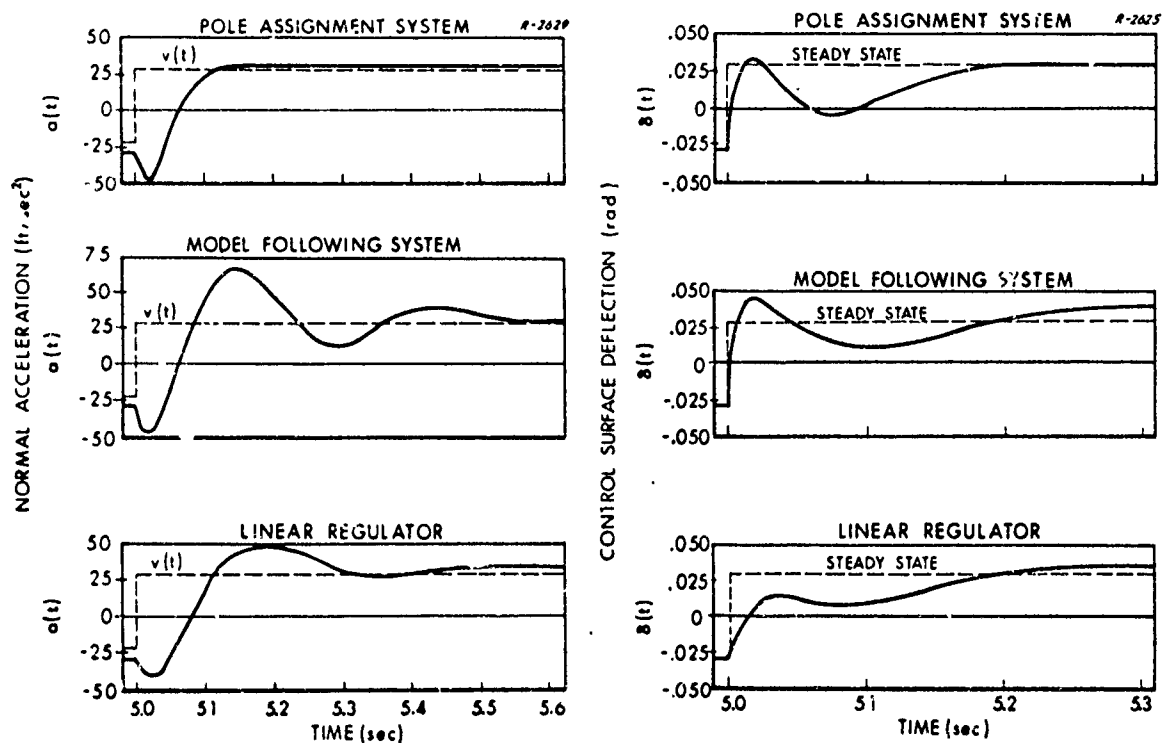
Figure 9.4-2 Autopilot Response Histories Along a Simulated Missile Trajectory for Three Adaptive Control Systems Using Explicit Plant Identification



(b) DYNAMIC PRESSURE  $\approx 300 \text{ lbs/ft}^2$   
MACH NUMBER  $\approx 0.45$

Figure 9.4-2 (Cont.)

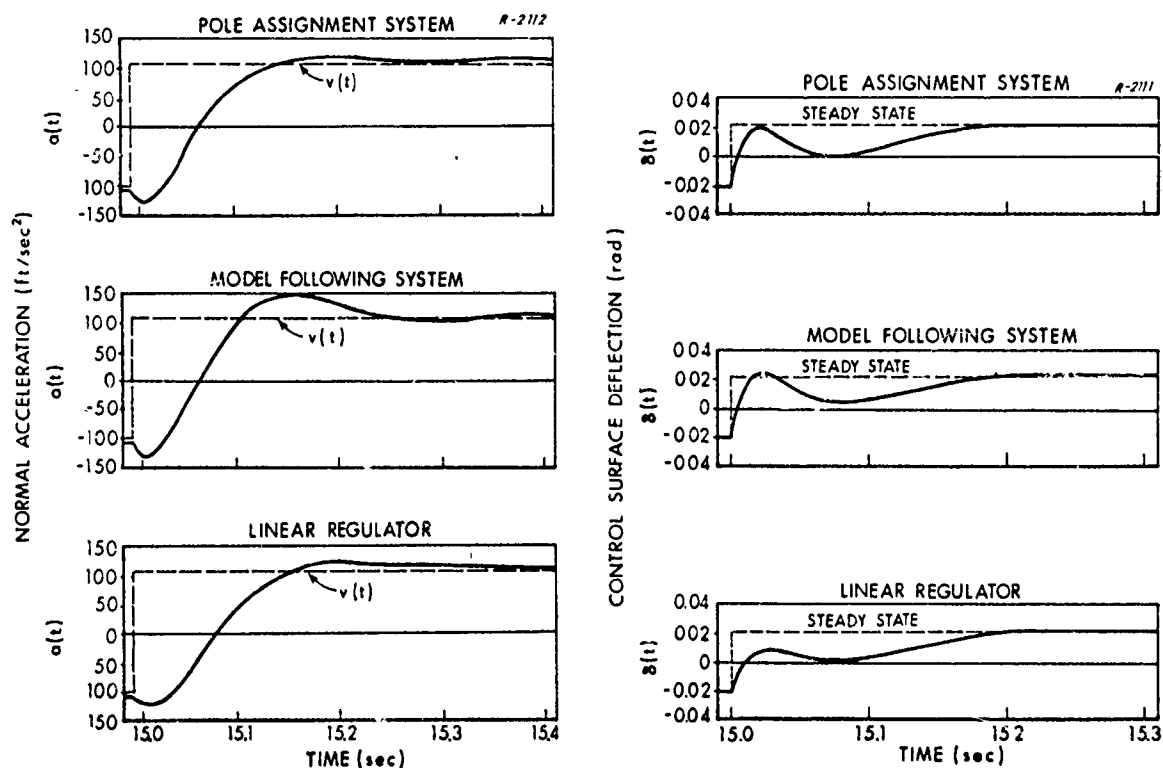
Autopilot Response Histories Along a Simulated Missile Trajectory for Three Adaptive Control Systems Using Explicit Plant Identification



(c) DYNAMIC PRESSURE  $\approx 1500 \text{ lbs/ft}^2$   
MACH NUMBER  $\approx 1.2$

Figure 9.4-2 (Cont.)

Autopilot Response Histories Along a Simulated Missile Trajectory for Three Adaptive Control Systems Using Explicit Plant Identification

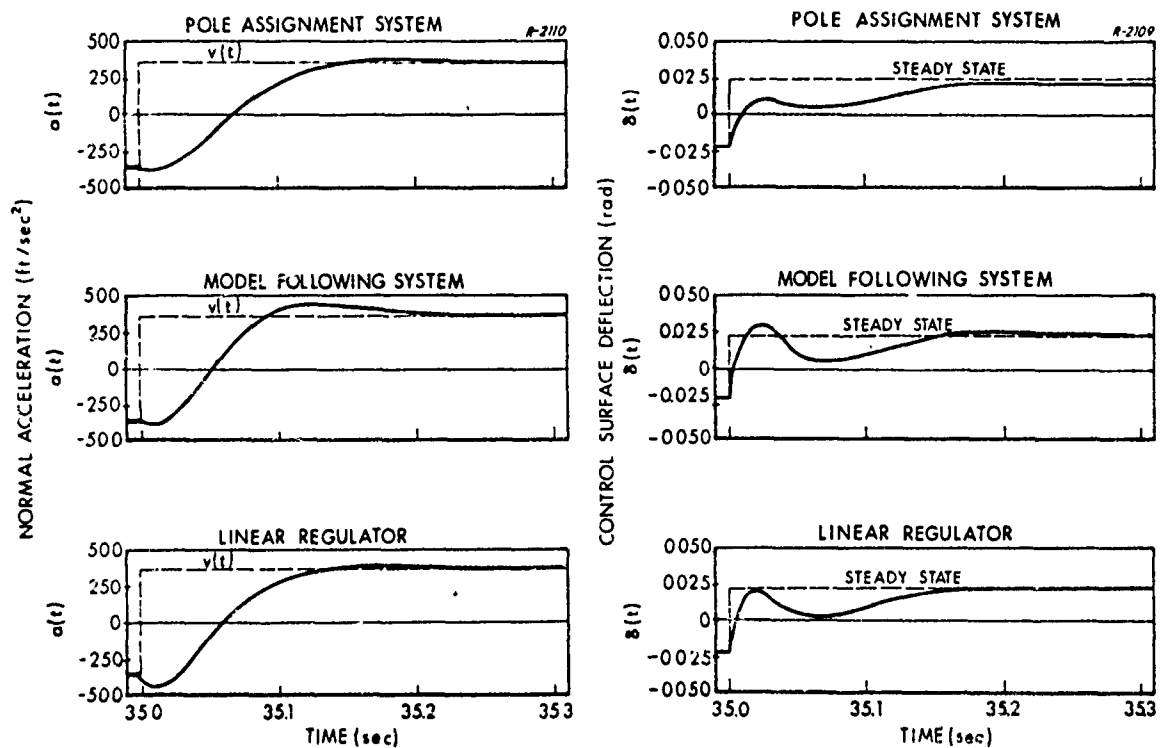


(d) DYNAMIC PRESSURE  $\approx 5000 \text{ lb}_s/\text{ft}^2$   
MACH NUMBER  $\approx 2.5$

Figure 9.4-2 (Cont.)

Autopilot Response Histories Along a Simulated Missile Trajectory for Three Adaptive Control Systems Using Explicit Plant Identification





(\*) DYNAMIC PRESSURE  $\cong 3600 \text{ lbs/ft}^2$   
MACH NUMBER  $\cong 4.5$

Figure 9.4-2 (Cont.)

Autopilot Response Histories Along a Simulated Missile Trajectory for Three Adaptive Control Systems Using Explicit Plant Identification

Recall that all three control methods are designed to give identical performance for the flight condition corresponding to  $t = 25$  seconds along the trajectory. Therefore on the interval  $25 \leq t \leq 26$ , the sets of time histories for  $a(t)$  and  $\delta(t)$  are identical as shown in Fig. 9.4-2(a), having negligible overshoot and a settling time of about 0.15 seconds. In Figs. 9.4-2(b) through (e),  $a(t)$  and  $\delta(t)$  are plotted at the beginning of several different one second intervals. At  $t = 0$  (Fig. (b)) when dynamic pressure and mach number are lowest, the greatest differences in response are observed among the three systems. The pole assignment method, which maintains constant closed loop pole locations throughout the trajectory, exhibits relatively large amplitude transient oscillations immediately after the command  $v(t)$  is applied. This behavior is caused by the fact that a relatively large change in angle of attack is required to produce a prescribed change in normal acceleration at this flight condition. Consequently in response to  $v(t)$  the control surface deflection must be relatively large, compared with its steady state value, to produce the required pitching moment and to compensate for the reduced control surface effectiveness. By contrast both optimal systems permit a much slower speed of response at this flight condition and consequently have smaller transient fluctuations. However, at the other times shown (Figs. (c) through (e)) the behavior of the pole assignment system is quite uniform without calling for excessive control surface deflection. As expected, the optimal system responses vary along the trajectory, generally becoming faster as dynamic pressure and mach number increase. Also they tend to exhibit some overshoot in acceleration, particularly in Fig. (c).

The conclusion from this demonstration is that the pole assignment method yields acceptable behavior over a wide range of flight conditions, excepting those where both mach number and dynamic pressure are lowest. The latter condition typically occurs just after launch, before the

missile has accelerated to its operating velocity. If one insists on a rapid response during the initial acceleration phase, the large transient pulse of acceleration in the wrong direction shown in Fig. 9.4-2(b) is physically unavoidable because of the required control surface deflection. To avoid excessive\* control surface deflections with the pole assignment technique the command input signal level must be kept low during this period. If nonuniform response characteristics can be tolerated during periods of low dynamic pressure and mach number, the adaptive optimal control techniques can be used to limit control surface deflections. However, as suggested in Section 9.1, the latter can also be accomplished by the pole assignment method, using different sets of poles (i.e., adaptive closed loop poles) for different ranges of flight conditions. This seems to be the preferred procedure in view of the fact that the optimal methods require more computer memory and more on-line computation for each recalculation of the adaptive gains.

The above observations are summarized in Table 9.4.1. Because the pole assignment technique has relatively low computational requirements it is considered to be the most promising. As suggested above, any requirement for variations in autopilot response characteristics can be accommodated by determining a few sets of closed loop poles,  $p_{m_i}$ ,  $i = 1, \dots, M$ , which are suitable for different flight regimes. The feedback gains are calculated adaptively according to Eq. (9.1-9). It is anticipated that only a few different sets of poles will be required in view of the generally good performance exhibited by the pole assignment method in Fig. 9.4-1.

---

\* In a practical situation there are limits on the allowable control surface deflection which the linear control system design techniques considered here do not take into account.

**TABLE 9.4-1**  
**COMPARISON OF ADAPTIVE CONTROL TECHNIQUES**  
**REQUIRING EXPLICIT PLANT IDENTIFICATION**

PERFORMANCE CRITERIA		MOST SATISFACTORY	LEAST SATISFACTORY
Computational Complexity	Programming Instructions, Storage, Amount of Computation per Gain Updating	Pole Assignment	Optimal Model Following System
	Number of Adaptive Gain Updatings Per Unit Time	Both Optimal Systems	Pole Assignment
Uniform Response Characteristics		Pole Assignment	Optimal Regulator
Control Level Required		Both Optimal Systems	Pole Assignment (Low Dynamic Pressure and Low Mach Number)

Optimal control techniques may be useful as an off-line design aid to determine suitable values for the closed loop poles. However, because the closed loop dynamics of adaptive optimal systems vary in an unknown fashion as plant parameters change, they are not as suitable for obtaining particular response characteristics as the pole assignment method. The added computational capability required to implement adaptive optimal methods is better devoted to estimating plant parameters as accurately as possible via the methods discussed in Chapter 6.

## 9.5 RAPIDLY VARYING PLANT PARAMETERS

In the preceding sections of this chapter, adaptive control techniques have been applied to a situation where plant parameters vary relatively slowly with respect to the response time of the closed loop control system. When missile flight conditions are changing very rapidly, as in dogfight applications, there is little theoretical justification for updating feedback gains by successively solving for the optimal control which minimizes the performance index in Eq. (9.2-2) or by determining those gains which maintain constant instantaneous closed loop poles as in Eq. (9.1-4). Nevertheless, these methods may still give satisfactory performance if the feedback gains are recomputed sufficiently often. In this section we demonstrate the autopilot acceleration response achieved by the pole assignment technique for the three second thrusting period of the trajectory given in Section H.1, during which time the missile's dynamic pressure changes by a factor of almost twenty.

Two sets of closed-loop poles are selected for the airframe:

$$p_{m_1} = \begin{bmatrix} -50.0 \\ -2.8 + j4.3 \\ -2.8 - j4.3 \end{bmatrix}; \quad p_{m_2} = \begin{bmatrix} -50.0 \\ -5.3 + j5.1 \\ -5.3 - j5.1 \end{bmatrix}$$

The set  $p_1$  is used in the interval  $4 \leq t < 6$  and  $p_2$  in the interval  $6 \leq t \leq 9$ . This design permits controlled variation in the response characteristics to allow for the changing effectiveness of aerodynamic control surfaces. The feedback gains  $h$  and the d-c gain  $k$  are computed forty times per second\* from Eqs. (9.1-9), (9.1-5), and (9.1-7) with  $a_m$ ,  $b_m$  and  $c_m$  determined by equating coefficients in the expression

\* Satisfactory behavior was also observed with twenty gain recomputations per second; however ten per second led to instability.

$$s^2 + a_m s + b_m = (s - p_{i1})(s - p_{i2})(s - p_{i3})$$

where  $p_{ij}$  is the  $j^{\text{th}}$  element of  $\underline{p}_{mi}$ . A piecewise constant input command

$$v(t) = \pm 16.0 \text{ ft/sec}^2$$

was applied, with the sign switched at one second intervals.

The acceleration response and the control surface deflection for the airframe control system are displayed in Fig. 9.5-1. Control surface deflection is plotted in terms of the normalized quantity\*

$$\bar{\delta} = |\delta|^{1/2} \text{sign}(\delta)$$

The curves indicate that the acceleration settles close to the commanded value in an interval equal to about three of the time constants associated with the dominant complex poles of  $\underline{p}_{m1}$  and  $\underline{p}_{m2}$ . During the first part of the trajectory, a large transient acceleration having an algebraic sign opposite to that of  $v(t)$  is produced by the control surface. This is another example of the behavior observed in Figs. 9.4-2(b) and (c). For this simulation the peak deflection required in Fig. 9.5-1(b) far exceeds the linear range of any missile control surface. Therefore in order to actually achieve the acceleration response time shown in the interval  $4.0 \leq t \leq 6.0$ , a much lower level of  $v(t)$  is required. Thus one concludes that this particular missile has little capability for following steering commands during the first part of its thrusting phase.

---

\* This normalization is defined to provide a convenient scale in Fig. 9.5-1.

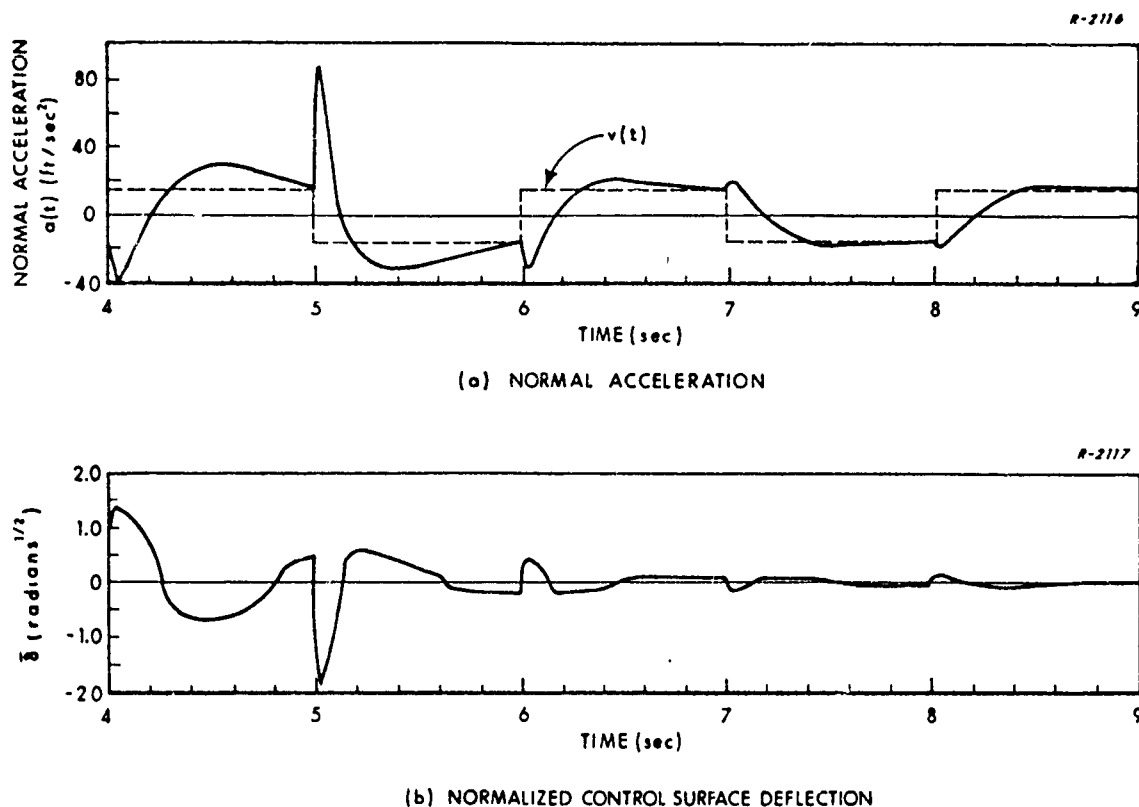


Figure 9.5-1 Response Characteristics While Airframe Parameters are Varying Rapidly: Autopilot Designed Using Pole Assignment Technique With Adaptive Closed Loop Poles

A more positive conclusion about the above simulation is that the airframe is successfully stabilized by the pole assignment method if the feedback gains are computed sufficiently rapidly and if the called for control levels are within the missile's capability. In other words, the instantaneous autopilot closed loop poles provide a good indication of the response characteristics, even though the airframe parameters vary a large amount in a period that is short with respect to the desired autopilot response time. Furthermore, these results have a strong bearing on the parameter identification procedure used to obtain  $\hat{a}$ . In this particular thrusting missile, parameter estimates must be obtained at a rapid rate --

on the order of twenty times per second. Further investigation is needed to determine which identification technique is best suited to meet this requirement. We have pointed out that the basic parameter identification technique described in Section 6.3 has the potential for generating estimates very rapidly.

## 9.6 SUMMARY AND CONCLUSIONS

Three methods of adaptive control which utilize explicit estimates of plant parameters have been evaluated for a missile autopilot. Each one operates on the principle of updating a set of feedback gains, assuming that the plant parameters remain constant at their estimated values for all future time, so that the instantaneous system closed loop poles provide an indication of the airframe response characteristics. The most promising method -- both in terms of mechanization and ability to provide uniform response characteristics -- is the pole assignment technique.

Each adaptive method is theoretically justifiable so long as plant parameters vary slowly compared with the desired airframe response. In a dogfight application this condition does not hold; however, the simulation results in Section 9.5 indicate that the pole assignment technique can still provide a stable autopilot, within the capability of the control surfaces. At low velocities, moderate acceleration steering commands and a rapid autopilot response can require control levels that exceed the bounds imposed by constraints on aerodynamic control surface deflections. To improve the control capability at low velocities, one of the alternative missile designs discussed in Section 8.4.2 may be attractive.



An important topic for additional study is an evaluation of parameter identification techniques for missile applications including the effects of noisy measurements. There is a special need to determine which methods can accomplish the extremely rapid parameter estimation required for thrusting missiles. In addition, it is worthwhile considering how to effectively utilize a priori information that may be available -- such as a known thrust level, a known launch altitude, etc. -- to determine air-frame parameters. These topics are beyond the scope of this report but they should be the subject of future investigation.

## 10. APPLICATIONS: LOW SENSITIVITY CONTROL SYSTEMS

In Chapter 7 a number of techniques useful for designing control systems that are insensitive to plant operating conditions have been described. Those methods which have the capability to desensitize the system to wide ranges of parameter variations are best suited for tactical missiles. In this chapter one such design procedure -- the Liapunov synthesis technique described in Section 7.4 -- is evaluated for a pitch rate autopilot having time-varying airframe dynamics. It is demonstrated that this method has the capability to null the difference between the outputs of the autopilot and a reference model.

### 10.1 DESIGN PROCEDURE

As described in Section 7.4, the Liapunov synthesis technique for designing an insensitive control system is similar to the Liapunov synthesis technique for an adaptive controller developed in Section 4.4.3. In fact the design steps are identical up to the point of defining a Liapunov function and selecting the control law. Consequently this discussion of an insensitive pitch rate autopilot parallels the first portion of Section 8.3.1; the latter material is repeated here for completeness.

Let the input-output relations for the design problem be represented by Fig. 10.1-1 in analogy with Fig. 8.3-1. To design an insensitive nonadaptive controller we proceed as in Eqs. (8.3-1) through (8.3-7). In Laplace transform notation the equations of motion for the plant and the model are

R-1987

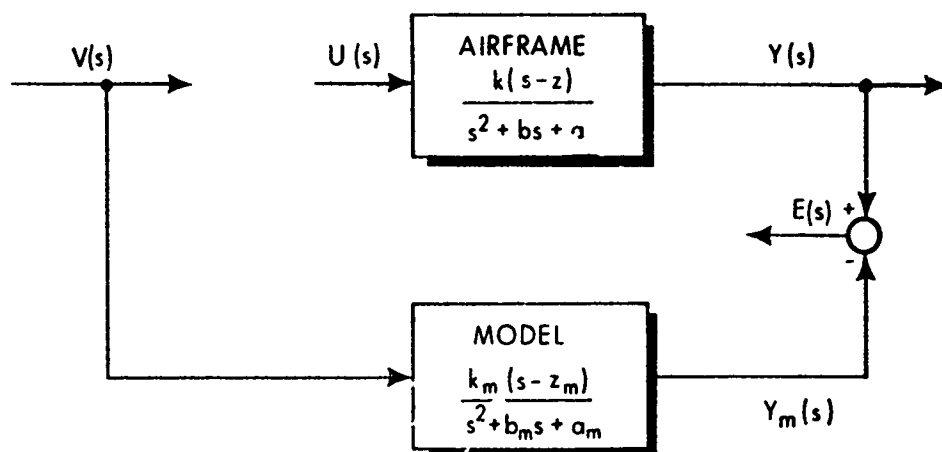


Figure 10.1-1 Plant-Reference Model Input-Output Relations for a Low Sensitivity Control System

$$\begin{aligned}
 (s^2 + bs + a)Y(s) &= k(s-z)U(s) \\
 (s^2 + b_m s + a_m)Y_m(s) &= k_m(s-z_m)V(s) \\
 E(s) &= Y(s) - Y_m(s)
 \end{aligned}
 \tag{10.1-1}$$

Subtracting these expressions and adding the quantity

$$(s^2 + b_m s + a_m)Y(s)$$

to both sides of the result produces the error equation

$$(s^2 + b_m s + a_m)E(s) = ((b_m - b)s + a_m - a)Y(s) + k(s-z)U(s) - k_m(s-z_m)V(s)
 \tag{10.1-2}$$

which is identified with Eq. (7.4-4).

Now we divide both sides of Eq. (10.1-2) by the polynomial

$$p_c(s) = s - p_1$$

where  $p_1$  is a negative number whose allowed range of values is to be determined presently. The result, after carrying out the required number of steps in dividing by  $p_c(s)$ , is

$$\begin{aligned} (s + b_m + p_1) E(s) = & - \left[ \frac{a_m + p_1(b_m + p_1)}{s - p_1} \right] E(s) + (b_m - b) Y(s) \\ & + \left[ \frac{a_m - a + p_1(b_m - b)}{s - p_1} \right] Y(s) + k U(s) \\ & + \frac{p_1 - z}{s - p_1} U(s) - \frac{k_m(p_1 - z_m)}{s - p_1} V(s) - k_m V(s) \quad (10.1-3) \end{aligned}$$

which has the same form as Eq. (7.4-5). Now for stability of the error signal we require that

$$b_m + p_1 > 0$$

on the left-hand-side of Eq. (10.1-3), or

$$p_1 > -b_m \quad (10.1-4)$$

This provides the condition needed on  $p_c(s)$ .

Referring to the right-hand side of Eq. (10.1-3) define new variables

$$\begin{aligned} Y_c(s) &= \frac{Y(s)}{s-p_1} & E_c(s) &= \frac{E(s)}{s-p_1} \\ U_c(s) &= \frac{U(s)}{s-p_1} & V_c(s) &= \frac{V(s)}{s-p_1} \end{aligned} \quad (10.1-5)$$

and vector quantities

$$\underline{\rho} \triangleq \begin{bmatrix} b_m - b \\ a_m - a + p_1(b_m - b) \\ p_1 - z \\ k_m(z_m - p_1) \\ -a_m - p_1(b_m + p_1) \end{bmatrix}; \quad \underline{f}(t) \triangleq \begin{bmatrix} y(t) \\ y_c(t) \\ u_c(t) \\ v_c(t) \\ e_c(t) \end{bmatrix} \quad (10.1-6)$$

Rewriting Eq. (10.1-3) in the time domain with the aid of Eqs. (10.1-5) and (10.1-6), produces a differential equation for the error in the form of Eq. (7.4-15),

$$\dot{e}(t) = - (b_m + p_1) e(t) + \underline{\rho}^T \underline{f}(t) + k u(t) - k_m v(t) \quad (10.1-7)$$

At this point the design procedure departs from that developed in Section 8.3 and continues as in Section 7.4, beginning with Eq. (7.4-16). A Liapunov function,

$$V(e) \triangleq \frac{1}{2} e^2 \quad (10.1-8)$$

is defined. Differentiating  $V$  and substituting for  $e(t)$  from Eq. (10.1-7) produces

$$\dot{V}(t) = -\left(b_m + p_1\right)e(t)^2 + \left[\underline{\rho}^T \underline{f}(t) + ku(t) - k_m v(t)\right]e(t) \quad (10.1-9)$$

To design a controller that is insensitive to variations in  $\underline{\rho}$  and  $k$ , choose the control  $u(t)$  in the form of Eq. (7.4-24),

$$u(t) = - \left[ \sum_{i=1}^5 \left| \frac{\rho_i}{k} \right|_{\max} |f_i(t)| + \left| \frac{k_m}{k} \right|_{\max} |v(t)| \right] \text{sign}(k) \text{sat}(e(t))$$

$$\text{sat}(e(t)) = \begin{cases} 1 & ; e > \epsilon \\ e/\epsilon & ; |e| \leq \epsilon \\ -1 & ; e < -\epsilon \end{cases}$$
(10.1-10)

where  $| \cdot |_{\max}$  denotes the maximum value of the argument over the range of allowable parameter variations. Observe that in addition to the ranges of parameter values, the sign of  $k$  must also be known in order to mechanize Eq. (10.1-10). Substitution for  $u(t)$  from Eq. (10.1-10) into Eq. (10.1-9) yields the following inequality for  $\dot{V}(t)$ :

$$\dot{V}(t) \leq -\left(b_m + p_1\right)e(t)^2; \quad |e(t)| > \epsilon \quad (10.1-11)$$

Using the definition of  $V$  in Eq. (10.1-8), the above inequality can be rewritten as

$$\dot{V}(t) \leq -2\left(b_m + p_1\right)V(t); \quad |e(t)| > \epsilon$$

Therefore it is inferred that

$$V(t) \leq V(0) \exp \left[ -2\left(b_m + p_1\right)t \right]; \quad |e(t)| > \epsilon \quad (10.1-12)$$

or, equivalently

$$e(t)^2 \leq e(0)^2 \exp \left[ -2 (b_m + p_1) t \right]; \quad |e(t)| > \epsilon \quad (10.1-13)$$

Consequently, by choosing  $p_1$  in Eq. (10.1-3) so that the quantity  $(b_m + p_1)$  is positive (as already required by Eq. (10.1-4)) and with knowledge of the ranges of plant parameter variations and the algebraic sign of the plant gain  $k$ , a controller can be designed which forces  $e(t)$  to the set of values,

$$|e(t)| \leq \epsilon \quad (10.1-14)$$

exponentially. Furthermore if the output error is initially less than  $\epsilon$ , Eq. (10.1-14) is always satisfied; that is, the error always remains below the saturation level. A block diagram of the control system is shown in Fig. 10.1-2. The choice of  $\epsilon$ , which specifies the saturation characteristics defined in Eq. (10.1-10), is determined by jointly considering the effects of system bandwidth and the error bound provided by Eq. (10.1-14). The former increases and the latter decreases as  $\epsilon$  decreases. In practice it is found that the error remains significantly less than  $\epsilon$  because the nonlinear gain term (in brackets) in Eq. (10.1-10) is usually conservatively large. This behavior is subsequently demonstrated in simulation results.

Before presenting simulation results it is worthwhile interpreting Eq. (10.1-10) in a way that leads to a less complicated, more familiar type of control law. The expression for  $u(t)$  can be viewed simply as a nonlinear gain multiplying a nonlinear function of the error, viz.,

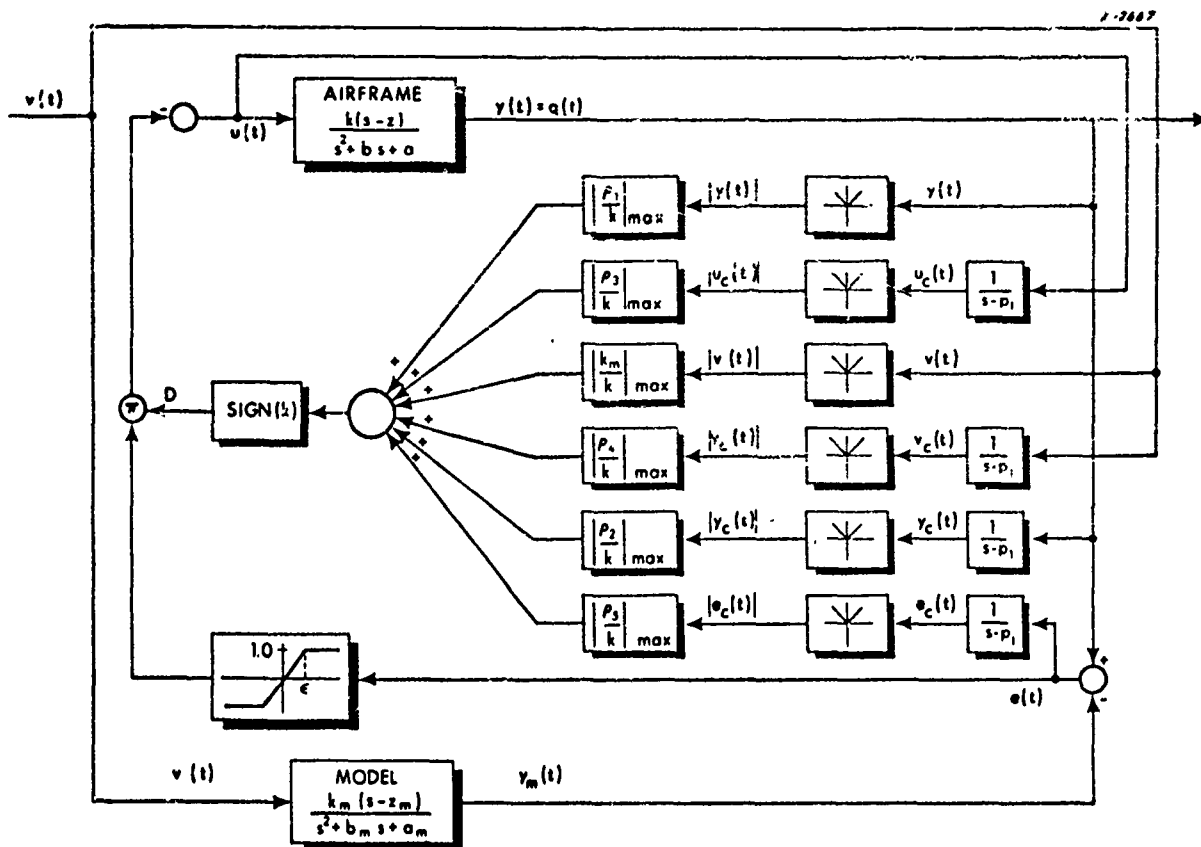


Figure 10.1-2 Mechanization of Insensitive Controller Based on Liapunov Design Procedure

$$u(t) = -D(\underline{f}(t), v(t)) \text{ sat}(e(t))$$

$$D(\underline{f}(t), v(t)) = \left[ \sum_{i=1}^5 \left| \frac{\rho_i}{k} \right|_{\max} |f_i(t)| + \left| \frac{k_m}{k} \right|_{\max} |v(t)| \right] \text{ sign}(k) \quad (10.1-15)$$

Disregarding the fact that  $D$  is a nonlinear function of the input and various system state variables, Fig. 10.1-2 can be redrawn much more simply as shown in Fig. 10.1-3. That is, the plant input  $u(t)$  is generated by passing the output error through a large saturating gain with drive (saturation) level



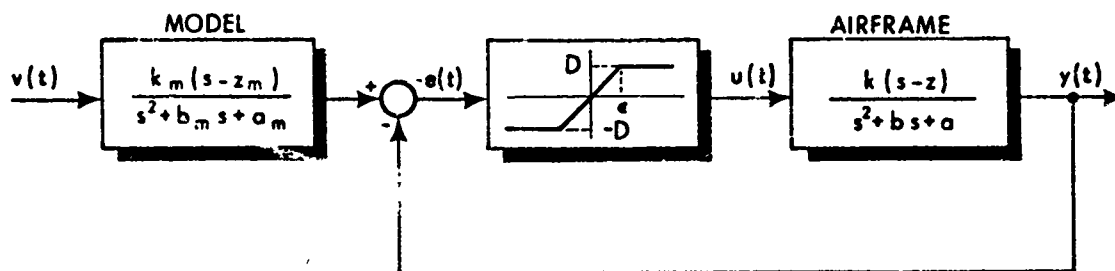


Figure 10.1-3 Alternative Representation for Fig. 10.1-2

$D(f(t), v(t))$ . Now the purpose of  $D$  in Eq. (10.1-15) is to make the second term on the right side of Eq. (10.1-9) sufficiently negative so that Eq. (10.1-11) holds. If it is conjectured that  $|f_1(t)|$  and  $|v(t)|$  always remain within known bounds, then it is possible to choose  $D$  constant and still obtain the desired stability properties. Such a control law is considerably simpler to mechanize than that given in Eq. (10.1-10). The performance of the system with a fixed value of  $D$  is compared with the control law in Eq. (10.1-15) in the simulation results reported below.

## 10.2 SELECTION OF PARAMETERS

For simulation purposes the airframe dynamics are taken from the trajectory data in Section H.1 with the actuator dynamics neglected. The dynamics of the reference model are taken from flight condition 6 in Table H.3. To implement the control law in Eq. (10.1-10), values for the quantities  $|\rho_1/k|_{\max}$  are required. Referring to Eq. (10.1-6) and the flight data in Table H.3 it follows that

$$\begin{aligned}
\left| \frac{\rho_1}{k} \right|_{\max} &= \left| \frac{b_m - b}{k} \right|_{\max} && \approx 1.5 \\
\left| \frac{\rho_2}{k} \right|_{\max} &= \left| \frac{a_m - a + p_1(b_m - b)}{k} \right|_{\max} && \approx 3.0 \\
\left| \frac{\rho_3}{k} \right|_{\max} &= \left| \frac{p_1 - z}{k} \right|_{\max} && \approx 3.0 \\
\left| \frac{\rho_4}{k} \right|_{\max} &= \left| \frac{k_m(z_m - p_1)}{k} \right|_{\max} && \approx 17.0 \\
\left| \frac{\rho_5}{k} \right|_{\max} &= \left| \frac{-a_m - p_1(b_m + p_1)}{k} \right|_{\max} && \approx 3.0 \\
\left| \frac{k_m}{k} \right|_{\max} &&& \approx 9.0
\end{aligned}$$

In addition, the saturation parameter  $\epsilon$  in Eq. (10.1-10) is assigned the value 0.01.

### 10.3 PERFORMANCE EVALUATION

To demonstrate the operation of the pitch rate control system illustrated in Fig. 10.1-2, a simulation of the autopilot was conducted with the airframe parameters fixed at values specified by flight condition 2 in Table H.1. In Fig. 10.3-1 the reference model response and the output error are plotted for a step input command. Except for the initial transient, the error is less than 2 percent of the model output. Furthermore the magnitude of the error is always considerably less than the theoretical upper bound of 0.01 specified by Eq. (10.1-14). This is to be

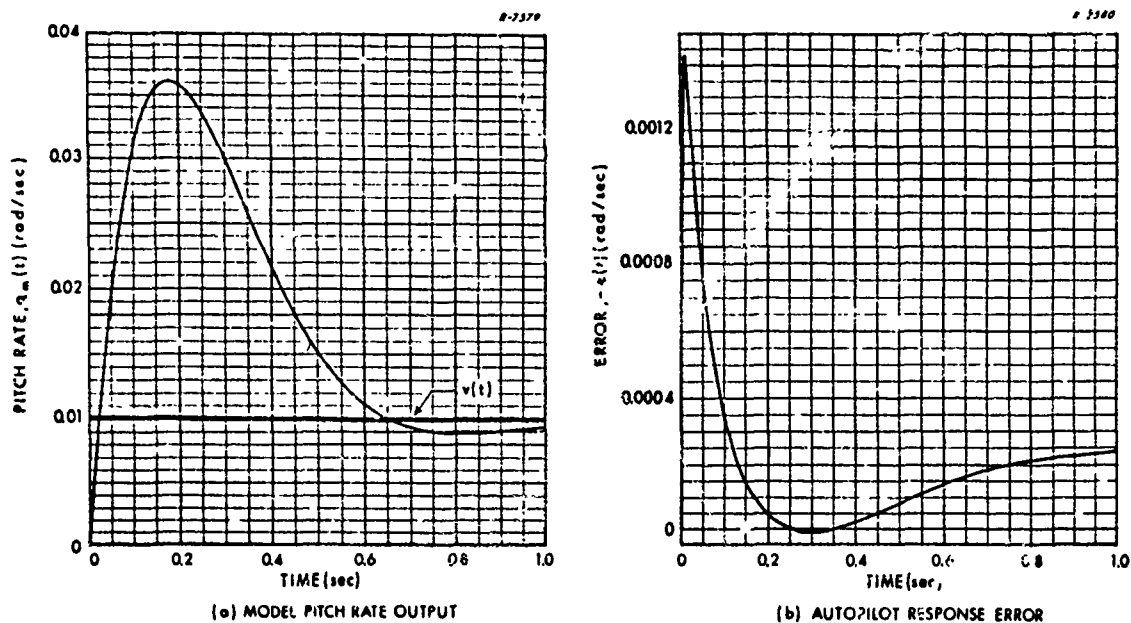
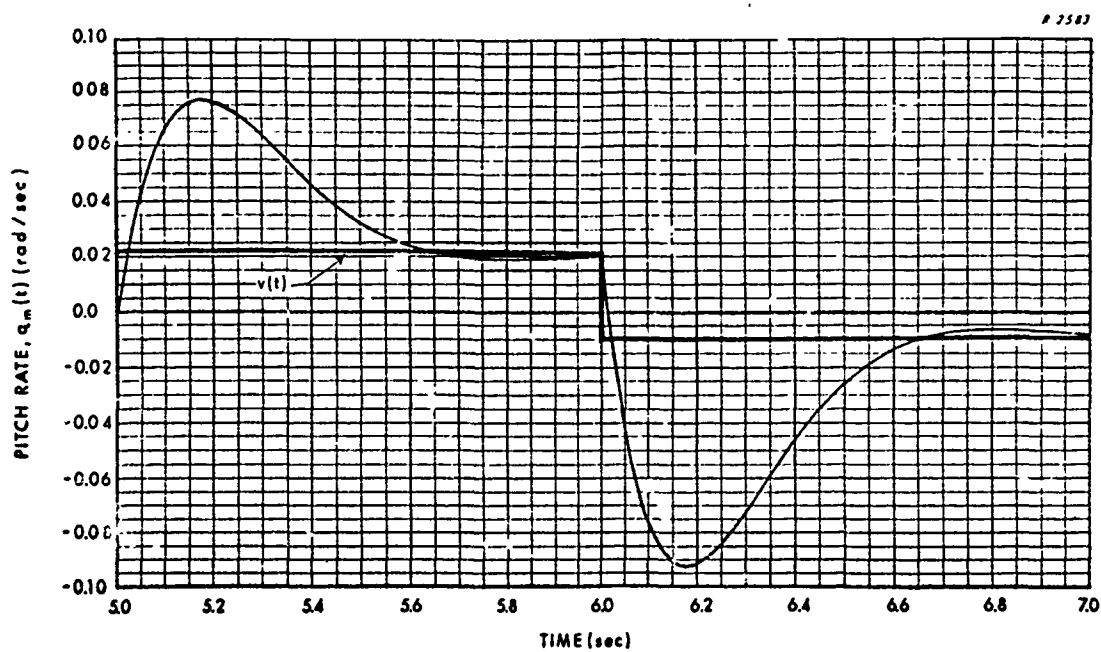


Figure 10.3-1 Step Response for the Pitch Rate Autopilot With a Time-Invariant Plant

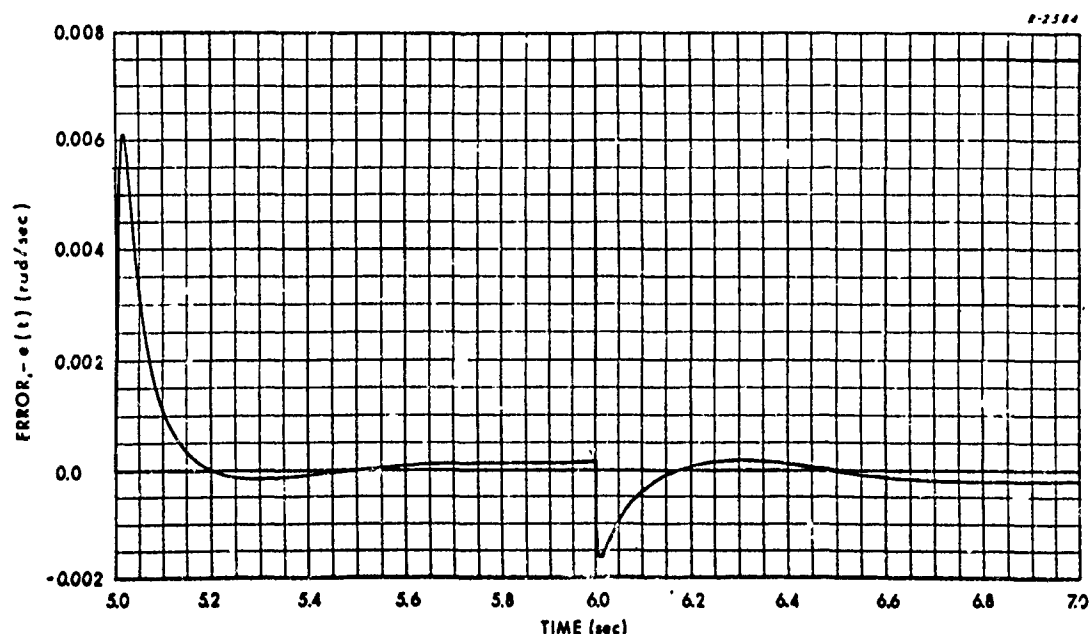
expected because the nonlinear gain  $D$  in Eq. (10.1-15) is conservatively large most of the time.

The behavior of this autopilot when parameters are time varying is illustrated in Fig. 10.3-2 for the first two seconds of thrusting flight (Table H.1), beginning in flight condition 1 at  $t = 5.0$  seconds. Both the pitch rate response of the reference model and the output error are shown. The latter is on the order of 1% of the former after an initial transient. Evidently the control system is quite capable of keeping the error small along such a trajectory.

The above performance compares favorably with that shown in Fig. 8.3-7 for the Liapunov adaptive design. However, against this advantage must be weighed the fact that Fig. 10.1-2 is basically a high gain design, as indicated in Fig. 10.1-3. Consequently higher order modes such as airframe structural vibrations may be excited and greater control levels are generally required.



(a) REFERENCE MODEL PITCH RATE OUTPUT



(b) AUTOPILOT RESPONSE ERROR

Figure 10.3-2 Step Response for the Pitch Rate Autopilot With a Time-Varying Plant

To compare the system in Fig. 10.1-2 with the case where the drive level of the nonlinearity in Fig. 10.1-3 is fixed, simulations were performed with  $D$  in Eq. (10.1-15) set equal to a constant. The results for two levels of  $D$  are presented in Fig. 10.3-3 for flight condition 2 in Table H.1; the airframe parameters and the input command have the same values as those used to generate Fig. 10.3-1. Evidently the use of a sufficiently large constant value of  $D$  gives performance which is comparable to the control law in Eq. (10.1-10). In these simulations the error never exceeds the linear range of the function  $\text{sat}(e(t))$  so the system operation remains linear. This controller configuration is much simpler to implement than that in Fig. 10.1-2; however the latter may have some operational advantage in that the nonlinear gain,  $D/\epsilon$ , becomes small when the signals in the system are small (see Eq. (10.1-15)), requiring a smaller control level.

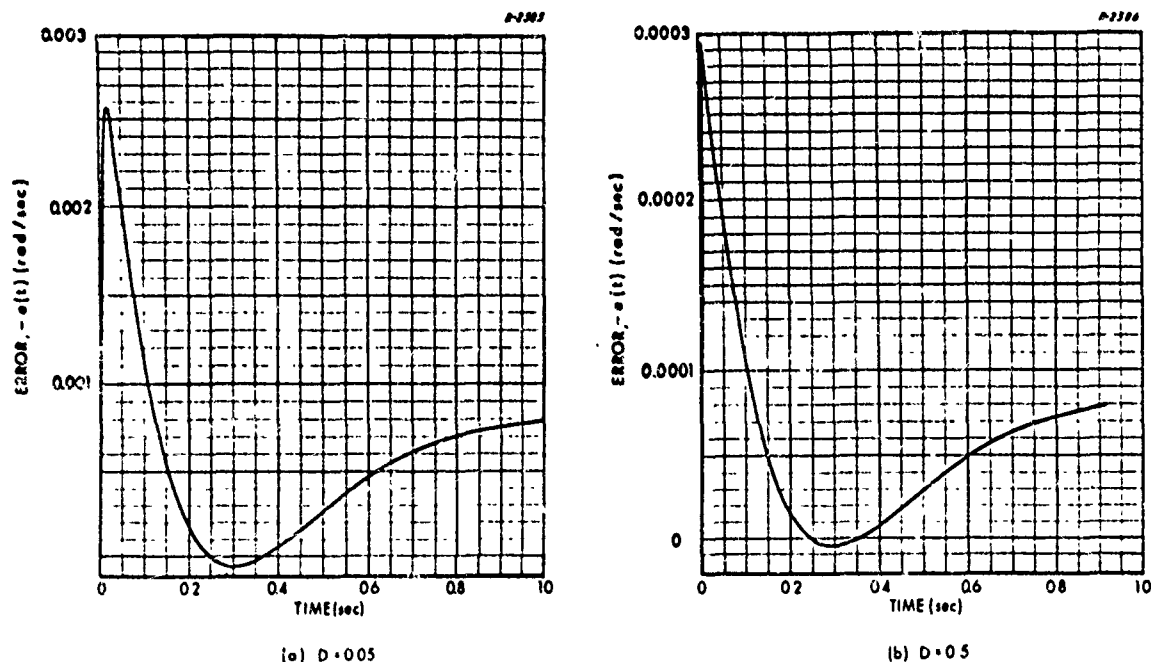


Figure 10.3-3 Autopilot Response for the Pitch Rate Autopilot With a Time-Invariant Plant and Constant Drive Level  $D$

## 10.4 SUMMARY AND CONCLUSIONS

The essential feature of the insensitive controller described in this chapter is that the system output error is passed through a saturating high gain element having a saturation level  $D$  that is a nonlinear function of variables generated by the plant and by various compensation networks. The system can be represented by Fig. 10.1-3 where  $D$  varies as prescribed in Eq. (10.1-15). Consequently, for an error signal that satisfies Eq. (10.1-14), the compensation operates essentially as a high gain with value  $D/\epsilon$ .

The use of high gain controllers is common practice for desensitizing a system to plant parameter variations, particularly for pitch rate and roll rate autopilots in aircraft and missile applications. As noted in Section 4.5, such techniques applied to autopilot design may be excessively sensitive to noise and may excite structural bending modes. The main contribution of the design approach evaluated here is that it generates the gain factor  $D$  as a nonlinear function of system variables such that the system has desired stability properties. Furthermore, if the signal levels are known to be bounded, the theory extends to the case where  $D$  is a sufficiently large constant.

As noted in Section 7.4 this design method is not suitable for nonminimum phase plants, for essentially the same reason given in Section 4.4.4. To make the output error small, the plant input  $u(t)$  must cancel the effect of any right-half-plane zeros, tending to make the system unstable. Consequently this technique is not directly applicable for achieving good normal acceleration response in tail-controlled missiles having fixed wings. However, using the artifice of an adaptive reference model in the same fashion described in Section 8.2.4, the system in

Figure 10.1-3 can be modified to provide adaptive normal acceleration response. This technique requires that enough plant parameters be identified so that the corresponding parameters in the reference model can be adjusted adaptively to yield a model pitch rate transfer function that corresponds to the desired normal acceleration response. For the application considered in this chapter, only a single plant zero,  $z$ , and the missile airspeed  $V$  need to be identified; the modification required to the control system in Fig. 10.1-3 is shown in Fig. 10.4-1. No simulation of this method is presented here.

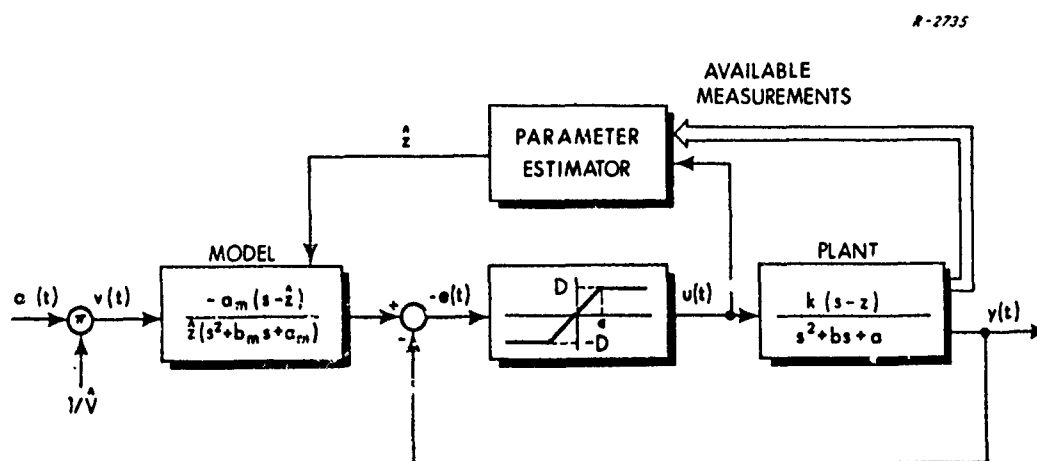


Figure 10.4-1 Adaptive Reference Model Configuration

PART IV  
GUIDANCE



11.            GUIDANCE SYSTEMS FOR TACTICAL MISSILES

The objective of guidance is to prescribe a steering law for the missile that will transfer it from the launcher to a target. To accomplish this task, different guidance laws may be used along different portions of the missile's trajectory, depending upon the information available, the maneuvers required, and the control mechanisms in use. For this discussion it is convenient to think of three distinctive guidance stages which can exist in a tactical mission; these are the post-launch, midcourse, and homing phases.

Post-launch guidance is concerned with the missile trajectory immediately after separation from the launcher. This stage includes any special maneuvers required (such as a 180 degree turn) to head the missile in the general direction of the target or to orient sensors so that they can acquire the target. For example, steering commands can be programmed in open loop fashion or provided by the launch vehicle during this phase of the trajectory.

Midcourse guidance is usually employed in a relatively long range mission. A midcourse guidance law is used to direct the missile to a region near the target, within which a homing sensor can provide accurate target information. An important requirement of this phase is a means for providing knowledge of missile position (e.g., inertial navigator, radio tracking, etc.) enroute to the target area. Midcourse guidance must be sufficiently accurate to enable the homing sensor to acquire the target.

Homing guidance is usually used during the final phase of missile flight. In a sense, this is the most critical period because steering actions taken during the last few seconds of flight have the most effect on

terminal miss distance. Overall mission success strongly depends upon having a homing sensor which provides accurate information about the target's location relative to the missile, and a steering law that is capable of achieving intercept in the presence of target maneuvers and measurement errors. Only the homing phase is treated in this chapter.

The chapter begins with a review of classical homing guidance techniques. The remainder concentrates on analyzing the accuracy of several homing guidance laws derived using techniques of optimal control theory to account for constant target maneuvers and autopilot dynamics. Graphs relating sensitivity of terminal accuracy and control effort expended to initial condition and measurement bias errors are presented. These curves aid in judging the relative performance capability of various designs; in particular they provide a quantitative comparison between optimal and suboptimal control techniques. The analysis presented here is essentially deterministic; it does not include measurement noise and randomly varying target maneuvers in the mathematical model of the guidance problem. As such, it provides a basis for making preliminary decisions about which guidance law is most appropriate. For a specific application further refinement of the conclusions obtained here should be made by investigating these random effects.

## 11.1 GUIDANCE EQUATIONS

For the purpose of guidance, the missile equations of motion are those which represent a point mass moving in three dimensions, acted upon by aerodynamic, gravitational, and thrust forces. To take the effect of the missile's rotational dynamics into account assuming the autopilot has already been designed, the airframe response is represented by some type

of transfer function. In addition to missile motion, the guidance equations must include the fact that the target is maneuvering (accelerating) in three dimensions. If accurate mathematical descriptions of all these factors are employed in formulating the guidance problem, the performance analysis for various steering laws is a difficult task. However, many of the essential features of the guidance problem can be studied by considering only planar motion of missile and target and by neglecting gravity and aerodynamic drag, as illustrated in Fig. 11.1-1. Furthermore it is assumed that both missile and target velocities,  $\underline{v}_m$  and  $\underline{v}_t$ , are constant in magnitude with variable directions that are controlled by lateral vehicle acceleration approximately normal to the velocity; losses of missile and target airspeed and/or altitude caused by maneuvers are neglected. For an aerodynamically controlled missile the above conditions imply the vehicle is in coasting flight with control forces provided by its lifting surfaces.

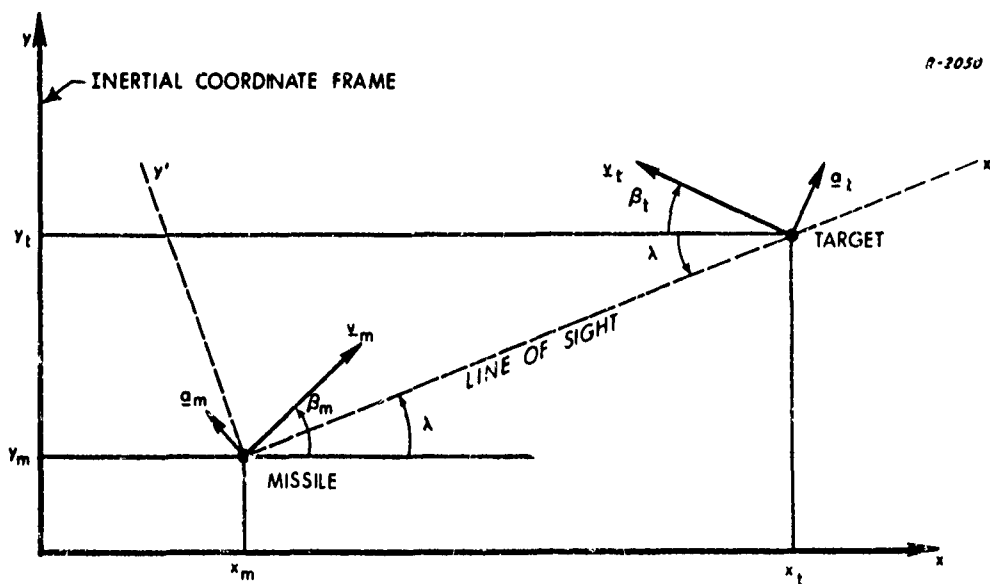


Figure 11.1-1 Definitions of Guidance Variables

With reference to Fig. 11.1-1 the missile equations of motion are

$$\begin{aligned}\ddot{x}_m(t) &= -a_m(t) \sin \beta_m(t) \\ \ddot{y}_m(t) &= a_m(t) \cos \beta_m(t) \\ \dot{a}_m(t) &= -\sigma a_m(t) + \sigma a_c(t) \\ a_m(t) &= v_m \dot{\beta}_m(t)\end{aligned}\tag{11.1-1}$$

where  $\sigma$  represents the pitch autopilot time constant associated with achieving a particular commanded normal acceleration and  $a_c(t)$  is the steering command. Similar expressions hold for the target:

$$\begin{aligned}\ddot{x}_t(t) &= a_t(t) \sin \beta_t(t) \\ \ddot{y}_t(t) &= a_t(t) \cos \beta_t(t) \\ a_t(t) &= v_t \dot{\beta}_t(t)\end{aligned}\tag{11.1-2}$$

To derive a feedback steering command some assumptions are required about target acceleration, and measurements of important state variables must be available. In addition the problem can be simplified if the nonlinear terms in Eqs. (11.1-1) and (11.1-2) are removed by appropriate linearizations. These tasks are accomplished in various ways, depending upon the particular guidance method used; specific details are given in subsequent sections for several homing guidance techniques.

## 11.2 HOMING GUIDANCE TECHNIQUES

A review of possible homing guidance methods naturally divides the subject into two categories -- those techniques which may be thought of as "classical", in the sense that they predate the development of modern control theory and those referred to as "optimal" which utilize more recently developed techniques for system design. In this section, a summary of the important features of these methods is presented.

### 11.2.1 Classical Homing Guidance Techniques

Three well known concepts for directing a missile during its homing phase are pursuit, beam rider, and proportional guidance (Refs. 133, 134, 135). The principles of each of these techniques are described here within the framework of Eqs. (11.1-1) and (11.1-2).

Pursuit Guidance -- One of the first ideas for guiding an interceptor vehicle was to point its velocity vector directly at the target. The implementation of this concept is the essential characteristic of pursuit guidance. In terms of the variables defined in Fig. 11.1-1, the objective is to turn the missile's velocity vector  $\underline{v}_m$  so that it lies along the line of sight -- i.e., achieve the condition,  $\beta_m = \lambda$ . The method of steering used to accomplish this task is to require that the commanded missile acceleration be given by

$$a_c(t) = -k \left( \beta_m(t) - \lambda(t) \right) \quad (11.2-1)$$

where  $k$  is an appropriate constant gain (Ref. 19).

An indication of the effectiveness of this steering command is obtained by assuming that the angles  $\beta_m(t)$  and  $\lambda(t)$  do not change very much during the homing phase and that their difference is small in magnitude. This allows the x-y coordinate axes in Fig. 11.1-1 to be chosen so that both angles remain small; e.g., define the x axis to be along the initial line of sight. Making the additional approximation that the effect of autopilot lag is negligible in Eq. (11.1-1) and using Eq. (11.2-1), one has

$$a_m(t) \cong a_c(t) = -k \left( \beta_m(t) - \lambda(t) \right) \quad (11.2-2)$$

The above assumptions permit our writing Eq. (11.1-1) as

$$\begin{aligned} \ddot{x}_m(t) &\cong -a_c(t) \beta_m(t) \\ \ddot{y}_m(t) &\cong a_c(t) \end{aligned} \quad (11.2-3)$$

To relate Eqs. (11.2-2) and (11.2-3), the small angle approximation is used in Fig. 11.1-1 to write

$$\begin{aligned} \beta_m(t) &\cong \frac{\dot{y}_m(t)}{\dot{x}_m(t)} \\ \lambda(t) &\cong \frac{y_t(t) - y_m(t)}{x_t(t) - x_m(t)} \end{aligned} \quad (11.2-4)$$

We now make the definitions

$$\gamma(t) \triangleq \beta_m(t) - \lambda(t) \quad r_{go}(t) \triangleq x_t(t) - x_m(t) \quad v_c \triangleq -\dot{r}_{go}(t) \cong \text{constant} \quad (11.2-5)$$

where  $r_{go}(t)$  is the range-to-go and  $v_c$  is the closing velocity. Remember that the objective of the guidance system is to drive  $\gamma(t)$  to zero. Differentiation of  $\gamma(t)$  in Eq. (11.2-5) with substitution from Eq. (11.2-2) through (11.2-5) and some algebraic manipulation produces a differential equation

$$\dot{\gamma}(t) = \left( \frac{v_m}{r_{go}(t)} - \frac{k}{v_m} \right) \gamma(t) - \frac{\dot{y}_t(t)}{r_{go}(t)} + \frac{\dot{x}_t(t)}{r_{go}(t)} \lambda(t) \quad (11.2-6)$$

where the approximation

$$v_m \cong \dot{x}_m(t)$$

is used, consistent with the small angle assumption.

If the target is stationary,  $\dot{x}_t(t) = \dot{y}_t(t) = 0$ . The range-to-go is given by

$$r_{go}(t) = r_{go}(0) - v_c t \triangleq v_c t_{go}$$

where  $t_{go}$  is the time-to-go until intercept. Consequently Eq. (11.2-6) becomes

$$\dot{\gamma}(t) = \left( \frac{v_m}{v_c t_{go}} - \frac{k}{v_m} \right) \gamma(t) \quad (11.2-7)$$

In this expression the coefficient of  $\gamma(t)$  contains a positive term which approaches infinity as  $t_{go}$  approaches 0. Therefore the differential equation for  $\gamma(t)$  becomes unstable just before intercept and  $\gamma(t)$  cannot be nulled. However, in practice it is possible to choose  $k$  sufficiently large so that the coefficient of  $\gamma(t)$  in Eq. (11.2-7) is negative until very near

intercept, yielding an acceptable terminal miss. This accounts for the satisfactory performance of pursuit guidance against surface targets (Ref. 19).

Against high velocity moving targets, the terms involving  $\dot{x}_t(t)$  and  $\dot{y}_t(t)$  in Eq. (11.2-6) are detrimental to the objective of driving  $\gamma(t)$  to zero. In addition, the path followed by the missile is not very efficient, as indicated in Fig. 11.2-1. For this reason pursuit guidance is not usually considered feasible against air targets (Ref. 23).

Beam Rider Guidance — The fundamental idea behind beam rider guidance systems is that the target is tracked by some type of active transmitter (e.g., a radar) external to the missile, often located in the launch vehicle (Ref. 133). The situation is depicted in Fig. 11.2-2. The missile is equipped with a sensor that provides a measure of the deviation of the missile from the beam centerline, e.g., the distance  $x$  in Fig. 11.2-2.

In order that the missile be directed toward the center of the beam, its lateral (commanded) inertial\* acceleration,  $z(t)$ , can be a linear function of  $x(t)$  and  $\dot{x}(t)$ , i.e.,

$$\ddot{z}(t) = -k_1 x(t) - k_2 \dot{x}(t) \quad (11.2-8)$$

In terms of the lateral acceleration,  $\ddot{y}(t)$ , of the beam we have

$$\ddot{z}(t) = \ddot{x}(t) + \ddot{y}(t) \quad (11.2-9)$$

---

\* Inertial acceleration (exclusive of the effects of gravity) is the quantity measured by the missile's sensors. Consequently the acceleration applied to control the missile is thought of as inertial although the quantity of interest is acceleration with respect to the beam.



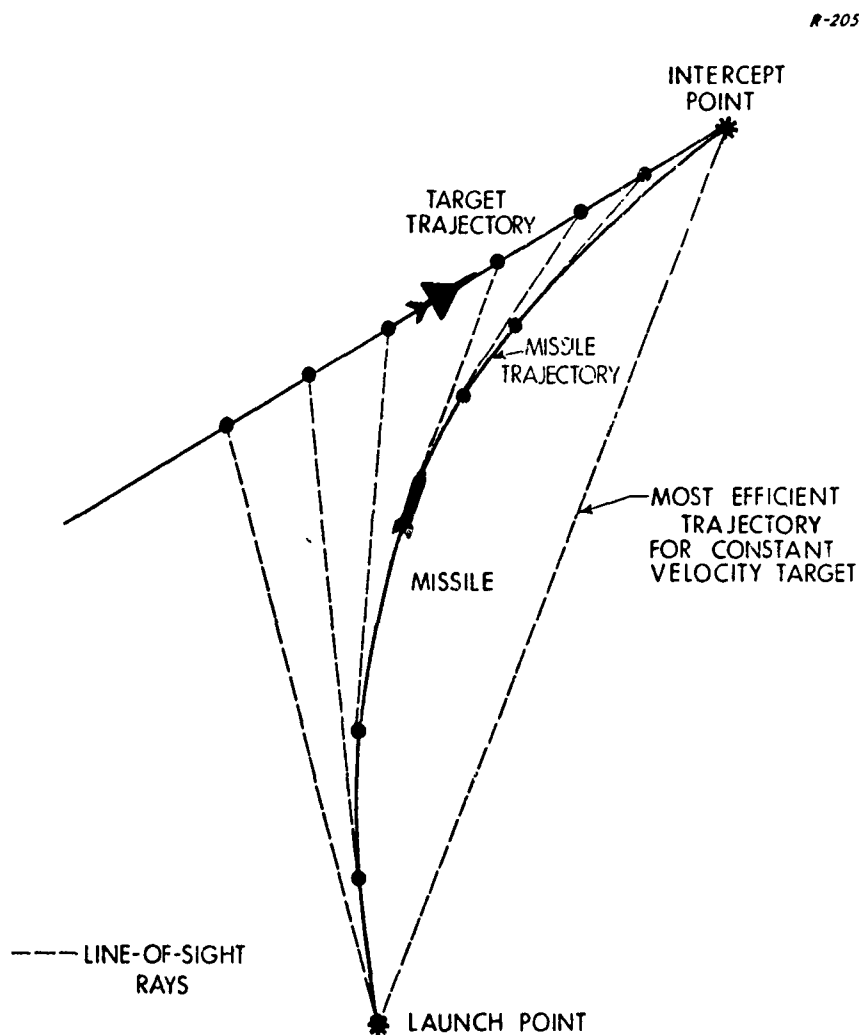


Figure 11.2-1 Pursuit Guidance Trajectory

As the missile approaches the target, the beam's acceleration is approximately equal to the component of target acceleration normal to the beam. If the latter is zero, then

$$\ddot{y}(t) \cong 0$$

and Eqs. (11.2-8) and (11.2-9) combine to yield

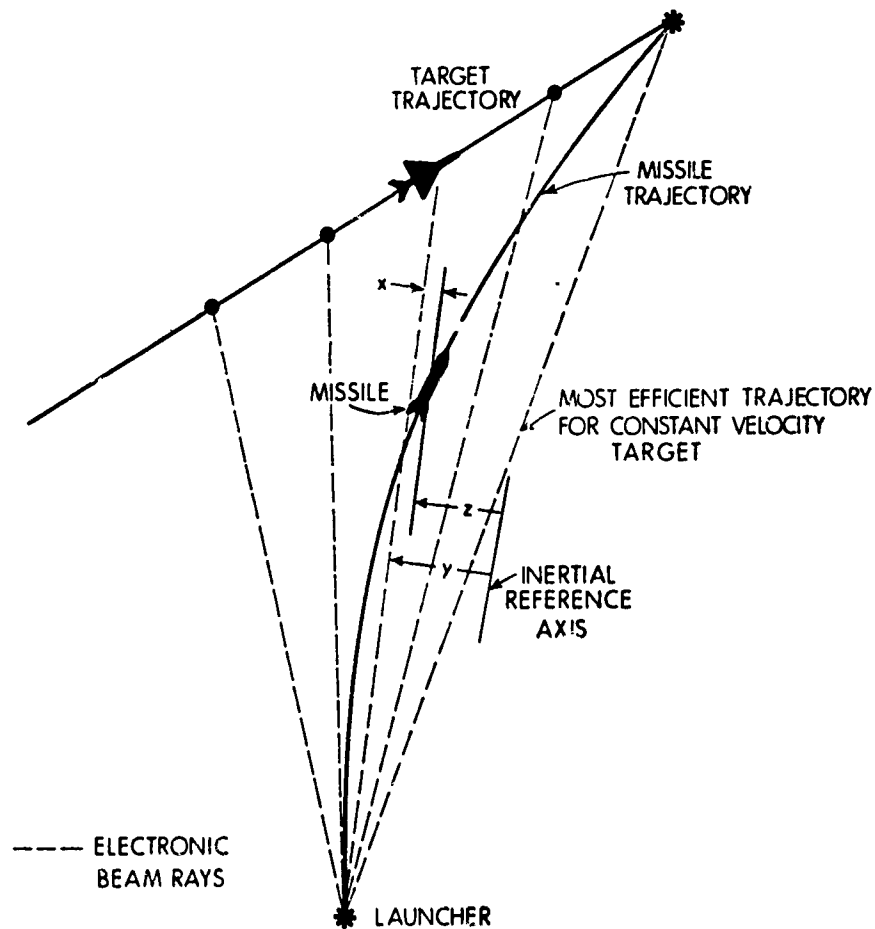


Figure 11.2-2 Beam Rider Guidance Trajectory

$$\ddot{x}(t) + k_2 \dot{x}(t) + k_1 x(t) = 0$$

(11.2-10)

Evidently both  $x(t)$  and  $\dot{x}(t)$  must be measured in order to have a damped response. Furthermore the damping must be sufficient so that  $x(t)$  is sufficiently close to zero by the time of intercept. As in the case of pursuit guidance, the missile does not follow the most efficient trajectory for a moving target.

The beam rider concept has the advantage that the missile need not have its own automatic target tracking mechanism. If it is launched within the radar beam, it is relatively easy to design a receiver for the missile that will tend to maintain a small distance  $x$  in Fig. 11.2-2. On the other hand, an objection for some applications is the dependence upon an external source to provide the beam. It is often desirable to have a self-contained system which frees the launcher vehicle from further guidance responsibility after firing the missile.

Proportional Guidance is an application of the principle that a collision course between two moving objects is one for which they approach each other at a constant relative bearing. In terms of Fig. 11.1-1 this means that the angular rate of the line of sight (LOS) is to be held at zero,

$$\dot{\lambda}(t) = 0$$

With reference to Fig. 11.2-3, this condition becomes

$$\dot{\phi}(t) + \dot{\theta}(t) = 0$$

The actual values of  $\dot{\phi}(t)$  and  $\dot{\theta}(t)$  can be measured with sensors to provide a measure of the deviation of line-of-sight rate from zero.

Assuming that this guidance scheme works well, the line-of-sight should not rotate very much along the intercept trajectory; hence for analysis purposes it is useful to define the relative coordinate system in Fig. 11.2-4. The x-axis of this coordinate frame is the LOS at the initial time,  $t = 0$ , and the rotation rate of the LOS is given by  $\dot{\lambda}(t)$ . Distance along the x axis is referred to as range-to-go,  $r_{go}$ . The steering law for proportional guidance dictates that an acceleration be applied normal to the LOS and proportional to  $\dot{\lambda}(t)$  in such a way as to reduce  $|\dot{\lambda}(t)|$ ; the conventional form of this relation is (Ref. 25)

R-2053

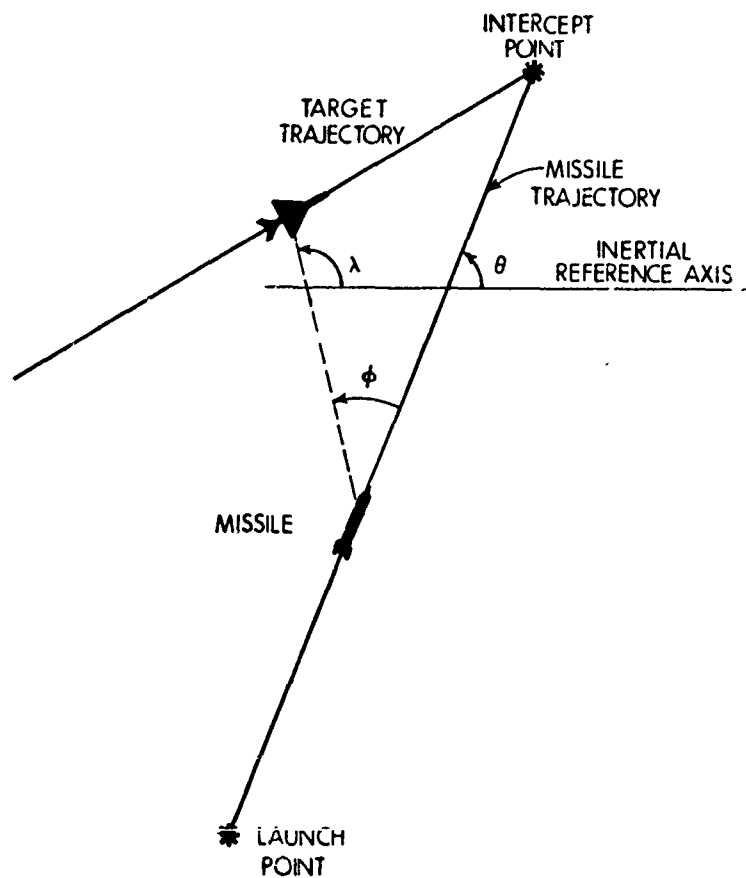


Figure 11.2-3 Proportional Guidance

$$\ddot{y}(t) = -\eta v_c \dot{\lambda}(t) \quad (11.2-11)$$

The quantity  $\eta$  is a constant of proportionality and  $v_c$  is the closing velocity (assumed constant in our analysis),

$$\dot{r}_{go}(t) \cong -v_c$$

The performance of this guidance law is ascertained by noting that for small  $\lambda(t)$ ,

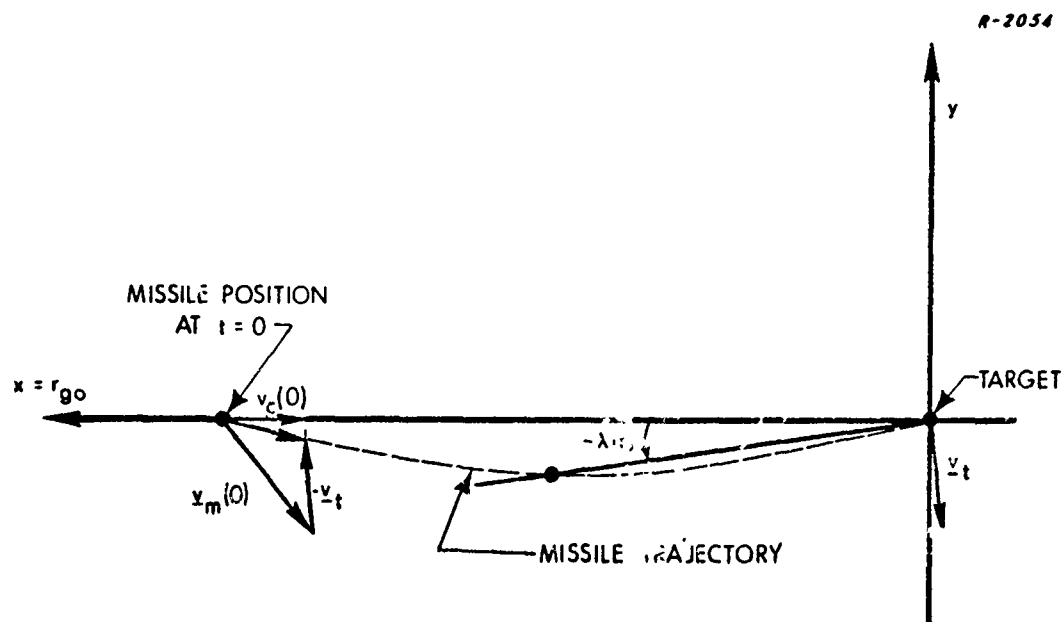


Figure 11.2-4 Relative Coordinate System in Proportional Guidance

$$\lambda(t) \approx \frac{y(t)}{r_{go}(t)} \quad (11.2-12)$$

Repeated differentiation of this expression with substitution from Eq. (11.2-11) yields

$$\ddot{\lambda}(t) = -\dot{\lambda}(t) \left( \frac{\eta - 2}{t_{go}} \right) \quad (11.2-13)$$

where

$$t_{go} = \frac{r_{go}(0)}{v_c} - t; \quad 0 \leq t \leq \frac{r_{go}(0)}{v_c}$$

The solution to Eq. (11.2-13) is

$$\dot{\lambda}(t) = \dot{\lambda}(0) \left( \frac{v_c}{r_{go}(0)} t_{go} \right)^{\eta-2} \quad (11.2-14)$$

Evidently  $\lambda(t)$  approaches zero with  $t_{go}$  if

$$\eta > 2$$

The conclusion is that if the constant of proportionality in Eq. (11.2-11) is large enough, this steering law does succeed in reducing the LOS rate (and hence also the terminal miss distance) to zero for a constant velocity target. Moreover, the missile's path in inertial space is nearly a straight line, which is the most efficient (minimum-time) trajectory against a nonmaneuvering target. Because of its ability to actually null the terminal miss and the simplicity of the acceleration command in Eq. (11.2-11), proportional guidance has been favored for use in most missile systems. Under the assumptions used in the foregoing analysis -- i. e., a constant velocity target with no autopilot lag -- good performance is achieved. However, as discussed in Chapter 3, the ability of a target to maneuver and the presence of autopilot dynamics do reduce terminal accuracy. This raises the question of whether such effects can be taken into account to derive a better steering law. In the next section, it is demonstrated that optimal control theory offers one means to this end.

### 11.2.2 Adaptive Optimal Guidance

To apply optimal control techniques to the design of missile guidance systems, the problem is mathematically described in terms of a set of first order differential equations. When the latter are linear and

a steering policy is sought which minimizes a quadratic performance index, one obtains a feedback steering law that is a linear function of the system state variables. In this manner desired performance characteristics can often be achieved by a design that is practical to implement in actual applications. Several optimal linear steering laws are described and evaluated in this and subsequent sections. The problem formulation is taken from Ref. (7).

The equations of motion for the guidance problem are obtained by consideration of Fig. 11.2-4. Just as in proportional guidance, it is assumed that the line-of-sight does not rotate very much from its initial position during the homing phase. The x-axis is the initial LOS. Because the range is decreasing at a relatively uncontrollable\* rate (i.e.,  $v_c$  is nearly constant), the principal variables of interest in Fig. 11.2-4 are  $y(t)$  and its time derivatives.

Problem Statement — We assume that the result of a positive command to the missile autopilot is acceleration along the negative y axis. Actually, the autopilot creates an acceleration vector that is approximately normal to the missile's velocity vector; any resulting acceleration component along the line-of-sight is being neglected. The autopilot dynamics are approximated by a first order lag,\*\* as in Eq. (11.1-1). In addition, we allow the possibility of the target's having a constant acceleration  $a_t$  normal to the LOS along the positive y-axis. With these specifications, a set of state variables can be defined as

---

\* It is tactically assumed that the missile has no capability for controlling its longitudinal thrust.

\*\* In Section 11.4 a higher order model is investigated which includes the right-half-plane zero associated with a tail-controlled missile.

$$\underline{x}(t) \triangleq \begin{bmatrix} x_1(t) \\ x_2(t) \\ x_3(t) \\ x_4(t) \end{bmatrix} \triangleq \begin{bmatrix} y(t) \\ \dot{y}(t) \\ a_t \\ a_m(t) \end{bmatrix} \quad (11.2-15)$$

and the differential equations of motion become

$$\begin{bmatrix} \dot{x}_1(t) \\ \dot{x}_2(t) \\ \dot{x}_3(t) \\ \dot{x}_4(t) \end{bmatrix} = \begin{bmatrix} 0 & 1 & 0 & 0 \\ 0 & 0 & 1 & -1 \\ 0 & 0 & 0 & 0 \\ 0 & 0 & 0 & -\sigma \end{bmatrix} \begin{bmatrix} x_1(t) \\ x_2(t) \\ x_3(t) \\ x_4(t) \end{bmatrix} + \begin{bmatrix} 0 \\ 0 \\ 0 \\ \sigma \end{bmatrix} a_c(t) \quad (11.2-16)$$

Because the autopilot dynamics are included in formulating the guidance problem -- i. e., the autopilot is predesigned -- we refer to this as a partially coupled set of guidance-autopilot equations. A completely coupled guidance-autopilot steering law, which incorporates missile airframe dynamics within the mathematical model, is investigated in Section 11.4.

For the purpose of guidance, it is desired that the terminal miss distance  $x_1(T)$  be made small within the capability of a limited amount of control  $a_c(t)$ . If unlimited acceleration were available, a zero miss distance could always be achieved in the absence of measurement errors. These considerations motivate the following choice for a quadratic performance index;

$$J = x_1(T)^2 + r \int_0^T a_c(t)^2 dt \quad (11.2-17)$$

where  $r$  is a positive weighting constant. The steering law is to be chosen such that  $J$  is minimized for a given value of  $T$ . The latter is assumed known from the relationship



$$T = \frac{r_{gc}^{(0)}}{v_c} \quad (11.2-18)$$

As we shall see, this problem formulation requires the existence of a capability for measuring range and range rate for implementing the resulting steering command.

The first term in  $J$  penalizes large values of terminal miss. The inclusion of the integral term,

$$J_u \triangleq \int_0^T a_c(t)^2 dt,$$

in the performance index has several objectives for a missile guidance application. First it tends to limit the peak normal acceleration output; this feature is required to prevent structural failure of the airframe. In addition, there are physical constraints on the maximum magnitude of the missile's control surface deflection. The latter saturates if the steering command is too large and the linear character of the autopilot dynamics is destroyed. Consequently the limitation on  $a_c(t)$  provided by minimizing  $J$  tends to keep the control surface deflection within required bounds. Missile maneuvers also require some expenditure of energy which ultimately results either in a loss of altitude or a loss of airspeed. These losses increase as the size of the integral term in  $J$  increases. Other energy consumption influenced by  $J_u$  is that required to drive the control surfaces. For a long trajectory, the continued presence of changing steering commands at the autopilot input can result in an appreciable drain on the actuator power supply; this effect is also limited by limiting the magnitude of  $a_c(t)$ . For all of the above reasons the integral term in Eq. (11.2-17) at least qualitatively regulates the actual control signals and control forces employed to reduce

the terminal miss distance. However it is emphasized that  $J_u$  is only an indirect measure of control surface deflection, actual normal acceleration, and energy losses.

Having specified a performance index, all of the remaining subjectivity in the design problem is contained in the parameter  $r$ . The larger its value, the heavier the penalty on the control relative to  $x_1(T)$ ; consequently the larger is the terminal miss. It should be chosen to provide an acceptable tradeoff between guidance accuracy and control effort.

The solution to the optimal control problem is derived analytically in Ref. 7. The optimal feedback steering law is given by:

$$\begin{aligned}
 a_{c_1}(t) &= -\underline{h}(t_{go})^T \underline{x}(t) & h_1(t_{go}) &= -\frac{\eta_1(t_{go})}{t_{go}^2} \\
 h_2(t_{go}) &= -\frac{\eta_1(t_{go})}{t_{go}} & h_3(t_{go}) &= -0.5 \eta_1(t_{go}) \\
 h_4(t_{go}) &= \frac{\eta_1(t_{go}) (\sigma t_{go} e^{\sigma t_{go}} - e^{\sigma t_{go}} + 1)}{\sigma^2 (e^{\sigma t_{go}} t_{go}^2)} \\
 \eta_1(t_{go}) &= \frac{6\sigma^2 t_{go}^2 (\sigma t_{go} - 1 + e^{-\sigma t_{go}})}{2\sigma^3 (3r + t_{go}^3) + 6\sigma t_{go} (1 - 2e^{-\sigma t_{go}}) - 6\sigma^2 t_{go}^2 + 3(1 - e^{-2\sigma t_{go}})} \\
 t_{go} &= T - t \cong \frac{r_{go}}{v_c}
 \end{aligned} \tag{11.2-19}$$

where  $h_i$  is the  $i^{\text{th}}$  element of  $\underline{h}$ . The feedback gains are written as functions of time-to-go rather than time. Because the range does not decrease exactly linearly with time, the value of  $t_{go}$  is not accurately predictable along the trajectory. However, given a capability for measuring range  $r_{go}$  and range rate  $(-v_c)$ ,  $t_{go}$  can be measured continuously and adaptively adjusted in the steering law, making this is an adaptive optimal guidance policy.

Aside from requiring some computational capability to implement the steering law, the above guidance policy assumes knowledge of all the system state variables; this is typical of feedback solutions to optimal control problems. At first sight, this requirement appears impractical because some of the states, defined in Eq. (11.2-15) are not readily available. In particular,  $x_1(t)$  and  $x_2(t)$  are position and velocity normal to an initial line-of-sight reference axis; neither of these quantities is easily measured. This situation can be improved if we differentiate Eq. (11.2-12) to obtain

$$\dot{\lambda}(t) \cong \frac{\dot{y}(t) r_{go}(t) - \dot{r}_{go}(t) y(t)}{r_{go}(t)^2} \quad (11.2-20)$$

Substitution for  $r_{go}(t)$  and  $\dot{r}_{go}(t)$  from Eqs. (11.2-5) and (11.2-19) produces

$$\dot{\lambda}(t) \cong \frac{1}{v_c} \left( \frac{y(t)}{t_{go}^2} + \frac{\dot{y}(t)}{t_{go}} \right) \quad (11.2-21)$$

Substitution of this expression into Eq. (11.2-19) to eliminate  $x_1(t)$  and  $x_2(t)$  yields a simpler, approximate steering law

$$a_{c_1}(t) \cong \eta_1 \left( t_{go} \right) v_c \dot{\lambda}(t) - h_3 \left( t_{go} \right) x_3(t) - h_4 \left( t_{go} \right) x_4(t) \quad (11.2-22)$$

The resemblance between the term dependent upon  $\dot{\lambda}$  and the steering law for proportional guidance, Eq. (11.2-11), is noteworthy. Its significance will be more evident presently.

Equation (11.2-22) is more easily mechanized than Eq. (11.2-19) because  $y(t)$  and  $\dot{y}(t)$  have been replaced by a more readily measured variable, the line-of-sight rate. The quantity  $x_4(t)$  is the missile's normal acceleration which can be measured by an accelerometer. The target's normal acceleration  $x_3(t)$  can be inferred by differentiating Eq. (11.2-20) to obtain

$$\ddot{\lambda}(t) = \frac{\ddot{y}(t)}{r_{go}} + \frac{2v_c}{r_{go}} \dot{\lambda}(t)$$

Using the fact that

$$\ddot{y}(t) = a_t - a_m(t)$$

one obtains

$$a_t = r_{go} \ddot{\lambda}(t) - 2v_c \dot{\lambda}(t) + a_m(t) \quad (11.2-23)$$

We have already postulated the capability to measure all quantities in Eq. (11.2-23) with the exception of  $\ddot{\lambda}(t)$ . The latter can be obtained by differentiating  $\dot{\lambda}(t)$ . The need to obtain angular acceleration of the line-of-sight

and to implement Eq. (11.2-23) makes  $a_t$  the most difficult state variable to estimate.

From Eq. (11.2-19) we can infer other optimal steering laws which neglect some of the dynamics in Eq. (11.2-16). In the limit of no autopilot lag ( $\sigma$  approaches infinity) the optimal control is

$$a_{c_2}(t) = \eta_2(t_{go}) \begin{bmatrix} \frac{1}{t_{go}^2} & \frac{1}{t_{go}} & 0.5 \end{bmatrix} \begin{bmatrix} x_1(t) \\ x_2(t) \\ x_3(t) \end{bmatrix}$$

$$\eta_2(t_{go}) = \frac{3t_{go}^3}{3r + t_{go}^3} \quad (11.2-24)$$

and use of Eq. (11.2-21) produces

$$a_{c_2}(t) \cong \eta_2(t_{go}) v_c \dot{\lambda}(t) + \frac{1}{2} \eta_2(t_{go}) x_3(t) \quad (11.2-25)$$

If both target acceleration and autopilot lag are neglected, the optimal steering law is

$$a_{c_3}(t) = \eta_2(t_{go}) \begin{bmatrix} \frac{1}{t_{go}^2} & \frac{1}{t_{go}} \end{bmatrix} \begin{bmatrix} x_1(t) \\ x_2(t) \end{bmatrix} \quad (11.2-26)$$

Again, substituting from Eq. (11.2-21),  $a_{c_3}(t)$  can be approximated as

$$a_{c_3}(t) \cong \eta_2(t_{go}) v_c \dot{\lambda}(t) \quad (11.2-27)$$

It is interesting to see what happens to Eq. (11.2-27) as the weighting  $r$  in the performance index goes to zero; i.e., from Eq. (11.2-24) it follows that

$$\lim_{r \rightarrow 0} a_{c_3}(t) = 3v_c \dot{\lambda}(t) \quad (11.2-28)$$

The right hand side of Eq. (11.2-28) is identical with the form\* of the proportional steering law, Eq. (11.2-11) with  $\eta = 3$ . In words Eq. (11.2-28) states that the classical proportional steering law with  $\eta = 3$  is the limit of the optimal law in Eq. (11.2-27) as the weighting on the control in the performance index approaches zero.

Steering law  $a_{c_1}(t)$  is optimal for minimizing  $J$  in Eq. (11.2-17) subject to Eq. (11.2-16);  $a_{c_2}(t)$  and  $a_{c_3}(t)$  are optimal when the equations of motion are modified to eliminate first autopilot lag and then both autopilot lag and target acceleration. However, we are concerned with the behavior of the state when all dynamics are present ( $\sigma < \infty$ ,  $a_t \neq 0$ ) and either  $a_{c_2}(t)$  or  $a_{c_3}(t)$  is used in place of the optimal control because the sensors or computation equipment required to implement  $a_{c_1}(t)$  may not be available. Consequently  $a_{c_2}(t)$  and  $a_{c_3}(t)$  are referred to as suboptimal steering laws.

Before making a decision to implement any of the steering laws derived above, one needs to know what sort of performance can be expected from each in the presence of all the effects included in Eq. (11.2-16) and

---

\* The minus sign is missing from Eq. (11.2-28) because of the definition of positive  $a_c(t)$  in Eq. (11.2-16).

also the influence of measurement errors. The purpose of the next section is to present a sensitivity analysis which determines the terminal miss caused by state variable initial conditions and measurement error biases for a range of values of the weighting parameter  $r$ . In addition, the measure of control effort

$$\int_0^T a_c(t)^2 dt,$$

is calculated for each case to provide an indication of the trade-off between terminal miss achieved and effort expended for a particular steering strategy.

### 11.3 STEERING LAW PERFORMANCE ANALYSIS

In this section we are interested in quantitatively evaluating the terms which define  $J$  in Eq. (11.2-17) for different linear steering laws applied to Eq. (11.2-16). In particular, the equations of motion have the form

$$\dot{\underline{x}}(t) = A\underline{x}(t) + \underline{b} a_{c_i}(t); \quad i = 1, 2, 3 \quad (11.3-1)$$

where

$$a_{c_i}(t) = -\underline{h}_i(t)^T \underline{x}(t) \quad (11.3-2)$$

and  $\underline{h}_i(t)$  is defined as follows -- using Eqs. (11.2-19), (11.2-24), and (11.2-26) and noting that  $t_{go} = T - t$ :

$$\begin{aligned}
\underline{h}_1(t) &\triangleq \underline{h}(T-t) \\
\underline{h}_2(t)^T &\triangleq -\eta_2(T-t) \begin{bmatrix} \frac{1}{(T-t)^2} & \frac{1}{T-t} & \frac{1}{2} & 0 \end{bmatrix} \\
\underline{h}_3(t)^T &\triangleq -\eta_2(T-t) \begin{bmatrix} \frac{1}{(T-t)^2} & \frac{1}{T-t} & 0 & 0 \end{bmatrix}
\end{aligned} \tag{11.3-3}$$

Therefore, for each steering law we can write Eq. (11.3-1) as

$$\begin{aligned}
\dot{\underline{x}}(t) &= A_i(t) \underline{x}(t); \quad i = 1, 2, 3 \\
A_i &\triangleq A - \underline{b} \underline{h}_i(t)^T \\
A &= \begin{bmatrix} 0 & 1 & 0 & 0 \\ 0 & 0 & 1 & -1 \\ 0 & 0 & 0 & 0 \\ 0 & 0 & 0 & -\sigma \end{bmatrix}; \quad \underline{b} = \begin{bmatrix} 0 \\ 0 \\ 0 \\ \sigma \end{bmatrix}
\end{aligned} \tag{11.3-4}$$

Associated with any steering law  $a_c(t)$  there is a value of the performance index for each missile trajectory, determined by the particular set of initial conditions and any state variable measurement errors that enter into the implementation of Eq. (11.3-2). We define

$$J_f \triangleq x_1(T)^2; \quad J_u \triangleq \int_t^T a_c(\tau)^2 d\tau \tag{11.3-5}$$

where  $J_u$  is referred to as the control effort expended or simply the "effort." Referring to Eq. (11.2-17), note that



$$J = J_f + rJ_u$$

where the lower limit of integration is changed from 0 to  $t$ , signifying that guidance can begin anytime prior to the intercept time  $T$ . Remember that the optimal value of  $J$  associated with Eq. (11.3-4) is achieved only when  $a_{c1}(t)$  is used as the steering command. Our purpose here is to compute  $x_1(T)$  and  $J_u$  for different trajectories using all three steering laws defined in Eqs. (11.3-2) and (11.3-3) and for different values of the weighting constant  $r$ .

### 11.3.1 Terminal Miss Sensitivity to Initial Conditions

Nonzero initial conditions on the state  $\underline{x}$  contribute to terminal miss and to the control effort expended; if  $\underline{x}$  were ever zero and the feedback steering command were perfectly implemented,  $a_c(t)$  would remain identically zero along the trajectory and both  $J_f$  and  $J_u$  in Eq. (11.3-5) would be zero. To economically determine the miss  $x_1(T)$  for a wide variety of trajectories, the adjoint techniques described in Section G.1 are helpful. There it is proved that the miss associated with Eq. (11.3-4) caused by initial conditions  $\underline{x}(t)$  for  $t \leq T$  is given by

$$\boxed{x_1(T) = \underline{\phi}_1(T, t)^T \underline{x}(t)} \quad (11.3-6)$$

where the sensitivity function,  $\underline{\phi}_1(T, t)$ , satisfies

$$\begin{aligned} \dot{\underline{\phi}}_1(T, t) &= -A_1(t)^T \underline{\phi}_1(T, t) \\ \underline{\phi}_1(T, T) &= \begin{bmatrix} 1 \\ 0 \\ \vdots \\ 0 \end{bmatrix} ; \quad i = 1, 2, 3 \end{aligned} \quad (11.3-7)$$

The sensitivity function is evaluated by integrating Eq. (11.3-7) (generally using a numerical method) backward in time. Once  $\varphi_i(T, t)$  is obtained and tabulated for any steering law  $a_{c_i}(t)$ , the effects of initial conditions at any initial time on terminal miss can be calculated.

The value of any element of  $\varphi_i(T, t)$  is the miss produced at time  $T$  by a unit initial condition at time  $t$  on the corresponding state and zero initial conditions on all the other state variables. For example, the terminal error produced by a unit velocity normal to the line of sight ( $\dot{y}(0) = 1.0$  ft/sec) is equal to  $\varphi_{i2}(T, 0)$  feet, where  $\varphi_{i2}(T, 0)$  is the second element of  $\varphi_i(T, 0)$  with units of ft/ft/sec. To introduce notation more suggestive of this property of the sensitivity function, we denote the normalized miss distance associated with the  $j^{\text{th}}$  element of  $\varphi_i(T, t)$  by  $\bar{m}_{ij}(T, t)$  where  $i$  refers to the particular steering law  $a_{c_i}(t)$  being employed. It is normalized by the units of  $\underline{x}(t)$ , as indicated by the over-bar notation.

Recall that the equations of motion for the optimal guidance problem are linearized about the initial line-of-sight. Therefore we can regard the initial value of  $y$  in Fig. 11.2-4 (hence also of  $x_1$  in Eq. (11.3-4)) as being zero. In addition, the initial value of the autopilot state  $x_4(t)$  represents an initial lateral acceleration of the missile at launch. If one exists, it is likely to be small and have relatively little effect upon terminal miss; therefore we consider  $x_4(0) = 0$  also. Consequently, the quantitative properties of  $\bar{m}_{i1}(T, t)$  and  $\bar{m}_{i4}(T, t)$  will not be displayed here.

At this point no sensitivity function has been defined for the line-of-sight rate  $\dot{\lambda}(t)$  in Eqs. (11.2-22), (11.2-25), and (11.2-27). If this state variable, rather than  $y(t)$  and  $\dot{y}(t)$ , is to be used in implementing the steering law, we are more interested in its associated normalized miss rather than that corresponding to an initial position and velocity normal to the

line of sight. To obtain this quantity, refer to Eq. (11.2-21) from which one can derive  $y(t)$  in terms of  $\dot{\lambda}(t)$  and  $\dot{y}(t)$ ,

$$y(t) \cong t_{go} \left( v_c t_{go} \dot{\lambda}(t) - \dot{y}(t) \right) \quad (11.3-8)$$

and define the normalized miss associated with  $\dot{\lambda}(t)$  to be  $\bar{m}_{15}(T, t)$ . Because Eqs. (11.2-19) and (11.2-22) are approximately equivalent mechanizations of the optimal steering command  $a_{c1}(t)$ , it follows that the terminal miss  $m$  caused by  $\lambda(t)$ ,  $y(t)$ , and  $\dot{y}(t)$  satisfies

$$\begin{aligned} m &= \bar{m}_{11}(T, t) y(t) + \bar{m}_{12}(T, t) \dot{y}(t) \\ m &= \bar{m}_{15}(T, t) \dot{\lambda}(t) \end{aligned} \quad (11.3-9)$$

Substitute for  $y(t)$  from Eq. (11.3-8) into the right hand side of the first expression in Eq. (11.3-9) and eliminate the variable  $m$  to obtain

$$\bar{m}_{15}(T, t) \dot{\lambda}(t) \cong \bar{m}_{11}(T, t) t_{go} \left( v_c t_{go} \dot{\lambda}(t) - \dot{y}(t) \right) + \bar{m}_{12}(T, t) \dot{y}(t) \quad (11.3-10)$$

This relation must hold for arbitrary values of  $y(t)$  and  $\dot{\lambda}(t)$ ; consequently, equating the coefficients of  $\dot{\lambda}(t)$  in Eq. (11.3-10), it follows that

$$\bar{m}_{15}(T, t) = \bar{m}_{11}(T, t) v_c (T-t)^2 \quad (11.3-11)$$

This gives us an expression for the normalized miss caused by  $\dot{\lambda}(t)$  in terms of that caused by  $y(t)$  for optimal steering law  $a_{c1}(t)$ . However, the same relation between position, velocity, and line-of-sight rate (Eq. 11.2-21) is used for all the steering policies under investigation. Therefore Eq. (11.3-11) holds for all values of the first subscript index;

$$\bar{m}_{i5}(T,t) = \bar{m}_{i1}(T,t) v_c (T-t)^2 ; \quad i = 1, 2, 3 \quad (11.3-12)$$

Graphs of the functions  $\bar{m}_{ij}(T,t)$  --  $i = 1, 2, 3$ ;  $j = 2, 3, 5$ , -- have been computed for different values of the control weighting  $r$  and autopilot natural frequency  $\sigma$ . Curves for  $\bar{m}_{i3}$  are normalized by  $g$  (one  $g = 32.2 \text{ ft/sec}^2$ ) and those for  $\bar{m}_{i5}$  are normalized by  $v_c$ . Values of 1 and 10 are chosen for  $\sigma$  to represent respectively slow and rapid autopilot responses. The results are plotted in Fig. 11.3-1 through 11.3-7. The time dependence of each normalized miss is in terms of the quantity  $(T-t)$ ; therefore the abscissa of each graph represents time-to-go in seconds. Recall from the definition of  $\bar{m}_{ij}(T,t)$  that the time  $(T-t)$  is the instant at which an initial condition on one of the state variables is assumed to exist; physically this can represent the time-to-go at launch or a point at which the target begins a constant maneuver.

Notice that the sensitivity curves caused by initial conditions on velocity ( $\bar{m}_{i2}$  in Fig. 11.3-2) and line-of-sight rate ( $\bar{m}_{i5}$  in Fig. 11.3-7) are identical for both of the suboptimal steering laws. This is due to the fact that the only difference between  $a_{c2}(t)$  and  $a_{c3}(t)$  is the term dependent upon the constant target acceleration in Eq. (11.2-24), which is zero for all time along the trajectories represented by these figures.

Figures 11.3-1(a) through 11.3-7(a) correspond to an autopilot time constant of 1 second; Figs. 11.3-1(b) through 11.3-7(b) present similar information for a time constant of 0.1 second. The principal comparison one can make from these curves is that miss distances for the guidance systems having the more rapid autopilot response are uniformly lower. Of course, nothing is said yet about the relative amounts of control effort expended, but it is not expected that this contribution to the

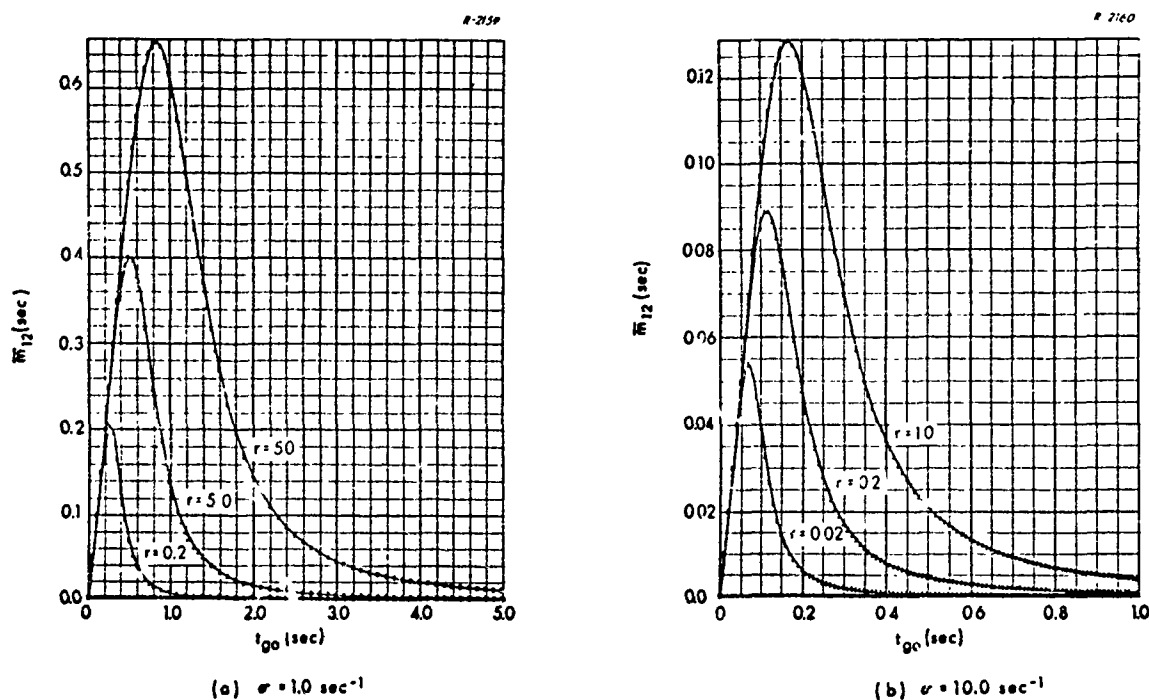


Figure 11.3-1 Normalized Miss Distance for an Initial Cross-Track Velocity: Optimal Steering Law  $a_{c1}(t)$

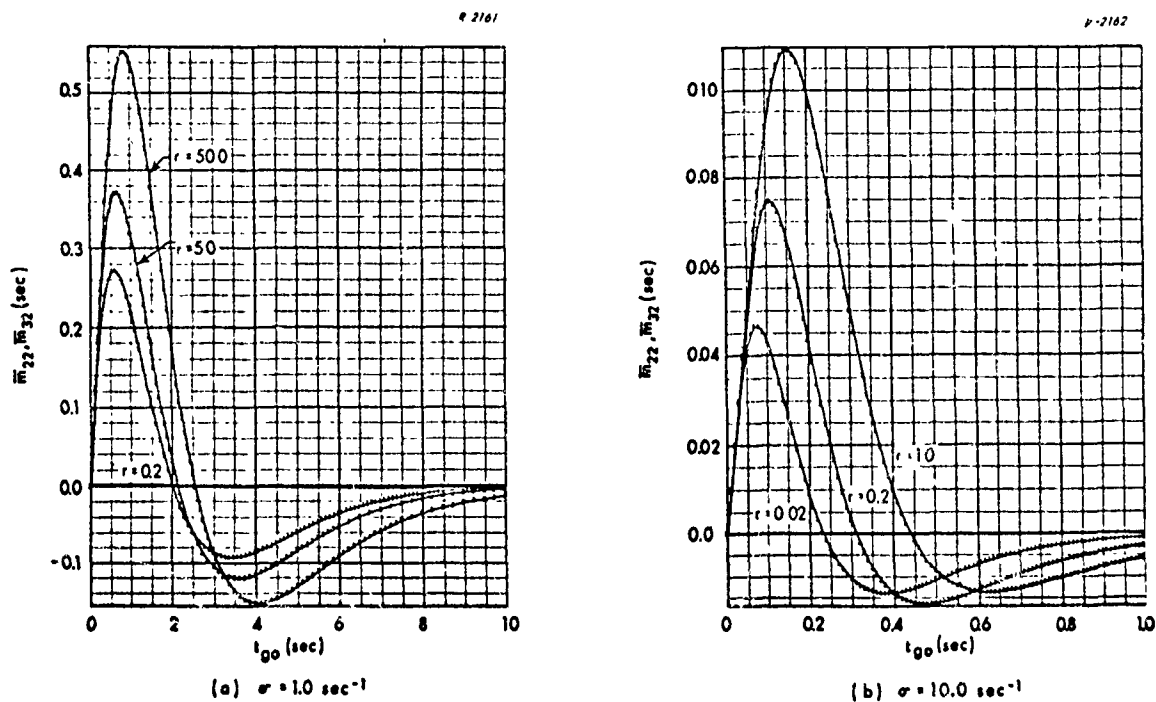


Figure 11.3-2 Normalized Miss Distance for an Initial Cross-Track Velocity: Suboptimal Steering Laws  $a_{c2}(t)$  and  $a_{c3}(t)$

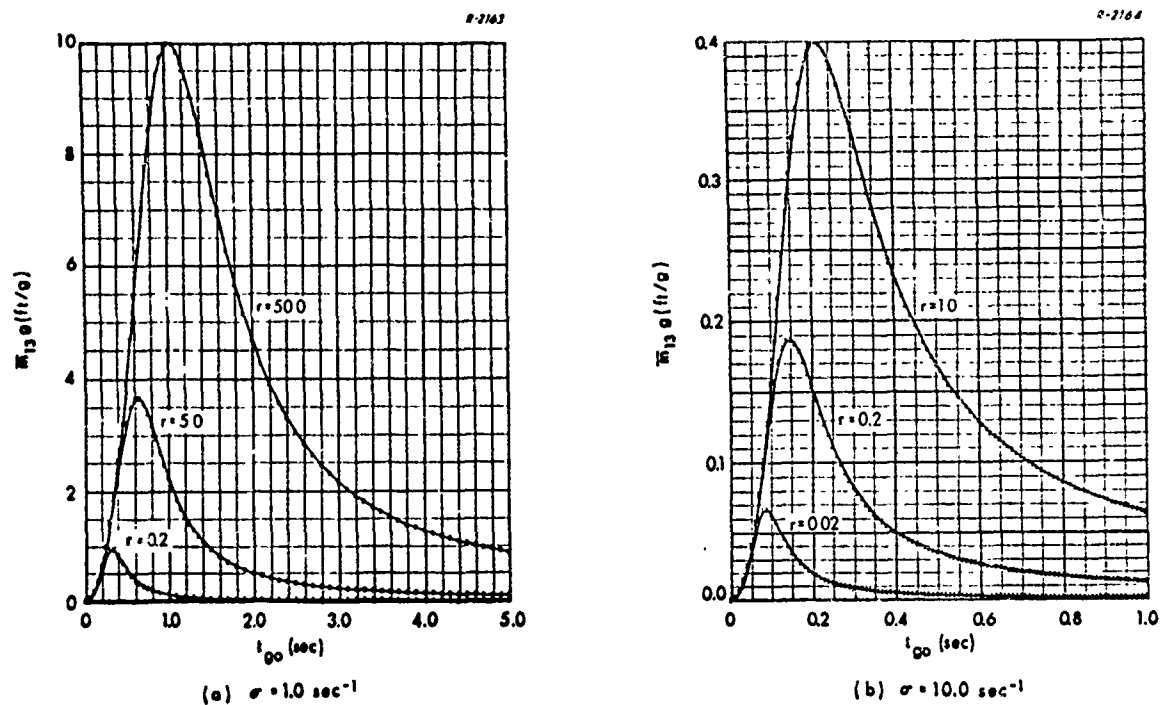


Figure 11.3-3 Normalized Miss Distance Caused by Target Acceleration: Optimal Steering Law  $a_{c1}(t)$

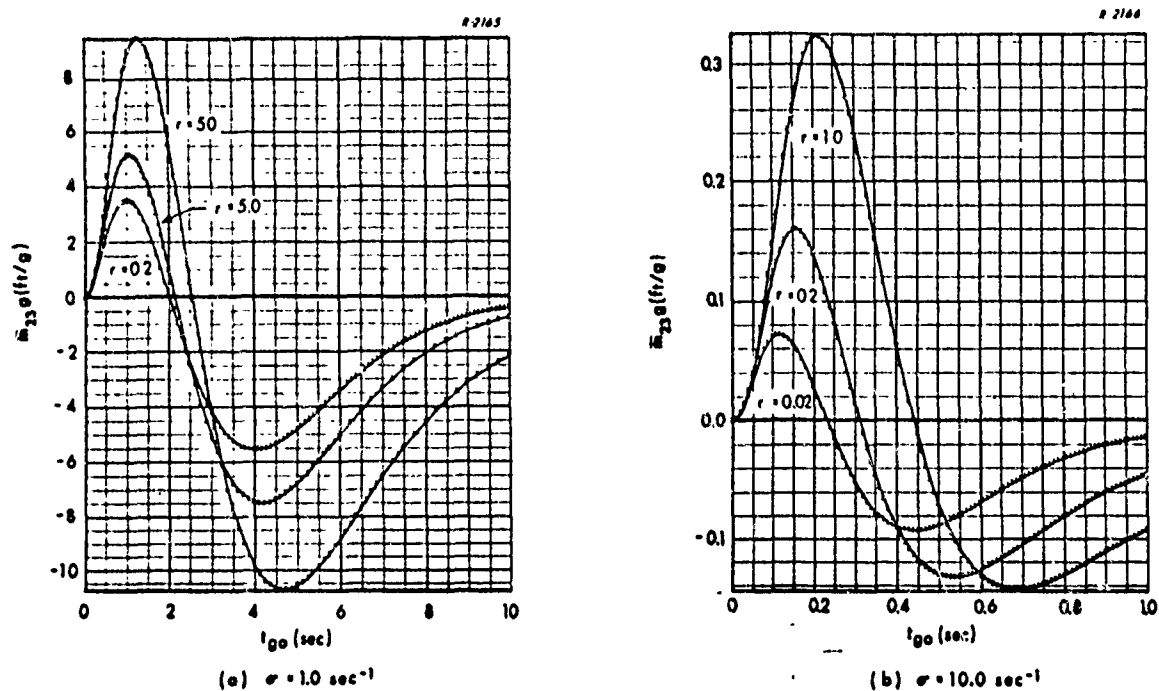


Figure 11.3-4 Normalized Miss Distance Caused by Target Acceleration: Suboptimal Steering Law  $a_{c2}(t)$

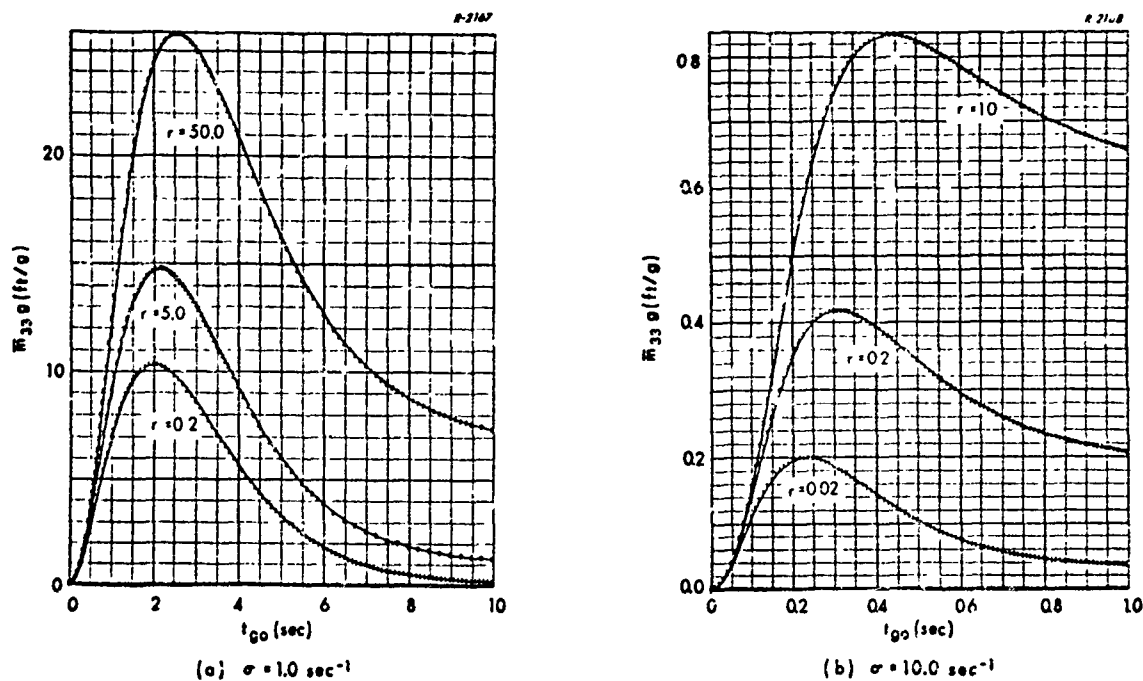


Figure 11.3-5 Normalized Miss Distance Caused by Target Acceleration: Suboptimal Steering Law  $a_{c_3}(t)$

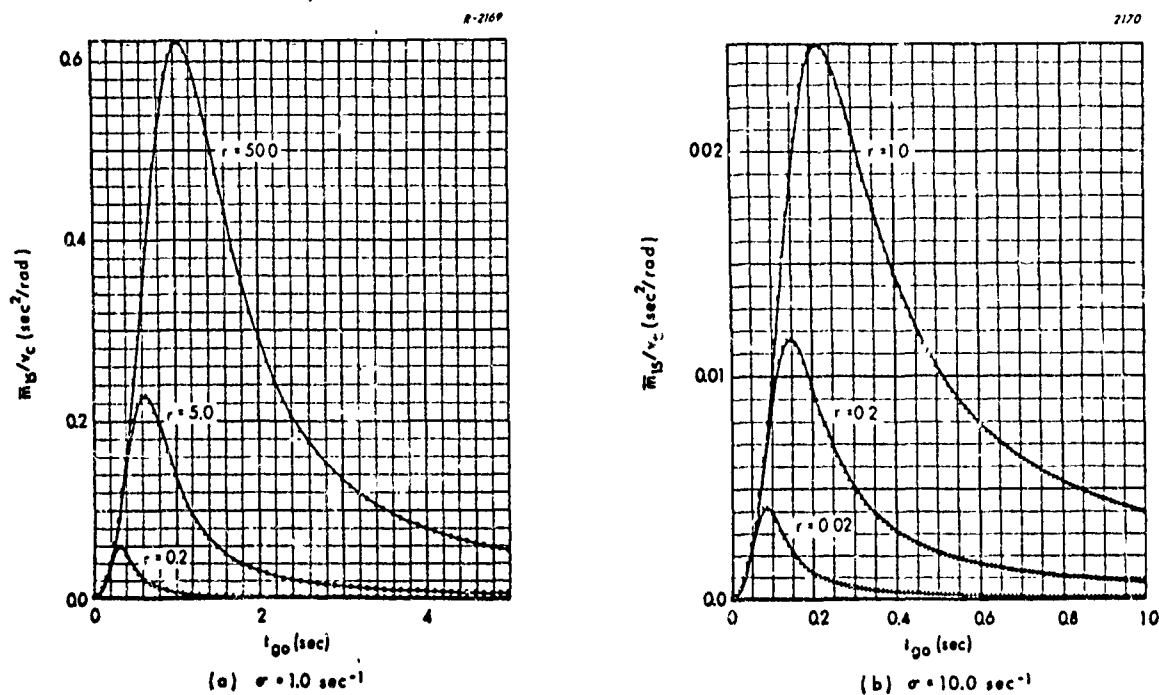


Figure 11.3-6 Normalized Miss Distance Caused by Initial Line-of-Sight Rate: Optimal Steering Law  $a_{c_1}(t)$

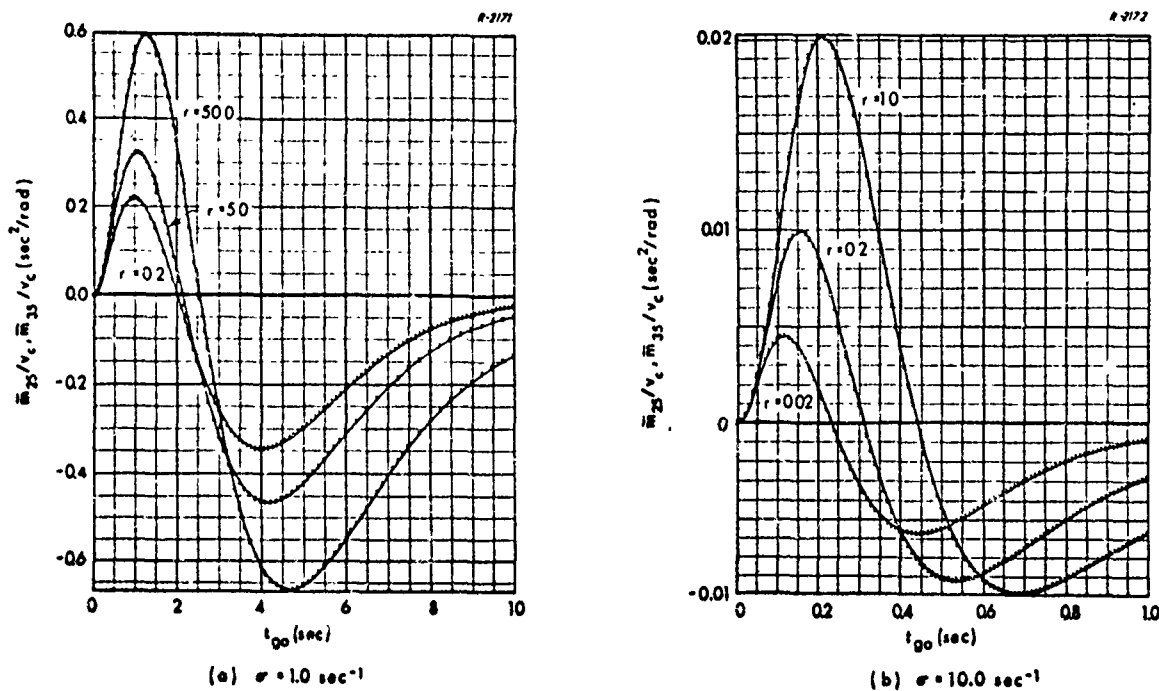


Figure 11.3-7 Normalized Miss Distance Caused by Initial Line-of-Sight Rate: Suboptimal Steering Laws  $a_{c2}(t)$  and  $a_{c3}(t)$

performance index in Eq. (11.2-17) will reverse the judgement that a faster autopilot is preferable. After all, given a system with no autopilot lag, the associated optimal steering law  $a_{c2}(t)$  does not call for one to be added. Also it is clear from inspection of individual figures that increasing the weighting on the control effort always increases the terminal miss for the optimal steering law, and almost always does so for the suboptimal steering laws. The maximum miss results when initial conditions occur at a time-to-go on the order of one autopilot time constant. Physically the latter is true because enough time remains for the initial condition to cause appreciable miss if no guidance action is taken while insufficient time remains for the autopilot to closely follow corrective steering commands.



Consequently, it is advantageous, from the target's point of view (Figs. 11.3-3 through 11.3-5), for the target to begin its constant acceleration maneuver at this most sensitive time.

Most of the above observations are qualitative judgements which are readily predictable on the basis of what is already known about trajectory sensitivity, e.g., see Figs. 3.1-1 through 3.1-4 of Section 3. To establish whether the optimal steering law  $a_{c_1}(t)$  has significant advantages over the other, suboptimal controls we must determine the control effort expended for representative sets of initial conditions. This is the subject of the next section.

### 11.3.2 Control Effort Sensitivity to Initial Conditions

The control effort  $J_u$  expended by the guidance system to null initial conditions, using any one of the steering laws under investigation, can be determined by the method described in Section G.4. Denote the values of  $J_u$  corresponding to  $a_c(t) = a_{c_i}(t)$  by  $J_{u_i}$ ,

$$J_{u_i} \triangleq \int_t^T a_{c_i}(\tau)^2 d\tau; \quad i = 1, 2, 3 \quad (11.3-13)$$

where, as before,  $t$  denotes the time at which the guidance problem begins. With application of Eq. (G-31)  $J_{u_i}$  is given by

$J_{u_i} = \underline{x}(t)^T C_i(t) \underline{x}(t); \quad i = 1, 2, 3$

 (11.3-14)

where  $C_i(t)$  satisfies the linear matrix differential equation

$$\begin{aligned}\dot{C}_i(t) &= -C_i(t) A_i(t) - A_i(t)^T C_i(t) - \underline{h}_i(t) \underline{h}_i(t)^T \\ C_i(T) &= 0 \quad i = 1, 2, 3\end{aligned}\tag{11.3-15}$$

with  $A_i(t)$  defined by Eq. (11.3-4). Equation (11.3-15) is evaluated by integrating backwards in time from the known terminal value of  $C_i(T)$ .

For the purpose of evaluating separately the effort caused by initial conditions on each state variable, we need to know only the diagonal elements of  $C_i(t)$  to perform the calculation in Eq. (11.3-14); i.e.,

$$J_{u_{ij}} = c_{ij}(t) x_j(t)^2\tag{11.3-16}$$

where  $x_j(t)$  is the initial condition on the  $j^{\text{th}}$  state variable at time  $t$  with all other initial conditions zero,  $c_{ij}(t)$  is the  $j^{\text{th}}$  diagonal element of  $C_i$ , and  $J_{u_{ij}}$  denotes the value of  $J_{u_i}$  produced by  $x_j(t)$ . Thus the control effort expended depends upon which steering law is in use and the magnitude of the nonzero initial condition. To facilitate the discussion it is convenient to define a root normalized control effort,  $\bar{J}_{u_{ij}}$ , according to

$$\bar{J}_{u_{ij}} \triangleq \sqrt{c_{ij}(t)/g^2}\tag{11.3-17}$$

For any particular values of  $i$  and  $j$  the effort is given by

$$J_{u_{ij}} = \left( \bar{J}_{u_{ij}} x_j(t) g \right)^2\tag{11.3-18}$$

Physically  $(\bar{J}_{u_{ij}})^2$  is the integral of the square of commanded normal acceleration (in g's) caused by a unit initial condition. Plots of the functions  $\bar{J}_{u_{ij}}(t_{go})$  --  $i = 1, 2, 3$ ;  $j = 2, 3, 5$ , -- corresponding to the miss sensitivity curves in the preceding section are given in Figs. 11.3-8 through 11.3-12.

As indicated in Figs. 11.3-8 and 11.3-9,  $\bar{J}_{u_{i5}}$  can be expressed in terms of  $\bar{J}_{u_{i2}}$ . To derive this relationship, refer to Eq. (11.2-21) and assume that  $y(t) = 0$  at the initial time  $t$ ; therefore

$$\dot{\lambda}(t) \cong \frac{\dot{y}(t)}{v_c t_{go}} \quad (11.3-19)$$

Substitution for  $y(t)$  from Eq. (11.3-19) into Eq. (11.3-16) produces

$$J_{u_{i2}} = c_{i2}(t) t_{go}^2 v_c^2 \lambda(t)^2$$

Defining the root normalized effort produced by the initial line-of-sight rate as

$$\bar{J}_{u_{i5}} \triangleq \sqrt{c_{i2}(t) t_{go}^2 v_c^2 / g^2}$$

it follows from Eq. (11.3-17) that

$$\boxed{\bar{J}_{u_{i5}} = \bar{J}_{u_{i2}} t_{go} v_c} \quad (11.3-20)$$

The curves corresponding to an initial cross-track velocity (Figs. 11.3-8 and 11.3-9) exhibit increasing maximum values as the

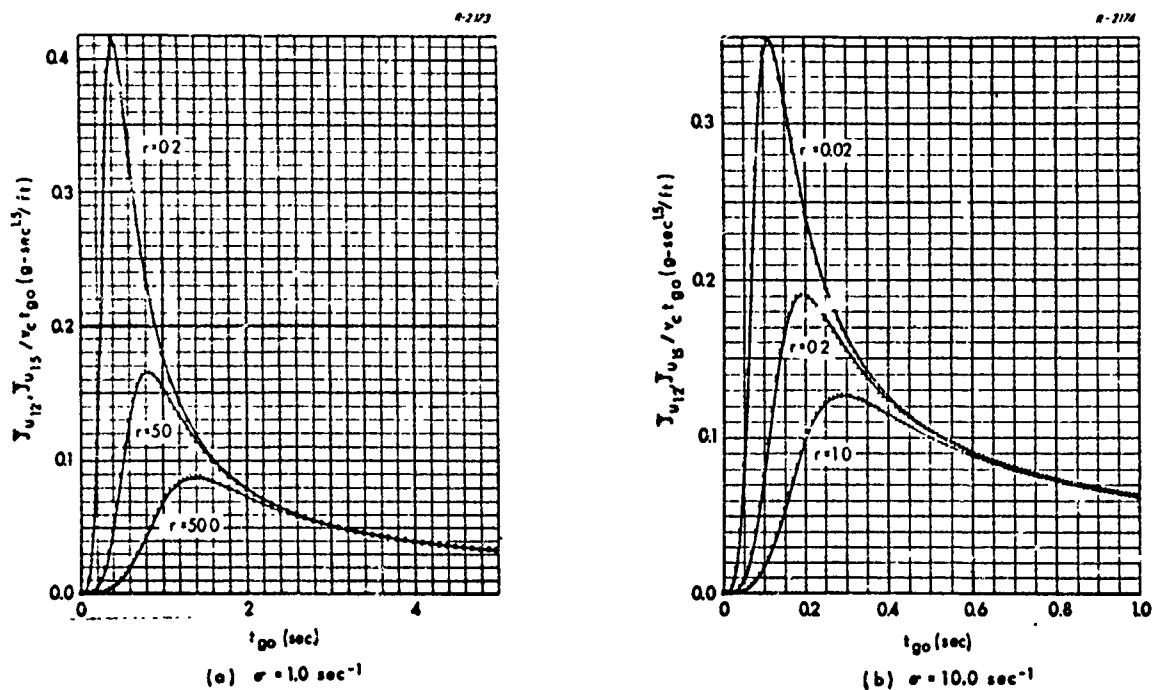


Figure 11.3-8 Root Normalized Effort Caused by Initial Cross-Track Velocity or Initial Line-of-Sight Rate: Optimal Steering Law  $a_{c1}(t)$

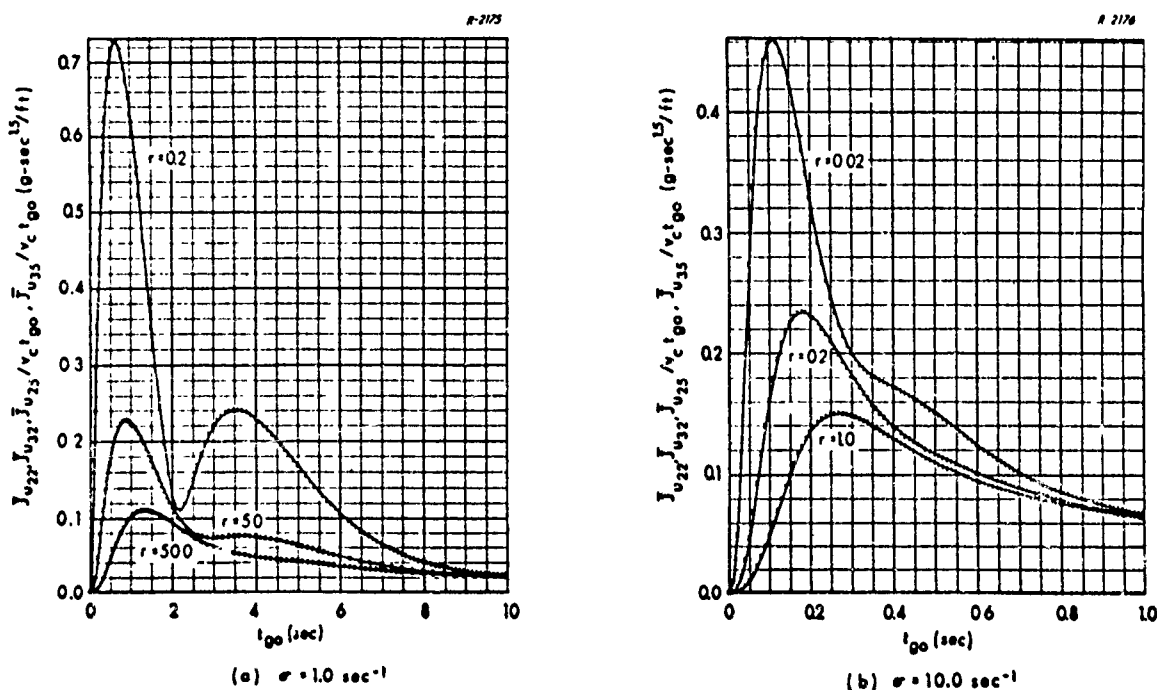


Figure 11.3-9 Root Normalized Effort Caused by Initial Cross-Track Velocity or Initial Line-of-Sight Rate: Suboptimal Steering Laws  $a_{c2}(t)$  and  $a_{c3}(t)$

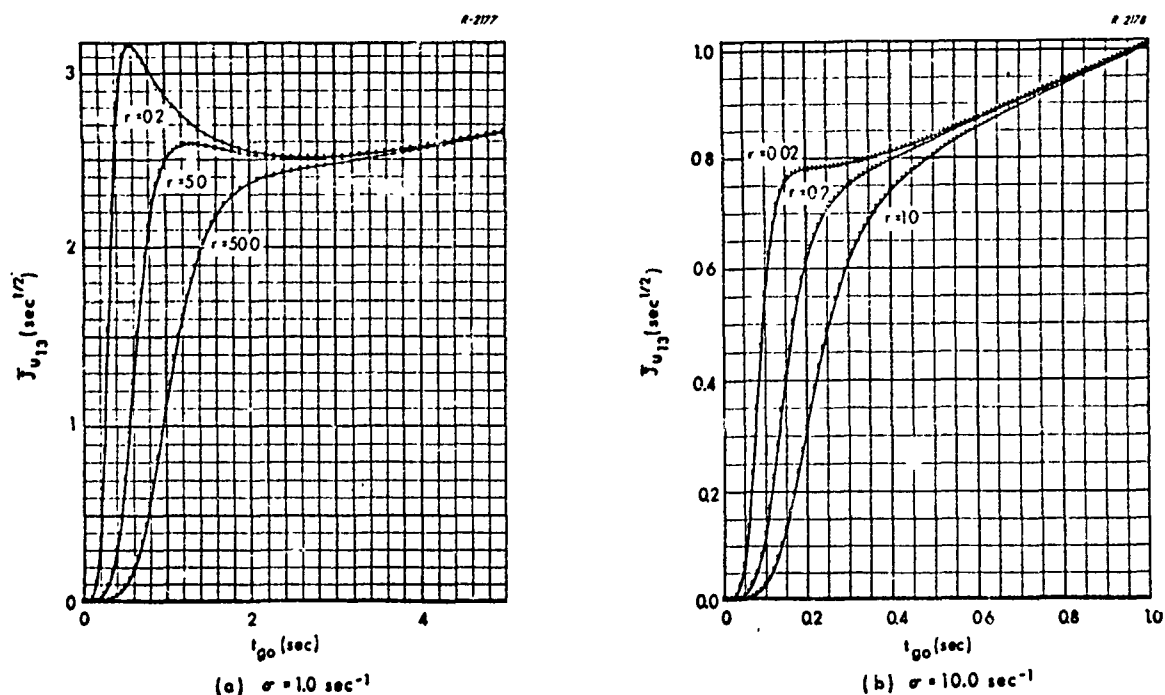


Figure 11.3-10 Root Normalized Effort Caused by Target Acceleration: Optimal Steering Law  $a_{c1}(t)$

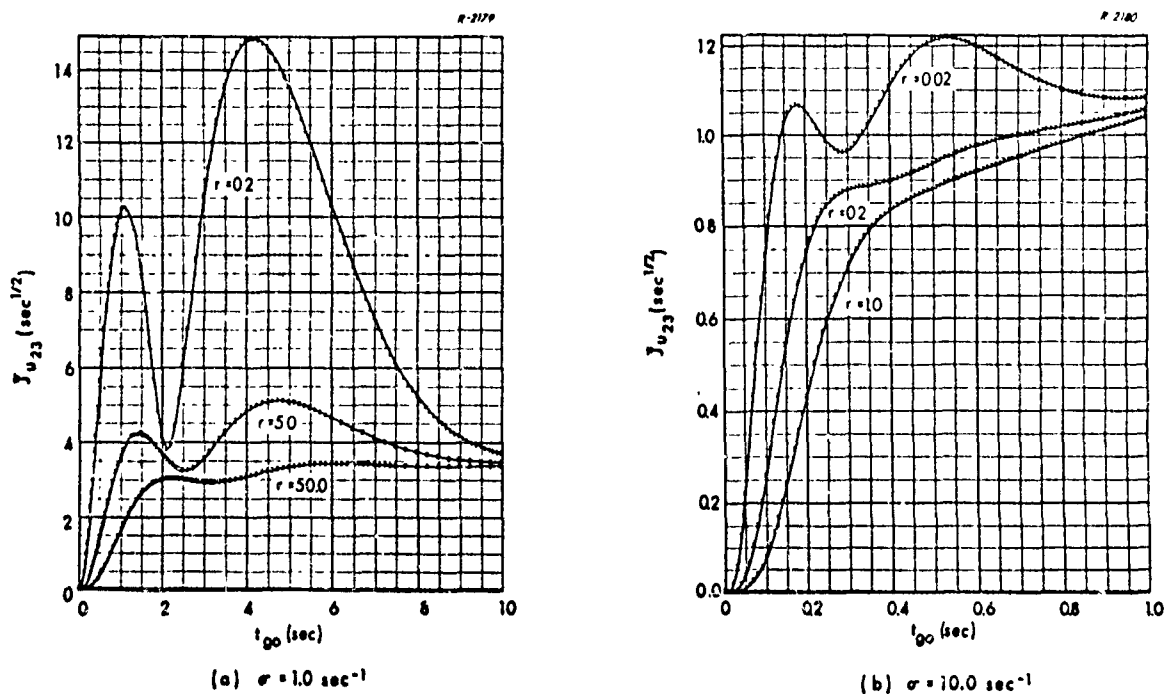


Figure 11.3-11 Root Normalized Effort Caused by Target Acceleration: Suboptimal Steering Law  $a_{c2}(t)$

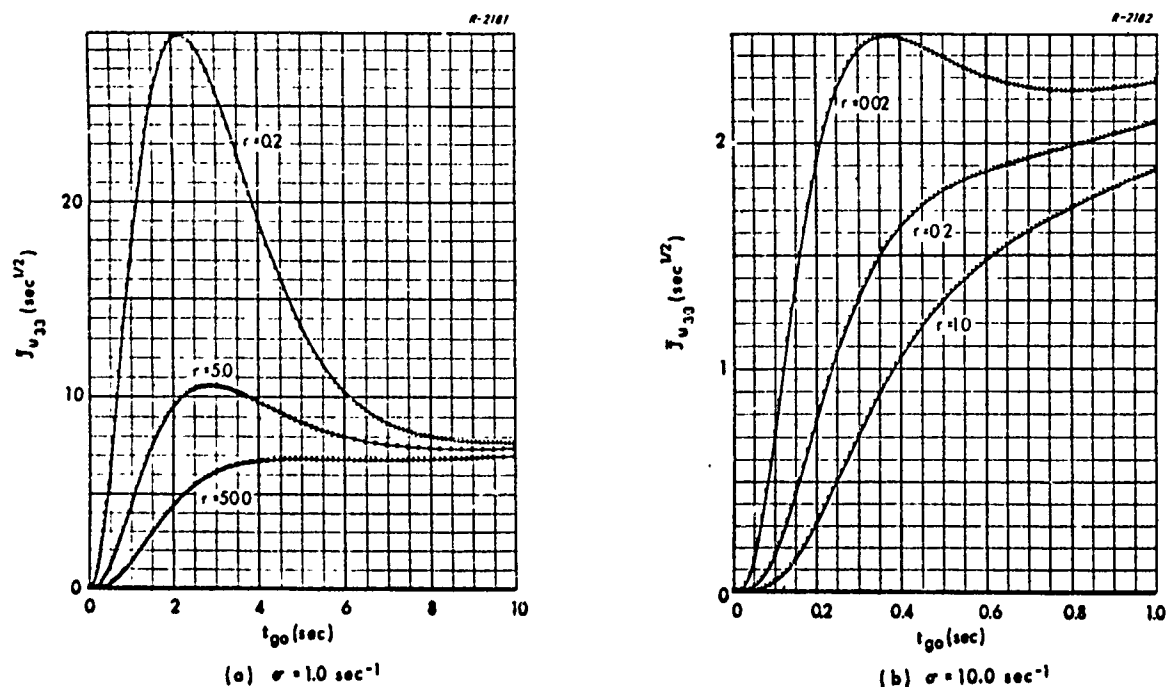


Figure 11.3-12 Root Normalized Effort Caused by Target Acceleration: for Suboptimal Steering Law  $a_{c3}(t)$

control weight  $r$  is decreased. As expected, this trend is opposite to that observed for the normalized terminal miss (Figs. 11.3-1) and 11.3-2). The sets of values of  $r$  for the cases,  $\sigma = 1$  and  $\sigma = 10$ , are different simply to scale the performance index so that each case exhibits about the same range of variation for  $\bar{J}_{u_{i2}}$ . In each figure for  $\bar{J}_{u_{i2}}$ , the curves converge toward zero as  $t_{go}$  increases because there is more time to reduce the terminal miss produced by the initial cross-track velocity and therefore less effort need be expended. Similar effects are observed for target acceleration (Figs. 11.3-10 through 11.3-12), except that the curves for  $\bar{J}_{u_{i3}}$  do not converge to zero with increasing  $t_{go}$ .

As suggested when justifying the choice of performance index in Eq. (11.2-17), besides energy expenditure the value of  $J_u$  provides an

indication of the magnitude of the airframe normal acceleration and control surface deflection. To provide an estimate of the latter a normalized root mean square commanded acceleration,  $\bar{a}_{ij}$ , can be calculated from

$$\bar{a}_{ij} \triangleq \bar{J}_{u_{ij}} / \sqrt{t_{go}} \quad (\text{g's/unit state}) \quad (11.3-21)$$

If it happened that the steering command were constant over the trajectory, it would have the value  $\bar{a}_{ij}$ . Consequently the latter provides an idea of the order of magnitude of the command; in fact it is a lower bound on its maximum magnitude.

To illustrate how the normalized rms steering command can be used to estimate the demands on control surface deflection, recall that the commanded normal acceleration is an input to the autopilot loop, as indicated in Fig. 11.3-13. Throughout the above discussion we have modeled the overall transfer function  $T(s)$  as a simple first order lag but in actual practice it consists of several components and can have more than one dominant pole. The control surface deflection  $\Delta(s)$  is related to commanded acceleration  $A_c(s)$  by the transfer function

$$\frac{\Delta(s)}{A_c(s)} = \frac{G_c(s) G_1(s)}{1 + G_c(s) G_1(s) G_2(s) H(s)} \triangleq T_\delta(s)$$

neglecting the sensor dynamics. If  $A_c(s)$  is known the control surface response can be calculated. In particular, if we assume that

$$a_c(t) \cong \bar{a}_{ij} x_j(0)$$

for a control law  $a_{c_i}(t)$  and a specified guidance initial condition  $x_j(0)$ , then

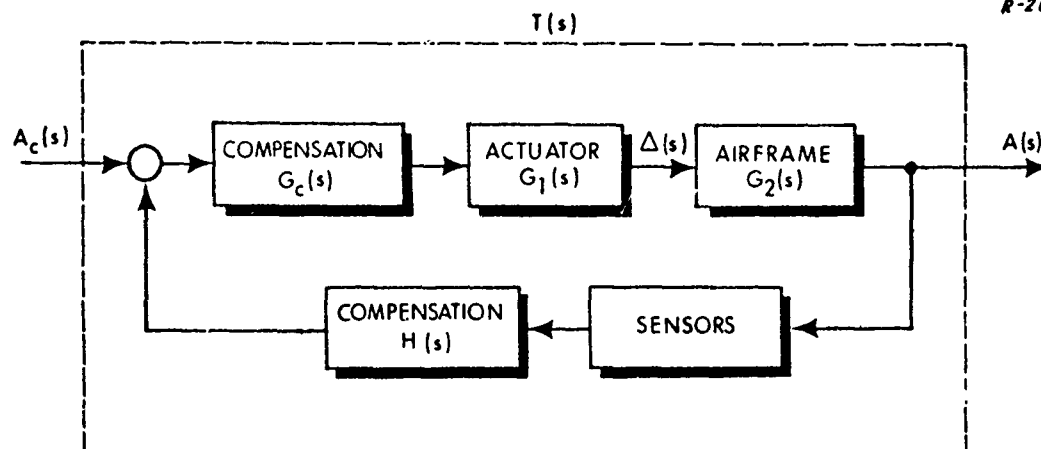


Figure 11.3-13 Autopilot Block Diagram

$$\Delta(s) = \frac{\bar{a}_{ij} x_j(0) T_{\delta}(s)}{s}$$

In this manner one can obtain some idea of the character of the response, recognizing that the assumption of a constant input command is a very rough approximation. Such information is useful for estimating whether the control surface deflection called for by the steering command exceeds the bounds imposed by mechanical constraints.

If one is interested in knowing the response of important autopilot variables to steering commands in more detail than outlined above, two possible courses of action can be taken. First, if detailed time behavior is desired, the actual autopilot equations of motion can be simulated. Alternatively, if the integral square values of various quantities are desired, they can be obtained using the adjoint techniques of Appendix G; this procedure is briefly outlined below for the application illustrated in Fig. 11.3-13.

The problem is to determine the integral square values of autopilot state or output variables for the steering commands  $a_{ci}(t)$  given in Eq.(11.3-2). These quantities can be determined in a manner similar to



that used for the performance index,  $J_u$ . In particular, let the autopilot equations of motion be written as

$$\begin{aligned}\dot{\underline{z}}(t) &= \underline{F}\underline{z}(t) + \underline{g}a_c(t) \\ a(t) &= \underline{c}^T \underline{z}(t) \\ y(t) &= \underline{d}^T \underline{z}(t)\end{aligned}\tag{11.3-22}$$

where  $\underline{z}(t)$  is the state of the autopilot,  $a(t)$  is normal acceleration, and  $y(t)$  is any variable (e.g., normal acceleration, control surface deflection, etc.) whose integral square value,  $J_y$ , is desired,

$$J_y = \int_t^T y(\tau)^2 d\tau$$

(Recall that in Eq. (11.3-4) the autopilot dynamics are assumed to be a first order lag.) To derive the actual equations of motion for the guidance system with the autopilot modeled by Eq. (11.3-22), replace  $x_4(t)$  in Eq. (11.3-4) by  $\underline{z}(t)$  and combine the result with Eq. (11.3-22) to obtain

$$\begin{bmatrix} \dot{x}_1(t) \\ \dot{x}_2(t) \\ \dot{x}_3(t) \\ \dot{\underline{z}}(t) \end{bmatrix} = \underline{F}_i(t) \begin{bmatrix} x_1(t) \\ x_2(t) \\ x_3(t) \\ \underline{z}(t) \end{bmatrix}$$

$$\underline{F}_i(t) \triangleq \begin{bmatrix} 0 & 1 & 0 & \underline{0}^T \\ 0 & 0 & 1 & -\underline{c}^T \\ 0 & 0 & 0 & \underline{0}^T \\ \underline{0} & \underline{0} & \underline{0} & \underline{F} \end{bmatrix} - \begin{bmatrix} 0 \\ 0 \\ 0 \\ \underline{g} \end{bmatrix} \underline{h}_i(t)^T \begin{bmatrix} 1 & 0 & 0 & \underline{0}^T \\ 0 & 1 & 0 & \underline{0}^T \\ 0 & 0 & 1 & \underline{0}^T \\ 0 & 0 & 0 & \underline{c}^T \end{bmatrix}\tag{11.3-23}$$

Equation (11.3-23) represents the actual dynamics of the guidance and control system with steering laws specified by Eq. (11.3-2). Defining

$$\underline{w}(t)^T \triangleq \begin{bmatrix} x_1(t) & x_2(t) & x_3(t) & \underline{z}(t)^T \end{bmatrix}$$

the equations of motion for the guidance system can be written compactly as

$$\dot{\underline{w}}(t) = F_i(t) \underline{w}(t) \quad (11.3-24)$$

and  $J_y$  as

$$J_y = \int_t^T \underline{w}^{(T)}(\tau) Q \underline{w}(\tau) d\tau$$

$$Q = \begin{bmatrix} [0] & [0] \\ [0] & \underline{d}\underline{d}^T \end{bmatrix} \quad (11.3-25)$$

Equations (11.3-24) and (11.3-25) have the same form as Eqs. (G-1) and (G-4); consequently Eq. (G-30) can be used to calculate  $J_y$  in terms of an initial condition on  $\underline{w}(t)$ ,

$$J_y = \underline{w}(t)^T D(T, t) \underline{w}(t)$$

$$\dot{D}(T, t) = -F_i(t)^T D(T, t) - D(T, t) F_i(t) - Q; \quad D(T, T) = 0 \quad (11.3-26)$$

The solution of Eq. (11.3-26) for  $D(T, t)$  provides a means for calculating the integral square value of any autopilot output variable defined by  $\underline{d}$  in Eq. (11.3-22). This type of analysis permits a more realistic

evaluation of the effect of a given steering law on the autopilot than does the value of integral square commanded acceleration.

### 11.3.3 Steering Law Evaluation

To make a judgement about the effectiveness of one steering law as opposed to another, we need to compare the values of control effort expended to produce a given level of normalized terminal miss. In making such a comparison the time-to-go, i. e., the time of missile launch or the time a target maneuver occurs, must be considered. One procedure for doing this is to compare miss distances and effort expended for different control weightings  $r$  at values of  $t_{go}$  which are related to the autopilot lag; e. g., take  $t_{go} = 1/\sigma, 2/\sigma, \dots, n/\sigma$ . Figure 11.3-14(a) is a graph of the normalized effort  $\bar{J}_u$ , defined in the preceding section, versus the magnitude of the normalized miss for a one second autopilot time constant, using both optimal and suboptimal control laws, required to remove an initial cross-track velocity. The data for these curves is read from Figs. 11.3-1(a), 11.3-2(a), 11.3-8(a) and 11.3-9(a) at the point  $t_{go} = 1.0$ . The significance of this plot is that if the missile is launched at a point one second away from the target with a unit cross-track relative velocity, then the curves give the resulting terminal miss and control effort expended using various steering laws. The value of the weighting constant  $r$  required to calculate each steering command is read as a parameter along the individual curves. This plot also indicates the degree of improvement obtained from the optimal steering law relative to the suboptimal methods. For example, if one can tolerate a normalized terminal miss no greater\* than 0.25, the superiority of the

---

\* A specification on normalized terminal miss can be arrived at through knowledge of the missile's velocity, likely target velocities, and likely launch heading angles. An illustration of how this can be done is given below in Example 11.3-1.

optimal steering law in terms of control effort expended is measured by the difference  $J_{u_{22}}(.25) - J_{u_{12}}(.25)$  in Fig. 11.3-14(a), which has a value of 0.290.

A significant observation is that an arbitrarily small miss-distance cannot be achieved using either suboptimal steering law. Recall from Eq. (11.2-28) that in the limit of zero control weighting,  $a_c(t)$  becomes proportional steering with  $\eta = 3$ . The normalized miss achieved with the latter for a unit initial cross track relative velocity can be read from Fig. 3.1-4, using the fact that

$$\dot{\lambda}(0) = \frac{\dot{y}(t)}{r_{go}}$$

It provides a lower bound for the normalized misses  $\bar{m}_{22}$  and  $\bar{m}_{32}$  obtained with the suboptimal steering laws, and it is achieved only in the limit as  $r$  approaches 0. With  $t_{go} = 1$  sec and  $\sigma = 1.0$ , the bound has the value 0.18 as indicated in Fig. 11.3-14(a).

If no steering at all is used ( $a_c(t) = 0$ ), the normalized terminal miss is numerically equal to  $t_{go}$ .\* Consequently the curves in Fig. 11.3-14(a) all terminate on the abscissa at  $\bar{m}_{12} = 1.0$ . An appreciable advantage is gained from optimal steering only when the desired normalized miss is significantly smaller than the "no-steering" value.

In a given application, graphs like Fig. 11.3-14(a) should be derived for several possible values of  $t_{go}$  at which the missile might be launched. As  $t_{go}$  increases relative to the autopilot time constant, the absolute values of control effort required to achieve a given miss distance become smaller, as illustrated by Fig. 11.3-14(b) for  $t_{go} = 4.0$ . This

---

\* If  $a_c(t) = 0$ , the normalized miss is equal to the product (1 ft/sec) ( $t_{go}$ ).

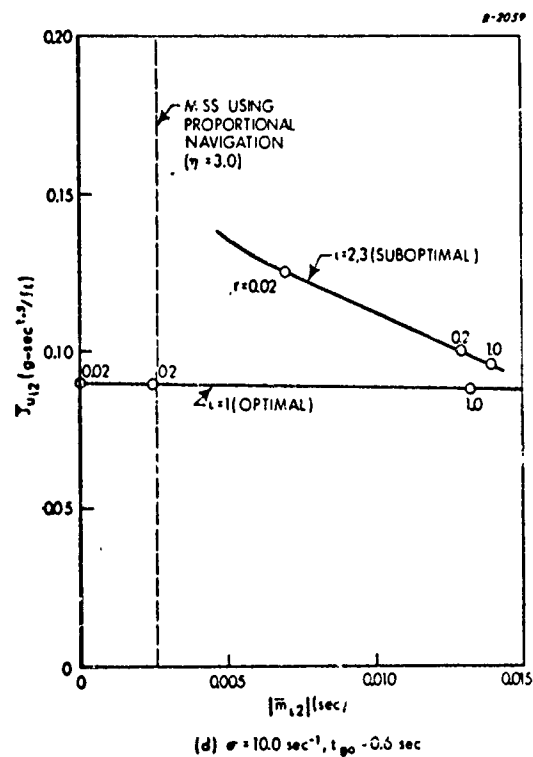
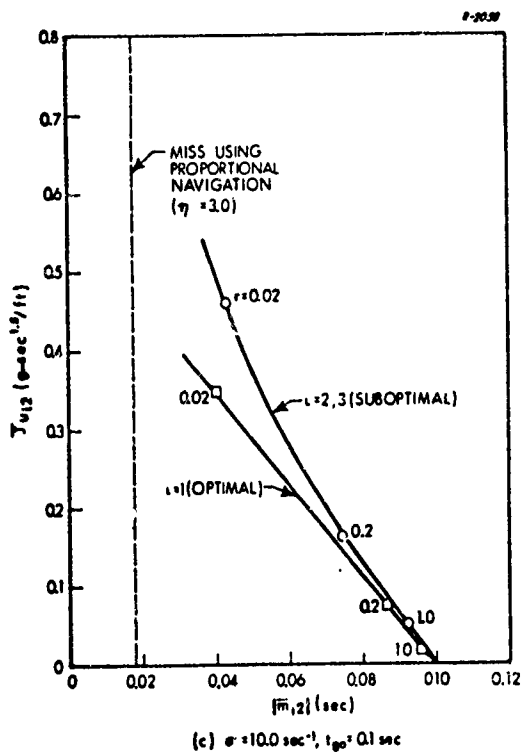
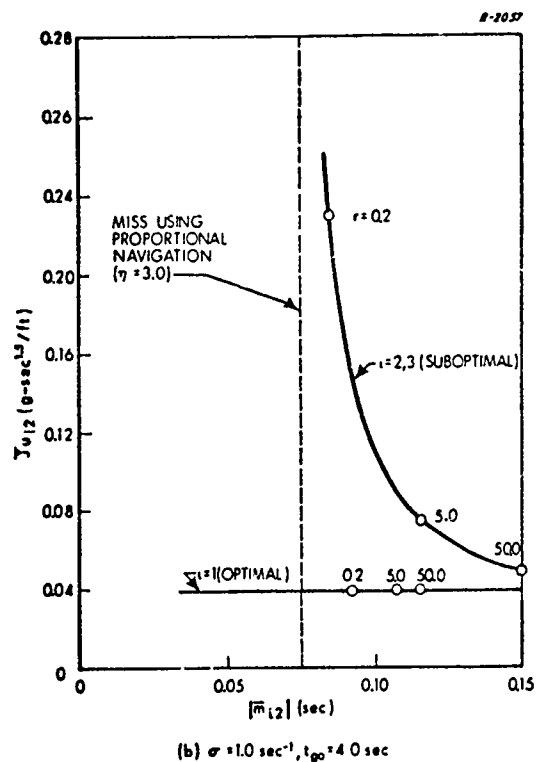
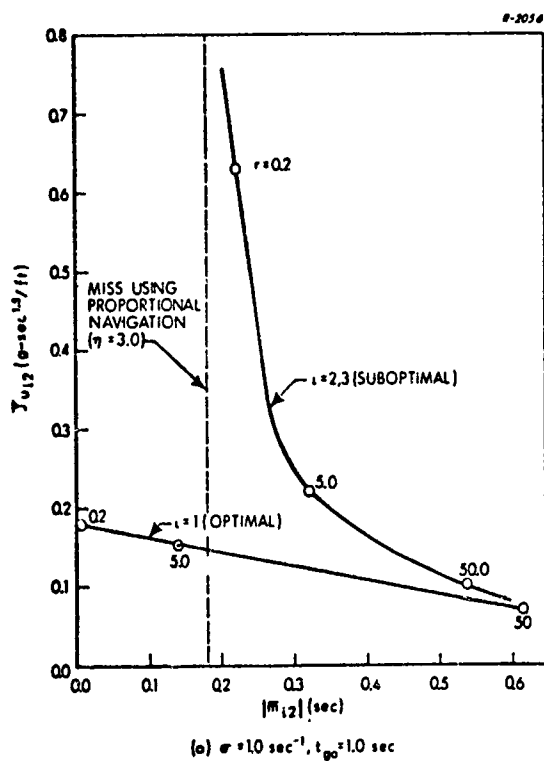


Figure 11.3-14 Root Normalized Effort Versus Normalized Terminal Miss Caused by an Initial Cross-Track Velocity

behavior is simply evidence of the fact that the longer the time until intercept, the more easily the guidance system can reduce the effects of initial condition errors.

Diagrams similar to Figs. 11.3-14(a) and (b) are displayed for the faster autopilot having a natural frequency of 10 rad/sec in Figs. 11.3-14(c) and (d). The data for the curves are obtained from Figs. 11.3-1(b), 11.3-2(b), 11.3-8(b), and 11.3-9(b). As one expects, the magnitudes of the effort and normalized miss are generally less than when  $\sigma = 1.0$ .

In addition to looking at the various terms contributing to the performance index in Eq. (11.2-17) one should insure that the absolute control magnitude is not excessive. This can be done exactly only by plotting the control as a function of time. However, an indication of control level can be obtained from the normalized root mean square commanded acceleration level defined in Eq. (11.3-21). Values of this quantity are simply obtained by scaling the ordinate in Fig. 11.3-14 by the factor  $(t_{go})^{-1/2}$ .

To summarize the evaluation of the guidance system response to relative cross-track velocity initial conditions, we shall illustrate the use of the graphs in Fig. 11.3-14 with an example:

**Example 11.3-1** — Consider the situation in Fig. 3.1-5 when the target has a velocity of 1000 feet/second. The relative cross-track velocity at launch is about 700 feet/second. To achieve a miss of seven feet, a normalized miss of about 0.01 is required. To see whether the various steering laws can achieve this level of accuracy, values of root normalized effort and normalized rms commanded acceleration for the various cases represented in Fig. 11.3-14 are tabulated in Table 11.3-1. The symbol \* denotes the fact that the desired miss is not achievable. When the cross-track velocity is 700 feet per second, the rms commanded acceleration

TABLE 11.3-1

STEERING LAW PERFORMANCE REQUIRED TO ACHIEVE  
A NORMALIZED TERMINAL MISS OF .01 FOR A  
CROSS-TRACK VELOCITY INITIAL CONDITION

Optimal Steering	Root Normalized Effort, $\bar{J}_{u_{12}}$	Normalized rms commanded acceleration, $\bar{a}_{12}$ (g's/ft/sec)
$\sigma = 1.0, \quad t_{go} = 1.0$	0.18	0.18
$\sigma = 1.0, \quad t_{go} = 4.0$	0.04	0.02
$\sigma = 10, \quad t_{go} = 0.1$	0.525	1.66
$\sigma = 10, \quad t_{go} = 0.6$	0.10	0.13
Suboptimal Steering	$\bar{J}_{u_{22}}, \bar{J}_{u_{32}}$	$\bar{a}_{22}, \bar{a}_{32}$
$\sigma = 1.0, \quad t_{go} = 1.0$	*	*
$\sigma = 1.0, \quad t_{go} = 4.0$	*	*
$\sigma = 10, \quad t_{go} = 0.1$	*	*
$\sigma = 10, \quad t_{go} = 0.6$	0.112	0.142

\* denotes "not achievable".

required is given by product ( $a_{12} \times 700$ ). In all cases except one (optimal steering,  $\sigma = 1.0, t_{go} = 4.0$ ) this quantity is greater than 90 g's. This information together with an autopilot analysis of the sort suggested at the end of Section 11.3.2 enables one to make a decision about which steering law to use when a range of possible launch conditions is known. Furthermore one can determine whether a given specification is reasonable; it may be physically impossible to destroy some targets with a given autopilot.

The effects of initial cross-track velocity are most relevant to dogfight applications where the pilot of a launch aircraft may be close to the target.

An analysis, such as that presented in the above example, aids one in obtaining the range of launch conditions, i.e., the "launch envelope," within which the launch aircraft must remain to make a successful attack.

We emphasize that throughout this chapter perfect knowledge of state variables in mechanizing the steering laws is assumed. In practice, appreciable measurement noise usually exists in the steering loop which should be included in a complete performance evaluation. The deterministic system analysis chiefly provides qualitative information about the ultimate performance that can be expected from a steering law.

Turning now to the effect of target maneuvers, a different criterion from that used above is suggested for comparing normalized miss and normalized effort associated with different steering laws. For a given value of the weighting constant  $r$  we choose that value of  $t_{go}$  which maximizes the terminal miss. Thus each steering law is being evaluated at those points where sudden application of a target maneuver has the maximum adverse effect upon guidance accuracy. These curves are relevant for any tactical situation because the target maneuver can begin anytime after the missile is launched.

Referring to Figs. 11.3-3(a) and 11.3-10(a) which illustrate the effects of a target maneuver, we want to tabulate or graph pairs of values of the maximum  $\bar{m}_{ij}$  and its associated normalized effort. To illustrate the procedure, in Fig. 11.3-3(a) note that for  $r = 0.2$ ,  $\bar{m}_{13}$  is 0.9 at  $t_{go} = 0.3$ . Entering the graph in Fig. 11.3-10(a) at  $t_{go} = 0.3$ , read out  $\bar{J}_{u13} = 1.6$ . This "point",  $(\bar{m}_{13}, \bar{J}_{u13}) = (0.9, 1.6)$ , and the two others that can be obtained from these figures for  $r = 5.0$  and  $r = 50$  are plotted and joined by a smooth curve labeled  $i = 1$  in Fig. 11.3-15(a). A similar plot is made in the same figure for the suboptimal control laws  $a_{c2}(t)$  and



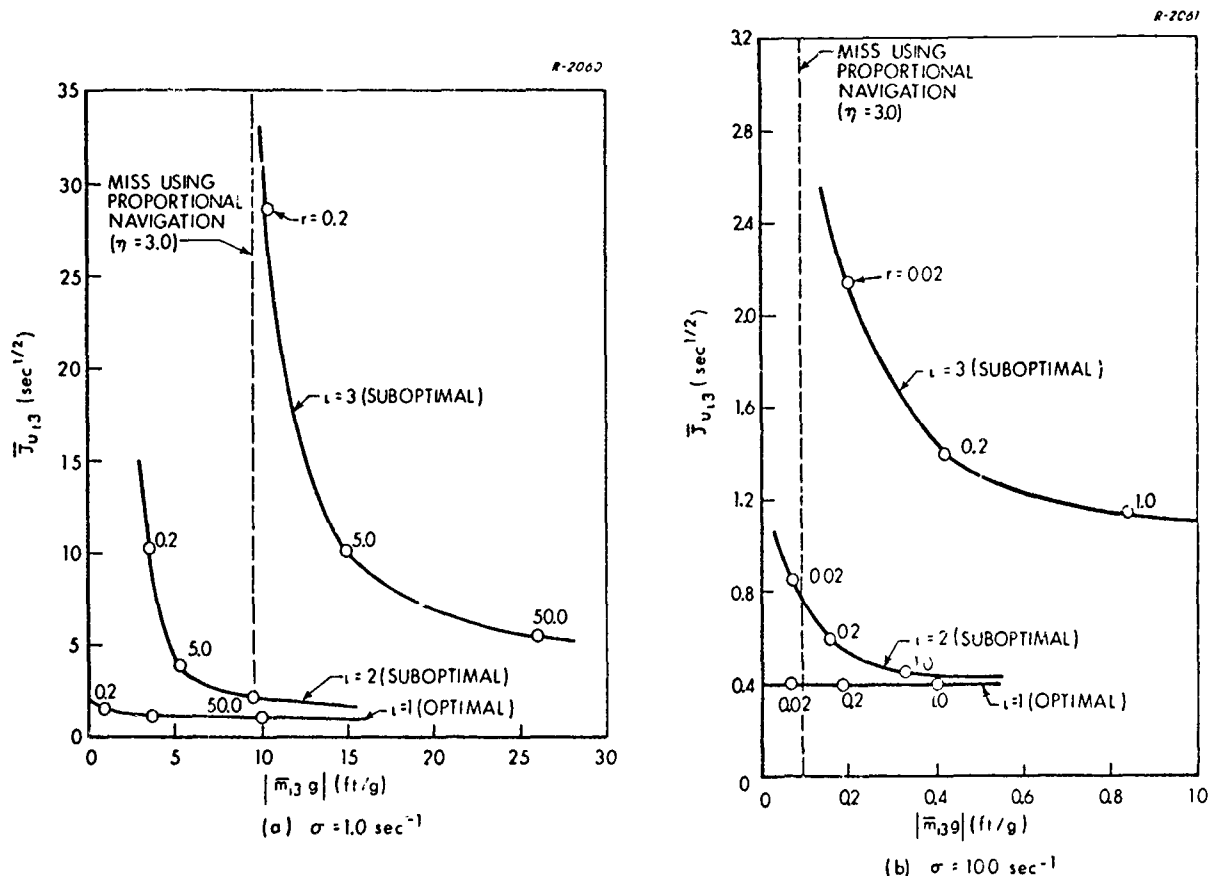


Figure 11.3-15 Root Normalized Effort Versus Peak Normalized Miss Produced by Target Acceleration

$a_{c3}(t)$  from the data in Figs. 11.3-4(a), 11.3-11(a), 11.3-5(a), and 11.3-12(a). The process is repeated in Fig. 11.3-15(b) for the case when the autopilot time constant is 0.1 sec.

In each of these graphs, the performance of the suboptimal steering law  $a_{c3}(t)$  approaches that of proportional guidance as the control weighting  $r$  approaches zero. Evidently the greatest relative improvement to guidance system performance is achieved by using  $a_{c2}(t)$  which includes compensation for the target maneuver. The additional advantage achieved by using the optimal steering law  $a_{c1}(t)$  is proportionately not so

large until relatively small values of normalized miss are desired. The following example illustrates the use of Fig. 11.3-15.

Example 11.3-2 — Suppose that one expects to encounter targets which can develop a normal acceleration up to 10 g's and insists upon a steering law that yields a peak terminal miss of 5 feet. The resulting required peak normalized miss in feet/g is 0.5. The corresponding values of normalized effort and normalized rms control level are read from Fig. 11.3-15 and tabulated in Table 11.3-2. For the slower autopilot the optimal steering law is significantly superior; it requires an rms commanded acceleration of 34 g's with a target maneuver of 10 g's. For the faster autopilot, there is little performance improvement in using  $a_{c1}(t)$  instead of  $a_{c2}(t)$ . However,  $a_{c2}(t)$  is distinctly preferable to  $a_{c3}(t)$ .

TABLE 11.3-2

STEERING LAW PERFORMANCE REQUIRED TO ACHIEVE A  
PEAK NORMALIZED TERMINAL MISS OF 0.5 IN THE  
PRESENCE OF TARGET ACCELERATION

Optimal Steering	Root Normalized Effort, $\bar{J}_{u13}$	Normalized rms commanded acceleration, $\bar{a}_{13}$ (g's/g)
$\sigma = 1.0$	1.7	3.4
$\sigma = 10.0$	0.4	0.8
Suboptimal Steering ( $a_{c2}(t)$ )	$\bar{J}_{u23}$	$\bar{a}_{23}$
$\sigma = 1.0$	very high; >20	very high; >20
$\sigma = 10.0$	0.44	0.88
Suboptimal Steering ( $a_{c3}(t)$ )	$\bar{J}_{u33}$	$\bar{a}_{33}$
$\sigma = 1.0$	*	*
$\sigma = 10.0$	1.44	1.2

\* denotes "not achievable".

#### 11.3.4 Terminal Miss Sensitivity to Measurement Bias Errors

The effects of measurement bias errors upon terminal miss distance can also be determined using adjoint techniques, as described in Section G-3. If a constant error  $\underline{\epsilon}$  is made in the measurement of the state  $\underline{x}(t)$  beginning at time  $t$ , the resulting terminal miss  $\underline{x}_1(T)$  is given by

$$\underline{x}_1(T) = \underline{\psi}_i(T, t)^T \underline{\epsilon}; \quad i = 1, 2, 3$$

where the subscript  $i$  still refers to the steering law being used. The differential equation for  $\underline{\psi}_i(T, t)$  is obtained by comparing Eq. (G-18) with Eqs. (11.3-1) and (11.3-2),

$$\dot{\underline{\psi}}_i(T, t) = \underline{h}_i(t) \underline{b}^T \underline{\varphi}_i(T, t); \quad \underline{\psi}_i(T, T) = \underline{0}$$

where  $\underline{h}_i(t)$  is defined in Eq. (11.3-3) and  $\underline{\varphi}_i(T, t)$  is defined by Eq. (11.3-7).

The value of any element of  $\underline{\psi}_i(T, t)$  at time  $t$  is the miss produced by a unit bias error in the corresponding measurement of the state and zero error in all other state measurements. All state initial conditions at time  $t$  are also assumed to be zero. In other words, the  $j^{\text{th}}$  element of  $\underline{\psi}_i(T, t)$  is the normalized miss  $\bar{b}_{ij}(T, t)$  produced by a single bias error in the measurement of state  $x_j$ .

Values of the normalized miss versus time-to-go for a target acceleration measurement error are plotted in Figs. 11.3-16 and 11.3-17 for the same values of autopilot time constant and control weighting used in the preceding graphs. Qualitatively it is seen that the miss becomes smaller as the control weighting  $r$  decreases. This is true because the decrease in  $r$  increases the feedback gains in the steering law, causing more rapid guidance system response to the error in line-of-sight rate

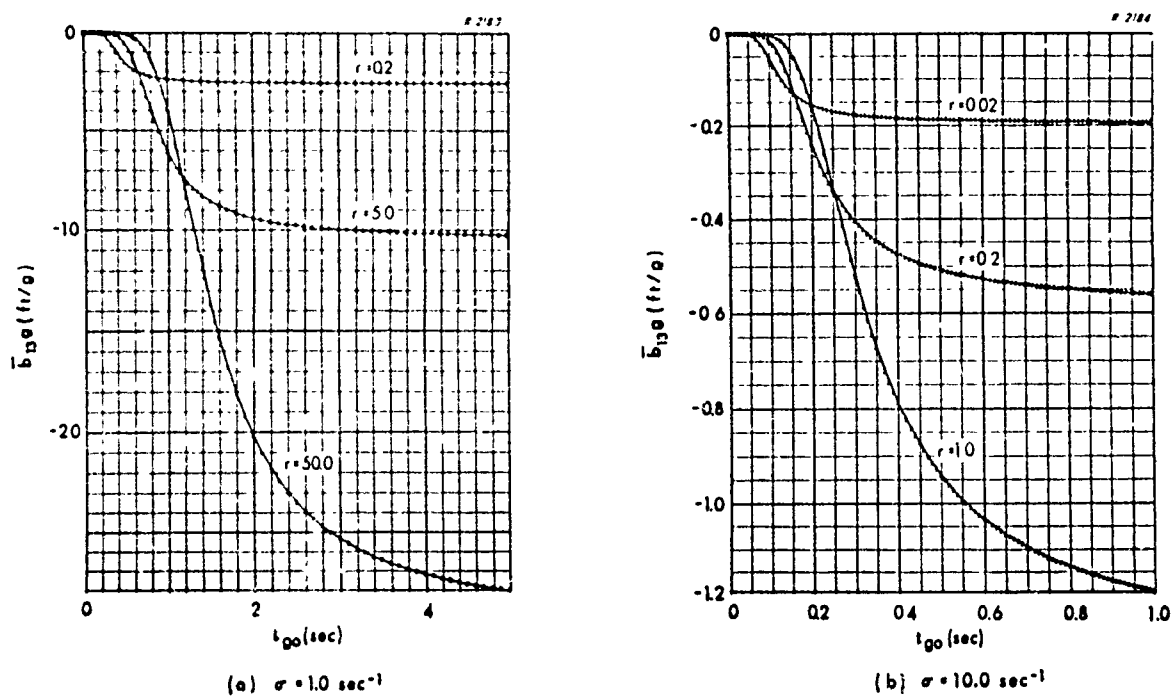


Figure 11.3-16 Normalized Miss Distance Caused by Target Acceleration Measurement Bias Error: Optimal Steering Law,  $a_{c1}(t)$

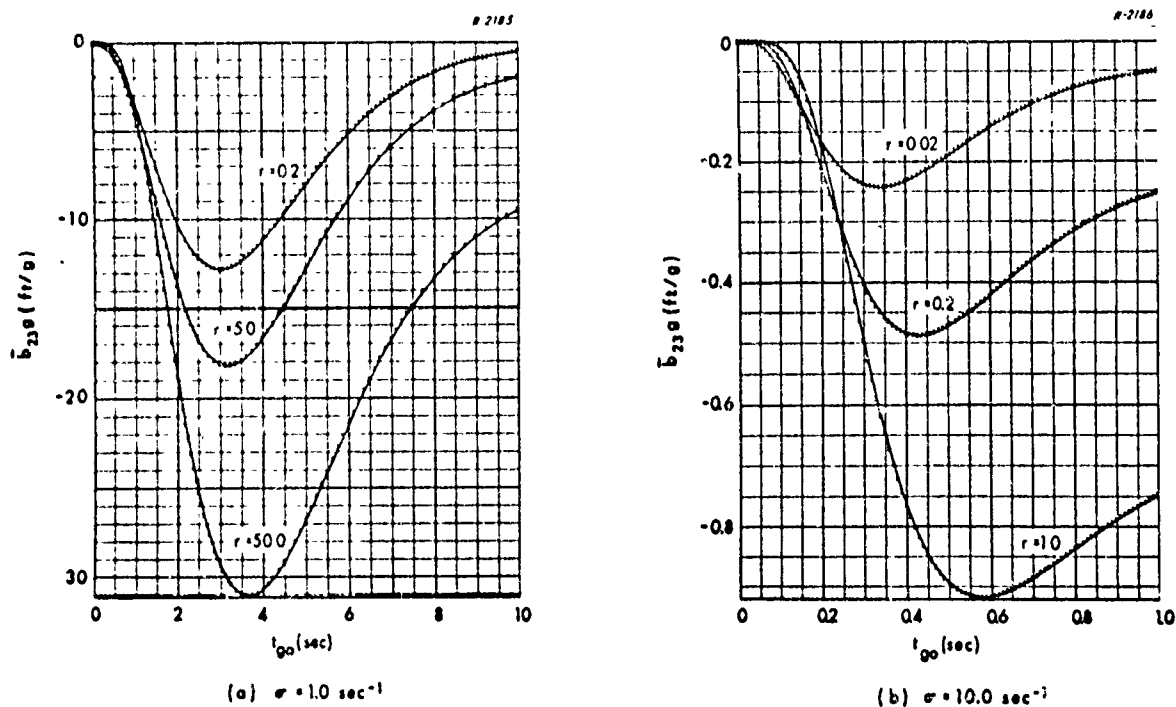


Figure 11.3-17 Normalized Miss Distance Caused by Target Acceleration Measurement Bias Error: Suboptimal Steering Law,  $a_{c2}(t)$

induced by the bias error, thus improving terminal accuracy. An increase in  $\sigma$  also improves accuracy because the autopilot lag decreases.

One useful comparison of the effects of bias errors on the accuracy of the steering laws is obtained by plotting the peak normalized miss from Figs. 11.3-16 and 11.3-17\* versus peak normalized miss caused by constant target acceleration in Figs. 11.3-3 and 11.3-4 for various values of the weighting  $r$ . The cases,  $\sigma = 1$  and  $\sigma = 10$ , are displayed separately in Figs. 11.3-18(a) and (b). Based on the comparison between the curves for these values of  $\sigma$  there is little difference in sensitivity to bias measurement errors between optimal and suboptimal steering laws. In the case  $\sigma = 10$  the curves are nearly superimposed on one another. This is to be expected because the optimal steering law  $a_{c1}(t)$  approaches the suboptimal law  $a_{c2}(t)$  as the autopilot time constant gets smaller.

An alternative comparison is afforded between the steering laws by the steady state values of  $\bar{b}_{13}$  incurred as time-to-go becomes large. Figures 11.3-16 and 11.3-17 indicate that the optimal steering law is more sensitive to measurement bias errors in terms of the steady state values of normalized terminal miss. This fact can have design implications for missiles which are launched at a time-to-go equal to several autopilot time constants. Because  $a_{c1}(t)$  has no built-in criterion for insuring an optimal response in the presence of bias errors, there is no reason to expect it to yield the best performance when such errors occur.

---

\* In Fig. 11.3-16 the peak normalized miss is taken to be the extrapolated steady state values of the curves.

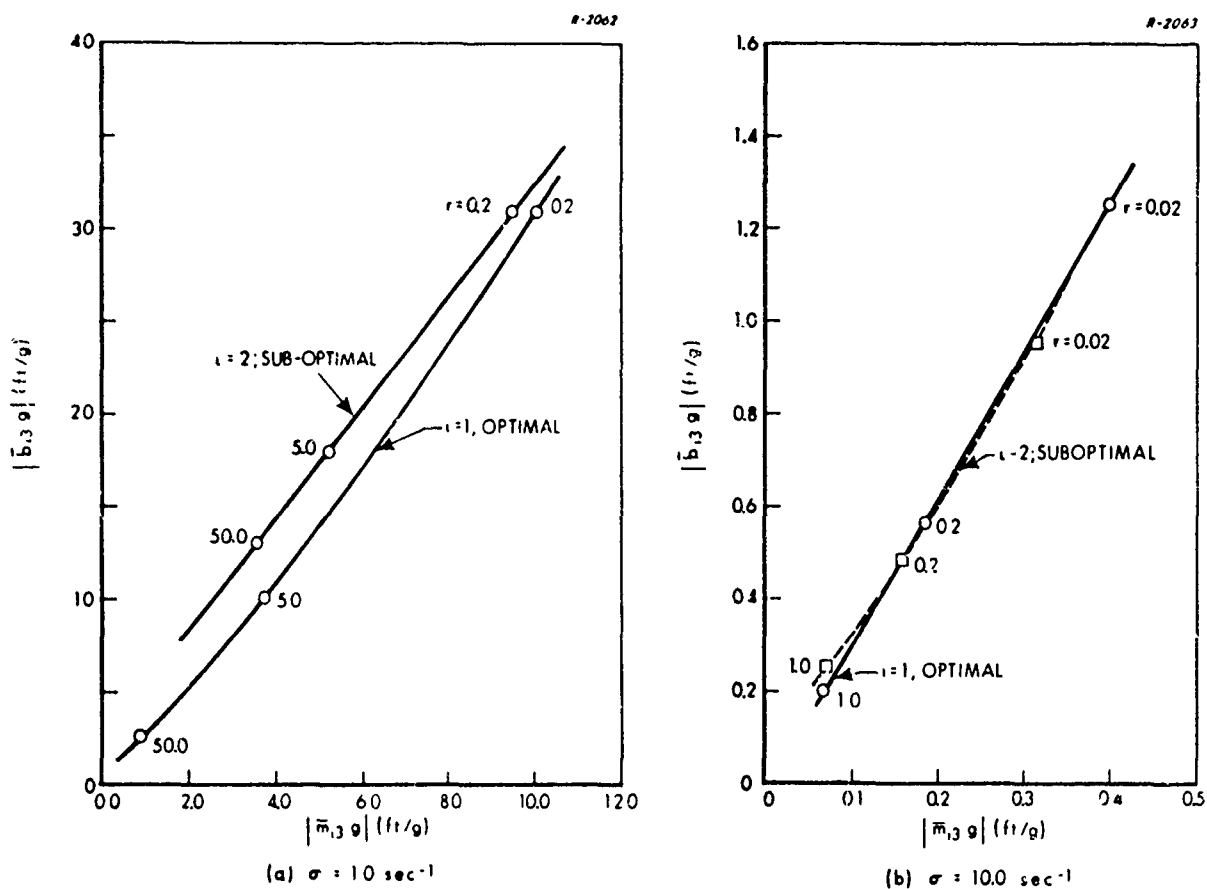


Figure 11.3-18 Peak Normalized Miss, Produced by Target Acceleration Measurement Bias Error, Versus Peak Normalized Miss Caused by Target Acceleration

### 11.3.5 Summary

This concludes our sensitivity analysis of the optimal and sub-optimal steering laws derived in Section 11.2. Its main purpose is to indicate an approach to evaluating different control policies in terms of the design objectives of an optimal control problem. Graphs of normalized miss and control effort of the type depicted in Figs. 11.3-14, 11.3-15 and 11.3-18 are the principal tools for making the performance analysis.

These curves can be used to determine actual values of miss distance and control effort if multiplied by an assumed value of the corresponding initial error -- e.g., cross-track velocity, target acceleration or bias error. Beyond this quantitative comparison of the specific steering laws, some general qualitative conclusions are:

- The faster the autopilot response, the smaller the absolute gain in terminal accuracy using optimal steering,  $a_{c1}(t)$ , as compared with  $a_{c2}(t)$ .
- In the presence of target maneuvers, suboptimal steering  $a_{c2}(t)$  offers a significant improvement over  $a_{c3}(t)$  because the latter has no provision for measuring target acceleration.
- In the presence of measurement bias errors the optimal steering law can exhibit worse performance than a suboptimal policy, depending upon the criteria used for evaluation. In particular, the terminal miss caused by a bias error for a missile launched at a time-to-go equal to several autopilot time constants away from the target is larger when optimal steering is used.

For a given autopilot lag, a definitive judgement about which steering law to use can be made only after considering a spectrum of possible initial values of time-to-go which are characteristic of the particular application. For a dogfight mission, sets of curves of the type shown in Figs. 11.3-14 and 11.3-18 should be obtained for values of  $t_{go}$  ranging over those values expected at launch. In missions where launch takes place at relatively long ranges from the target, initial cross-track velocity (Fig. 11.3-14) is not so important but the steady state effects of measurement errors (e.g., Fig. 11.3-18) must be evaluated. In addition to the bias errors treated above, the effects of continuously varying random measurement errors ("noise") should be analyzed as outlined in Section G.3.

Similarly, graphs like those in Fig. 11.3-15 can be obtained for a set of values of  $t_{go}$  over the range in which target maneuvers are expected to occur, usually within a few seconds before intercept. Performance data displayed in this fashion yield enough quantitative information to permit a rational choice of steering law.

The performance criteria throughout the above discussion are integral square control and the squared terminal miss. The former is somewhat inappropriate because excessive peak control magnitudes can be required. The normalized root mean square acceleration defined in Eq. (11.3-21) gives an optimistic bound on the commanded acceleration level. For any application it should be checked by actually computing the steering command as a function of time for representative cases.

#### 11.4 A COUPLED GUIDANCE-AUTOPILOT STEERING LAW

The statement is made in Section 2.1 that the steering and autopilot control loops for a tactical missile are usually treated as separate entities because their associated response times are considerably different. This is a valid procedure when time-to-go until intercept is large with respect to the autopilot response time; however, when the latter condition does not hold, performance can be improved by considering guidance and control as coupled functions.

The effect of including autopilot dynamics (assumed to be a first order lag) in designing an optimal steering law is demonstrated in Sections 11.2 and 11.3. Only a partially coupled design is considered there in that the autopilot characteristics are taken into account by the guidance law but the guidance dynamics are not taken into account when designing the autopilot. It is shown that an optimal steering law which



accounts for the autopilot lag is significantly better than a suboptimal law that neglects autopilot dynamics if the initial time-to-go\* is of the same order of magnitude as the autopilot time constant. In this section we determine what further performance benefits can be gained by treating the autopilot and steering law design tasks as completely coupled problems.

#### 11.4.1 Problem Formulation

In this section we formulate the optimal guidance-control problem in a manner similar to that used in Section 11.2.2. Both optimal and suboptimal control laws are derived for comparison purposes.

Our first task is to develop a set of state equations which describe the dynamics of the overall system. The missile airframe dynamics are taken to be second order, as in Eqs. (9.2-9) and (9.2-10) (the actuator dynamics are neglected). To obtain the equations of motion it is convenient to define a new state variable

$$a(t)' \triangleq VL_{\alpha} \alpha(t) \quad (11.4-1)$$

Combining Eqs. (9.2-9), (9.2-10) and (11.4-1) with the missile translational dynamics from Eq. (11.2-16) produces

---

\* The initial time-to-go is regarded as the point when the target begins a constant maneuver or, in the case of an initial cross-track velocity, the time at which the missile is launched.

$$\dot{\underline{z}}(t) = \underline{F}\underline{z}(t) + \underline{g}\delta(t)$$

$$\underline{z}(t)^T \triangleq [y(t) \dot{y}(t) a_t(t) q(t) a(t)'] \triangleq [z_1(t) z_2(t) z_3(t) z_4(t) z_5(t)]$$

$$\underline{F} \triangleq \begin{bmatrix} 0 & 1 & 0 & 0 & 0 \\ 0 & 0 & 1 & 0 & -1 \\ 0 & 0 & 0 & 0 & 0 \\ 0 & 0 & 0 & M_q & M_\alpha/VL_\alpha \\ 0 & 0 & 0 & VL_\alpha & -L_\alpha \end{bmatrix}; \quad \underline{g} \triangleq \begin{bmatrix} 0 \\ -VL_\delta \\ 0 \\ M_\delta \\ -VL_\delta L_\alpha \end{bmatrix} \quad (11.4-2)$$

Thus Eq. (11.2-16) is altered by replacing  $x_4(t)$  with two airframe state variables and the control variable becomes control surface deflection,  $\delta(t)$ , instead of commanded acceleration. By analogy with Eq. (11.2-17) the design objective is to choose a feedback control law that minimizes the quadratic performance index

$$J = z_1(T)^2 + r_c \int_0^T \delta(t)^2 dt \quad (11.4-3)$$

As before,  $z_1(T)$  is the terminal miss. However the integral expression in Eq. (11.4-3) is not stated in terms of commanded acceleration; instead it is the integral of the square of the control surface deflection. Consequently the contribution of the control effort to the performance index has a different physical significance here than it does in Eq. (11.2-17). If the control surface actuator is driven electromagnetically, the effort in Eq. (11.4-3) is proportional to the energy consumed. If the actuators are hydraulically driven, the quantity

$$\int_0^T \dot{\delta}(t)^2 dt$$

is a better measure of energy expenditure; however, it is usually observed that increasing  $r_c$  in Eq. (11.4-3) also tends to reduce the value of the integral-square control surface rate. Therefore the above expression for  $J$  has useful properties for most actuator systems. With the above qualifications in mind, we shall speak of the control penalty term in Eq. (11.4-3) as a measure of actuation energy.

Because the above optimal control problem has the same structure as that discussed in Section 11.2, analytical solutions for the optimal, time-varying feedback gains can be obtained using the procedures described in Refs. 7 and 136. However, we are primarily interested in evaluating the performance of the guidance system, a task that must be accomplished numerically. Closed form expressions for the feedback gains offer no particular advantage for this purpose; therefore they are not presented here. From the known properties of the optimal regulator problem (see Appendix B) the solution for control surface deflection that minimizes  $J$  in Eq. (11.4-3) is given by

$$\begin{aligned} \delta_1(t) &= -\underline{k}_1(t)^T \underline{z}(t) \\ \underline{k}_1(t)^T &= \frac{1}{r_c} \underline{g}^T S(t) \end{aligned} \quad (11.4-4)$$

where the matrix  $S(t)$  is the solution to

$$\begin{aligned} \dot{S}(t) &= -S(t) F - F^T S(t) + \frac{1}{r_c} S(t) \underline{g} \underline{g}^T S(t) \\ S(T) &= \begin{bmatrix} 1 & 0 & \cdot & 0 \\ 0 & 0 & \cdot & 0 \\ \cdot & \cdot & \cdot & \cdot \\ 0 & \cdot & \cdot & 0 \end{bmatrix} \end{aligned} \quad (11.4-5)$$

It is desirable to compare the optimal control law given above with the steering law,  $a_{c_1}(t)$ , derived in Section 11.2 under the assumption that the autopilot is already designed with dynamics given approximately by a first order lag. Recall that the latter is an optimal steering policy for minimizing  $J$  in Eq. (11.2-17); however it is not optimal for the problem posed in this section. Because  $a_{c_1}(t)$  is a commanded acceleration and  $\delta(t)$  is a control surface deflection, some algebraic manipulation is required to obtain the associated suboptimal control  $\delta_2(t)$ . This is accomplished by defining the suboptimal control law according to

$$\delta_2(t) \triangleq -c_1 q(t) - c_2 a(t)' + c_3 a_{c_1}(t) \quad (11.4-6)$$

The fixed gains  $c_1$  and  $c_2$  are chosen to provide a stabilized airframe having specified response characteristics and  $c_3$  is selected so that the d-c gain between  $a_{c_1}(t)$  and the normal acceleration of the airframe,  $a(t)$ , is unity. The implementation of Eq. (11.4-6) is illustrated in Fig. 11.4-1. Equation (11.4-6) simulates the application of the steering law  $a_{c_1}(t)$ , derived assuming a first order autopilot, to the actual second order autopilot.

Recall that  $a_{c_1}(t)$  is derived assuming the transfer function  $G(s)$  in Fig. 11.4-1 is of the form

$$\frac{\sigma}{s + \sigma}$$

representing a first order lag. The value of  $\sigma$  is required for mechanizing the steering law. However, in the case treated here the autopilot is actually second order. Consequently the first order lag can be considered only as an approximation. With the fixed gain compensation provided by  $c_1$  and  $c_2$  in Fig. 11.4-1 the autopilot closed loop poles are obtained by substituting

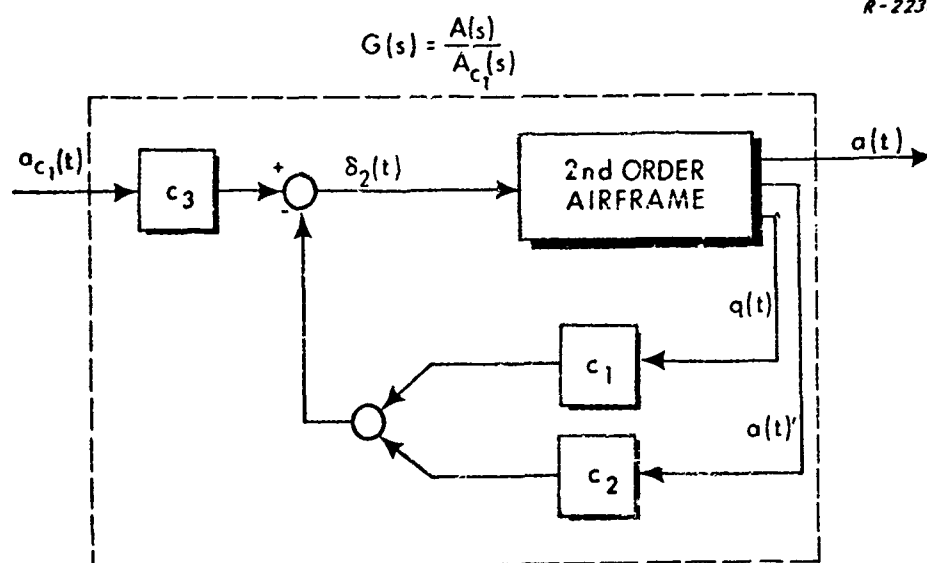


Figure 11.4-1 A Second Order Autopilot Design  
for a Suboptimal Steering Law

$\delta_2(t)$  from Eq. (11.4-6) for  $\delta(t)$  in Eq. (11.4-2) and considering only the dynamics of  $z_4(t)$  and  $z_5(t)$ ; these poles are the eigenvalues  $\lambda_i$  of the matrix

$$F_a = \begin{bmatrix} M_q - M_\delta c_1 & \frac{M_\alpha}{VL_\alpha} - M_\delta c_2 \\ VL_\alpha(1 + c_1 L_\delta) & -L_\alpha + VL_\alpha L_\delta c_2 \end{bmatrix} \quad (11.4-7)$$

We define  $-\sigma$  to be the real part of that eigenvalue of  $F_a$  which has the smallest magnitude; i.e.,

$$\sigma = -\text{sign} \left[ \text{Re}(\lambda_i) \right] \min_i \left| \text{Re}(\lambda_i) \right|; \quad i = 1, 2 \quad (11.4-8)$$

This is certainly not the only rational choice possible for  $\sigma$ . If the closed loop poles are close together a smaller value than that given by Eq.(11.4-8)

may be better. However it seems to be a reasonable selection when the poles have sizeable imaginary parts.

To express the suboptimal control  $\delta_2(t)$  in terms of the state variables  $\underline{z}(t)$  defined in Eq. (11.4-2), a relation is needed for the airframe acceleration  $a(t)$  which is required to generate  $a_{c1}(t)$ . From the airframe equations of motion -- Eq. (8.1-3) and (11.4-1) -- with actuator dynamics neglected, it can be shown that

$$a(t) = a(t)' + VL_\delta \delta(t) \quad (11.4-9)$$

Combining Eqs. (11.2-19), (11.4-6), and (11.4-9),  $\delta_2(t)$  can be written as

$$\delta_2(t) = -\underline{k}_2(t)^T \underline{z}(t)$$

$$\underline{k}_2(t) \triangleq \begin{bmatrix} c_3 h_1(t) \\ c_3 h_2(t) \\ c_3 h_3(t) \\ c_1 \\ c_2 + c_3 h_4(t) \end{bmatrix} \left( \frac{1}{1 + c_3 h_4(t) VL_\alpha} \right) \quad (11.4-10)$$

where the gains  $h_i(t)$ ,  $i = 1, 2, 3, 4$ , are calculated from Eq. (11.2-19).

Equations (11.4-4) and (11.4-10) provide respectively optimal and suboptimal control laws for the system in Eq. (11.4-2). The former is a result of considering the tasks of autopilot and steering law design as a coupled control problem. By comparison the suboptimal control law

does not take the guidance function into account when designing the autopilot, and it approximates the autopilot second order dynamics as a first order lag in deriving the steering law. In the next section the relative performance of these two control policies is compared and evaluated, using the same sensitivity analysis techniques applied in Section 11.3.

#### 11.4.2 Performance Analysis

By analogy with Eq. (11.3-4), the closed loop form of Eq. (11.4-2) is

$$\begin{aligned}\dot{\underline{z}}(t) &= \underline{F}_i(t) \underline{z}(t) \\ \underline{F}_i(t) &\triangleq \underline{F} - \underline{g} \underline{k}_i(t)^T ; \quad i = 1, 2\end{aligned}\tag{11.4-11}$$

The terminal miss  $\underline{z}_1(T)$  caused by a nonzero initial value of  $\underline{z}(t)$  is calculated from the equations,

$$\begin{aligned}\underline{z}_1(T) &= \underline{\varphi}_i(T, t)^T \underline{z}(t) \\ \dot{\underline{\varphi}}_i(T, t) &= - \underline{F}_i(t)^T \underline{\varphi}_i(T, t) \\ \underline{\varphi}_i(T, T) &= \begin{bmatrix} 1 \\ 0 \\ 0 \\ 0 \\ 0 \end{bmatrix} \quad i = 1, 2\end{aligned}\tag{11.4-12}$$

As in Section 11.3.1 we define  $\bar{m}_{ij}(T, t)$  to be the normalized miss caused by a unit initial value for the  $j^{\text{th}}$  element of  $\underline{z}$ ; i.e.,  $\bar{m}_{ij}(T, t)$  is the  $j^{\text{th}}$  element of  $\underline{\varphi}_i(T, t)$ . Only the characteristics of the sensitivity to cross-track velocity,  $\bar{m}_{12}(T, t)$ , are displayed here to illustrate the type of performance achieved with this optimal guidance law. It is expected that conclusions for this case will also hold qualitatively for other sensitivities of interest.

Figure 11.4-2(a) shows curves of the normalized miss  $\bar{m}_{12}$  for the optimal control law  $\delta_1(t)$  given in Eq. (11.4-4). Curves for  $\bar{m}_{22}$  corresponding to the suboptimal control law in Eq. (11.4-10) are given in Figs. 11.4-1(b) and (c) for two different sets of parameter values given in Table 11.4-1 below. The first set (case #1) has values of fixed feedback gains  $c_1$  and  $c_2$  which produce a relatively slowly responding autopilot having a time constant of 0.83 sec; the second set (case #2) yields a faster response with a time constant of 0.13 sec. The values of the airframe parameters --  $M_q$ ,  $M_\alpha$ ,  $M_\delta$ ,  $L_\alpha$ ,  $L_\delta$ , and  $V$  -- are taken from Appendix H, Table H-2, flight condition 4. The curves for  $\bar{m}_{12}$  correspond to different values of the performance index weighting  $r_c$  in Eq. (11.4-3) and those for  $\bar{m}_{22}$  to values of the weighting  $r$  in Eq. (11.2-17).

Qualitatively, the curves in Fig. 11.4-2 are much the same as those in Figs. 11.3-1 and 11.3-2 with respect to their dependence on  $r_c$ ,  $r$ , and  $t_{go}$ . However, the oscillations in the curves corresponding to the suboptimal control law (Figs. 11.4-2(b) and (c)) are much more persistent than we have encountered previously. This behavior results from the fact that  $\delta_2(t)$  is derived assuming first order autopilot dynamics; however, the actual dynamics prescribed by Eq. (11.4-7) are second order and their associated closed loop poles have significant imaginary parts. The situation is quantitatively pictured in Fig. 11.4-3 where the actual autopilot



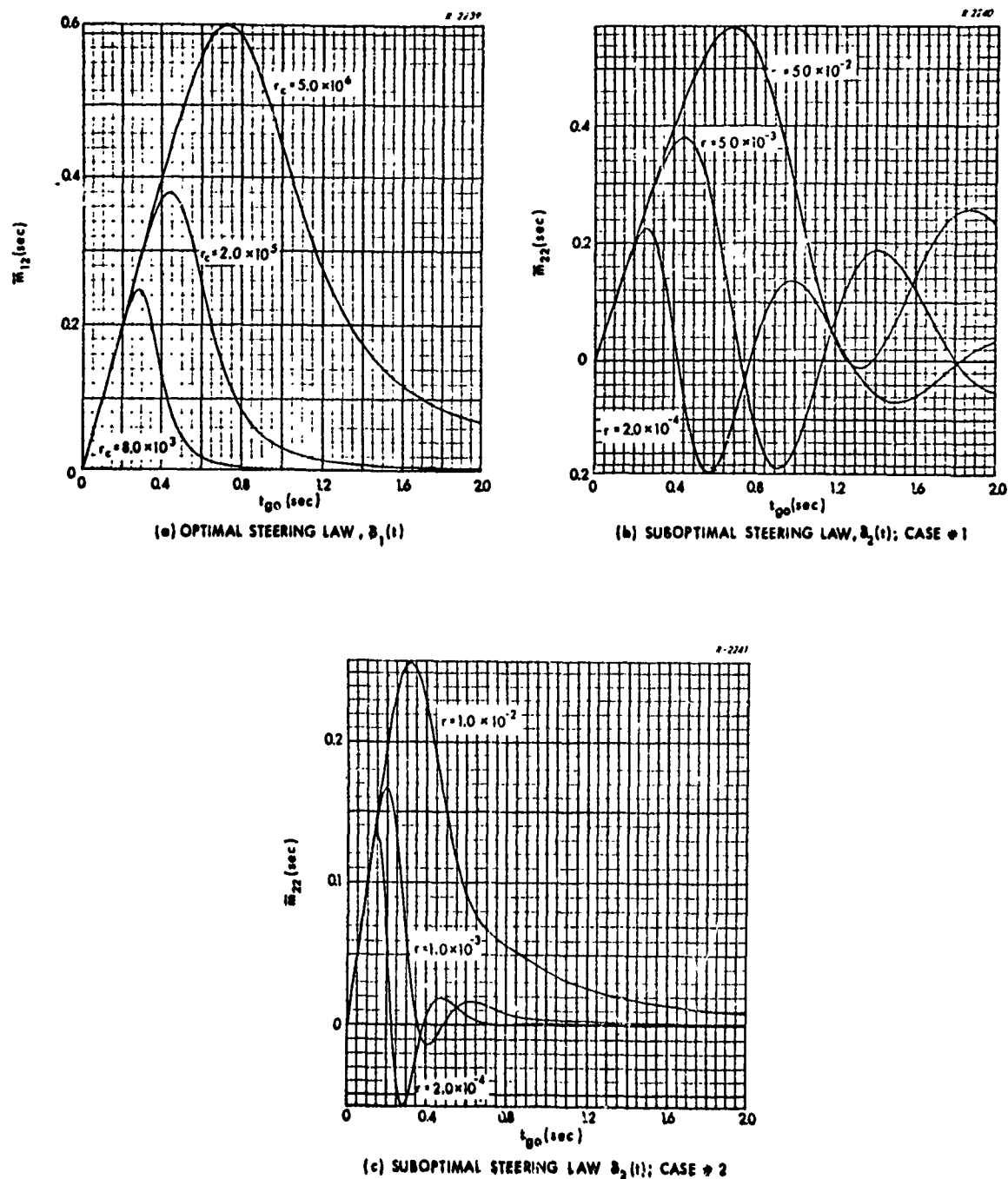


Figure 11.4-2 Normalized Terminal Miss Distance Produced by an Initial Cross-Track Velocity

TABLE 11.4-1  
PARAMETER VALUES FOR SUBOPTIMAL  
CONTROL LAW  $\delta_2(t)$

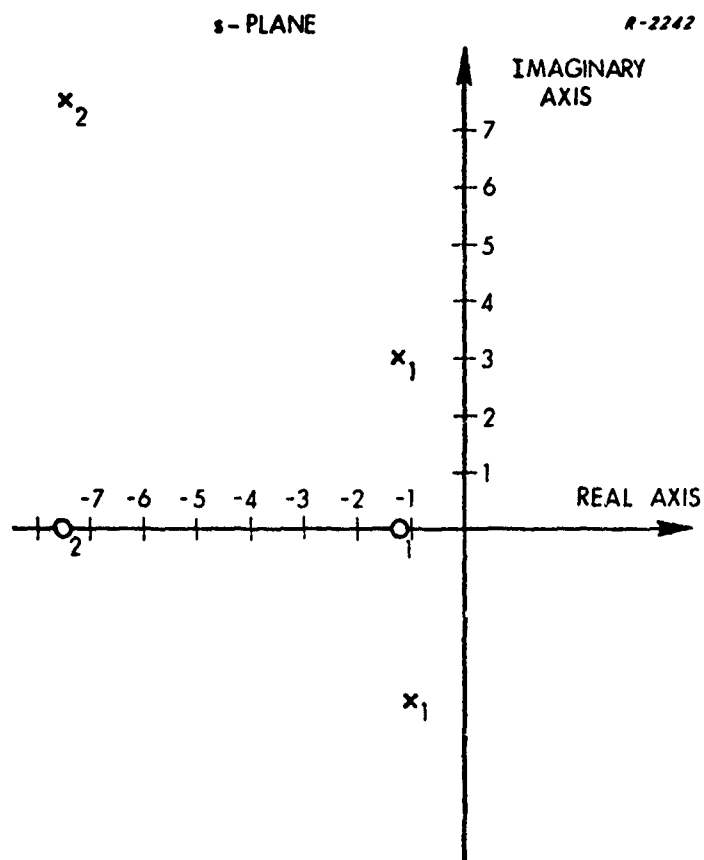
Suboptimal Control Law Parameter	Case No.	
	#1	#2
$c_1$	$2.31 \times 10^{-2}$	0.198
$c_2$	$1.91 \times 10^{-5}$	$1.42 \times 10^{-3}$
$c_3$	$-1.61 \times 10^{-4}$	$-1.65 \times 10^{-3}$
$1/\sigma(\text{sec})$	0.83	0.13

poles and the assumed first order pole,  $-\sigma$ , are displayed for both sets of control parameters in Table 11.4-1. Evidently there is reason to expect that the first order lag is not always a good approximation, especially for case #1 where the autopilot dynamics are more nearly those of a harmonic oscillator. The significance of these observations is that an "optimal" guidance law based on an inaccurate description of autopilot dynamics may not perform nearly so well as expected from the analysis.

In addition to terminal accuracy, another quantity of interest in evaluating performance is the control effort

$$J_{u_i} \triangleq \int_t^T \delta_i(\tau)^2 d\tau \text{ (rad}^2 \text{ sec)} \quad (11.4-13)$$

which is a measure of the control surface deflection required for controlling the missile. This is determined by a set of expressions similar to Eqs. (11.3-14) and (11.3-15); i.e.,



$x_2$

$x_i$ : ACTUAL AUTOPILOT POLES  
FOR  $i^{\text{th}}$  SUBOPTIMAL CASE

$o_i$ : AUTOPILOT POLE FOR FIRST ORDER  
APPROXIMATION FOR  $i^{\text{th}}$  SUBOPTIMAL CASE

Figure 11.4-3 Closed Loop Pole Locations for the Second Order Autopilot and its First Order Approximation

$$J_{u_i} = \underline{z}(t)^T C_i(t) \underline{z}(t)$$

$$\dot{C}_i(t) = -C_i(t) F_i(t) - F_i(t)^T C_i(t) - \underline{k}_i(t) \underline{k}_i(t)^T$$

$$C_i(T) = 0 \quad (11.4-14)$$

where  $\underline{k}_i(t)$  and  $F_i(t)$  are obtained from Eqs. (11.4-4), (11.4-10) and (11.4-11). As in preceding sections we define a root normalized effort

$$\bar{J}_{u_{ij}} = \sqrt{c_{ij}} \quad (\text{rad-sec}^{1/2}/\text{unit state}) \quad (11.4-15)$$

where  $c_{ij}$  is the  $j^{\text{th}}$  diagonal element of  $C_i$  so that the effort produced by an initial condition  $z_j(t)$  is calculated from

$$J_{u_{ij}} = \left[ \bar{J}_{u_{ij}} z_i(t) \right]^2$$

Note that the units of  $\bar{J}_{u_{ij}}$  are different here than in Eq. (11.3-21) because of the different definitions in Eqs. (11.3-13) and (11.4-13). Plots of  $\bar{J}_{u_{12}}$  corresponding to Fig. 11.4-2 are given in Fig. 11.4-4.

To effectively compare the optimal and suboptimal control laws, we crossplot values of  $\bar{m}_{i2}$  and  $\bar{J}_{u_{i2}}$  from Figs. 11.4-2 and 11.4-4 for given values of time-to-go, in the same fashion as Fig. 11.3-14 is derived. The curves are given in Fig. 11.4-5 for  $t_{go} = 0.4$  sec and 1.0 sec.\* These data can be used to analyze the effects of various initial values of cross track velocity on guidance accuracy and control effort, as is done in Table 11.3-1. The only difference is that the effort is now integral square control surface deflection rather than integral square commanded acceleration.

---

\* Note that the number of data points is too small to draw a smooth connecting curve in some cases. This is because the oscillatory nature of the curves for the suboptimal laws in Fig. 11.4-2 causes wide fluctuations in the values of  $|\bar{m}_{22}|$ .

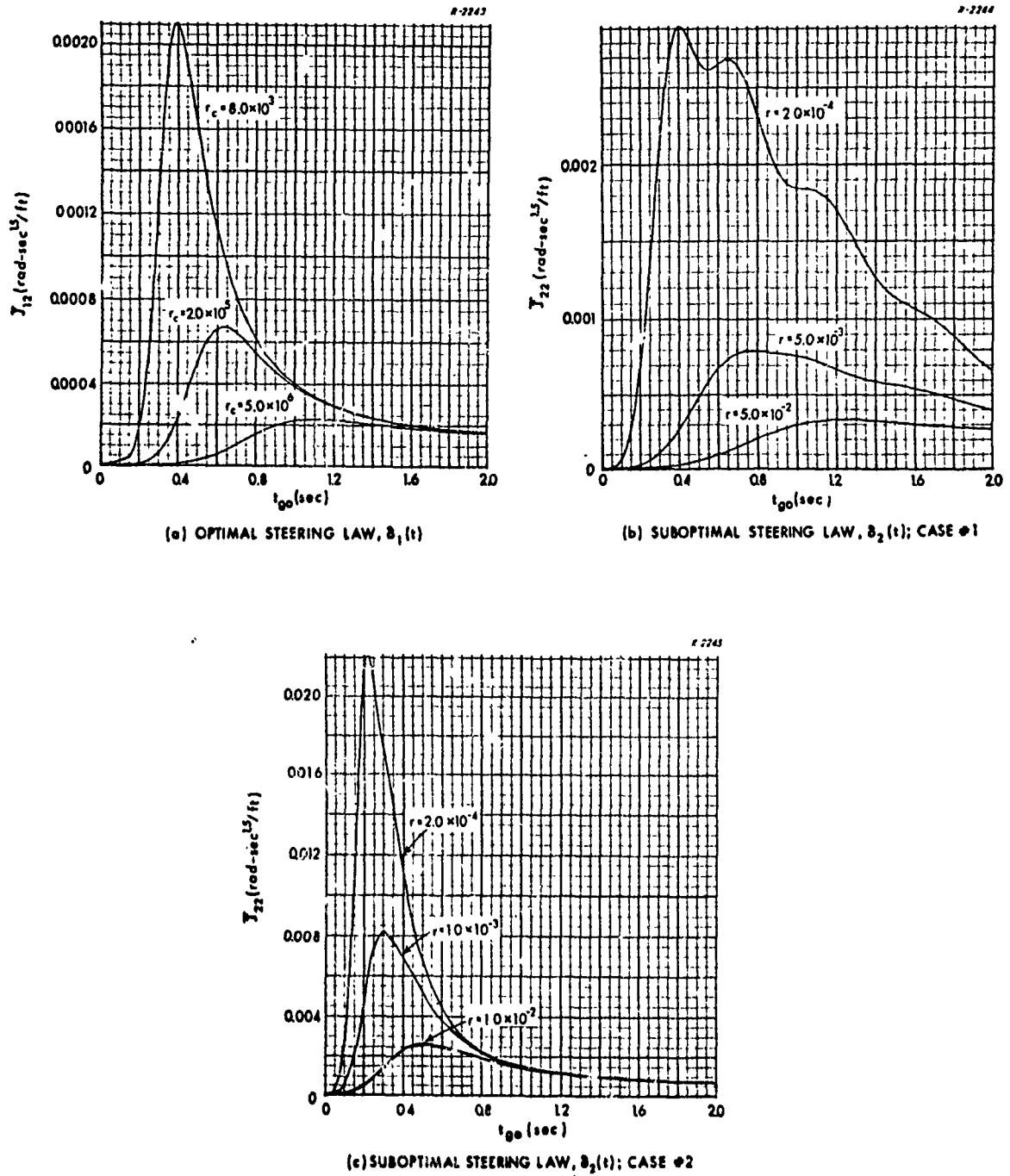


Figure 11.4-4 Root Normalized Effort Caused by an Initial Cross-Track Velocity

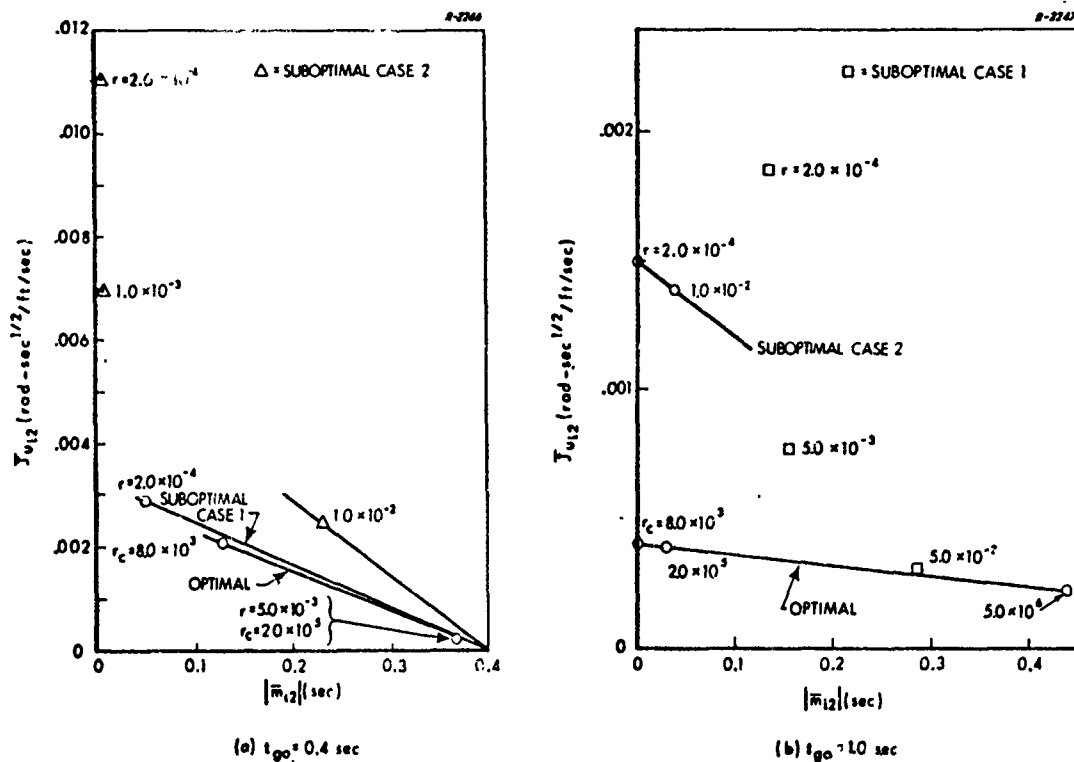


Figure 11.4-5 Root Normalized Effort Versus Normalized Terminal Miss Caused by an Initial Cross-Track Velocity

Recall that there are two aspects of the suboptimal law  $\delta_2(t)$  that make it inferior to the optimal control law when judged on the basis of the index  $J$ , in Eq. (11.4-3). First it is derived with commanded acceleration considered as the control variable rather than control surface deflection and the autopilot feedback gains are preselected constants  $c_1$  and  $c_2$ . Second, it is derived assuming the autopilot is a first order lag, but the actual autopilot dynamics are second order. Both of these assumptions are responsible for the deviations of the suboptimal performance curves from those for the optimal control law in Fig. 11.4-5; the reasons for this are outlined below.

First of all, the fixed feedback gains  $c_1$  and  $c_2$  in the suboptimal design tend to make the autopilot response faster than it needs to be when the missile is some distance from the target. Consequently an initial

cross-track velocity causes more control surface deflection (in the integral square sense) than is necessary to achieve the desired terminal accuracy. This effect is most significant in suboptimal case #2 and contributes to the deviations from optimum of the corresponding performance curves in Fig. 11.4-5.

In the second place, as the weighting constant  $r$  decreases, the feedback gains  $h_1(t)$  in the suboptimal steering law  $\delta_2(t)$  increase and the overall system response becomes more sensitive to the use of a wrong (first order) model for the autopilot. This effect is observed through the oscillatory behavior of the curves in Fig. 11.4-2, particularly case #1 where it has already been noted that the first order lag approximation is especially poor. The resulting contribution to terminal miss distance depends upon  $t_{go}$ . Thus a value of  $r = 2.0 \times 10^{-4}$ , which gives good performance at  $t_{go} = 0.4$  sec in Fig. 11.4-5, gives poor performance at  $t_{go} = 1.0$  sec, relative to the optimal control. If the weighting constant  $r$  gets very low, the suboptimal guidance system actually becomes unstable because the denominator of the factor

$$\frac{1}{1 + c_3 h_4(t) \sqrt{L_\alpha}}$$

in Eq. (11.4-10) becomes negative as  $h_4(t)$  increases in magnitude, making all the gains in  $k_2(t)$  have the wrong sign. The conclusion is that optimal control theory can be helpful in designing laws that account for missile dynamics, provided these dynamics are reasonably accurately modeled. Otherwise the true system performance may be substantially poorer than that prescribed by the theory.

Heretofore nothing has been said about the behavior of the feedback gains in optimal guidance systems. It has been possible to ascertain

their effect on system performance using adjoint theory, without knowing their specific time history. However the optimal gains associated with  $\delta_1(t)$  are of special interest. Figure 11.4-6(a) is a plot of the first element of  $\underline{k}_1(t)$  corresponding to the simulation data in Figs. 11.4-2(a) and 11.4-4(a). For comparison purposes the first element of the set of gains  $\underline{k}_2(t)$  for suboptimal case 2 is shown in Fig. 11.4-6(b). Only one gain from each set is required because they all behave qualitatively in the same fashion.

The point of interest is the fact that the optimal gains become slightly negative just before intercept; this happens for all the elements of  $\underline{k}_1(t)$ . Consequently the guidance system is driven into what can be considered an unstable condition for a short period of time. The reason for this behavior is that the guidance law takes advantage of the fact that the particular missile represented by these simulations can achieve a limited amount of lift from its tail control surfaces as well as from its fixed wings. Normally the principal lift force is supplied by the wings; the tail controls provide the pitching moment required to change angle of attack, thereby varying the magnitude of the lift. However very near intercept there is insufficient time to change the lift force on the wings, since this requires rotating the entire missile; therefore steering commands can best be realized using the faster responding control surfaces. No such behavior is observed for the suboptimal gains because the action of the control surface is not included in the model dynamics.\* Typically this gain reversal is small in magnitude and it occurs just before intercept; consequently it has little net effect on guidance accuracy. However,

---

\* Analytically speaking, the behavior of the optimal gains is a reflection of the fact that the airframe transfer function between control surface deflection and normal acceleration has a right-half-plane zero.



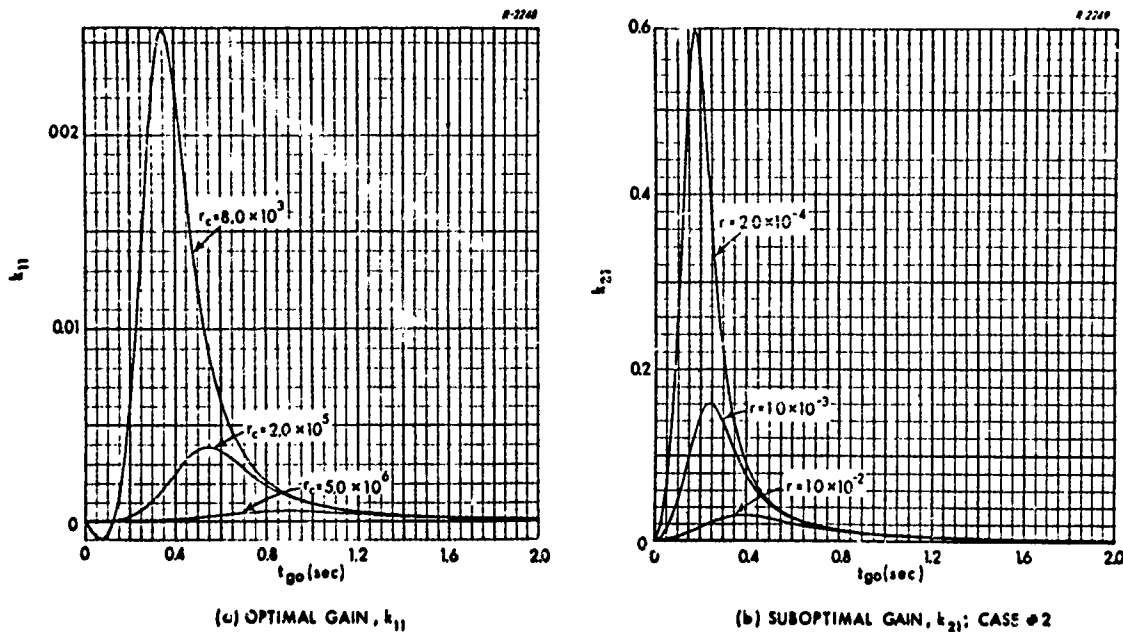


Figure 11.4-6 Comparison of Representative Time Histories for Optimal and Suboptimal Gains

it suggests that if the vehicle had rapidly responding rotatable wings mounted near the center of gravity in addition to tail control surfaces, then an optimal control law would make use of the wing controls to generate the primary lift force, using the tail controls only to balance the resulting lift-induced moments. That is, the entire missile airframe would not have to rotate to develop an angle of attack; instead the wings would rotate with respect to the missile body, presumably resulting in more rapid control system response characteristics. Such a design seems attractive for lifting vehicles in those flight regimes where tail controls alone are incapable of providing sufficiently rapid response. Of course against this potential advantage, the weapons designer must weigh the need for two sets of control surfaces and must consider whether the resulting configuration has desirable aerodynamic properties.

Another point of interest about the set of optimal feedback gains (see Fig. 11.4-6(a)) is that they are generally increasing as time-to-go decreases (except very close to the end of the trajectory). Physically this is reasonable behavior because rapid system response near the end of the trajectory is required to achieve a low value of terminal miss. The gains decrease at the end because the lag associated with the guidance system dynamics reduces the sensitivity of the terminal miss distance to the control level. If the optimal gains associated with the airframe state variables --  $k_{13}(t)$  and  $k_{14}(t)$  in Eq. (11.4-4) -- are considered together with the airframe dynamics it is found that the primary effect of the gains is to produce a time-varying autopilot whose instantaneous pole locations move to the left (right) in the complex plane as  $k_{13}$  and  $k_{14}$  increase (decrease) in magnitude. Consequently, the optimal coupled guidance-autopilot steering law effectively produces an autopilot whose response characteristics vary along the trajectory. The advantage of this over the control methods discussed in Section 11.2 is that less control energy is consumed along the trajectory. However, if energy consumption is not important, good terminal accuracy can also be achieved by predesigning the autopilot to have as good response characteristics as possible everywhere along the trajectory and then formulating the guidance problem with the autopilot dynamics neglected, as in deriving  $a_{c2}(t)$  and  $a_{c3}(t)$  in Eqs. (11.2-24) and (11.2-26). The conclusion is that it is useful to include airframe dynamics in the formulation of the guidance problem only if expenditure of control actuation energy is an important consideration\*; otherwise the usual convention of separating the design of the autopilot and guidance loop is valid.

The purpose of this section has been to demonstrate the effects on performance of simultaneously designing the autopilot and guidance

---

\* See the discussion immediately following Eq. (11.4-3) regarding the significance of  $J_u$  as a measure of control energy.

loops for a tactical missile. Three important conclusions are drawn from the above discussion.

- If autopilot dynamics are included in the problem formulation for an optimal steering law, they must be accurately modeled; otherwise the guidance accuracy may be adversely affected. In particular, the assumption that the autopilot is a first order lag when it actually is second order with lightly damped complex poles is a relatively poor approximation.
- If control actuation energy expenditure is not an important consideration, the usual convention of separating the design of the autopilot and guidance loops is valid.
- Guidance loop performance may be significantly improved if a faster responding control technique, such as rotatable wings in conjunction with tail controls is used.

The need for adaptive control or identification of missile airframe dynamics is implied throughout this discussion. If the autopilot is to be predesigned to achieve as good response as possible everywhere along a trajectory that has variable flight conditions, then adaptive control techniques are needed. Alternatively, if airframe dynamics are to be incorporated in the guidance problem formulation, as in Eq. (11.4-2), then the parameters  $M_\alpha$ ,  $M_\delta$ , etc. must be identified. These tasks can be accomplished by any of the methods described in previous chapters.

## 11.5 SUMMARY AND CONCLUSIONS

This chapter begins with a review of classical homing guidance techniques -- pursuit, beam rider, and proportional guidance. Proportional guidance is generally considered the best of the classical methods because

it is a self contained system that is theoretically able to null the terminal miss when attacking a moving target. However the presence of target maneuvers, autopilot lag, control effort constraints, and control magnitude limitations suggests that steering laws designed with optimal control techniques may offer improvement in performance.

Several optimal steering laws are investigated in Sections 11.2, 11.3, and 11.4, each taking into account a number of different effects. These are summarized in Table 11.5-1. The steering laws are evaluated with respect to one another by applying them to a common set of equations of motion. The principal conclusions are:

- In the presence of target maneuvers, optimal steering laws that include a term proportional to measured target acceleration offer substantial improvement in guidance accuracy over those that do not, as indicated in Fig. 11.3-15.
- Optimal steering laws that correctly include the effects of autopilot dynamics offer significantly improved guidance accuracy for steering commands that are initiated at a value of time-to-go having the same order of magnitude as the effective autopilot lag. This is illustrated by Figs. 11.3-14 and 11.3-15.
- If autopilot dynamics are imperfectly known (e.g., if a second order autopilot having a low damping factor is approximated by a first order lag) the performance of the optimal steering law may be significantly degraded from that predicted by analysis.
- From the standpoint of implementation, the improvement in performance obtained by measuring target acceleration may justify the added computation required in the guidance laws, as compared with conventional proportional guidance. However, the additional complexity required to include autopilot or uncompensated airframe dynamics in the guidance law, even if accurately known, is probably not worthwhile unless control actuation

**TABLE 11.5-1**  
**SUMMARY OF OPTIMAL STEERING LAWS**

Steering Laws*	Conditions for Optimality					
	Maneuvering Target	Neglect Autopilot Dynamics	First/Order Autopilot	Second/Order Airframe	Minimize $x_1(T)^2 + r \int_t^T a_c(\tau)^2 d\tau$	Minimize $z_1(T)^2 + r_c \int_t^T \delta(\tau)^2 d\tau$
$a_{c_1}(t)$	X		X		X	
$a_{c_2}(t)$	X	X			X	
$a_{c_3}(t)$		X			X	
$\delta_1(t)$	X			X		X
$\delta_2(t)$	X		X		X	
<p><math>a_c(t)</math> = commanded normal acceleration</p> <p><math>\delta(t)</math> = commanded control surface deflection</p> <p><math>x_1(\tau), z_1(\tau)</math> = terminal miss distance</p> <p><math>r, r_c</math> = weighting constants</p> <p>* See Eqs. (11.2-19), (11.2-24), (11.2-26), (11.4-4) and (11.4-6).</p>						

effort is a critical consideration; a more practical method for improving guidance accuracy is to pre-design the best possible autopilot.

- Given a set of candidate steering laws, it is possible to generate graphical displays of performance data using linear sensitivity analysis. The plots permit rational comparisons of the techniques, based on guidance accuracy and control effort expended. This information, considered together with the computational complexity of each steering law, will aid in making a specific selection.

The above conclusions should be regarded as tentative, subject to further refinement in a particular application, after considering effects of random measurement noise, control level and normal acceleration limiting, and time-varying, random or intelligent target maneuvers.

The above observations have a direct bearing on missile guidance system design. First of all, the optimal steering laws use time-varying feedback gains which may require more computer storage than is available for a particular application. Therefore a designer might choose to use constant feedback gains instead; if so, the optimal design can be used as a standard of comparison to evaluate the suboptimal system.

If the effort expended by the missile control actuators is an important consideration, there is some advantage in including the dynamics of autopilot ( $a_{c_1}(t)$  in Section 11.2-19) or the uncompensated airframe ( $\delta_1(t)$  in Section 11.4) in the guidance problem formulation. The resulting optimal guidance law effectively provides an autopilot having time-varying feedback gains that tend to increase as the range-to-go decreases. Thus over a long trajectory, some saving in control effort is achieved because the autopilot bandwidth is large only near the end of the trajectory. However, if the actuator power supply is more than sufficient

for the mission under consideration, it is reasonable to predesign the autopilot to have as good a response as possible at all flight conditions (using any of the methods discussed elsewhere in this report) and then to utilize a linear guidance law that neglects the resulting autopilot dynamics.

Another important consideration is the conclusion that autopilot or airframe dynamics should be accurately modeled if they are to be included in an optimal steering law; otherwise the performance benefit expected from the more complex steering law (e. g., compare the complexity of Eqs. (11.2-19) and (11.2-24)) may not be realized. Therefore when flight conditions are time-varying an adaptive capability -- either for identifying airframe parameters or for producing an adaptive autopilot that has predictable dynamics -- is desirable.

Finally, it may be feasible to solve the problem of achieving good guidance accuracy, as it is related to the autopilot response time, by using rapidly acting missile control mechanisms such as rotatable wings. The latter would overcome the inherently slower response characteristics of the conventional tail-controlled, fixed-wing vehicle.

## APPENDIX A

LINEAR DYNAMICAL SYSTEMS

## A.1 STATE SPACE NOTATION

Almost all of the recent advances in control theory -- work by Pontryagin, Bellman, Liapunov, Kalman and others -- are formulated in state space notation. In addition, this manner of stating a problem keeps it closer to physical reality than the classical transform techniques.

A Dynamic System -- The dynamics of a linear system can be represented by a first order vector-matrix differential equation in which  $\underline{x}(t)$  is the system state vector and  $\underline{u}(t)$  is a forcing function, viz:

$$\dot{\underline{x}}(t) = F(t) \underline{x}(t) + G(t) \underline{u}(t) \quad (A-1)$$

This is the continuous form employed in most modern control theory. Figure A-1 illustrates the equation. The state vector of a dynamic system is composed of any set of quantities sufficient to completely describe the unforced motion of that system; given the state vector at a particular point in time and a history of the system forcing function, the state at any other time can be computed. The state vector is not necessarily a unique set of variables; several sets may be able to fulfill the above requirement.

Given a high-order linear differential equation,

$$\left( D^n + a_{n-1}(t) D^{n-1} + \dots + a_1(t) D + a_0(t) \right) y(t) = f(t)$$

where  $D^j \triangleq d^j/dt^j$ , we can define a set of state variables  $x_1(t), \dots, x_n(t)$  by



R-230

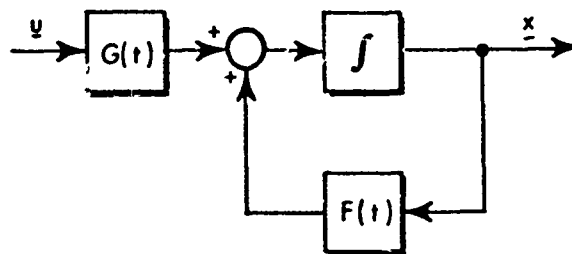


Figure A-1 Illustration of Continuous Representation of Linear Dynamic Equations

$$x_1(t) = y(t)$$

$$x_2(t) = \dot{x}_1(t)$$

$$\vdots$$

$$x_n(t) = \dot{x}_{n-1}(t)$$

These variables can be used to write the high order differential equation as a set of first order linear differential equations:

$$\dot{x}_1(t) = x_2(t)$$

$$\dot{x}_2(t) = x_3(t)$$

$$\vdots$$

$$\dot{x}_n(t) = -a_0(t) x_1(t) - a_1(t) x_2(t) - \dots - a_{n-1}(t) x_n(t) + f(t)$$

Or, in the form of Eq. (A-1);

$$\begin{bmatrix} \dot{x}_1 \\ \dot{x}_2 \\ \vdots \\ \dot{x}_{n-1} \\ \dot{x}_n \end{bmatrix} = \begin{bmatrix} 0 & 1 & 0 & \dots & 0 & 0 \\ 0 & 0 & 1 & \dots & 0 & 0 \\ \vdots & \vdots & \vdots & \ddots & \vdots & \vdots \\ 0 & 0 & 0 & \dots & 0 & 1 \\ -a_0 & -a_1 & -a_2 & \dots & -a_{n-2} & -a_{n-1} \end{bmatrix} \begin{bmatrix} x_1 \\ x_2 \\ \vdots \\ x_{n-1} \\ x_n \end{bmatrix} + \begin{bmatrix} 0 \\ 0 \\ \vdots \\ 0 \\ f \end{bmatrix} \quad (\text{A-2})$$

Equation (A-2) is illustrated in block diagram form in Fig. A-2. Notice that the state variables are in each case the outputs of integrations.

R-223

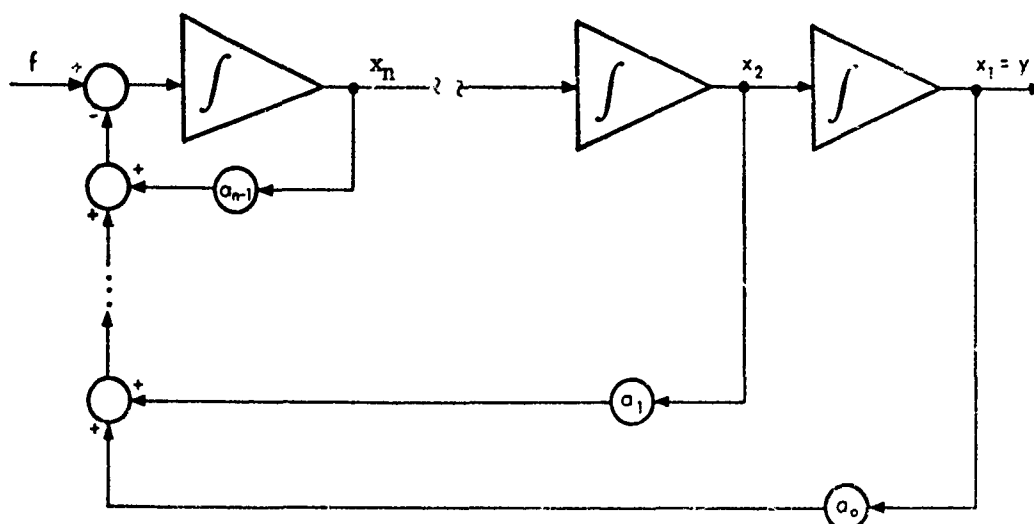


Figure A-2 Block Diagram Representation of Eq. (A-2)

In many linear systems of interest the forcing function is multi-variable; that is,  $\underline{u}(t)$  in Eq. (1) is composed of several nonzero functions. Also, the individual elements of  $\underline{u}(t)$  may drive several state variables simultaneously, causing  $G(t)$  to be a matrix with significant elements at locations not on its diagonal. In these cases the system dynamics may be determined directly from the physical description of the problem.

For example, a block diagram of the physical system may be sketched and the first order vector-matrix differential equation determined by inspection. Figure A-3 illustrates a hypothetical linear dynamic system forced by several inputs. The outputs of all the integrators constitute a convenient set of state variables. The system dynamic equations can be written in the form of Eq. (A-1);

$$\begin{bmatrix} \dot{x}_1 \\ \dot{x}_2 \\ \vdots \\ \dot{x}_n \end{bmatrix} = \begin{bmatrix} a_1 & 1 & c_1 & \dots \\ a_2 & b_1 & 1 & \\ \vdots & \vdots & \vdots & \\ a_n & b_n & c_n & \dots \end{bmatrix} \begin{bmatrix} x_1 \\ x_2 \\ \vdots \\ x_n \end{bmatrix} + \begin{bmatrix} g_1 & \dots & h_1 \\ g_2 & \dots & h_2 \\ \vdots & \vdots & \vdots \\ g_n & \dots & h_n \end{bmatrix} \begin{bmatrix} u_1 \\ u_2 \\ \vdots \\ u_r \end{bmatrix}$$

Reference 34 demonstrates the steps required to convert a higher order differential equation into a set of state variables driven by a multi-variable forcing function.

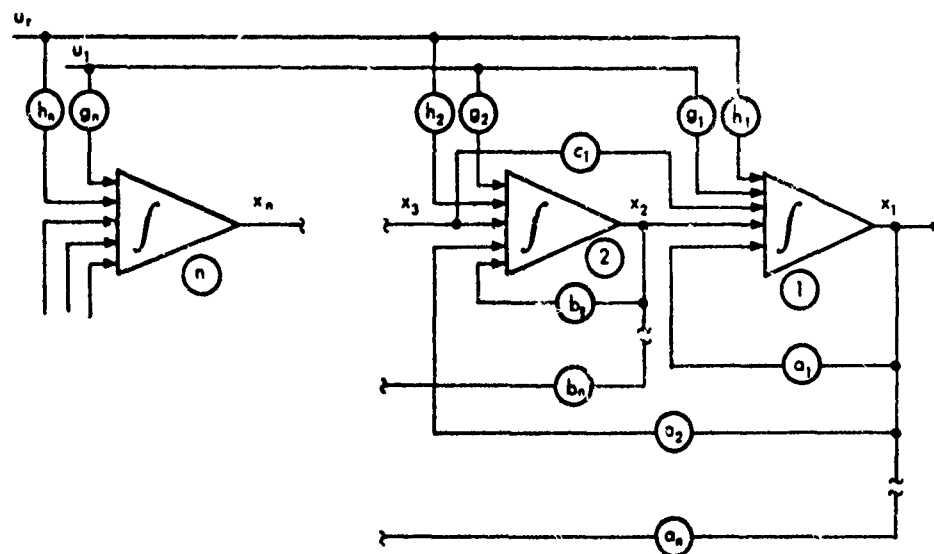


Figure A-3 Block Diagram of a Hypothetical Linear Dynamic System

## A.2 THE TRANSITION MATRIX

The homogeneous unforced matrix differential equation corresponding to Eq. (A-1) is

$$\dot{\underline{x}}(t) = F(t) \underline{x}(t) \quad (A-3)$$

Suppose that at some time,  $\tau$ , all but one of the outputs of the integrators in Fig. A-3 were set to zero and no inputs,  $u_i$ , are present. Also assume that the nonzero integrator output was given the value, one. The behavior of the state vector for all times after  $\tau$  could be expressed in terms of a time-varying "solution vector,"  $\varphi_j(t, \tau)$ , where the subscript refers to the integrator whose output is nonzero.

$$\varphi_j(t, \tau) = \begin{bmatrix} x_1(t, \tau)_j \\ x_2(t, \tau)_j \\ \vdots \\ x_n(t, \tau)_j \end{bmatrix} \quad (A-4)$$

If the initial condition on the  $j^{\text{th}}$  integrator is something other than unity,  $c$  for example, then from the linear nature of the system

$$\varphi_j(t, \tau, c) = c \varphi_j(t, \tau)$$

Also, if integrators  $i$  and  $j$  both have nonzero outputs  $c_i$  and  $c_j$  at time  $\tau$ , the response for the system is just the sum of the individual response vectors

$$\varphi_{i,j}(t, \tau, c_i, c_j) = c_i \varphi_i(t, \tau) + c_j \varphi_j(t, \tau)$$

But this can be written as a product of the matrix

$$\begin{bmatrix} \varphi_i & \varphi_j \end{bmatrix}$$

and the vector

$$\begin{bmatrix} c_i \\ c_j \end{bmatrix}$$

In general every integrator can have a nonzero value at  $\tau$  and the time history of the state becomes the sum of the individual effects

$$\underline{x}(t) = \begin{bmatrix} \varphi_1(t, \tau) & \varphi_2(t, \tau) & \dots & \varphi_n(t, \tau) \end{bmatrix} \underline{x}(\tau)$$

which is written for compactness as

$$\underline{x}(t) = \Phi(t, \tau) \underline{x}(\tau)$$

The matrix  $\Phi(t, \tau)$  is called the transition matrix for the system of Eq. (A-3). The transition matrix allows calculation of the state vector at some time,  $t$ , given the state vector at  $\tau$ .

Returning to Eq. (A-4), it can be seen that the solution vectors obey the differential equation

$$\frac{d\varphi_j(t, \tau)}{dt} = F(t) \varphi_j(t, \tau)$$

where

$$\varphi_j(\tau, \tau) = \underline{\epsilon}_j$$

$$\underline{\epsilon}_1 = \begin{bmatrix} 1 \\ 0 \\ 0 \\ \vdots \\ 0 \end{bmatrix}; \quad \underline{\epsilon}_2 = \begin{bmatrix} 0 \\ 1 \\ 0 \\ \vdots \\ 0 \end{bmatrix}, \text{ etc.}$$

Therefore, the transition matrix, composed of the vectors  $\underline{\phi}_j$ , obeys the equation

$$\frac{d}{dt} \Phi(t, \tau) = F(t) \Phi(t, \tau)$$

$$\Phi(\tau, \tau) = I$$

The transition matrix  $\Phi(t_1, t_0)$  relates  $\underline{x}(t_1)$  to  $\underline{x}(t_0)$  in Eq. (A-3);

$$\underline{x}(t_1) = \Phi(t_1, t_0) \underline{x}(t_0)$$

Similarly,

$$\begin{aligned} \underline{x}(t_2) &= \Phi(t_2, t_1) \underline{x}(t_1) \\ &= \Phi(t_2, t_1) \Phi(t_1, t_0) \underline{x}(t_0) \end{aligned}$$

Therefore,

$$\Phi(t_2, t_0) = \Phi(t_2, t_1) \Phi(t_1, t_0)$$

This principle is illustrated in Fig. A-4 for a first order system having a scalar transition matrix,  $\phi(t, \tau)$ . It is a general property of the state transition matrix, independent of the order of  $t_0$ ,  $t_1$  and  $t_2$  in time. In addition,

$$\Phi(t, t) = \Phi(t, \tau) \Phi(\tau, t) = I$$

Premultiplying this expression by  $\Phi^{-1}(t, \tau)$  provides the useful relation

$$\Phi^{-1}(t, \tau) = \Phi(\tau, t)$$

Transition Matrix for Stationary Systems — For a stationary system, the F matrix is time-invariant and the transition matrix depends only on the time interval considered:

$$\Phi(t, \tau) = \Phi(t - \tau)$$

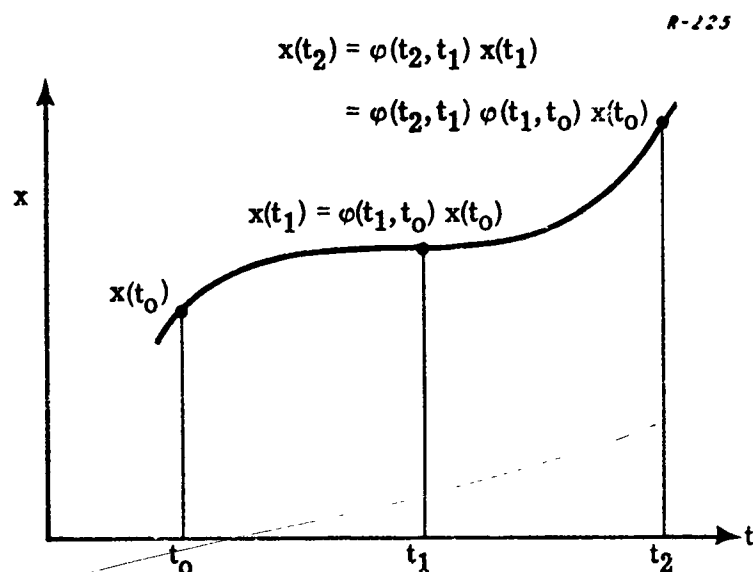


Figure A-4 Illustration of the Behavior of the State for a First Order Homogeneous System

Equation (A-3) can be used to expand  $\underline{x}(t)$  in a Taylor's series about some time,  $t_0$ ,

$$\underline{x}(t) = \underline{x}(t_0) + \underline{\dot{x}}(t_0)(t-t_0) + \underline{\ddot{x}}(t_0) \frac{(t-t_0)^2}{2!} + \dots$$

But

$$\begin{aligned} \underline{\dot{x}}(t_0) &= F \underline{x}(t_0) \\ \underline{\ddot{x}}(t_0) &= F \underline{\dot{x}}(t_0) = F^2 \underline{x}(t_0) \\ &\vdots \\ &\vdots \\ &\text{etc.} \end{aligned}$$

Substituting, the expansion becomes

$$\begin{aligned} \underline{x}(t) &= \underline{x}(t_0) + F(t-t_0) \underline{x}(t_0) + \frac{F^2(t-t_0)^2}{2!} \underline{x}(t_0) + \dots \\ &= \left[ I + F(t-t_0) + \frac{1}{2!} F^2(t-t_0)^2 + \dots \right] \underline{x}(t_0) \end{aligned} \quad (A-5)$$

By analogy to the scalar case the matrix exponential is defined by

$$e^F \triangleq I + F + \frac{F^2}{2!} + \frac{F^3}{3!} + \dots \quad (A-6)$$

Consequently, the transition matrix for the stationary system can be identified from Eq. (A-5) as

$$\Phi(t-t_0) = e^{F(t-t_0)}$$

which depends only on the stationary system dynamics (F) and the interval  $t-t_0$ .

In stationary systems,  $t_0$  may often be assigned the value zero. A useful expression for the transition matrix  $\Phi(t, 0)$  can be obtained by taking Laplace transforms in Eq. (A-3). Defining  $\underline{X}(s)$  as the transform of  $\underline{x}(t)$ , one obtains

$$s\underline{X}(s) = F\underline{X}(s) + \underline{x}(0)$$

or alternatively

$$\underline{X}(s) = (Is - F)^{-1} \underline{x}(0) \quad (A-7)$$

Comparison of Eq. (A-7) with the expression

$$\underline{x}(t) = \Phi(t, 0) \underline{x}(0)$$

implies that

$$\Phi(t, 0) = L^{-1} \{ (Is - F)^{-1} \}$$

where  $L^{-1} \{ \}$  denotes the inverse Laplace transform. Defining  $\bar{\Phi}(s)$  to be the Laplace transform of  $\Phi(t, 0)$ , one has

$$\bar{\Phi}(s) = (Is - F)^{-1} \quad (A-8)$$



### A.3 THE MATRIX SUPERPOSITION INTEGRAL

Consider now the general linear system of Eq. (A-1), including the forcing function  $\underline{u}(t)$ ;

$$\dot{\underline{x}} = \underline{F}\underline{x} + \underline{G}\underline{u} \quad (\text{A-9})$$

Referring to Fig. A-5 we can see that the effect of the input to the  $i^{\text{th}}$  integrator of Fig. A-3 over a small interval  $(\tau - \Delta\tau, \tau)$  can be represented as an impulse whose area is the value of the  $i^{\text{th}}$  element of the vector  $\underline{G}(\tau)\underline{u}(\tau)$  times the interval  $\Delta\tau$ . Temporarily assuming that the initial conditions on all the integrators are zero, this impulse will cause a small change  $\Delta x_i$  in the integrator output;

$$\Delta x_i(\tau) = \left( \underline{G}(\tau) \underline{u}(\tau) \right)_i \Delta\tau$$

The change in the entire state vector can be expressed as

$$\Delta \underline{x}(\tau) = \begin{bmatrix} \Delta x_1 \\ \Delta x_2 \\ \vdots \\ \Delta x_n \end{bmatrix} = \underline{G}(\tau) \underline{u}(\tau) \Delta\tau$$

The effect of this small change on the state at some subsequent point in time can be expressed by

$$\Delta \underline{x}(t), \text{ given an impulse input } \underline{G}(\tau) \underline{u}(\tau) \Delta\tau = \Phi(t, \tau) \underline{G}(\tau) \underline{u}(\tau) \Delta\tau$$

Because the system is linear the response to the complete input history can be viewed as the sum of the responses to individual impulses. In the limit as  $\Delta\tau \rightarrow 0$  the effect of the input on the state at some time,  $t$ , can be represented by

$$\underline{x}(t) = \int_{-\infty}^t \Phi(t, \tau) \underline{G}(\tau) \underline{u}(\tau) d\tau$$

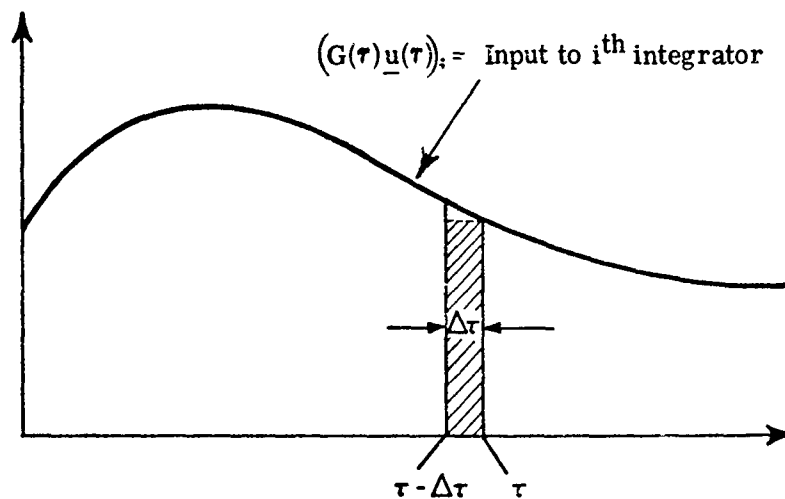


Figure A-5 Representation of the Input to the  $i$ th Integrator as an Impulse

Now because the system is linear, the effects of initial conditions at time  $t_0$  and the presence of a forcing function after time  $t_0$  can be combined to yield

$$\underline{x}(t) = \Phi(t, t_0) \underline{x}(t_0) + \int_{t_0}^t \Phi(t, \tau) G(\tau) \underline{u}(\tau) d\tau \quad (\text{A-10})$$

The integral in Eq. (A-10) is often called the matrix superposition integral.

Of possible use in solving Eq. (A-10) is the relation

$$\frac{d}{d\tau} (\Phi(t, \tau)) = -\Phi(t, \tau) F(\tau)$$

which can be derived from

$$\begin{aligned} \Phi(t, \tau - \Delta\tau) &= \Phi(t, \tau) \Phi(\tau, \tau - \Delta\tau) \\ &= \Phi(t, \tau) \left( I + F(\tau)(\Delta\tau) + \frac{F(\tau)^2(\Delta\tau)^2}{2!} + \dots \right) \end{aligned}$$

The derivative is given by

$$\begin{aligned}\frac{d}{d\tau} \Phi(t, \tau) &= \lim_{\Delta\tau \rightarrow 0} \frac{\Phi(t, \tau) - \Phi(t, \tau - \Delta\tau)}{\Delta\tau} \\ &= \lim_{\Delta\tau \rightarrow 0} \frac{-\Phi(t, \tau) F(\tau) (\Delta\tau) + O(\Delta\tau^2)}{\Delta\tau} \\ &= -\Phi(t, \tau) F(\tau)\end{aligned}$$

#### A.4 CONTROLLABILITY AND OBSERVABILITY

Consider a linear dynamical system for which a set of linear measurements  $\underline{y}(t)$  is defined by

$$\begin{aligned}\dot{\underline{x}}(t) &= F(t) \underline{x}(t) + G(t) \underline{u}(t) \\ \underline{y}(t) &= H(t) \underline{x}(t)\end{aligned}\tag{A-11}$$

The measurements are those quantities which can be directly observed at various system output "terminals"\*. For this system of equations,  $\underline{u}(t)$  is the control and  $\underline{y}(t)$  is the observation. Two fundamental properties of the system, related to these sets of variables are defined as follows:

A system is controllable at time  $t_1 > t_0$  if it is possible to choose  $\underline{u}(t)$  in the interval  $t_0 \leq t \leq t_1$  to "drive" any state  $\underline{x}(t_0) = \underline{\xi}$  to any point  $\underline{x}(t_1) = \underline{\gamma}$ .

A system is observable at time  $t_1 > t_0$  if it is possible to determine the state  $\underline{x}(t_0)$  by observing  $\underline{y}(t)$  in the interval  $t_0 \leq t \leq t_1$ .

Controllability determines whether one can achieve any desired state by manipulating  $\underline{u}(t)$  and observability determines whether one can determine the value of the state at any time by measuring  $\underline{y}(t)$ .

---

\* This terminology is suggested by the input and output terminals of electric networks.

Conditions which determine whether the linear system in Eq. (A-11) has these properties are determined by the algebraic properties of the matrices  $F(t)$ ,  $G(t)$ , and  $H(t)$  (Ref. 30). For constant systems, necessary and sufficient conditions are:

A constant,  $n^{\text{th}}$  order, linear, dynamical system is controllable if, and only if, the matrix

$$\Theta = \left[ G \mid FG \mid F^2G \mid \dots \mid F^{n-1}G \right] \quad (\text{A-12})$$

has rank\*  $n$ .

A constant  $n^{\text{th}}$  order linear dynamical system is observable if, and only if, the matrix

$$\Lambda = \left[ H^T \mid F^T H^T \mid (F^T)^2 H^T \mid \dots \mid (F^T)^{n-1} H^T \right] \quad (\text{A-13})$$

has rank  $n$ .

Note that because the system is time invariant, the time  $t_1$ , does not appear in Eqs. (A-12) and (A-13), implying that  $t_1$  is arbitrary so long as

$$t_1 > t_0$$

This concludes a brief summary of the important properties of linear systems used in this report. The reader is referred to Refs. 30 and 34 for more details on the subject.

---

\* That is, at least one set of  $n$  columns of  $\Theta$  form a set of linearly independent vectors.

## APPENDIX B

OPTIMAL CONTROL OF LINEAR SYSTEMS

## B.1 INTRODUCTION

The basic task faced by a control system designer can often be expressed in terms of the solution  $\underline{x}(t)$  to a set of first order differential equations

$$\dot{\underline{x}}(t) = \underline{f}[\underline{x}(t), \underline{u}(t), t]; \quad \underline{x}(t_0) = \underline{x}_0 \quad (\text{B-1})$$

The vector  $\underline{x}(t)$  is called the state of the system and  $\underline{u}(t)$  is a vector set of control variables which can be specified by the designer. The objective is to determine  $\underline{u}(t)$  such that  $\underline{x}(t)$  achieves some desired behavior subject to the cause-effect relationship provided by Eq. (B-1). For example, it may be required that certain elements of the state vector take on specified values at a given terminal time  $t_f$ , or that the solution to Eq. (B-1) (also referred to as the trajectory of the state) should possess certain stability properties.

Generally speaking, design criteria that are related only to the behavior of  $\underline{x}(t)$ , are not sufficient to determine a unique control  $\underline{u}(t)$ . Clearly if one's purpose is to transfer the state from one point  $\underline{x}(t_0) = \underline{x}_0$  in "state space" to another  $\underline{x}(t_f) = \underline{x}_f$  without any specification on the path taken by  $\underline{x}(t)$  or limits upon the control, then there are likely to be an infinite number of paths and control functions that can be employed. Consequently additional design requirements can be accommodated.

Usually it is true that the implementation of different controllers, all of which satisfy the desired criteria on the state, costs different amounts

of some important measure of acceptability, --e.g., system complexity, weight, and/or volume. For example, a controller for a self-contained tactical missile guidance system that requires a large computer to mechanize  $\underline{u}(t)$  would be unacceptable with respect to all of these characteristics. Often this "cost," although quite recognizable in the resulting system design, is difficult to describe mathematically. Therefore it may not be possible to include it in the design criteria in any systematic fashion. In such circumstances a satisfactory mechanization is achieved using a combination of intuition, experience, and trial and error. In other situations the cost can be expressed as a mathematical quantity; a common example is a time integral, such as

$$\int_{t_0}^{t_f} |\underline{u}(t)| \, dt$$

or

$$\int_{t_0}^{t_f} \underline{u}(t)^T \underline{u}(t) \, dt$$

Expressions of this type may represent the total amount of fuel or energy consumed, in which case it is desired to keep their values small. For this case a reasonable design procedure is to determine the control so that the associated cost is minimized, subject to any constraints on the behavior of  $\underline{x}(t)$  or  $\underline{u}(t)$ . The solution to a problem posed in this fashion, called an optimal control problem, is referred to as an optimal control law; it is the best control to use for the particular design criteria selected. More generally, an optimal control law is one which minimizes a specified performance index, defined as a functional of the state

and the control, while satisfying the specific design constraints. Thus an optimal control problem provides a means for selecting one control law from the many which are permissible when there is no performance index.

Another property one desires to have in any controller design is feedback; that is, the optimal control should be explicitly a function of the state  $\underline{x}(t)$ . When it has this form,  $\underline{u}(t)$  is referred to as a closed loop or feedback control. This arrangement is needed because there are always forces or disturbances acting upon a physical system which are not accounted for in the mathematical model given by Eq. (B-1). These cause the state to deviate from the path which is predicted by integrating Eq. (B-1) with a specified  $\underline{u}(t)$ . If the latter is explicitly a function of time only (i.e. it is an open loop control) the controller never senses the effect of disturbances on the state, and the latter may drift away from its desired path, possibly in an unstable fashion.

The above-mentioned considerations are important in any control system design problem. This appendix presents analytical details for formulating and obtaining a feedback solution for a special kind of optimal control problem associated with linear dynamical systems. Basic textbook references for this subject are Athans and Falb (Ref. 97) and Bryson and Ho (Ref. 137).

## B.2 THE LINEAR OPTIMAL REGULATOR

A linear dynamical system is described by a differential equation of the form

$$\dot{\underline{x}}(t) = A(t) \underline{x}(t) + B(t) \underline{u}(t); \quad \underline{x}(t_0) = \underline{x}_0 \quad (B-2)$$

where  $\underline{x}(t)$  is a set of state variables which describe the response of the system to a set of control inputs  $\underline{u}(t)$ . An important optimal control problem associated with this system requires the selection of  $\underline{u}(t)$  such that the "quadratic" performance index

$$J[\underline{x}(t), \underline{u}(t)] = \underline{x}(t_f)^T F \underline{x}(t_f) + \int_{t_0}^{t_f} \left[ \underline{x}(t)^T Q(t) \underline{x}(t) + \underline{u}(t)^T R(t) \underline{u}(t) \right] dt \quad (B-3)$$

is minimized for a given terminal time  $t_f$ . The weighting matrices  $F$ ,  $Q(t)$ , and  $R(t)$  are to be specified by the designer where  $F$  and  $Q(t)$  are positive semidefinite and  $R(t)$  is positive definite.\*

Physically speaking, the terms in  $J$  involving the state provide a measure of the magnitude of  $\underline{x}(t)$  both at the termination time and during the interval  $(t_0, t_f)$ . The term involving  $\underline{u}(t)$  is a measure of the control effort expended. The objective is to make  $\underline{x}(t)$  small in the sense defined by the magnitudes of the individual indices

$$\begin{aligned} J_f &\triangleq \underline{x}(t_f)^T F \underline{x}(t_f) \\ J_{\underline{x}} &\triangleq \int_{t_0}^{t_f} \underline{x}(t)^T Q(t) \underline{x}(t) dt \end{aligned} \quad (B-4)$$

---

\* A positive semidefinite matrix  $F$  is one for which the condition

$$\underline{x}^T F \underline{x} \geq 0$$

holds for all vectors  $\underline{x}$ . If this condition holds with strict inequality for all  $\underline{x} \neq 0$ ,  $F$  is said to be positive definite. The quantity  $\underline{x}^T F \underline{x}$  is known as a quadratic form.



This is to be accomplished with the competing requirement that excessive control levels not be used, as measured by

$$J_{\underline{u}} \triangleq \int_{t_0}^{t_f} \underline{u}(t)^T R(t) \underline{u}(t) dt \quad (B-5)$$

The total performance index is the sum of  $J_f$ ,  $J_{\underline{x}}$  and  $J_{\underline{u}}$ ; therefore minimization of  $J$  prevents any one of the individual indices from being too large at the expense of the others.

The significance of using quadratic forms to measure the size of the control and the state is that they heavily penalize large values of  $\underline{x}(t)$  and  $\underline{u}(t)$ . In addition, the squares of state and control variables are often identified as power and their integral square values are interpreted as energy; e.g.,  $J_{\underline{u}}$  in Eq. (B-5) can be a measure of energy expended. An additional nonincidental reason for the popularity of quadratic performance indices is that the solution for the optimal feedback control is readily derived and it is a linear function of the state; hence it is relatively easy to mechanize. Other types of optimal design criteria often permit a solution for the open-loop optimal control but the corresponding feedback control is usually not readily obtained.

The solution to the optimal control problem described above is given by

$$\underline{u}(t) = -R(t)^{-1} B(t)^T S(t) \underline{x}(t) \quad (B-6)$$

where  $S(t)$  is the solution to a matrix Riccati differential equation,

$$\dot{S}(t) = -S(t) A(t) - A(t)^T S(t) + S(t) B(t) R(t)^{-1} B(t)^T S(t) - Q(t)$$

$$S(t_f) = F \quad (B-7)$$

The matrix  $S(t)$  can be determined by integrating Eq. (B-7) backwards from the terminal time. Then a set of time-varying gains,

$$K(t) \triangleq R^{-1}(t) B(t)^T S(t), \quad (B-8)$$

can be calculated and stored in a controller to implement the feedback control law

$$\underline{u}(t) = -K(t) \underline{x}(t); \quad t_0 \leq t \leq t_f \quad (B-9)$$

In this form the control is optimal for all time in the interval  $(t_0, t_f)$  with  $\underline{x}(t)$  regarded as the initial state. The value of the performance index for any initial condition  $\underline{x}(t)$  at time  $t \geq t_0$  evaluated over the interval  $(t, t_f)$  is given by

$$J = \underline{x}(t)^T S(t) \underline{x}(t)$$

From the standpoint of implementation, observe that Eq. (B-9) assumes all the elements in the state vector are available to generate  $\underline{u}(t)$ . Often in a practical situation some state variables cannot be measured directly; instead there may be a set of measurements  $\underline{m}(t)$  related to  $\underline{x}(t)$  by a linear transformation

$$\underline{m}(t) = H(t) \underline{x}(t) \quad (B-10)$$

To implement the optimal control law,  $\underline{x}(t)$  must be obtained from  $\underline{m}(t)$  as accurately as possible. Methods for accomplishing this task when the system of equations, Eqs. (B-2) and (B-10), is observable (see Appendix A) are discussed in Refs. 138, 139, and 140. The result is that an estimate  $\hat{\underline{x}}(t)$  of the state can be obtained by implementing a multi-dimensional "filter" defined by differential equations of the form

$$\dot{\hat{\underline{x}}}(t) = F(t) \hat{\underline{x}}(t) + G(t) \underline{m}(t) \quad (B-11)$$

where  $F(t)$  and  $G(t)$  are derived either from the principles of estimation theory (Ref. 138) or from linear observer theory (Refs. 139 and 140). Consequently when all state variables are not directly measurable ( $H(t)$  in Eq. (B-10) cannot be inverted), the need to implement an expression such as Eq. (B-11), as well as Eq. (B-9) with  $\hat{\underline{x}}(t)$  substituted for  $\underline{x}(t)$ , complicates the structure of the controller.

### B.3 CHOICE OF PERFORMANCE WEIGHTING MATRICES

A critical step in defining the optimal control problem is the selection by the designer of the weighting matrices  $F$ ,  $Q(t)$  and  $R(t)$  in Eq. (B-3). There is no direct procedure for accomplishing this task; it embodies all of the subjectivity remaining in the design problem. The elements in any one matrix can be selected with respect to each other on the basis of the relative importance of various products of state variables, as indicated in Ref. 137. Often none of the cross products --  $x_i(t) x_j(t)$  or  $u_i(t) u_j(t)$ ,  $i \neq j$  -- in the quadratic forms are of interest so that the off-diagonal terms in the weighting matrices are taken as zero. The diagonal elements of each matrix can be sized according to the desired relative magnitudes of the elements in  $\underline{x}(t)$  and  $\underline{u}(t)$ . For instance if the desired magnitudes of  $x_j(t_f)$  and  $x_i(t_f)$  are known relative to each other, say

$$\frac{x_j(t_f)^2}{x_i(t_f)^2} = r_{ji}, \quad (B-12)$$

then require that the diagonal elements  $f_{ii}$  and  $f_{jj}$  of  $F$  satisfy

$$\frac{f_{ii}}{f_{jj}} = \frac{x_j(t_f)^2}{x_i(t_f)^2} = r_{ji} \quad (B-13)$$

This determines  $f_{ii}$  relative to  $f_{jj}$ ; hopefully the resulting optimal control will operate to yield values of the terminal state which approximately satisfy Eq. (B-12). Relative values of the elements in two different weighting matrices can be chosen from rough, a priori knowledge of the magnitudes of the penalty terms  $J_f$ ,  $J_{\underline{x}}$  and  $J_{\underline{u}}$  which might result in a reasonable case. For example, suppose it is known that the level of control  $u_1(t)$  required to yield a desired value of  $x_1(t_f)$  has a magnitude on the order of  $M_1$ . Then let

$$\frac{q_{11}}{f_{11}} = \frac{x_1(t_f)^2}{M_1^2(t_f - t_0)} \quad (\text{B-14})$$

Using some heuristic method of this type, one arrives at trial values of  $F$ ,  $Q(t)$  and  $R(t)$ . If the resulting optimal control yields trajectories for  $\underline{x}(t)$  and  $\underline{u}(t)$  which appear unsatisfactory, adjustments can be made to the weighting matrices to change the system behavior.

The fact that trial and error are required to determine appropriate weighting matrices for the performance index tends to contradict the basic philosophy of optimal control. The latter implicitly contains the idea that, given required constraints upon the state and control variables of a dynamical system, a performance index which accurately represents the cost of designing and implementing the system can be devised. It is desired that this index, and no other, be minimized; however, in practical applications considerations often arise which modify this design concept. In particular, frequently one has certain performance criteria in mind which cannot be easily incorporated into the mathematical formulation of an optimal control problem. As an illustration note that the performance index in Eq. (B-3) is a weighted sum of several different cost

factors which compete with one another. The designer may be primarily interested in the values of individual terms, such as

$$\int_{t_0}^{t_f} u_i(t)^2 dt$$

Each term of this type is, for the optimal control situation, dependent upon the weighting matrices used to define the performance index and it cannot be evaluated without actually solving the control problem for specific choices of  $F$ ,  $Q(t)$  and  $R(t)$ . Thus several trial designs may be needed before the designer is satisfied with the collective behavior of the state and control variables and some compromise in his "true" objectives may be required. Other examples of design criteria that are difficult to treat mathematically are ranges of allowable settling time and overshoot in response to step commands. In these cases quadratic performance indices can also be used as an artifice to generate a family of trajectories from which one, having the additional desired features, is selected. In view of these contingencies, optimal control theory for linear systems using quadratic performance indices can be a useful design aid but it is no panacea.

#### B.4 THE TIME-INVARIANT LINEAR REGULATOR

An important special case of the linear optimal regulator described in Section B.2 occurs when Eq. (B-2) and the weighting matrices are time invariant --  $A(t)$  and  $B(t)$  are constant matrices,  $A$  and  $B$  -- and

$$F = 0; \quad Q(t) = Q; \quad R(t) = R$$

For this application interest is focused on the form of the optimal control law as  $t_f$  approaches infinity. Under the added restriction that the linear constant system

$$\dot{\underline{x}}(t) = A \underline{x}(t) + B \underline{u}(t); \quad \underline{x}(t_0) = \underline{x}_0 \quad (\text{B-15})$$

is controllable\* it has been shown (Ref. 141) that the feedback control which minimizes

$$J = \int_{t_0}^{\infty} \left[ \underline{x}(t)^T Q \underline{x}(t) + \underline{u}(t)^T R \underline{u}(t) \right] dt \quad (\text{B-16})$$

is given by

$$\underline{u}(t) = -R^{-1} B^T S \underline{x}(t) \quad (\text{B-17})$$

The constant matrix  $S$  is the unique positive semidefinite solution to the "steady state" matrix Riccati equation\*\*

$$SA + A^T S - SBR^{-1} B^T S + Q = 0 \quad (\text{B-18})$$

The feedback gain matrix

$$K = R^{-1} B^T S,$$

is also constant, requiring much less storage than the time-dependent controller.

Perhaps the most important property of the above control law is that the closed loop system

$$\dot{\underline{x}}(t) = \left( A - BR^{-1} B^T S \right) \underline{x}(t) \quad (\text{B-19})$$

---

\* See Appendix A for a definition of controllability.

\*\* When any eigen values of  $A$  have nonnegative real parts, some additional restrictions on the weighting matrix  $Q$  are required (Ref. 147) in order that there be a unique positive semidefinite solution to Eq. (B-17).

is asymptotically stable in the large (Ref. 141). Hence even though there is some subjectivity in the choice of  $Q$  and  $R$ , various trial values of the latter always lead to a set of feedback gains for which the system has desirable stability properties. When the dimensions of the state and control are large, solving Eq. (B-18) is a convenient method for selecting various values of  $K$  which have this property.

## B.5 VARIATIONS ON THE LINEAR OPTIMAL REGULATOR

One objection to the optimal regulator problem as posed in Sections B.2 and B.4 is that the control law requires knowledge of all state variables. If a filtering operation as suggested in Eq. (B-11) must be performed on the available measurements to accomplish this task, the system complexity increases. To avoid this difficulty it may be desirable to formulate an optimal control problem which requires only partial state feedback. This is done simply by requiring that a control  $\underline{u}(t)$  having the restricted form

$$\underline{u}(t) = - \left[ \begin{array}{c} K_r(t) \\ [0] \end{array} \right] \underline{x}(t) \quad (B-20)$$

be determined such that a performance index  $J$  (either Eq. (B-3) or (B-16)) is minimized subject to the equations of motion; e. g.,

$$\dot{\underline{x}}(t) = A\underline{x}(t) + B\underline{u}(t) \quad (B-21)$$

The zeros in the gain matrix defined in Eq. (B-20) multiply those elements of  $\underline{x}(t)$  which are not available for feedback. This is a seemingly minor modification to the optimal regulator problem; however it considerably complicates the procedure for determining the feedback control law. A numerical method for determining the gains  $K_r(t)$  is given in Ref. 142.

Another technique for determining a restricted set of feedback gains is given in Ref. 143. Here the condition on  $\underline{u}(t)$  is the same as Eq. (B-20) but the quadratic performance index includes cross product terms in the state and control. This leads to a simpler solution for  $K_r(t)$  but the physical significance of the cost functional becomes obscured by the special techniques used to select certain of its weighting matrices.

In Section B.3 it is mentioned that trial and error are often required to design the optimal regulator because the performance index is really a weighted sum of several competing indices. To eliminate the need to select weighting constants, it can be required that each separate term of  $J$  take on specified values, except the one which is to be minimized. This results in an optimal control problem with integral constraints. To illustrate this idea, consider the problem of choosing a control  $\underline{u}(t)$  for the system

$$\dot{\underline{x}}(t) = A \underline{x}(t) + B \underline{u}(t); \quad \underline{x}(t_0) = \underline{x}_0 \quad (\text{B-22})$$

such that the performance index

$$J_{\underline{u}} = \int_{t_0}^{t_f} \underline{u}(t)^T R \underline{u}(t) dt \quad (\text{B-23})$$

is minimized subject to the constraint

$$J_{\underline{x}} = \int_{t_0}^{t_f} \underline{x}(t)^T Q \underline{x}(t) dt = c \quad (\text{B-24})$$

where  $c$  is a specified constant. For this illustration we take  $F = 0$  in Eq. (B-4). The motivation for this problem formulation is the desire to



insure that  $\underline{x}(t)$  is "small enough" in the interval  $(t_0, t_f)$ . Therefore a specific value is assigned to  $J_{\underline{x}}$  rather than including it in the performance index, as is done for the optimal regulator in Eq. (B-3). Consequently there is no need to consider what the "size" of  $Q$  should be relative to  $R$ .

To solve the above problem it is convenient to proceed as if we want to minimize the quantity

$$J = J_{\underline{u}} + \lambda \int_{t_0}^{t_f} \underline{x}(t)^T Q \underline{x}(t) dt \quad (B-25)$$

where  $\lambda$  is a weighting constant to be specified presently; for the moment we ignore Eq. (B-24). The solution to this problem is obtained directly from Section B.2; the optimal control is given by

$$\underline{u}(t) = -R^{-1} B^T S(t) \underline{x}(t) \quad (B-26)$$

where  $S(t)$  satisfies

$$\dot{S}(t) = -S(t) A - A^T S(t) + S(t) B R^{-1} B^T S(t) - \lambda Q \quad (B-27)$$

$$S(t_f) = 0$$

This equation can be solved once  $\lambda$  is known. If  $\lambda$  can be chosen so that Eq. (B-24) is satisfied, the solution to the problem with  $J_{\underline{x}}$  constrained is determined.

Appealing to the adjoint theory for linear systems\* we know that for any feedback control law

---

\* See Appendix G.

$$\underline{u}(t) = -K(t) \underline{x}(t) \quad (B-28)$$

applied to Eq. (B-21), the value of  $J_{\underline{x}}$  caused by initial conditions  $\underline{x}(t)$  at any time  $t$  is determined by the relation

$$J_{\underline{x}} = \underline{x}(t)^T C(t) \underline{x}(t) \quad (B-29)$$

where  $C(t)$  is the solution to

$$\begin{aligned} \dot{C}(t) &= - \left( A - B K(t) \right)^T C(t) - C(t) \left( A - B K(t) \right) - Q(t) \\ C(t_f) &= 0 \end{aligned} \quad (B-30)$$

If an optimal control law is used we know from Eq. (B-26) that

$$K(t) = R^{-1} B^T S(t) \quad (B-31)$$

Substituting from Eq. (B-31) into Eq. (B-30) and combining with Eq. (B-26) yields the following control law for minimizing the performance index  $J_{\underline{u}}$ , subject to the constraint on  $J_{\underline{x}}$  in Eq. (B-24):

$$\begin{aligned} \underline{u}(t) &= - R^{-1} B^T S(t) \underline{x}(t) \\ \dot{S}(t) &= S(t) A - A^T S(t) + S(t) B R^{-1} B^T S(t) - \lambda Q \\ \dot{C}(t) &= - \left( A - B R^{-1} B^T S(t) \right)^T C(t) - C(t) \left( A - B R^{-1} B^T S(t) \right) - Q \\ S(t_f) &= C(t_f) = 0 \\ \underline{x}(t_0)^T C(t_0) \underline{x}(t_0) &= c \end{aligned} \quad (B-32)$$

Because  $\lambda$  is unknown, Eq. (B-32) is a set of coupled non-linear differential equations with boundary conditions at both end points.

Consequently they must generally be solved by some numerical method.

An iterative type procedure can be used as follows:

- Guess a value of  $\lambda$ .
- Integrate the differential equations for  $S(t)$  and  $C(t)$  backward from  $t_f$  to  $t_0$ .
- Check to see whether the expression

$$\underline{x}^T(t_0) C(t_0) \underline{x}(t_0) = c$$

is satisfied. If so,  $S(t)$  yields the desired feedback gains; if not, choose a new value of  $\lambda$  and repeat the above steps.

Successive choices of  $\lambda$  can be made by any convenient finite-difference type method.

Because the last expression in Eq. (B-32) depends upon the initial value of the state, the solutions for  $S(t)$  and  $K(t)$  also depend upon  $\underline{x}(t_0)$ , making the control law partially open loop in character. To avoid this situation it is desirable to modify the condition on  $J_{\underline{x}}$  by normalizing the integral in Eq. (B-24). Thus require instead that

$$\bar{J}_{\underline{x}} \triangleq \max_{\underline{x}(t_0)} \left[ \frac{\int_{t_0}^{t_f} \underline{x}(t)^T Q \underline{x}(t) dt}{\underline{x}(t_0)^T \underline{x}(t_0)} \right] = c \quad (B-33)$$

Referring to Eq. (B-29) it follows that

$$\bar{J}_{\underline{x}} = \max_{\underline{x}(t_0)} \left[ \frac{\underline{x}(t_0)^T C(t_0) \underline{x}(t_0)}{\underline{x}(t_0)^T \underline{x}(t_0)} \right] \triangleq |C(t_0)| = c \quad (\text{B-34})$$

The scalar quantity  $|C(t_0)|$  is referred to as the norm of the matrix  $C(t_0)$ ; it can be evaluated from the relation (Ref. 144)

$$|C(t_0)| = \max_i \rho_i(C(t_0)) = c \quad (\text{B-35})$$

where  $\rho_i$  is the  $i^{\text{th}}$  eigenvalue of  $C(t_0)$ .

Replacement of the fifth expression in Eq. (B-32) by Eq. (B-35) eliminates the dependence of the optimal control law upon the initial state; however it still depends upon the initial time. The last objection is eliminated in the steady state situation where  $t_f$  approaches infinity. Just as in the optimal regulator, the corresponding feedback gains become constants which satisfy

$$\begin{aligned} \underline{u}(t) &= -K \underline{x}(t) \\ K &= R^{-1} B^T S \\ SA + A^T S - S B R^{-1} B^T S + \lambda Q &= 0 \\ (A - B R^{-1} B^T S)^T C + C (A - B R^{-1} B^T S) + Q &= 0 \\ \max_i \rho_i(C) &= c \end{aligned} \quad (\text{B-36})$$

The relations in Eq. (B-36) provide a method for choosing constant feedback gains so that Eq. (B-34) is satisfied as  $t_f$  approaches infinity. The numerical effort required to determine  $K$  is considerably greater than for the optimal regulator; however there is less subjectivity in defining a performance index. The extension to more than one

quadratic integral constraint can be made quite readily by introducing more "multipliers"  $\lambda$ . However each new constraint requires an additional matrix equation similar to that for  $C$  in Eq. (B-36) and an additional eigenvalue condition. It is possible that the conditions leading to the matrix norm in Eq. (B-34) can be changed to permit a simpler computation than determining the maximum eigenvalue of  $C$ . This procedure for selecting a set of constant feedback gains is largely experimental at present and little experience with the resulting system performance or the feasibility of possible modifications in the problem formulation is currently available.\*

This concludes a summary of several important features of modern optimal control theory. It is intended only as a review of the material considered in this report; for additional information the reader is referred to the aforementioned textbooks (Refs. 97, 137) and the literature.

---

\* There are apparently some unanswered questions about existence of solutions to this type of problem formulation.

## APPENDIX C

AN ANALYSIS OF THE M.I.T. GRADIENT METHOD

This appendix is concerned with an examination of the M.I.T. parameter adjustment rule (Ref. 40), to determine the extent to which it achieves the gradient algorithm described in Section 4.2 and given in Eq. (4.2-10). Recall that the objective is to change a parameter value  $h_i$  by an amount  $\Delta h_i$ , given by

$$\Delta h_i(t_j) = -\alpha_i \int_{t_j}^{t_{j+1}} \left[ L_e(t) e_{h_i}(t) \right]_{h_i(t_j)} dt \quad (C-1)$$

where

$$t_{j+1} - t_j = T$$

and subscripts  $e$  and  $h_i$  denote partial differentiation with respect to  $e$  and  $h_i(t_j)$  (see Eq. (4.2-11)). The quantity  $L[e(t)]$  is a positive function of the error signal. As an alternative to Eq. (C-1) the M.I.T. rule uses the analog gain adjustment algorithm

$$\dot{h}_i(t) = -\alpha_i L_e(t) e_{h_i}(t) \quad (C-2)$$

The actual total change in  $h_i(t)$  is not completed until time  $t_{j+1}$  and is given by

$$\Delta \tilde{h}_i(t_{j+1}) \triangleq -\alpha_i \int_{t_j}^{t_{j+1}} L_e(t) e_{h_i}(t) dt \quad (C-3)$$

with continuous updating of  $h_i(t)$ . In order that this procedure be justified on the basis of gradient arguments, it is required that

$$\Delta \tilde{h}_i(t_{j+1}) \cong \Delta h_i(t_j) \quad (C-4)$$

The first observation is that in general strict equality does not hold in Eq. (C-4) because  $h_i$  is held constant in Eq. (C-1) at the value  $h_i(t_j)$ , whereas in Eqs. (C-2) and (C-3)  $h_i(t)$  is continuously updated. Because  $e(t)$  is a functional of  $h(t)$  through Eq. (4.2-6), the integrands of the two expressions differ. This fact can be detrimental to system performance if Eq. (C-2) adjusts the adaptive gains in the wrong direction near the beginning of the interval, thereby causing significant variations in  $L_e(t)$  and  $e_{h_i}(t)$  later in the interval. It is possible that the resulting closed loop adaptive system could be made unstable by this behavior. This potential difficulty can be avoided by updating  $h_i$  only at discrete times  $t_j$ , as suggested in Section 4.2.2.

Another comparison between Eqs. (C-1) and (C-3) is afforded by the M.I.T. procedure for computing  $e_{h_i}(t)$  for  $t \geq t_j$  given in Eq. (4.2-18), and repeated here as

$$\begin{aligned} e_{h_i}(t) &\cong \underline{c}^T \tilde{\underline{x}}_{h_i}(t) \\ \dot{\tilde{\underline{x}}}_{h_i}(t) &= A_m \tilde{\underline{x}}_{h_i}(t) - b_m x_i(t); \quad \tilde{\underline{x}}_{h_i}(t_0) = \underline{0} \end{aligned} \quad (C-5)$$

In order that Eq. (C-4) hold for successive integration intervals, the quantity  $\tilde{\underline{x}}_{h_i}(t)$  should be reinitialized to zero in the adaptive controller at times  $t_j$ ,  $j = 0, 1, \dots$ . This corresponds to beginning the integration in Eq. (C-1) over successive intervals, with

$$e_{h_i}(t) \Big|_{h_i(t_j)} = 0$$

However, in the M.I.T. method Eq. (C-5) is implemented continuously from  $t = t_0$  without ever resetting  $\tilde{\underline{x}}_{h_i}$  to zero. Presumably this is a

matter of convenience to avoid the digital logic associated with reinitialization. Thus at first glance, the M.I.T. adaptation rule looks like a gradient procedure only over the first T seconds; for subsequent intervals, the integral in Eq. (C-3) might be substantially different from that in Eq. (C-1).

To analyze this aspect of the M.I.T. method, suppose the adaptive system is in equilibrium at time  $t_\ell > t_0$  with

$$\dot{h}(t) = 0; \quad e(t) = 0$$

At this instant let a change in some system parameter occur so that an error begins to develop. For  $t \geq t_\ell > t_0$  the solution of Eq. (C-5) is

$$e_{h_i}(t) = -c^T \int_{t_0}^t \Phi_m(t, \tau) \underline{b}_m x_i(\tau) d\tau \quad (C-6)$$

where  $\Phi_m(t, \tau)$  is the transition matrix\* for the system model. On the other hand, if  $\tilde{x}_{h_i}(t)$  is set to zero at  $t_\ell$ , then

$$e_{h_i}(t)^\dagger = -c^T \int_{t_\ell}^t \Phi_m(t, \tau) \underline{b}_m x_i(\tau) d\tau \quad (C-7)$$

where the superscript  $\dagger$  means that the differential equations for  $\tilde{x}_i(t)$  are reinitialized at  $t = t_\ell$ . The error incurred in using the solution of (C-6) rather than (C-7) in the parameter adjustment algorithm of Eq. (C-2) is related to the quantity

---

\* See Appendix A for a definition of transition matrix.



$$\begin{aligned}
\Delta e_{h_i}(t) &\triangleq e_{h_i}(t) - e_{h_i}(t)^{\dagger} \\
&= - \underline{c}^T \int_{t_0}^{t_\ell} \Phi_m(t, \tau) \underline{b}_m x_i(\tau) d\tau
\end{aligned} \tag{C-8}$$

Assuming the linear time-invariant reference model is chosen to be asymptotically stable, the elements of the transition matrix approach zero exponentially at a rate determined by the dominant time constant associated with model pole locations; i.e., the magnitudes of the elements of  $\Phi_m(t, \tau)$  in Eq. (C-8) regarded as functions of  $t$  approach zero as  $ce^{-\sigma(t-\tau)}$  for some positive values of  $c$  and  $\sigma$ . Consequently  $|\Delta e_{h_i}(t)|$  as given by Eq. (C-8) is small if

$$\sigma(t - \tau) \gg 0; \quad t_0 \leq \tau \leq t_\ell \tag{C-9}$$

The condition expressed by Eq. (C-9) holds for most values of  $t$  within the gain adjustment interval,  $t_\ell \leq t \leq t_\ell + T$ , if

$$T \gg \tau_m \tag{C-10}$$

where  $\tau_m$  is the model settling time. If Eq. (C-10) is satisfied, the resulting integrated effect of  $\Delta e_{h_i}(t)$  upon  $h_i$  also tends to be small.

The conclusion is that the analog adaptive algorithm reliably produces the weighting function  $e_{h_i}(t)$  required in Eq. (C-1) only for an integration interval which is significantly longer than the model settling time. Therefore if the gain  $\alpha_i$  is assigned a value much greater than is justified for such a long interval, or if the system parameters and command input vary

considerably, the real-time parameter adjustment rule expressed by Eq. (C-2) does not necessarily correspond to a gradient method.

The object here is to provide a qualitative measure of the conditions under which an analogy between the M.I.T. method and gradient techniques can be made. It may be observed in particular applications that the adaptive system of Fig. 4.2-1 behaves satisfactorily even when the design assumptions do not hold; such characteristics are fortuitous but they cannot be predicted from the theory. A by-product of this discussion is recognition that by discretely updating the adaptive gains and reinitializing  $\tilde{x}_{h_i}$  in Eq. (C-5) at times  $t_j$ ,  $j = 0, 1, \dots$ , the analogy between M.I.T. and gradient methods can be made for any value of  $T$  in Eq. (C-1). A short integration interval is desirable to achieve a rapid convergence rate because many adjustments of the type given in Eq. (C-1) are required to achieve the minimum of  $J$  in Eq. (4.2-1), for fixed values of the plant parameters. Because the increments,  $\Delta h_i$ , are to be computed in real time over successive intervals of length  $T$ , sufficient total time is required to provide enough steps for adequate convergence. Assuming that the allowable change in  $\underline{h}$  which satisfies condition (C-4) with adequate accuracy is independent of the length of the interval and assuming the cost function is invariant with time, the convergence rate of the gradient technique is inversely proportional to  $T$ . Typically then, recalling the condition given by Eq. (4.2-4),  $T$  should be specified by

$$T \cong \tau_m \quad (C-11)$$

provided that  $\tilde{x}_{h_i}(t)$  is reset to zero at the beginning of each adjustment interval. This reasoning leads to the discrete form of the M.I.T. method described in Section 4.2.2.

## APPENDIX D

### STABILITY THEORY

In this appendix definitions and theorems related to stability theory which are helpful in analyzing and designing adaptive control systems are given. An extensive body of literature exists on this subject, some of which is provided in Refs. 64-71. Excellent basic treatments are provided in Refs. 64, 67, 68 and 71. No attempt is made to give a complete survey of the subject here; only material required in this report is presented.

#### D.1 DEFINITIONS

We begin by introducing definitions of various types of stability which apply to the asymptotic behavior of solutions of a set of time-invariant, first order differential equations beginning at time  $t_0$ ;

$$\dot{\underline{x}} = \underline{f}(\underline{x}); \quad \underline{x}(t_0) = \underline{x}_0 \quad (\text{D-1})$$

We are interested in the properties of  $\underline{x}(t)$  for  $t > t_0$  near the equilibrium point,  $\underline{x}_e$ , which satisfies

$$\underline{f}(\underline{x}_e) = \underline{0} \quad (\text{D-2})$$

By redefining the state with a shift of origin,

$$\underline{x}(t) \triangleq \underline{x}_e - \underline{z}(t)$$

one can always make the equilibrium solution for  $\underline{z}(t)$  equal to zero.

Therefore without loss of generality, assume  $\underline{x}_e = \underline{0}$ .

The solution to Eq. (D-1) near the origin can be qualitatively described in terms of the following definitions (Refs. 64 and 67):

1. The origin is a stable equilibrium point of Eq. (D-1) if for every real number  $\delta > 0$ , there exists a real number,  $\epsilon(\delta)$  (depending upon  $\delta$ ), such that the condition

$$|\underline{x}_0| \leq \epsilon$$

implies

$$|\underline{x}(t)| \leq \delta; \quad t \geq t_0$$

In other words,  $\underline{x}(t)$  is bounded in magnitude by an arbitrarily small number if the initial conditions are sufficiently small.

2. The origin is an asymptotically stable equilibrium point of Eq. (D-1) whenever it is stable and, in addition,

$$\lim_{t \rightarrow \infty} |\underline{x}(t)| = 0$$

More precisely, there is some real number  $\gamma > 0$  such that for every  $\delta > 0$  there is also a number  $T(\delta, \underline{x}_0)$  for which

$$|\underline{x}_0| \leq \gamma$$

implies

$$|\underline{x}(t)| \leq \delta \text{ for all } t > t_0 + T$$

These definitions provide only local descriptions of system behavior. That is, the number  $\epsilon(\delta)$  might have a finite upper bound over all values of  $\delta$ . This would mean that for some value of the initial state whose magnitude is larger than the bound, the convergence properties expressed in the definitions would not hold. In many cases one

desires a stronger condition on system behavior such as that provided by:

3. The solution to Eq. (D-1) is globally asymptotically stable if it is stable (in the sense of definition 1 above) and

$$\lim_{t \rightarrow \infty} |\underline{x}(t)| = 0$$

for all  $\underline{x}_0$ .

Definition 3 guarantees a well behaved system no matter how large is  $|\underline{x}_0|$ .

The above definitions can be applied to an adaptive missile autopilot having constant, possibly unknown, plant parameters and a constant input. Ideally, global asymptotic stability of the equations of motion (e.g., Eq. (4.4-15)) for the plant and adaptive gains about their equilibrium solution is desired. Some theorems which are helpful in achieving this condition are provided in the following sections.

## D.2 LINEAR TIME-INVARIANT SYSTEMS

Conditions for achieving stability and global asymptotic stability of solutions to the time-invariant linear equations,

$$\dot{\underline{x}}(t) = A \underline{x}(t) \tag{D-3}$$

are readily stated. Because the solution to Eq. (D-3) can be obtained analytically as a linear combination of terms like

$$t^k e^{\lambda_i(t-t_0)}; \quad 0 \leq k \leq j_i - 1$$

where  $\lambda_i$  is an eigenvalue of  $A$  having multiplicity\*  $j_i$ , a necessary and sufficient condition for stability is:

$\text{Re}(\lambda_i) \leq 0$  for all  $i$ ; if  $\text{Re}(\lambda_i) = 0$  then there exist  $j_i$  linearly independent eigenvectors  $\underline{x}_k$  --  $k = 1, \dots, j_i$  -- which satisfy

$$A \underline{x}_k = \lambda_i \underline{x}_k$$

For global asymptotic stability, it is necessary and sufficient that  $\text{Re}(\lambda_i) < 0$  for all values of  $i$ .

### D.3 LINEAR PERIODIC SYSTEMS (Floquet Theory)

The special type of time-varying linear system

$$\dot{\underline{x}}(t) = A(t) \underline{x}(t) \quad (D-4)$$

which can be treated in terms of the definitions stated in Section D.1 is the case when  $A(t)$  is periodic with period  $T$ ,

$$A(t + T) = A(t)$$

It can be shown (Ref. 71) that the transition matrix\*\* associated with  $A(t)$  is of the form

$$\Phi(t, t_0) = P(t, t_0) e^{R(t-t_0)} \quad (D-5)$$

where  $P(t, t_0)$  is periodic in  $T$  and  $R$  is a constant matrix;  $e^R$  is defined in Eq. (A-6). The solution  $\underline{x}(t)$  to Eq. (D-4) at times  $t_0 + nT$  --  $n = 0, 1, \dots$  -- is given by\*\*

$$\underline{x}(t_0 + nT) = \Phi(t_0 + nT, t_0) \underline{x}_0 \quad (D-6)$$

\* That is, there are  $j_i$  eigenvalues of  $A$  which have the value  $\lambda_i$ .

\*\* See Section A.2.

Substitution of Eq. (D-5) into Eq. (D-6) and using the fact --  
 $P(t_0 + nT, t_0) = P(t_0, t_0) = I$  -- produces

$$\underline{x}(t_0 + nT) = e^{RnT} \underline{x}_0 = \Phi(t_0 + T, t_0)^n \underline{x}_0$$

Thus the behavior of  $\underline{x}(t)$  at integral periods can be described by a difference equation,

$$\underline{x}(t_0 + nT) = \Phi(t_0 + T, t_0) \underline{x}(t_0 + (n-1)T) \quad (D-7)$$

where  $\Phi$  is independent of  $n$ . In terms of the eigenvalues  $\lambda_i$  of  $\Phi(t_0 + T, t_0)$ , each having multiplicity  $j_i$ , a necessary and sufficient condition for stability<sup>\*</sup> of solutions to this difference equation is (Ref. 68):

$|\lambda_i| \leq 1$  for all  $i$ ; if  $|\lambda_i| = 1$  then there exist  $j_i$   
 linearly independent eigenvectors  $\underline{\xi}_k$  --  $k = 1, \dots,$   
 $j_i$  -- which satisfy

$$\Phi(t_0 + T, t_0) \underline{\xi}_k = \lambda_i \underline{\xi}_k$$

For global asymptotic stability it is necessary and sufficient that

$$|\lambda_i| < 1; \quad \text{all } i$$

These conditions together with Eq. (D-5) imply the respective stability and asymptotic stability of  $\underline{x}(t)$  for all time.

The above discussion demonstrates that the stability properties of Eq. (D-4) depend upon the eigenvalues of the matrix

$$\Phi(t_0 + T, t_0) = e^{RT} \quad (D-8)$$

---

\* Stability and asymptotic stability of difference equations are defined in the same manner as in Section D.1 except that  $t$  is replaced by  $nT$ .

In general the matrix  $R$  on the right side of Eq. (D-8) cannot be determined analytically; however, it may be practical to obtain  $\Phi(t_0 + T, t_0)$  by numerically integrating its differential equation

$$\dot{\Phi}(t, t_0) = A(t) \Phi(t, t_0) ; \quad \Phi(t_0, t_0) = I$$

over the interval  $t_0 \leq t \leq t_0 + T$ , especially if  $T$  is relatively small. In this manner the stability of periodic systems can often be ascertained.

#### D.4 NONLINEAR SYSTEMS (Linearization)

When presented with a nonlinear system to analyze, as in Eq. (D-1), commonly one's first approach is to linearize the equations about an equilibrium point and study their behavior with higher order terms neglected. To this end suppose Eq. (D-1) can be written as

$$\dot{\underline{x}}(t) = \underline{f}[\underline{x}(t)] = A \underline{x}(t) + \underline{g}[\underline{x}(t)] \quad (D-9)$$

where

$$\lim_{|\underline{x}| \rightarrow 0} \frac{|\underline{g}(\underline{x})|}{|\underline{x}|} = 0$$

and  $A$  is a constant matrix. Typically  $A$  is determined by calculating

$$A = \left. \frac{\partial \underline{f}(\underline{x})}{\partial \underline{x}} \right|_{\underline{x} = 0}$$

The behavior of  $\underline{x}(t)$  about the origin can be expressed in terms of properties of the matrix  $A$ . Recall that local stability properties are



expressed by Definitions 1 and 2 in Section D.1. In particular, it has been proved (Ref. 71) that the solution to Eq. (D-9) is (locally) asymptotically stable if the eigenvalues  $\lambda_i$  of A satisfy

$$\operatorname{Re}(\lambda_i) < 0 ; \quad \text{for all } i$$

and that the origin is unstable (i.e., it is not stable in the sense defined in Section D.1) if

$$\operatorname{Re}(\lambda_i) > 0 ; \quad \text{for any } i$$

In a similar manner the Floquet theory described in Section D.3 can be applied to determine local stability properties when A is periodic.

An important observation is the fact that nothing general can be said when

$$\operatorname{Re}(\lambda_i) \leq 0 ; \quad \text{all } i$$

$$\operatorname{Re}(\lambda_j) = 0 ; \quad \text{some } j$$

For this case the effect of the nonlinear terms must be investigated; this fact is effectively demonstrated in Eq. (4.2-44). One special case where some eigenvalues of A have nonzero real parts is treated in Appendix E.

#### D.5 NONLINEAR SYSTEMS (Liapunov Theory)

For the nonlinear system,

$$\dot{\underline{x}}(t) = \underline{f}[\underline{x}(t)] \tag{D-10}$$

global stability properties can often be determined by methods associated

principally with Liapunov (Refs. 65, 67, 68). The relevant theorems are stated without proof in this section.

Theorem 1 (Ref. 67)

Let there exist a scalar function  $V(\underline{x})$  associated with the state of Eq. (D-10) and having the following properties:

- (a)  $V(\underline{x})$  and its first order partial derivatives are continuous in a certain open region  $R$  about the origin in  $n$ -dimensional Euclidean space.
- (b)  $V(\underline{x}) > 0$ ;  $\underline{x} \neq 0$ ,  $\underline{x}$  in  $R$
- (c)  $V(0) = 0$

Then the following statements are true with respect to solutions  $\underline{x}(t)$  of Eq. (D-10):

- 1(a) If  $\dot{V}(\underline{x}(t)) \leq 0$  along solutions of Eq. (D-10) in  $R$ , the origin is stable. A  $V(\underline{x})$  with this property and which satisfies conditions (a), (b) and (c) above is called a Liapunov function.
- 1(b) If  $\dot{V}(\underline{x}(t)) < 0$  along solutions of Eq. (D-10) in  $R$ , the origin is asymptotically stable.
- 1(c) If 1(b) holds and  $R$  is the whole Euclidean space, denoted by the symbol  $E^n$ , with

$$\lim_{|\underline{x}| \rightarrow \infty} V(\underline{x}) = \infty,$$

then the origin is globally asymptotically stable.

- 1(d) If 1(a) holds, if  $R = E^n$ , if  $\dot{V}(\underline{x}(t))$  does not vanish identically in  $t \geq t_0$  for any  $t_0$  and any  $\underline{x}_0 \neq 0$ , and if

$$\lim_{|\underline{x}| \rightarrow \infty} V(\underline{x}) = \infty$$

then the origin is globally asymptotically stable.

The details of the above theorem can be motivated by Fig. D-1 which illustrates possible trajectories for  $\underline{x}(t)$ . The contours of constant  $V(\underline{x})$  are closed in the vicinity of the origin. If the contour

$$V(\underline{x}) = V(\underline{x}_0)$$

is contained in  $R$  as indicated and if condition 1(a) of the theorem holds,  $V(\underline{x}(t))$  is never increasing and the trajectory, denoted by  $\underline{x}_{1a}(t)$ , must remain within the contour. On the other hand if condition 1(b) holds,  $V(\underline{x}(t))$  is constantly decreasing and the trajectory, denoted by  $\underline{x}_{1b}(t)$ , must eventually approach the origin. Similar arguments apply to the other conditions of the theorem.

Notice that the conditions of the theorem require one to find an appropriate  $V(\underline{x})$ , i.e., a Liapunov function; however there is no general systematic method for doing this. This matter receives a great deal of attention in the literature; suitable functions have been found for

R-2724

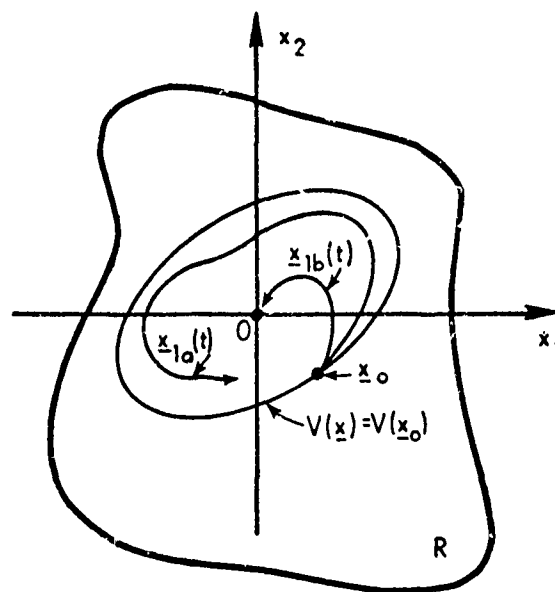


Figure D-1 Illustration of Theorem 1

various special types of nonlinear systems. The failure to find a form of  $V(\underline{x})$  which has the desired properties for a specific case does not mean that one doesn't exist. Consequently proving stability with Liapunov techniques is an ad hoc procedure.

The next theorem treats the case where  $\dot{V}(\underline{x}(t)) = 0$  along some solution to Eq. (D-10).

Theorem 2: (Ref. 65)

Let there be a scalar function  $V(\underline{x})$  satisfying conditions (a) and (b) of Theorem 1 with  $R = E^n$  and  $\dot{V}(\underline{x}(t)) \leq 0$  along solutions of Eq. (D-10) and

$$\lim_{|\underline{x}| \rightarrow \infty} V(\underline{x}) = \infty$$

Let  $T$  be the set of values of  $\underline{x}$  such that

$$\dot{V}(\underline{x}(t)) = 0; \quad \underline{x} \in T$$

and let  $S$  be the largest subset of  $T$  such that

$$\underline{x}(t_0) \text{ in } S \Rightarrow \underline{x}(t) \text{ in } S; \quad t \geq t_0$$

Then all solutions converge to  $S$  as  $t \rightarrow \infty$ .

Theorem 2 says that under suitable conditions,  $\underline{x}(t)$  must approach a set of values  $S$  such that  $\dot{V}(\underline{x}) = 0$  for all  $\underline{x}$  contained in the set. This result is particularly useful when Eq. (D-10) does not have a unique equilibrium point. In such a situation,  $S$  may be the set of all solutions to the equation

$$\underline{f}(\underline{x}) = \underline{0}$$

and one can establish the convergence of  $\underline{x}(t)$  to  $S$ .

All of our discussion thus far has been related to time-invariant systems. Some remarks about the time-varying case are given in the next section.

## D.6 TIME-VARYING SYSTEMS

The equations under consideration in this section are of the form

$$\begin{aligned}\dot{\underline{x}}(t) &= \underline{f}[\underline{x}(t), t] ; & \underline{x}(t_0) &= \underline{x}_0 \\ \underline{f}(0, t) &= \underline{0} & & (D-11)\end{aligned}$$

Most of the definitions and theorems of the preceding sections can be modified to give general stability conditions for solutions to Eq. (D-11); the essential difference is that conditions which are uniform with time must be imposed. One useful result applicable to Eq. (D-11) is a simple extension of the theorems in Section D.5 given by the following:

### Theorem 3

Suppose we are given a function  $V_1(\underline{x})$  which satisfies the conditions on  $V(\underline{x})$  in respectively Theorems 1 and/or 2 of Section D.5 and also a continuous function  $V_2(\underline{x})$  satisfying both

$$V_2(\underline{0}) = 0$$

and the set of conditions on  $\dot{V}(\underline{x})$  in Theorems 1 and/or 2 respectively. Then if

$$\dot{V}_1(\underline{x}(t), t) \leq V_2(\underline{x}(t))$$

along solutions of Eq. (D-11), the solution of Eq. (D-11) has the stability properties described in Theorems 1 and/or 2 respectively.

This can be viewed as a special case of the general theorems for time-varying systems; that is,  $V_1(\underline{x})$  has all the properties required of a time-varying Liapunov function for Eq. (D-11) (Refs. 65, 67).

Thus far conditions have been given for convergence of  $\underline{x}(t)$  to a set where the Liapunov function satisfies the condition

$$\dot{V}(\underline{x}(t)) = 0$$

It has been assumed that motion is restricted to a region where

$$\dot{V}(\underline{x}(t)) \leq 0 \quad (D-12)$$

However, acceptable operation can sometimes be attained even though  $\dot{V}(\underline{x}(t)) \geq 0$  inside a small region about an equilibrium point; one might expect convergence of  $\underline{x}(t)$  to some type of oscillatory condition within the region. Limit cycling, steady state solutions achieved in some non-linear control systems are examples of this type of behavior. These considerations motivate a discussion of a somewhat different type of stability than that defined in Section D.1.

## D.7 PRACTICAL STABILITY

Practical stability deals with the behavior of the solution  $\underline{x}(t)$  to a set of differential equations

$$\dot{\underline{x}}(t) = \underline{f}[\underline{x}(t), t] \quad (D-13)$$

when a positive scalar function  $V(\underline{x})$  exists such that  $\dot{V}[\underline{x}(t), t]$  does not satisfy the condition in Eq. (D-12) everywhere in the vicinity of the equilibrium point. In this case a different type of stability from that associated with Liapunov theory can sometimes be established (Refs. 65 and 67). A useful result of this type is the following:

Theorem 4

Let a function  $V_1(\underline{x})$  be given which satisfies the following:

- (a)  $V_1(\underline{x})$  and its first partial derivatives are continuous in  $E^n$ .
- (b)  $V_1(\underline{x}) > 0$ ;  $\underline{x} \neq 0$
- (c)  $\lim_{|\underline{x}| \rightarrow \infty} V_1(\underline{x}) = \infty$

Also let there be a continuous function  $V_2(\underline{x})$  satisfying:

- (d)  $V_2(\underline{x}) > 0$ ;  $\underline{x} \neq 0$
- (e)  $V_2(0) = 0$

Now define a set of  $S$  by the condition

$$V_2(\underline{x}) \leq M \Leftrightarrow \underline{x} \text{ in } S$$

Then if

$$\dot{V}_1(\underline{x}(t), t) < -V_2(\underline{x}(t)) + M$$

along solutions of Eq. (D-13), it follows that  $\underline{x}(t) \rightarrow T$  as  $t \rightarrow \infty$ , where  $T$  is a set defined by

$$V_1(\underline{x}) \leq L \Leftrightarrow \underline{x} \in T$$

$$L = \text{Max}_{\underline{x} \text{ in } S} \{V_1(\underline{x})\}$$

The content of the theorem is illustrated by Fig. D-2. Any solution  $\underline{x}_1(t)$  which starts outside  $T$  must converge to  $T$  since

$$\dot{V}_1 < 0; \text{ for all } \underline{x} \text{ outside } T$$

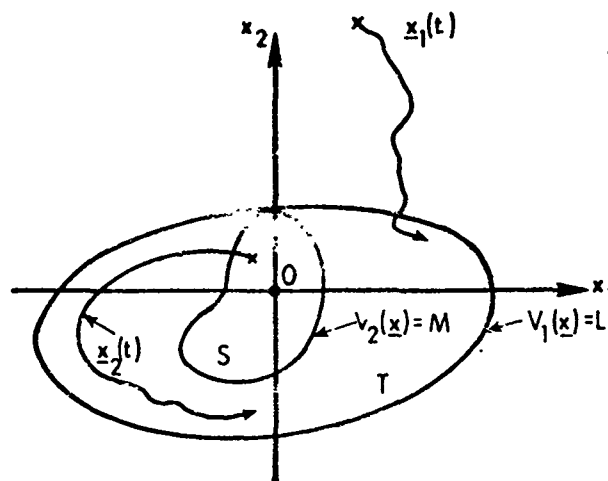


Figure D-2 Illustration of Motion that Exhibits Practical Stability

Furthermore, any solution  $\underline{x}_2(t)$  which begins within  $T$  must remain in  $T$  since

$$\dot{V}_1 < 0; \quad \underline{x} \text{ in the boundary of } T$$

This concludes our summary of several methods for determining stability properties of differential equations. These techniques are important for achieving satisfactory designs for adaptive controllers because they provide a qualitative description of the behavior of non-linear and linear time-varying systems.



## APPENDIX E

A LOCAL STABILITY THEOREM FOR ADAPTIVE SYSTEMS

In this appendix, conditions are established for local stability of a nonlinear system having equations of motion similar to Eq. (4.2-40). The need for this arises because conventional stability theorems cannot be applied to a linearized system when it has some closed loop poles at the origin of the complex plane.

Consider the nonlinear, time-invariant system described by

$$\dot{\underline{x}}(t) = \tilde{A}\underline{x}(t) + \underline{f}[\underline{x}(t)] ; \quad \underline{x}(0) = \underline{x}_0 \quad (\text{E-1})$$

with the partitioned form

$$\begin{bmatrix} \dot{\underline{x}}_1(t) \\ \dot{\underline{x}}_2(t) \end{bmatrix} = \begin{bmatrix} A_{11} & A_{12} \\ A_{21} & [0] \end{bmatrix} \begin{bmatrix} \underline{x}_1(t) \\ \underline{x}_2(t) \end{bmatrix} + \begin{bmatrix} \underline{f}_1[\underline{x}_1(t), \underline{x}_2(t)] \\ \underline{f}_2[\underline{x}_1(t)] \end{bmatrix} \quad (\text{E-2})$$

where  $\underline{x}_1(t)$  is an  $n$ -dimensional vector,  $\underline{x}_2(t)$  an  $m$ -dimensional vector,  $A_{11}$  an  $n \times n$  matrix,  $A_{12}$  an  $n \times m$  matrix, and  $A_{21}$  an  $m \times n$  matrix. Let the total dimension of  $\underline{x}(t)$  be  $\ell = n + m$ . Equation (E-2) has a special uncoupled nature in that  $\underline{x}_2(t)$  is driven by only  $\underline{x}_1(t)$ . It has the same structure as Eq. (4.2-40) without the forcing terms; the effects of the latter will be investigated subsequently.

Our purpose is to establish conditions for which stability of the equations

$$\dot{\underline{y}}(t) = \tilde{A}\underline{y}(t)$$

implies local stability of Eq. (E-1); in particular we are interested in the case where  $\tilde{A}$  has some eigenvalues at the origin of the complex plane. The results of this investigation are summarized in the following theorem:

Theorem

Suppose the system described by Eq. (E-2) satisfies the conditions:

- (a) The eigenvalues  $s_i$ ,  $i=1, 2, \dots, \ell$ , of  $\tilde{A}$  satisfy\*

$$\operatorname{Re}(s_i) < 0 ; \quad i = 1, \dots, r$$

$$s_i = 0 ; \quad i = r+1, \dots, \ell$$

That is to say, the nonzero eigenvalues of  $\tilde{A}$  have negative real parts and there are  $\ell - r = q$  eigenvalues with the value zero.

- (b)  $\operatorname{Rank}(A_{12}) = m - q \geq 1$

- (c) If  $|\underline{x}_2| = \alpha$ , then there exists a  $\gamma > 0$  such that

$$\lim_{|\underline{x}_1| \rightarrow 0} \frac{|f_1(\underline{x}_1, \underline{x}_2)|}{|\underline{x}_1|} = \gamma \alpha < \infty$$

- (d) 
$$\lim_{|\underline{x}_1| \rightarrow 0} \frac{|f_2(\underline{x}_1)|}{|\underline{x}_1|} = 0$$

Then it follows that the solution to Eq. (E-1) is locally stable, and furthermore locally we have

$$\lim_{t \rightarrow \infty} |\underline{x}_1(t)| = 0 \quad (\text{E-3})$$

---

\*  $\operatorname{Re}(s)$  denotes the real part of the complex number  $s$ .

The proof of this theorem is similar to that given by Coddington and Levinson (Ref. 71) for the case when the eigenvalues of  $\tilde{A}$  are strictly in the left-half complex plane. The hypotheses of the theorem are motivated by the various steps required to verify Eq. (E-3). It is clear that in general Eq. (E-3) must hold for stability because the state  $\underline{x}_2(t)$  in Eq. (E-2) is given by

$$\underline{x}_2(t) = \underline{x}_2(0) + \int_0^t \left[ A_{21} \underline{x}_1(\tau) + \underline{f}_2(\underline{x}_1(\tau)) \right] d\tau \quad (E-4)$$

If  $\underline{x}_1(t)$  does not approach zero sufficiently rapidly,  $\underline{x}_2(t)$  will tend to become arbitrarily large for some functions  $\underline{f}_2(\underline{x}_1)$ . The main task is to demonstrate that the zero eigenvalues of  $\tilde{A}$  do not contribute to the solution for  $\underline{x}_1(t)$ .

From Appendix A we know the solution to Eq. (E-1) satisfies

$$\underline{x}(t) = \Phi(t, 0) \underline{x}(0) + \int_0^t \Phi(t, \tau) \underline{f}[\underline{x}(\tau)] d\tau \quad (E-5)$$

where  $\Phi(t_2, t_1)$  is the transition matrix associated with  $\tilde{A}$ . Write  $\Phi(t, 0)$  in partitioned form

$$\Phi(t, 0) = \begin{bmatrix} \Phi_{11}(t, 0) & | & \Phi_{12}(t, 0) \\ \hline \Phi_{21}(t, 0) & | & \Phi_{22}(t, 0) \end{bmatrix} \quad (E-6)$$

with the same partition dimensions as  $\tilde{A}$  and expand Eq. (E-5) to obtain an expression for  $\underline{x}_1(t)$ ,

$$\begin{aligned} \underline{x}_1(t) = & \Phi_{11}(t,0)\underline{x}_1(0) + \Phi_{12}(t,0)\underline{x}_2(0) \\ & + \int_0^t \left\{ \Phi_{11}(t,\tau) \underline{f}_1 \left[ \underline{x}_1(\tau), \underline{x}_2(\tau) \right] + \Phi_{12}(t,\tau) \underline{f}_2 \left[ \underline{x}_1(\tau) \right] \right\} d\tau \end{aligned} \quad (E-7)$$

From Eq. (E-7) it is clear that in order for Eq. (E-3) to be satisfied, it should be true that

$$\lim_{t \rightarrow \infty} |\Phi_{11}(t,0)| = \lim_{t \rightarrow \infty} |\Phi_{12}(t,0)| = 0 \quad (E-8)$$

where  $|\Phi|$  is the matrix norm.\* Otherwise the contributions of the initial conditions to  $\underline{x}_1(t)$  may not approach zero. Eq. (E-8) is verified below by examining the detailed construction of  $\Phi(t,0)$  under the hypotheses of the theorem.

The Laplace transform  $\bar{\Phi}(s)$  of  $\Phi(t,0)$  is given in Section A.2 as

$$\bar{\Phi}(s) = (Is - \tilde{A})^{-1} \quad (E-9)$$

Denote  $F_{ij}(s)$  as the element in the  $i^{\text{th}}$  row and  $j^{\text{th}}$  column of  $\bar{\Phi}(s)$  and define the cofactor (Ref. 145) associated with the  $i$ - $j^{\text{th}}$  element of the matrix  $(Is - \tilde{A})$  as  $p_{ij}(s)$ . Recall that

$$p_{ij}(s) = (-1)^{i+j} \text{Det} \left[ M_{ij}(s) \right] \quad (E-10)$$

\* The appropriate definition of a matrix norm  $|A|$  for this application is (the maximum eigenvalue of  $A^T A$ )<sup>1/2</sup>. This definition is "compatible" (Ref. 144) with the euclidean norm of a vector  $|\underline{x}| = (\underline{x}^T \underline{x})^{1/2}$ , in the sense that

$$|A\underline{x}| \leq |A| |\underline{x}|$$

where  $M_{ij}(s)$  is the minor (submatrix) obtained by deleting the  $i^{\text{th}}$  row and  $j^{\text{th}}$  column of  $(Is - \tilde{A})$ . From the definition of the inverse of a matrix (Ref. 145) it follows that

$$F_{ij}(s) = \frac{p_{ji}(s)}{\text{Det}(Is - \tilde{A})} \quad (\text{E-11})$$

Because  $\tilde{A}$  has  $q$  eigenvalues at the origin (hypothesis (a))

$$\text{Det}(Is - \tilde{A}) = s^q p(s) \quad (\text{E-12})$$

where  $p(s)$  is a polynomial with strictly left-half plane zeros (i.e., none have zero real parts). Conditions (a) and (b) of the theorem imply that the first  $n$  columns of  $\tilde{A}$  are linearly independent, both of each other and of the last  $m$  columns in  $\tilde{A}$ , and also the rank of  $\tilde{A}$  is equal to  $r$ . Therefore,

$$\text{Rank}(M_{ij}(0)) = r - 1; \quad \begin{cases} i = 1, \dots, \ell \\ j = 1, \dots, n \end{cases} \quad (\text{E-13})$$

Consequently, because the dimension of  $M_{ij}(s)$  is  $\ell - 1$ ,

$$\text{Det}(M_{ij}) = s^c q_{ij}(s); \quad \begin{cases} i = 1, \dots, \ell \\ j = 1, \dots, n \end{cases} \quad (\text{E-14})$$

$$c \geq (\ell - 1) - (r - 1) = \ell - r = q$$

where  $q_{ij}(s)$  is a polynomial. Substitution of Eqs. (E-12) and (E-14) into Eq. (E-11) produces

$$F_{ij}(s) = (-1)^{i+j} s^{(c-q)} \frac{q_{ji}(s)}{p(s)} \quad \begin{cases} i = 1, \dots, n \\ j = 1, \dots, \ell \end{cases} \quad (\text{E-15})$$

where  $c - q \geq 0$ . Referring to Eqs. (E-6) and (E-9), each element of  $\bar{\Phi}_{11}(s)$  and  $\bar{\Phi}_{12}(s)$  is given by  $F_{ij}(s)$  in Eq. (E-15) which has its poles -- i.e., the zeros of  $p(s)$  -- strictly in the left-half complex plane. This implies that the elements of  $\Phi_{11}(t, 0)$  and  $\Phi_{12}(t, 0)$  decay exponentially and therefore the associated matrix norms have exponential bounds (Ref. 34),

$$\left. \begin{aligned} |\Phi_{11}(t, 0)| &\leq k_1 e^{-\sigma t} \\ |\Phi_{12}(t, 0)| &\leq k_2 e^{-\sigma t} \end{aligned} \right\} \sigma > 0 \quad (\text{E-16})$$

where  $k_1$  and  $k_2$  are some positive constants. This establishes Eq. (E-8); now we can proceed directly to the proof of the theorem, following Ref. 71.

For convenience take  $k_1 = k_2 = k$  in Eq. (E-16). Taking norms of both sides of Eq. (E-7) and substituting Eq. (E-16), one obtains

$$\begin{aligned} |\underline{x}_1(t)| &\leq k e^{-\sigma t} (|\underline{x}_1(0)| + |\underline{x}_2(0)|) \\ &\quad + k \int_0^t e^{-\sigma(t-\tau)} (|f_1(\underline{x}_1(\tau), \underline{x}_2(\tau))| + |f_2(\underline{x}_1(\tau))|) d\tau \end{aligned} \quad (\text{E-17})$$

Hypotheses (c) and (d) of the theorem imply that for any  $\epsilon > 0$ , there exists an  $\alpha$  and a  $\delta$  such that if

$$\begin{aligned} |\underline{x}_1(t)| &\leq \delta \\ |\underline{x}_2(t)| &\leq \alpha \end{aligned} \quad (\text{E-18})$$

then

$$\begin{aligned} |f_1(\underline{x}_1(t), \underline{x}_2(t))| &\leq \frac{\epsilon |\underline{x}_1(t)|}{2k} \\ |f_2(\underline{x}_1(t))| &\leq \frac{\epsilon |\underline{x}_1(t)|}{2k} \end{aligned} \quad (\text{E-19})$$

The first condition in Eq. (E-19) follows from condition (c) of the theorem; in particular take

$$\alpha \leq \frac{\epsilon}{2k\gamma} \quad (\text{E-20})$$

The second condition in Eq. (E-19) follows from condition (d) of the theorem; i.e.,  $f_2[\underline{x}_1] \rightarrow 0$  faster than  $\underline{x}_1$ . Substitution of Eq. (E-19) into Eq. (E-17) and transposing  $e^{-\sigma t}$  produces

$$e^{\sigma t} |\underline{x}_1(t)| \leq k \left( |\underline{x}_1(0)| + |\underline{x}_2(0)| \right) + \epsilon \int_0^t e^{\sigma \tau} |\underline{x}_1(\tau)| d\tau \quad (\text{E-21})$$

subject to Eq. (E-18). This inequality yields (Ref. 71, p315)

$$|\underline{x}_1(t)| \leq k \left( |\underline{x}_1(0)| + |\underline{x}_2(0)| \right) e^{-(\sigma-\epsilon)t} \quad (\text{E-22})$$

Now if we require

$$\epsilon < \sigma$$

$$|\underline{x}_1(0)| + |\underline{x}_2(0)| \leq \frac{\delta}{k} \quad (\text{E-23})$$

Eq. (E-22) becomes

$$|\underline{x}_1(t)| \leq \delta e^{-(\sigma-\epsilon)t} \leq \delta \quad (\text{E-24})$$

The conclusion is that for sufficiently small initial conditions on the state,  $\underline{x}_1(t)$  is indeed less than or equal to  $\delta$  as required by Eq. (E-18), but still subject to the requirement,

$$|\underline{x}_2(t)| \leq \alpha$$

To check the latter condition, we calculate a bound on  $\underline{x}_2(t)$ . Substitution into Eq. (E-4) from Eqs. (E-18), (E-19) and (E-24) produces

$$|\underline{x}_2(t)| \leq |\underline{x}_2(0)| + \left( |A_{21}| + \frac{\epsilon}{2k} \right) \delta \int_0^{\infty} e^{-(\sigma-\epsilon)t} dt \quad (E-25)$$

which reduces to

$$|\underline{x}_2(t)| \leq |\underline{x}_2(0)| + \left( |A_{21}| + \frac{\epsilon}{2k} \right) \frac{\delta}{\sigma - \epsilon} \quad (E-26)$$

Given the quantities  $\alpha, \epsilon, k, |A_{21}|$ , and  $\sigma$  as specified by Eqs. (E-20), (E-23), (E-16), (E-2), and (E-16) respectively, one can choose  $\delta$  and  $|\underline{x}_2(0)|$  sufficiently small so that by Eq. (E-26)

$$|\underline{x}_2(t)| \leq \alpha; \quad t \geq 0$$

Therefore the assumptions in Eq. (E-18) made in deriving Eq. (E-24) are consistent and  $\underline{x}_1(t) \rightarrow \underline{0}$  exponentially, thus proving the theorem.

To apply the theorem to Eq. (4.2-40) neglecting the forcing terms, make the identifications

$$\begin{aligned} \underline{x}_1(t) &= \delta \underline{x}(t); & \underline{x}_2(t) &= \delta \underline{h}(t) \\ A_{11} &= A - \underline{b} \underline{h}_0^T; & A_{12} &= -\underline{b} \underline{x}_m^T \\ A_{21} &= B' \underline{x}_m \underline{c}^T; & B' &= \begin{bmatrix} \beta'_1 & 0 & \cdot & 0 \\ 0 & \beta'_2 & \cdot & \cdot \\ \cdot & \cdot & \cdot & \cdot \\ 0 & \cdot & \cdot & \beta'_n \end{bmatrix} \\ f_1(\underline{x}_1(t), \underline{x}_2(t)) &= -\underline{b} \delta \underline{h}(t)^T \delta \underline{x}(t) \\ f_2(\underline{x}_2(t)) &= B' \delta \underline{x}(t) \underline{c}^T \delta \underline{x}(t) \end{aligned} \quad (E-27)$$



The conditions of the theorem are checked as follows:

- (a) The eigenvalues of  $\tilde{A}$  are determined by expanding  $\text{Det} (Is - \tilde{A})$ . Using the Schur identities for the determinant of a partitioned matrix (Ref. 146) it follows that

$$\text{Det}(Is - \tilde{A}) = s^n \text{Det} \left( Is - A_{11} - \frac{1}{s} A_{12} A_{21} \right)$$

Substitution for  $A_{11}$ ,  $A_{12}$ , and  $A_{21}$  with some algebraic manipulation produces

$$\text{Det}(Is - \tilde{A}) = s^{n-1} \text{Det} (Is - A_{11}) T(s)$$

$$T(s) = s + k_e G_o(s)$$

$$k_e \triangleq \sum_{i=1}^n \beta_i' x_{m_i}^2$$

$$G_o(s) \triangleq \underline{c}^T (Is - A_{11})^{-1} \underline{b}$$

where  $k_e$  and  $G_o(s)$  are defined as in Eqs. (4.2-47) and (4.2-50). Note that the zeros of  $\text{Det}(Is - A_{11})$  are cancelled by the poles of  $T(s)$ . Now we assume that the adaptation gains  $\beta_i'$  and the quantity  $\underline{n}_o$  in  $A_{11}$  can be chosen so that  $T(s)$  has  $n+1$  zeros located strictly in the left half complex plane, as discussed in Section 4.2.6. Therefore

$$r = n+1$$

$$q = n-1$$

- (b) From the structure of  $A_{12}$  in Eq. (E-27) it follows that

$$\text{Rank}(A_{12}) = 1$$

Using the results from (a) above,

$$m - q = n - (n - 1) = 1 = \text{Rank}(A_{12})$$

Therefore condition (b) is satisfied.

(c) Condition (c) is satisfied because

$$|f_1(\underline{x}_1, \underline{x}_2)| \leq |b| |\underline{x}_1| |\underline{x}_2| \leq \alpha \gamma |\underline{x}_1|$$

where we identify

$$|\underline{x}_2(t)| \leq \alpha$$

$$\gamma = |b|$$

(d) Condition (d) of the theorem is satisfied because  $f_2(\underline{x}_1)$  is quadratic in  $\underline{x}_1$

Therefore Eq. (4.2-40) is locally stable in the sense defined in the theorem, subject to the condition that the zeros of  $T(s)$  have negative real parts.

The above development provides sufficient conditions on the matrix  $\tilde{A}$  and the nonlinearities  $f_1$  and  $f_2$  in order that the solution to Eq. (4.2-40) be locally stable, neglecting forcing terms. To assess the effect of the latter, modify Eq. (E-2) as follows

$$\dot{\underline{x}}(t) = \tilde{A}\underline{x}(t) + \underline{d} + \underline{f}(\underline{x}(t)) \quad (E-28)$$

where  $\underline{d}$  is a constant forcing term added to account for the corresponding quantity in Eq. (4.2-40).

Assume Eq. (E-28) has a steady state solution  $\underline{x}_s$  which satisfies

$$\tilde{A}\underline{x}_s + \underline{d} + \underline{f}(\underline{x}_s) = \underline{0} \quad (E-29)$$

Define a new variable  $\underline{z}(t)$  by

$$\underline{z}(t) = \underline{x}(t) - \underline{x}_s \triangleq \begin{bmatrix} z_1 \\ z_2 \end{bmatrix} \quad (E-30)$$

where the partitions correspond to those for  $\underline{x}(t)$  in Eq. (E-2). Substitution from Eqs. (E-29) and (E-30) into Eq. (E-28) and expanding the nonlinear term about  $\underline{x}_s$  produces

$$\dot{\underline{z}}(t) = \tilde{A} \underline{z}(t) + \left. \frac{\partial f}{\partial \underline{x}} \right|_{\underline{x}_s} \underline{z}(t) + \text{higher order terms} \quad (\text{E-31})$$

where  $\partial f / \partial \underline{x}$  is the matrix with its  $i$ - $j^{\text{th}}$  element equal to  $\partial f_i / \partial x_j$ . Now define the partitioned matrix

$$\left. \frac{\partial f}{\partial \underline{x}} \right|_{\underline{x}_s} = \begin{bmatrix} \frac{\partial f_1}{\partial x_1} & \frac{\partial f_1}{\partial x_2} \\ \frac{\partial f_2}{\partial x_1} & \frac{\partial f_2}{\partial x_2} \end{bmatrix}_{\underline{x}_s} \triangleq \begin{bmatrix} F_{11} & F_{12} \\ F_{21} & F_{22} \end{bmatrix} \triangleq F \quad (\text{E-32})$$

The result of combining terms in Eq. (E-31) and using Eq. (E-32) is

$$\dot{\underline{z}}(t) = (\tilde{A} + F) \underline{z}(t) + \text{higher order terms} \quad (\text{E-33})$$

Using Eq. (E-27) we can evaluate the partial derivatives in Eq. (E-32) as follows:

$$\begin{aligned} F_{11} &= -\underline{b} \delta \underline{h}_s^T; & F_{12} &= -\underline{b} \delta \underline{x}_s^T \\ F_{21} &= B'(\underline{c}^T \delta \underline{x}_s I + \delta \underline{x}_s \underline{c}^T); & F_{22} &= 0 \end{aligned}$$

The higher order terms in Eq. (E-33) are quadratic functions similar to  $\underline{f}_1$  and  $\underline{f}_2$  in Eq. (E-2). Therefore from the above relations it follows that the

unforced nonlinear equations of motion for  $\underline{z}(t)$  have the same structure as Eq. (E-2) and the stability theorem can be applied to the matrix  $(\tilde{A} + F)$ .

This concludes the investigation of conditions for the stability of Eq. (E-2). The results obtained enable one to make some qualitative statements about the behavior of Eq. (4.2-40) as described in Section 4.2.6.

## APPENDIX F

### THE STEADY-STATE MATRIX RICCATI EQUATION

In determining the optimal control  $\underline{u}(t)$  for a linear time invariant system which minimizes a quadratic performance index

$$J = \int_{t_0}^{t_f} \left[ \underline{x}(t)^T Q \underline{x}(t) + \underline{u}(t)^T R \underline{u}(t) \right] dt \quad (F-1)$$

subject to the equations of motion,

$$\dot{\underline{x}}(t) = A \underline{x}(t) + B \underline{u}(t); \quad \underline{x}(t_0) = \underline{x}_0 \quad (F-2)$$

the matrix Riccati equation

$$\begin{aligned} \dot{S}(t) &= -S(t) A - A^T S(t) + S(t) B R^{-1} B^T S(t) - Q \\ S(t_f) &= 0 \end{aligned} \quad (F-3)$$

has an important role.\* Its solution enables one to mechanize the optimal linear feedback control law

$$\underline{u}(t) = -R^{-1} B^T S(t) \underline{x}(t) \quad (F-4)$$

An important special case of the above is when the terminal time is infinite,  $t_f = \infty$ , so that  $S(t)$  becomes a constant  $S$  which is the solution to the steady state equation

$$SA + A^T S - SBR^{-1} B^T S + Q = 0 \quad (F-5)$$

---

\* See Appendix B

This is an important result because the linear control law requires only constant feedback gains; therefore techniques for determining  $S$  are of interest. The latter are the subject of this appendix. Our emphasis will be upon methods that are feasible for solving Eq. (F-5) on-line in an adaptive control system as described in Section 5.4. To guarantee that there is a unique positive semidefinite solution for  $S$ , it is assumed throughout this discussion that  $Q$  is positive semidefinite,  $R$  is positive definite, the system represented by Eq. (F-2) is controllable,\* and all the eigenvalues of  $A$  have nonnegative real parts. If the last of these conditions does not hold,  $Q$  must be further restricted, as discussed in Ref. 147.

Because Eq. (F-5) is a nonlinear matrix equation, it usually has no closed form solution and consequently some numerical technique must be used to obtain a close approximation to  $S$ . Three methods described in the literature are

- Numerical Integration
- Newton's Method
- Eigenvector Method

The essential features of each are summarized and then comparisons of their relative computational complexity are made.

Numerical Integration — Perhaps the most obvious technique for solving Eq. (F-5) is to integrate Eq. (F-3) to a nearly steady state condition. It has been established (Ref. 147) that beginning with any positive semidefinite value of  $S(t_f)$  and integrating Eq. (F-3) backwards in time, the solution for  $S(t)$  satisfies

---

\* See Appendix A for a definition of controllability

$$\lim_{t \rightarrow -\infty} S(t) = S,$$

converging exponentially. That is,

$$|S - S(t)| \leq \alpha e^{-\sigma t} \quad (\text{F-6})$$

for some positive constants,  $\alpha$  and  $\sigma$ , where  $| \cdot |$  denotes the matrix norm. The significance of Eq. (F-6) is that over an interval of time having length  $\Delta$ , the bound on the error in the solution is reduced by the factor  $e^{-\sigma \Delta}$

$$\max |S - S(n\Delta)| \leq e^{-\sigma \Delta} \max |S - S((n-1)\Delta)| \quad (\text{F-7})$$

In the terminology of numerical analysis (Ref. 148) the method has first order convergence properties.

Newton's Method — Newton's method is an important recursive technique for solving nonlinear algebraic equations (Ref. 148). Several authors have described its use for the matrix Riccati equation (e.g., Refs. 147 and 149) in Eq. (F-5). Applied to this problem it results in the expression

$$\left( A - BR^{-1}B^T S_k \right)^T S_{k+1} + S_{k+1} \left( A - BR^{-1}B^T S_k \right) + S_k BR^{-1}B^T S_k + Q = 0 \quad (\text{F-8})$$

Given a value for  $S_k$ , Eq. (F-8) is a solvable linear relation in  $S_{k+1}$  under our assumptions on  $Q$ ,  $R$ , and  $A$ . Because  $S_{k+1}$  is symmetric, the total number of unknowns to be determined is

$$\frac{n(n+1)}{2}$$

If the recursion begins with any positive semidefinite matrix  $S_0$  such that the eigenvalues of the matrix

$$A - BR^{-1} B^T S_0$$

all have negative real parts, then the sequence  $\{S_k\}$  generated by Eq. (F-8) converges to the solution of Eq. (F-5) (Ref. 147).

With respect to the convergence rate of this technique, it is known (Ref. 148) that as  $S_k$  approaches the solution  $S$ , the error behaves as

$$|S - S_k| \leq \eta^{2^k} |S - S_{k-1}| \quad (F-8)$$

where  $\eta$  is a positive constant less than one. Compared with Eq. (F-7) Eq. (F-8) indicates a much more rapid convergence rate as  $S_k$  approaches  $S$  because the factor  $\eta^{2^k}$  decreases rapidly with  $k$  whereas  $e^{-\sigma\Delta}$  is constant. Therefore Newton's method exhibits second order convergence properties.

Eigenvector Method — The third technique is found to be most efficient when the dimension of  $S$  is large. It is based upon the fact that  $S(t)$  in Eq. (F-3) can also be determined from the relations (Ref. 97)

$$\dot{\Omega}(t) = \begin{bmatrix} A & -BR^{-1}B^T \\ -Q & -A^T \end{bmatrix} \Omega(t)$$

$$\Omega(0) = I$$

$$\Omega(T, t) = \begin{bmatrix} \Omega_{11}(T, t) & \Omega_{12}(T, t) \\ \Omega_{21}(T, t) & \Omega_{22}(T, t) \end{bmatrix}$$

$$S(t, T) = -\Omega_{22}(T, t)^{-1} \Omega_{21}(T, t) \quad (F-9)$$



where  $\Omega$  is a  $2n \times 2n$  matrix ( $A$  being of dimension  $n$ ),  $\Omega_{ij}(T, t)$  --  $i, j, = 1, 2$  -- is an  $n \times n$  matrix and  $S$  is regarded as both a function of  $t$  and  $T$ . The solution to Eq. (F-5) is obtained from

$$S = \lim_{T \rightarrow \infty} S(T, t) = \lim_{T \rightarrow \infty} \left\{ -\Omega_{22}(T, t)^{-1} \Omega_{21}(T, t) \right\} \quad (F-10)$$

or alternatively

$$S = \lim_{t \rightarrow -\infty} \left\{ -\Omega_{22}(T, t)^{-1} \Omega_{21}(T, t) \right\} \quad (F-11)$$

Because the differential equation for  $\Omega(t)$  is time independent, we can take  $T = 0$  in Eq. (F-11) so that  $S$  can be determined by

$$S = \lim_{t \rightarrow -\infty} \left\{ -\Omega_{22}(0, t)^{-1} \Omega_{21}(0, t) \right\} \quad (F-12)$$

The details of the method involve determining the eigenvalues and eigenvectors of the matrix

$$\begin{bmatrix} A & | & -BR^{-1}B^T \\ \hline Q & | & -A^T \end{bmatrix}$$

which permit the limit in Eq. (F-12) to be easily calculated. Several algebraic steps must be completed and they are described in Refs. 150 and 151. For large values of  $n$  ( $n$  = the dimension of  $S$ ), less computation time is required for this procedure than for Newton's method. Newton's method requires inversion of a matrix whose dimension is  $(1/2)(n)(n+1)$  and the associated computation time is proportional to  $n^6$ ; furthermore when  $n$  is large or if the matrix to be inverted is ill-conditioned (Ref. 144),

excessive numerical errors may be incurred. By contrast, the computation time required for the eigenvalue method is proportional to  $n^3$ .

For tactical missile applications, Newton's method seems to be a feasible procedure for solving Eq. (F-5). The order of the system is sufficiently low so that the required matrix inversion can be accurately accomplished and the associated programming instructions are less complicated than those required by the eigenvalue method. The total computation time required to obtain a solution in the cases considered in Chapter 9 is roughly  $1/100^{\text{th}}$  of that required by the numerical integration technique. The integration technique has also been compared with the eigenvector method (Ref. 151); for the cases reported the former typically requires a computation time 100 times longer than the latter to obtain a solution for S.

## APPENDIX G

ADJOINT THEORY FOR LINEAR SYSTEMS

When designing a control law  $\underline{u}(t)$  for any known system of equations,

$$\dot{\underline{x}}(t) = \underline{f}(\underline{x}(t), \underline{u}(t))$$

it is desirable to be able to analyze the system performance for various choices of  $\underline{u}(t)$ . This can always be done numerically simply by integrating the equations of motion. Different sets of initial conditions and types of measurement errors can be tried to obtain representative simulations of actual system operation. In general, a great deal of computational labor is involved in examining a satisfactory number of cases to obtain a measure of "average" system behavior. However, if the equations of motion are linear, the task of performance evaluation can be greatly simplified by the use of sensitivity functions which analytically determine the effects of initial conditions and measurement errors. These functions are derived here using so-called "adjoint theory" for linear systems.

## G.1 PROBLEM FORMULATION

Consider the linear dynamical system

$$\dot{\underline{x}}(t) = \underline{A}(t)\underline{x}(t) + \underline{B}(t)\underline{u}(t); \quad \underline{x}(t_0) = \underline{x}_0 \quad (G-1)$$

where  $\underline{u}(t)$  is a linear feedback controller given by

$$\underline{u}(t) = \underline{K}(t) \underline{x}(t) \quad (G-2)$$

and  $K(t)$  is a specified matrix. Define three performance measures for the system as follows:

$$J_f \triangleq \underline{x}(t_f)^T F \underline{x}(t_f) \quad (G-3)$$

$$J_{\underline{x}} \triangleq \int_{t_0}^{t_f} \underline{x}(t)^T Q(t) \underline{x}(t) dt \quad (G-4)$$

$$J_{\underline{u}} \triangleq \int_{t_0}^{t_f} \underline{u}(t)^T R(t) \underline{u}(t) dt \quad (G-5)$$

where  $F$ ,  $Q(t)$ , and  $R(t)$  are assumed to be symmetric, positive semi-definite matrices. The quantity  $J_f$  is a measure of the magnitude of the terminal state at time  $t_f$ ,  $J_{\underline{x}}$  indicates the size of the state along a solution to Eq. (G-1) and  $J_{\underline{u}}$  represents the amount of control "effort" expended. These are all familiar quadratic performance indices used in optimal control theory.\* Our purpose here is to indicate how  $J_f$ ,  $J_{\underline{x}}$ , and  $J_{\underline{u}}$  can be evaluated, given any linear feedback control law, in terms of initial conditions  $\underline{x}(t_0)$  on the state and measurement errors incurred in implementing Eq. (G-2).

## G.2 TERMINAL STATE SENSITIVITY TO INITIAL CONDITIONS

To determine the sensitivity of the terminal state to initial conditions, rewrite Eqs. (G-1) and (G-2) as

$$\begin{aligned} \dot{\underline{x}}(t) &= \tilde{A}(t) \underline{x}(t); & \underline{x}(t_0) &= \underline{x}_0 \\ \tilde{A}(t) &\triangleq A(t) + B(t) K(t) \end{aligned} \quad (G-6)$$

---

\* See Appendix B.

We know from linear system theory\* that the transition matrix  $\Phi(t, t_0)$  associated with  $\tilde{A}(t)$  satisfies

$$\dot{\Phi}(t, t_0) = \tilde{A}(t) \Phi(t, t_0); \quad \Phi(t_0, t_0) = I \quad (G-7)$$

Knowledge of  $\Phi$  obtained by integrating Eq. (G-7) permits us to write

$$\underline{x}(t) = \Phi(t, t_0) \underline{x}_0$$

That is  $\underline{x}(t)$  can be determined for any values of  $t$  and  $\underline{x}_0$ , given the solution to Eq. (G-7) for a particular initial time  $t_0$ . Consequently we can regard the state as a function of both  $t_0$  and  $t$ , written as  $\underline{x}(t, t_0)$ . However, in many applications it is desirable to know the terminal state resulting from initial conditions imposed on the system at different initial times. For example, this is the case in the missile guidance problem discussed in Chapter 11 where the effects of launching the missile at different ranges relative to the target are to be evaluated. In other words, if  $\underline{x}(t)$  is the state at any initial time  $t < t_f$ , one is interested in evaluating

$$\underline{x}(t_f, t) \triangleq \Phi(t_f, t) \underline{x}(t) \quad (G-8)$$

Accomplishing this for a range of values of  $t$  requires knowledge of  $\Phi(t_f, t)$  where the initial time is regarded as an independent variable. Notice that  $\underline{x}(t_f, t)$  is obtained from  $\underline{x}(t, t_0)$  by making the change of variables --  $t \rightarrow t_f$  and  $t_0 \rightarrow t$ .

To obtain  $\Phi(t_f, t)$  from Eq. (G-7) requires that a complete integration of the matrix differential equation be performed over the interval  $(t, t_f)$  for each initial time  $t$  of interest. Often this must be done numerically and a great deal of computational labor is entailed. However, the

---

\* See Appendix A.

procedure can be greatly simplified if a differential equation for  $\Phi(t_f, t)$  itself can be determined with  $t$  as the independent variable. To derive an equation for  $\Phi(t_f, t)$ , we begin with the property

$$\Phi(t_f, t_f) = \Phi(t_f, t) \Phi(t, t_f) = I$$

Differentiate both sides of this expression to obtain

$$\dot{\Phi}(t_f, t) \Phi(t, t_f) + \Phi(t_f, t) \dot{\Phi}(t, t_f) = 0$$

and therefore, using the fact that  $\Phi(t, t_f)^{-1} = \Phi(t_f, t)$ ,

$$\dot{\Phi}(t_f, t) = -\Phi(t_f, t) \dot{\Phi}(t, t_f) \Phi(t_f, t) \quad (G-9)$$

Now observe that the differential equation for  $\Phi(t, t_0)$ , Eq. (G-7), can be written as

$$\dot{\Phi}(t, t_f) = \tilde{A}(t) \Phi(t, t_f) \quad (G-10)$$

because Eq. (G-7) holds for any  $t_0$  -- in particular  $t_0 = t_f$ . Substitution from Eq. (G-10) into Eq. (G-9) produces the desired equation for  $\Phi(t_f, t)$ :

$$\begin{aligned} \dot{\Phi}(t_f, t) &= -\Phi(t_f, t) \tilde{A}(t) \\ \Phi(t_f, t_f) &= I \end{aligned} \quad (G-11)$$

Equation (G-11) is said to be adjoint to Eq. (G-7) and  $\Phi(t_f, t)$  is referred to as a sensitivity function.

In the missile guidance application, only one element of the terminal state vector is of interest, the miss distance. This can be obtained from knowledge of only one row of the transition matrix, taken without loss of generality to be the first row. Denoting the first row of  $\Phi(t_f, t)$

by the column vector  $\underline{\phi}$ , it follows from Eq. (G-11) that

$$\dot{\underline{\phi}}(t_f, t) = -\tilde{A}(t)^T \underline{\phi}(t_f, t); \quad \underline{\phi}(t_f, t_f) = \begin{bmatrix} 1 \\ 0 \\ \cdot \\ \cdot \\ 0 \end{bmatrix} \quad (G-12)$$

To calculate  $\Phi(t_f, t)$  and  $\underline{\phi}(t_f, t)$ , Eqs. (G-11) and (G-12) are integrated backwards in time from  $t = t_f$ . Once evaluated these sensitivity functions determine the terminal state resulting from any given initial condition  $\underline{x}(t)$ , according to Eq. (G-8). The performance index in Eq. (G-3) is then determined by

$$J_f = \underline{x}(t)^T \Phi(t_f, t)^T F \Phi(t_f, t) \underline{x}(t) \quad (G-13)$$

### G.3 TERMINAL STATE SENSITIVITY TO MEASUREMENT ERRORS

Another important contribution to the terminal state can be produced by errors in implementing the linear control law in Eq. (G-2). These errors may result from imperfect observations provided by sensors; they can often be represented as random fluctuations or as (possibly time-varying) bias errors. To examine such effects, suppose that the control law for Eq. (G-1) is given by

$$\underline{u}(t) = K(t) (\underline{x}(t) + \underline{\epsilon}(t)) \quad (G-14)$$

where  $\underline{\epsilon}(t)$  is an error vector. The resulting equations of motion for the linear system are

$$\dot{\underline{x}}(t) = \tilde{A}(t) \underline{x}(t) + B(t) K(t) \underline{\epsilon}(t)$$

where  $\tilde{A}(t)$  is defined in Eq. (G-6). According to linear system theory,\* the terminal state at time  $t_f$  caused by the action of  $\underline{\epsilon}(t)$  on the interval  $(t, t_f)$ , with zero initial conditions on the state at time  $t$ , is given by

$$\underline{x}(t_f, t) = \int_t^{t_f} \Phi(t_f, \tau) B(\tau) K(\tau) \underline{\epsilon}(\tau) d\tau \quad (G-15)$$

where  $\underline{x}(t_f, t)$  is regarded as a function of both  $t_f$  and  $t$ , just as in Eq. (G-8). A differential equation for the terminal state is obtained simply by differentiating Eq. (G-15) to obtain

$$\begin{aligned} \dot{\underline{x}}(t_f, t) &= -\Phi(t_f, t) B(t) K(t) \underline{\epsilon}(t) \\ \underline{x}(t_f, t_f) &= \underline{0} \end{aligned} \quad (G-16)$$

In the special case when the measurements contains only bias errors, i.e.,  $\underline{\epsilon}(t)$  is a constant  $\underline{\epsilon}$ , the terminal state is given by

$$\begin{aligned} \underline{x}(t_f, t) &= \Psi(t_f, t) \underline{\epsilon} \\ \dot{\Psi}(t_f, t) &= -\Phi(t_f, t) B(t) K(t) \\ \Psi(t_f, t_f) &= \underline{0} \end{aligned} \quad (G-17)$$

If one is interested in only a single element of  $\underline{x}(t_f)$ , then only one row (which can be taken as the first) of  $\Psi(t_f, t)$  -- denoted by  $\underline{\psi}(t_f, t)$  -- need be determined; that is,

$$\begin{aligned} x_1(t_f, t) &= \underline{\psi}(t_f, t)^T \underline{\epsilon} \\ \dot{\underline{\psi}}(t_f, t) &= -K(t)^T B(t)^T \underline{\varphi}(t_f, t) \\ \underline{\psi}(t_f, t_f) &= \underline{0} \end{aligned} \quad (G-18)$$

---

\* See Appendix A.



where  $\underline{\varphi}(t_f, t)$  is the first row of  $\Phi(t_f, t)$ , defined by Eq. (G-12).

All of the integrations in Eqs. (G-16), (G-17) and (G-18) are performed backward in time and require knowledge of the transition matrix  $\Phi(t_f, t)$ ; the latter is evaluated from Eqs. (G-11) or (G-12) which are also integrated backward in time. Therefore the sensitivity functions for initial conditions and measurement errors can be generated simultaneously.

Another form the measurement errors  $\underline{\epsilon}(t)$  can take is that of a random process (noise) having zero mean and second moments

$$E\{\underline{\epsilon}(t_1) \underline{\epsilon}(t_2)^T\} = W(t_1) \delta(t_1 - t_2); \text{ for all } t_1 \text{ and } t_2 \quad (\text{G-19})$$

where  $W(t_1)$  is a known positive definite matrix and  $\delta(t_1 - t_2)$  is the unit Dirac delta (impulse) function. The mean value of the terminal state produced by this noise is also zero. If we denote the second moment characteristics of the state by

$$P(t_f, t) = E\{\underline{x}(t_f, t) \underline{x}(t_f, t)^T\}$$

where  $E\{\}$  denotes mathematical expectation, then it can be shown that

$$\dot{P}(t_f, t) = -\Phi(t_f, t) B(t) K(t) W(t) K(t)^T B(t)^T \Phi(t_f, t)^T; \quad P(t_f, t_f) = 0 \quad (\text{G-20})$$

This equation is also integrated backward in time.\*

With the terminal miss (or its statistics) caused by measurement errors calculated from either Eq. (G-17), (G-18), or (G-20), the value of the performance index  $J_f$  is readily calculated. For example, if

---

\*  $P(t_f, t)$  is called the state covariance matrix.

$\underline{\epsilon}(t)$  is a constant bias error,

$$J_f = \underline{\epsilon}^T \Psi(t_f, t)^T F \Psi(t_f, t) \underline{\epsilon} \quad (G-21)$$

If  $\underline{\epsilon}(t)$  is a random process, the expected value of  $J_f$  is given by

$$E\{J_f\} = E\{\underline{x}(t_f, t)^T F \underline{x}(t_f, t)\} = \text{Trace}(P(t_f, t) F) \quad (G-22)$$

where  $\text{Trace}(PF)$  denotes the sum of the diagonal elements of the matrix product,  $PF$ .

#### G.4 INTEGRAL-TYPE PERFORMANCE INDEX SENSITIVITY TO INITIAL CONDITIONS

In this section we want to determine an efficient method for calculating the values of the performance indices in Eqs. (G-4) and (G-5) produced by initial conditions  $\underline{x}(t)$ . Beginning with Eq. (G-5),  $J_u$  can be written explicitly as a function of  $t_f$  and  $t$  by substituting for  $\underline{u}(t)$  from Eq. (G-2) and regarding  $t_0$  as a variable,  $t$ . Thus

$$J_u(t_f, t) = \int_t^{t_f} \underline{x}(\tau)^T K(\tau)^T R(\tau) K(\tau) \underline{x}(\tau) d\tau \quad (G-23)$$

Equation (G-23) can be expressed in terms of the initial conditions  $\underline{x}(t)$  by substituting the relation (see Eq. (G-8))

$$\underline{x}(\tau) \triangleq \underline{x}(\tau, t) = \Phi(\tau, t) \underline{x}(t) \quad (G-24)$$

to obtain

$$J_u(t_f, t) = \underline{x}(t)^T \left\{ \int_t^{t_f} \Phi(\tau, t)^T K(\tau)^T R(\tau) K(\tau) \Phi(\tau, t) d\tau \right\} \underline{x}(t) \quad (G-25)$$

where  $\underline{x}(t)$ , being independent of  $\tau$ , is factored outside the integration.

Evidently the control effort in Eq. (G-25) can be expressed as

$$J_{\underline{u}}(t_f, t) = \underline{x}(t)^T C_{\underline{u}}(t_f, t) \underline{x}(t) \quad (G-26)$$

where  $C_{\underline{u}}(t_f, t)$  is a sensitivity function identified as

$$C_{\underline{u}}(t_f, t) \triangleq \int_t^{t_f} \Phi(\tau, t)^T K(\tau)^T R(\tau) K(\tau) \Phi(\tau, t) d\tau \quad (G-27)$$

A differential equation can be obtained for this quantity by differentiating both sides of Eq. (G-27) with respect to  $t$  producing

$$\begin{aligned} \dot{C}_{\underline{u}}(t_f, t) = & \int_t^{t_f} \left[ \dot{\Phi}(\tau, t)^T K(\tau)^T R(\tau) K(\tau) \Phi(\tau, t) \right. \\ & + \Phi(\tau, t)^T K(\tau) R(\tau) K(\tau) \dot{\Phi}(\tau, t) \left. \right] d\tau \\ & - \Phi(t, t)^T K(t)^T R(t) K(t) \Phi(t, t) \end{aligned} \quad (G-28)$$

Noting that  $\Phi(t, t) = I$  and substituting from Eqs. (G-11) and (G-27) into Eq. (G-28) yields

$$\dot{C}_{\underline{u}}(t_f, t) = -\tilde{A}(t)^T C_{\underline{u}}(t_f, t) - C_{\underline{u}}(t_f, t) \tilde{A}(t) - K(t)^T R(t) K(t) \quad (G-29)$$

This differential equation can be integrated backward in time from the terminal condition

$$C_{\underline{u}}(t_f, t_f) = 0$$

to determine the solution for the sensitivity function in Eq. (G-26). Once known, it can be used to evaluate  $J_{\underline{u}}$  for any desired initial conditions.

In an exactly analogous fashion, a sensitivity function  $C_{\underline{x}}(t_f, t)$  can be derived for evaluating  $J_{\underline{x}}$  in Eq. (G-4). The appropriate equations are listed below without proof:

$$J_{\underline{x}} = \underline{x}(t)^T C_{\underline{x}}(t_f, t) \underline{x}(t)$$

$$\dot{C}_{\underline{x}}(t_f, t) = -\tilde{A}(t)^T C_{\underline{x}}(t_f, t) - C_{\underline{x}}(t_f, t) \tilde{A}(t) - Q(t); \quad C_{\underline{x}}(t_f, t_f) = 0 \quad (G-30)$$

Finally, in some cases it is desirable to evaluate a composite performance index

$$J = J_f + J_{\underline{x}} + J_{\underline{u}}$$

in terms of initial conditions  $\underline{x}(t)$  on the state. This can be accomplished from the relations

$$J = \underline{x}(t)^T C(t_f, t) \underline{x}(t)$$

$$\dot{C}(t_f, t) = -\tilde{A}(t)^T C(t_f, t) - C(t_f, t) \tilde{A}(t) - Q(t) - K(t)^T R(t) K(t)$$

$$C(t_f, t_f) = F \quad (G-31)$$

Using the sensitivity functions developed in this appendix, one can evaluate various linear control laws for a linear dynamical system. The importance of these functions is that they provide an efficient method of evaluating quadratic performance indices and determining the terminal state at a fixed terminal time caused by initial conditions or measurement errors which are applied to the system at a variable initial time.

## APPENDIX H

### TRAJECTORY DATA

In this appendix numerical values for the parameters which define equations of motion for a missile airframe are presented. The reader is referred to Section 8.1 for definitions of terms.

#### H.1 AIR-TO-SURFACE TRAJECTORY DATA

One set of data applies to an air-to-surface trajectory for an aerodynamically controlled missile and is summarized in Tables H.1, H.2, H.3, and H.4. The aerodynamic coefficients defined in Eq. (8.1-2) are given for several different flight conditions in Table H.1. Included are values of time at which the particular flight condition occurs along a sample trajectory. The corresponding stability derivatives  $M_q$ ,  $M_\alpha$ , etc. which appear in Eq. (8.1-3) are listed in Table H.2.

The elements of  $A$  and  $\underline{b}$  in Eq. (8.1-4),

$$A = \begin{bmatrix} a_{11} & a_{12} & a_{23} \\ a_{21} & a_{22} & a_{23} \\ 0 & 0 & a_{33} \end{bmatrix}; \quad \underline{b} = \begin{bmatrix} 0 \\ b_1 \\ b_2 \end{bmatrix} \quad (H-1)$$

are calculated from the data in Tables H.1 and H.2; their values are tabulated in Table H.3. When simulations with continuously varying parameters are performed, values of  $A$  and  $\underline{b}$  at times between those listed in Table H.3 are obtained by linear interpolation, i.e.,

TABLE H.1

MISSILE AIRFRAME DATA ALONG AN  
AIR-TO-SURFACE TRAJECTORY

Flight Condition	1	2	3	4	5	6	7
Time (seconds)	0-5	6	8	23	62	71	80
Altitude (feet)	35,000	35,000	35,000	35,000	0	0	0
Velocity (ft/sec)	683	1459	2920	2920	2791	2791	2791
Dynamic Pressure (psf)	171	786	3146	3146	9258	9258	9258
Mass (slugs)	47.2	42.6	28.6	34.2	33.8	33.1	27.4
$I_{yy}$ (slug-ft <sup>2</sup> )	715	664	497	506	482	441	432
$C_{N\alpha}$	7.28	9.22	8.14	8.14	8.31	8.31	8.31
$C_{N\delta}$	4.53	4.18	1.49	1.49	1.95	1.95	1.95
$C_{Mq}$	-86	-295	-222	-222	-225	-225	-225
$C_{M\alpha}$	-5.82	-4.24	-.597	-.879	-.515	-1.27	-.665
$C_{M\delta}$	-17.8	-18.1	-7.40	-7.45	-9.21	-9.39	-9.25
Constants: $S = 1.23 \text{ ft}^2$ ; $d = 1.25 \text{ ft}$ .							

TABLE H.2

STABILITY DERIVATIVES ALONG AIR-TO-SURFACE TRAJECTORY

Flight Condition	1	2	3	4	5	6	7
$M_q$	-0.029	- 0.230	- 0.462	- 0.455	- 1.49	- 1.63	- 1.66
$M_\alpha$	-2.14	- 7.72	- 5.81	- 8.40	- 15.2	- 41.0	- 21.9
$M_\delta$	-6.56	-33.0	-72.0	-71.2	-272.0	-303.0	-305.0
$L_\alpha$	0.0478	0.144	0.379	0.379	1.01	1.03	1.24
$L_\delta$	0.0298	0.0652	0.0699	0.0699	0.237	0.242	0.292

TABLE H.3  
ENTRIES IN A AND b (Eq. (H-1))

Flight Condition	1	2	3	4	5	6	7
a <sub>11</sub>	- 0.029	- 0.230	- 0.462	- 0.455	- 1.49	- 1.63	- 1.66
a <sub>12</sub>	- 0.065	- 0.0367	- 0.00526	- 0.0054	- 0.0054	- 0.0142	- 0.0063
a <sub>13</sub>	- 5.23	- 29.5	- 70.9	- 69.7	- 268.0	- 293.0	- 300.0
a <sub>21</sub>	32.7	210.0	1100.0	926.0	2817.0	2880.0	3470.0
a <sub>22</sub>	- 0.0478	- 0.144	- 0.378	- 0.317	- 1.0	- 1.03	- 1.24
a <sub>23</sub>	-1015.0	-4760.0	-10200.0	-8486.0	-33100.0	-33900.0	-40800.0
a <sub>33</sub>	- 50.0	- 50.0	- 50.0	- 50.0	- 50.0	- 50.0	- 50.0
b <sub>2</sub>	1015.0	4760.0	10200.0	8486.0	33100.0	33900.0	40800.0
b <sub>3</sub>	50.0	50.0	50.0	50.0	50.0	50.0	50.0

TABLE H.4  
AIRFRAME UNDAMPED NATURAL FREQUENCY  
AND DAMPING RATIO

Flight Condition	1	2	3	4	5	6	7
ζ	0.026	0.067	0.172	0.132	0.305	0.203	0.296
ω <sub>n</sub>	1.46	2.78	2.44	2.92	4.09	6.54	4.89

$$A(t) = \left[ A(t_i) (t_{i+1} - t) + A(t_{i+1}) (t - t_i) \right] \frac{1}{t_{i+1} - t_i}$$
$$\underline{b}(t) = \left[ \underline{b}(t_i) (t_{i+1} - t) + \underline{b}(t_{i+1}) (t - t_i) \right] \frac{1}{t_{i+1} - t_i} \tag{H-2}$$

where t<sub>i</sub> is the time that the i<sup>th</sup> flight condition occurs.

Additional important quantities are the three open loop poles of the airframe and actuator. One pole is produced by the actuator and has a fixed value

$$p_1 = -\lambda = -50.0 \text{ sec}^{-1}$$

The other two,  $p_2$  and  $p_3$ , are complex conjugate airframe poles which are the roots of the second order polynomial

$$s^2 + 2\zeta\omega_n s + \omega_n^2$$

where

$$\omega_n^2 = a_{11}a_{22} - a_{12}a_{21} = |p_2|^2 = |p_3|^2$$

$$2\zeta\omega_n = -a_{11} - a_{22} = -p_2 - p_3$$

The quantities  $\omega_n$  and  $\zeta$  are referred to as the undamped natural frequency and the damping ratio respectively;\*  $\omega_n$  is the magnitude of  $p_2$  and  $\zeta$  is the cosine of the angle  $p_2$  makes with the negative real axis in the complex plane. The values of these quantities are given in Table H.4.

## H.2 SURFACE-TO-AIR TRAJECTORY DATA

A second set of airframe data used for simulations described in this report is for a surface-to-air trajectory. Airframe dynamics are specified in terms of the transfer function  $T(s)$  relating commanded control surface deflection to normal acceleration,

---

\* See Ref. 21 for definitions of these terms.



$$T(s) = \frac{k(s - z_1)(s - z_2)}{(s - p_a)(s^2 + 2\zeta\omega_n s + \omega_n^2)} \quad (\text{H-3})$$

The pole  $p_a$  is associated with the actuator and the remaining terms represent the airframe rotational dynamics. Values of these quantities together with the time, velocity, altitude, and dynamic pressure profiles are given in Table H.5. In order to convert this data to the form shown in Table H.2, relationships must be found between the quantities  $M_\alpha$ ,  $M_\delta$ , etc., and the variables in Eq. (H-3). This can be done using Eqs. (8.1-3), (8.1-4) and (8.1-8) with the result,

$$\begin{aligned} L_\delta &= \frac{k}{p_a V} \\ L_\alpha &= z_1 + z_2 + 2\zeta\omega_n \\ M_q &= z_1 + z_2 \\ M_\alpha &= -L_\alpha M_q - \omega_n^2 \\ M_\delta &= \frac{L_\delta}{L_\alpha} (M_\alpha + z_1 z_2) \end{aligned} \quad (\text{H-4})$$

Substitution of these quantities into Eq. (8.1-3) permits the calculation of the elements defined in Eq. (H-1); their values are entered in Table H.6.

The data supplied for these two trajectories has been obtained by fitting sets of parameters for actual missile airframes to hypothetical trajectories. Consequently, although the behavior of the airframe parameters is qualitatively representative of actual flight conditions and is adequate to test feasibility of various control methods, the specific numerical values are not real flight data.

TABLE H.5

MISSILE AIRFRAME TRANSFER FUNCTION  
PARAMETERS FOR SURFACE-TO-AIR TRAJECTORY

Flight Condition	1	2	3	4	5	6	7
k	6750.0	27900.0	39600.0	48800.0	51300.0	41600.0	33750.0
$z_1$	- 10.9	- 45.0	- 68.4	- 90.9	- 99.2	- 90.2	- 82.7
$z_2$	9.98	40.4	61.7	82.3	90.1	82.5	76.2
$\omega_n$	8.50	17.2	20.5	22.9	23.4	21.4	19.3
$\zeta$	0.0471	0.095	0.139	0.131	0.138	0.128	0.121
$p_a$	- 50.0	- 50.0	- 50.0	- 50.0	- 50.0	50.0	50.0
Velocity (ft/sec)	500.0	2059.0	3124.0	4031.0	4470.0	4330.0	4220.0
Dynamic Pressure (psf)	297.0	4482.0	6180.0	4755.0	3618.0	1415.0	640.0
Altitude (thous. ft.)	0	4.0	20.0	40.0	50.0	68.4	83.6
time (secs)	0	10.0	20.0	30.0	35.0	45.0	55.0

TABLE H.6

ENTRIES IN A AND b (Eq. (H-1)) FOR  
SURFACE-TO-AIR TRAJECTORY

Flight Condition	1	2	3	4	5	6	7
$a_{11}$	- 1.0	- 4.60	- 6.70	- 8.59	- 9.10	- 7.70	- 6.50
$a_{12}$	- 0.24	- 0.0729	- 0.0463	- 0.0357	- 0.038	- 0.0307	- 0.0296
$a_{13}$	- 49.4	- 256.0	- 382.0	- 526.0	- 544.0	- 443.0	- 352.0
$a_{21}$	300.0	3970.0	8770.0	13900.0	16900.0	14000.0	12500.0
$a_{22}$	- 0.60	- 1.93	- 2.81	- 3.46	- 3.79	- 3.25	- 2.85
$a_{23}$	-6750.0	-27900.0	-39700.0	-48800.0	-57350.0	-41640.0	-33700.0
$a_{33}$	- 50.0	- 50.0	50.0	- 50.0	- 50.0	- 50.0	- 50.0
$b_2$	6750.0	27900.0	39700.0	48800.0	57350.0	41640.0	33700.0
$b_3$	50.0	50.0	50.0	50.0	50.0	50.0	50.0

## REFERENCES

1. Stear, E.B. and Gregory, P.C., "Adaptive Flight Control-Past, Present, and Future," Flight Control Laboratory, Aeronautical Systems Division, Air Force Systems Command Report N63-10008.
2. Buscher, R.G., "Self-Adaptive Flight Control Without Test Signals," Space/Aeronautics, December 1961.
3. Haas, R.L., "Simulation Study of Proposed Yaw Damper Systems for the B-58 Aircraft," AFFDL-TR-66-136, September 1966.
4. Goldshine, G.D. and Lacey, G.T., "All-Electric Nonlinear Actuator Steers Advanced Tactical Missiles," Space/Aeronautics, September 1969.
5. Bernadyn, J., et.al., "Off-Line Adaptive Flight Control System," Technical Report AFFDL-TR-65-182, April 1966 (AD 487901).
6. Ehlers, H.L. and Smyth, R.K., "Survey of Adaptive Control Applications to Aerospace Vehicles," AIAA Guidance Control and Flight Dynamics Conference, Pasadena, California, August 12-14, 1968, paper no. 68-970.
7. Willems, G., "Optimal Controllers for Homing Missiles," Report No. RE-TR-68-15, September 1968, U.S. Army Missile Command, Redstone Arsenal, Alabama. (AD-843725).
8. Jacobs, O.L.R., "Two Uses of the Term 'Adaptive' in Automatic Control" IEEE Trans. on Automatic Control, Vol. AC-9 No. 4 October 1964.
9. Mishkin, E. and Braun, L., Jr., editors, Adaptive Control Systems, McGraw-Hill, New York, New York, 1961.
10. Mendel, J.M., "Survey of Learning Control Systems for Space Vehicle Applications," 1966 Joint Automatic Control Conference, Seattle, Washington.
11. Tou, J.T. and Hill, J.D., "Steps Toward Learning Control," 1966 Joint Automatic Control Conference, Seattle, Washington.

12. Barron, R.L., et al., "Self-Organizing Control of Aircraft Pitch Rate and Normal Acceleration," Technical Report AFFDL-TR-66-41, August 1966 (AD 801157).
13. Hoppe, S.G., Semmelhack, H.P., and Swonger, C.W., "A Feasibility Study of Self-Learning Adaptive Flight Control for High Performance Aircraft," Technical Report AFFDL-TR-67-18, February 1967.
14. LaBounty, R.H., "Root Locus Analysis of a High-Gain-Linear System with Variable Coefficients," Master's Thesis, School of Engineering, Air Force Institute of Technology Air University, August 26, 1964.
15. Makus, D.T., Haake, H.B., and Briggs, P., "Investigation of Advanced Flight Control Systems Through Application of Linear Sensitivity Techniques," Tech. Report AFFDL-TR-66-142, Vol. I, October 1966.
16. Horowitz, I., "Optimum Linear Adaptive Design of Dominant Type Systems with Large Parameter Variations, IEEE Trans. on Automatic Control, June 1969.
17. Trueblood, R.B., "Inertial Guidance for Air-to-Air Missiles,"(U) Instrumentation Laboratory Report No. R-430, Massachusetts Institute of Technology, November 15, 1963 (AD 375867). (SECRET)
18. Herget, C.J. et.al., "Adaptive Flight Control System for Missile Performance Optimization-Phase II(U)," Report No. P69-358, Hughes Aircraft Company, Aeronautical Systems Division, Culver City, California, September 1969. (CONFIDENTIAL)
19. Leistikow, L., et. al., "Optimum Control of Air-to-Surface Missiles," Technical Report AFFDL-TR-66-64, March 1967 (AD 815389).
20. "ASM Guidance Effectiveness Studies, Volume I: Tactical ASM Requirements (U)," Technical Report AFAL-TR-68-279, Vol. I, November 1968 (AD 397686). (SECRET)
21. Truxal, J.G., Control Systems Synthesis, McGraw-Hill Book Co., Inc., New York, New York, 1955.

22. Fossier, M.W., "An Analysis of Combat Experience with Sparrow III Air-to-Air Missiles (U)," AIAA Tactical Missile System Conference (U), Redstone Arsenal, Alabama, February 10-12, 1969. (SECRET)
23. Amlie, T.S., "Design Trends in Guidance for Air-to-Air Weapons," Symposium in Analysis and Design of Fighter Systems for Air-to-Air Combat (U), The Rand Corp., January 10-12, 1968, Santa Monica, California. Proceedings published September 1968 (AD 393279). (SECRET)
24. Lapin, L.L., "The Aircraft Jinking Maneuver-A Descriptive and Quantitative Analysis (U)," NWC TP 4430, Naval Weapons Center, China Lake, California, January 1968. (CONFIDENTIAL)
25. Stallard, D.V., "Classical and Modern Guidance of Homing Interceptor Missiles," Report P 247, Raytheon Company, Missile Systems Division, Bedford, Mass. April 1968.
26. Christie, K.V., "The Impact of Tactical Air Defenses," Symposium on Analysis and Design of Fighter Systems for Air-to-Air Combat (U)," AIAA Tactical Missile System Conference, Redstone Arsenal, Alabama, February 10-12, 1969. (SECRET)
27. Augustine, Norman R., "Tactical Missiles and Ordnance in Southeast Asia: Lessons Learned (U)," AIAA Tactical Missile System Conference, Redstone Arsenal, (U), Alabama, February 10-12, 1969. (SECRET)
28. Attinello, J.S., "Southeast Asia Air-to-Air-Combat (U)," Symposium on Analysis and Design of Fighter Systems for Air-to-Air Combat (U), The Rand Corp., January 10-12 1968, Santa Monica, California. Proceedings published September 1968 (AD 393279). (SECRET)
29. Younkin, W.G., "Error Sources in Infrared Seekers," notes for short course, Guidance and Control of Tactical Missiles, July 21-25, 1969, UCLA, Los Angeles, California.
30. Kalman, R.E., Arbib, M.A., and Falb, P.L., Topics in Mathematical System Theory, McGraw-Hill Book Co., New York, 1969.

31. Sutherland, A. A., Jr., "Variable Frequency Compensation for Sampled Data Control Systems," Massachusetts Institute of Technology Patent Application, 21 February 1968, Serial No. 707268.
32. Tyler, J. S., Jr., "The Characteristics of Model-Following Systems as Synthesized by Optimal Control," 1964 Joint Automatic Control Conference.
33. Rediess, H. A., "A New Model Performance Index for the Engineering Design of Control Systems," Doctoral Thesis TE-26, Dec. 9, 1968, Experimental Astronomy Laboratory, Massachusetts Institute of Technology, Cambridge 39, Massachusetts.
34. Zadeh, L. A., and Desoer, C. A., Linear System Theory, McGraw-Hill Book Company, 1963, New York, New York.
35. Hofmann, L. G., and Best, J. J., "New Methods in Adaptive Flight Control," NASA Report CR-1152, September 1968.
36. Eveleigh, V. W., Adaptive Control and Optimization Techniques, McGraw-Hill Book Co., New York 1967.
37. Gibson, J. E., Nonlinear Automatic Control, McGraw-Hill Book Co., New York, New York, 1963.
38. Margolis, M., and Leondes, C. T., "A Parameter Tracking Servo for Adaptive Control Systems," IRE Transactions in Automatic Control, PGAC 4, No. 2, pp 100-111, November 1959.
39. Margolis, M., "On the Theory of Process Adaptive Control Systems, The Learning Method Approach," AFOSR-TN-60-618 Report No. 60 - 32, May 1960.
40. Osburn, P. V., "Investigation of a Method of Adaptive Control," ScD Thesis, Department of Aeronautics and Astronautics, 1961, Massachusetts Institute of Technology, Cambridge, Massachusetts.
41. Osburn, P. V., Whitaker, H. P., and Kezer, A., "New Developments in the Design of Model Reference Adaptive Control Systems," IAS Paper No. 61-39, IAS 29th Annual Meeting, New York, New York, January 23-25, 1961.

42. Horrocks, T., "Investigations into Model Reference Adaptive Control Systems," Proceedings of the Institution of Electrical Engineers, Vol. 111, No. 11, November 1964.
43. Donalson, D.D., and Leondes, C.T., "A Model Referenced Parameter Tracking Technique for Adaptive Control Systems, I - The Principle of Adaptation," IEEE Transactions on Applications and Industry, September 1963.
44. Dressler, R.M., "A Simplified Technique for the Synthesis of Model-Referenced Adaptive Control Systems," Technical Report No. 6764-3, U.S. Army Material Command, Redstone Arsenal, Alabama, March 1966, (AD 483444).
45. Pearson, A.E. and Noonan, F., "On the Model Reference Adaptive Control Problem," 1968 Joint Automatic Control Conference June 26-28, The University of Michigan.
46. Winsor, C.A., "Model Reference Adaptive Design," Report No. N6928388, 1968.
47. Chang, S.H., "On the Relative Time of Adaptive Processes," IEEE Trans. on Automatic Control, January 1965.
48. Klein, D.W., "Pitch Attitude Adaptive Control for VTOL Aircraft," Master's Thesis, June 1969, Department of Aeronautics and Astronautics, The Massachusetts Institute of Technology, Cambridge, Massachusetts.
49. James, D.J.G., "Stability Analysis of a Model Reference Adaptive Control System with Sinusoidal Inputs," Int. J. Control, 1969, Vol. 9, No. 3.
50. Donalson, D.D. and Leondes, C.T., "A Model Referenced Tracking Technique for Adaptive Control Systems II - Stability Analysis by the Second Method of Liapunov," IEEE Transactions on Applications and Industry, September 1963.
51. Dressler, R.M., "An Approach to Model-Referenced Adaptive Control Systems," IEEE Trans. on Automatic Control, Vol. AC-12 No. 1, February 1967.

52. Lee, Y.S. and Toivanen, T.W., "Application of Mark III-SOC (Self-Organizing Control) to Multivariable Control Problems. Part I High-Gain Decoupling Control Applied to the Longitudinal Axis of the XV-4B VTOL Aircraft", Technical Report AFFDL-TR-68-10, Part I, September 1968.
53. Yore, E.E., "Application of Mark III - SOC (Self-Organizing Control) to Multivariable Control Problems. Part II. Optimal Decoupling Control Applied to the Lateral-Directional Axes of a Sweep Wing Aircraft," Technical Report AFFDL-TR-68-10, Part II, February 1968.
54. Smith, F.B., Jr., "Application of Mark III-SOC (Self-Organizing Control) to Multivariable Control Problems. Part II. Optimal Decoupling Control Applied to the Lateral-Directional Axes of a Sweep Wing Aircraft," Technical Report AFFDL-TR-68-10, Part II, February 1968.
54. Smith, F.B., Jr., "Application of Mark III-SOC (Self-Organizing Control) to Multivariable Control Problems Part III. An Application of Decoupling in the Control of Pitch and Airspeed During Approach," Technical Report AFFDL-TR-68-10, Part III, September 1968.
55. McKechine, R.M. III and Barron, R.L., "Design Principles for Self-Organizing Control System Flight Hardware," Proc. 19th Annual NAECON, 1967, pp. 465-473.
56. Barron, R., "Self-Organizing Control: The Next Generation of Controllers; Part I the Elementary SOC," Control Engineering, February 1968.
57. Barron, R., "Self-Organizing Control: The Next Generation of Controllers; Part II, the General Purpose SOC," Control Engineering, February 1968.
58. Heasley, J.E., "The Application of Self-Organizing Control Techniques to the Control of a Tactical Air-to-Ground-Missile," Master's Thesis, Air Force Institute of Technology, Air University, Wright-Patterson Air Force Base, Ohio, June 1968.
59. Barron, R.L., et. al., "Application of Self-Organizing Control Techniques to High-Performance Missiles (U)," Final Technical Report under Contract N00019-68-C-0159, April 1969 (AD 852869).



60. Narendra, K.S. and Baker, T.S., "Simultaneous Multiple Parameter Adjustment in Adaptive Systems Using a Single Perturbation Signal," ONR Report NR-375-732, April 15, 1967, (AD 653474).
61. Narendra, K.S. and McBride, L.E., "Multiparameter Self-Optimizing Systems Using Correlation Techniques," IEEE Trans. on Automatic Control, January 1964.
62. Hagen, K.E., "The Dynamic Behavior of Parameter-Adaptive Control Systems," Ph.D. Thesis, Department of Aeronautics and Astronautics, Massachusetts Institute of Technology, Cambridge, Massachusetts, June 1964.
63. Gersho, A., "Linear Adaptation," P.I.B. Symposium in Computer Processing in Communications, April 1969.
64. Brockett, R.W., Finite Dimensional Linear Systems, J. Wiley and Sons, Inc., 1970.
65. LaSalle, J. and Lefschetz, S., Stability by Liapunov's Direct Method, Academic Press, New York, 1961.
66. Lefschetz, S., Stability of Nonlinear Control Systems, Academic Press, New York, 1965.
67. Kalman, R.E. and Bertram, J.E., "Control System Design via the 'Second Method' of Liapunov - I Continuous-Time Systems," Trans. ASME, June 1960.
68. Kalman, R.E. and Bertram, J.E., "Control System Design via the 'Second Method' of Liapunov - II Discrete-Time Systems," Trans. ASME, June 1960.
69. Brockett, R.W., "The Status of Stability Theory for Deterministic Systems," IEEE Trans. on Automatic Control, July 1966.
70. Lefevre, C. and Richalet, J., "Energy Stability Criteria," Automatika i Telemekhanika, No.4, April 1968.
71. Coddington, E.A. and Levinson, N., Theory of Ordinary Differential Equations, McGraw-Hill Book Co., New York, New York, 1955.

72. Winsor, C.A. "Design of Model Reference Adaptive Control Systems by Liapunov's Second Method", IEEE Trans. on Automatic Control, April 1968.
73. Parks, P.C., "Liapunov Redesign of Model Reference Adaptive Control Systems," IEEE Trans. on Automatic Control, Vol. AC-11, No. 3, July 1966.
74. Phillipson, P.H., "Concerning 'Liapunov Redesign of Model Reference Adaptive Control Systems,' " IEEE Trans. on Automatic Control, Vol. AC-12, No. 5, October 1967.
75. Monopoli, R.V. and Gilbert, J.W., "A Modified Liapunov Design for Model Reference Adaptive Control Systems," Manuscript submitted to IEEE Trans. on Automatic Control, June 1969.
76. Monopoli, R.V. and Gilbert, J.W., "Model Reference Adaptive Control Based on Liapunov-Like Techniques," Second IFAC Symposium on System Sensitivity and Adaptivity, Dubrovnik, Yugoslavia, August 26-31, 1968.
77. Pasdera, J.S. and Epstein, J.S., "On Liapunov Designed Model-Reference Control Systems," Midwest Symposium on Circuit Theory, April, 1969, University of Texas, Austin, Texas.
78. Phillipson, P.H., "Design Methods for Model-Reference Adaptive Systems," Proceedings, The Institution of Mechanical Engineers, 1968-69, Vol. 183, Part I, No. 35.
79. Monopoli, R.V. and Gilbert, J.W., "Model Reference Adaptive Control Systems With Feedback and Prefilter Adjustable Gains," Fourth Annual Princeton Conference on Information Sciences and Systems, March 26-27, 1970, Princeton, New Jersey.
80. Gelb, A. and Vander Velde, W.E., Multiple-Input Describing Functions and Nonlinear System Design, McGraw-Hill Book Co., New York, New York, 1968.
81. Gelb, A. and Blashke, T.C., "Design for Adaptive Roll Control of a Missile," The Journal of the Astronautical Sciences, Vol. IX, No. IV, Winter 1962.

82. Smyth, R.K. and Nahi, N.E., "Phase and Amplitude Sinusoidal Dither Adaptive Control System," IEEE Trans. on Automatic Control, Vol. AC-8, October 1963.
83. Stallard, D.V., "A Missile Adaptive Roll Autopilot With a New Dither Principle," IEEE Trans. on Automatic Control, Vol. AC-11, No. 3 July 1960.
84. Coffey, T.C., "The Phase and Amplitude Sinusoidal Dither Adaptive Control System (PASDACS) - Results from a Preliminary Study ATN-64(40-40-60)-1, October 1, 1963, Aerospace Corporation, P.O. Box 95085, Los Angeles, 45, California.
85. Trueblood, R.B. and Kezer, A., "Advanced Flight Control System Concepts for VTOL Aircraft; Phase I Technical Report," R428, Instrumentation Laboratory, M.I.T., Cambridge, Massachusetts, October 1963.
86. Newton, G.C., Jr., Gould, L.A., and Kaiser, J.F. Analytical Design of Feedback Controls, John Wiley & Sons, Inc., New York 1957.
87. Young, P.C., "Adaptive Pitch Autostabilization of an Air-to-Surface Missile," Presented at Southwestern IEEE Conf. San Antonio, Texas, April 1969.
88. Ho, Y.C. and Whalen, B.H., "An Approach to the Identification and Control of Linear Dynamic Systems with Unknown Parameters," IEEE Trans. on Automatic Control, Vol. AC-8, July 1963, No. 3.
89. Pottle, C., "The Digital Adaptive Control of a Linear Process Modulated by Random Noise," IEEE Trans. on Automatic Control, Vol. AC-8, July 1963, No. 3.
90. Jenkins, K.W. and Roy, R.J., "A Design Procedure for Discrete Adaptive Control Systems," 1966 Joint Automatic Control Conference, Univ. of Washington, August 17-19.
91. Farison, J.B., Graham, R.E., and Shelton, R.C., Jr., "Identification and Control of Linear Discrete Systems," IEEE Trans. on Automatic Control, August 1969.

92. Farison, J.B. and Weigman, C.L., "Identification-Adaptive Quadratic-Cost-Linear System Control," Report TR 6812, October 1968, Department of Electrical Engineering, The University of Toledo, Toledo, Ohio.
93. Farison, J.B., "A Review of Linear Discrete-Time System Identification and Control," Report TR-6911, July 1969, Department of Electrical Engineering, University of Toledo, Toledo, Ohio.
94. Tyler, J.S., Jr., "The Characteristics of Model-Following Systems as Synthesized by Optimal Control," Joint Automatic Control Conference, 1964.
95. Young, P.C., "Optimal Design of an Aircraft Pitch Axis Control System," Technical Note 404-67-68, May, 1968, Naval Weapons Center, China Lake, California.
96. Young, P.C. and Yancey, C.B., "A Preliminary Investigation into the Problem of Autostabilizing an Air-to-Surface Missile," Technical Note 404-78-68, 1 October 1968, Naval Weapons Center, China Lake, California.
97. Athans, M. and Falb, P., Optimal Control, Mc-Graw-Hill Book Co., 1966, New York.
98. Lee, Y.S., "A Time-Optimal Adaptive Control System via Adaptive Switching Hypersurface," IEEE Trans. on Automatic Control, Vol. AC-12, No. 4, August 1967.
99. Durboraw, I.N.III, "Control System Performance Limitations and a Near-Optimal Control Synthesis," ScD Thesis, Department of Aeronautics and Astronautics, Massachusetts Institute of Technology, Cambridge, Massachusetts, June 1967.
100. Lion, P.M., "Rapid Identification of Linear and Nonlinear Systems," AIAA Journal, Vol. 5, No. 10, October 1967.
101. Astrom, K.J. and Eykhoff, P., "System Identification," survey paper presented at IFAC Symposium, Prague, June 1970.
102. Kopp, R.E. and Orford, R.J., "Linear Regression Applied to System Identification for Adaptive Control Systems," AIAA Journal, Vol. 1, No. 10, October 1963.

103. Young, P.C., "An Instrumental Variable Method for Real Time Identification of a Noisy Process," Automatica, March 1970.
104. Kushner, H.J., "On the Convergence of Lion's Identification Method with Random Inputs," 1969 Report, Division of Applied Mathematics, Brown University, Rhode Island.
105. Derman, C., "Stochastic Approximation," Ann. Math. Statistics, Vol. 27 (1956).
106. Horowitz, I.M., Synthesis of Feedback Systems, New York Academic Press, Inc., 1963.
107. Bode, Hendrik, W., Network Analysis and Feedback Amplifier Design, Van Nostrand Book Company, 1945.
108. Cruz, J.B., Jr., and Perkins, W.R., "A New Approach to the Sensitivity Problem in Multivariable Feedback System Design," IEEE Transactions on Automatic Control, July 1964.
109. Kriendler, E., "Closed Loop Sensitivity Reduction of Linear Optimal Control Systems," IEEE Transactions on Automatic Control, June 1968.
110. Lee, Y. "Sensitivity Analysis and Synthesis of Linear Feedback Systems," Joint Automatic Control Conference, University of Pennsylvania, June 1967.
111. Lancaster, P., Lambda-Matrices and Vibrating Systems, Pergamon Press, 1966.
112. Tomovic, R., Sensitivity Analysis of Dynamic Systems, McGraw Hill Book Company, 1963.
113. Wilkie, D.F., and Perkins, W.R., "Generation of Sensitivity Functions for Linear Systems Using Low-Order Models," IEEE Transactions on Automatic Control, April 1969.
114. Perkins, W.R., Cruz, J.B., Jr., and Gonzales, R.L., "Design of Minimum Sensitivity Systems," IEEE Transactions on Automatic Control, April, 1968.

115. Price, C.F., and Deyst, J.J., "A Method for Obtaining Desired Sensitivity Characteristics With Optimal Controls," 1968 Joint Automatic Control Conference, The University of Michigan, June 26-28.
116. Burzio, A., and Siljak, D.D., "Minimization of Sensitivity with Stability Constraints in Linear Control Systems," IEEE Transactions on Automatic Control, July 1966.
117. McClamroch, N.H., Clark, L.G., and Aggarwal, J.K., "Sensitivity of Linear Control Systems to Large Parameter Variations," Automatica, Vol. 5, 1969.
118. Salmon, D., "Minimax Controller Design," IEEE Transactions on Automatic Control, August 1968.
119. Michael, G.J., and Merriam, C.W., III, "Stability of Parametrically Disturbed Linear Control Systems," J. Math. Anal. and Appl., Vol. 28, Nov. 1969.
120. Monopoli, R.V., "Controller Design for Nonlinear and Time Varying Plants," NASA Contractor Report, NASA CR-152, January 1965.
121. Giesekeing, D., "An Optimum Bistable Controller for Increased Missile Autopilot Performance," IEEE Transactions on Automatic Control, October, 1963.
122. Lindorff, D.P., "Relay Control of Systems with Parameter Uncertainties and Disturbances," Automatica, Vol. 5, 1969.
123. Bakken, O.A., Brueske, R.A., Kratzke, W.A., Rath, R.J., and Riel, R.C., "Application of Modern Control Theory to Defense Missiles," Boeing Company Report No. 81205, October 1966, (AD 803142).
124. Monopoli, R.V., "Control of Linear Plants with Zeros and Slowly Varying Parameters," IEEE Transactions on Automatic Control, February 1967.
125. Wonham, W.M. and Johnson, C.D., "Optimal Bang-Bang Control with Quadratic Performance Index," Journal of Basic Engineering, Trans. ASME, Vol. 86, March 1964.

126. Johnson, C.D. and Wonham, W.M., "Another Note on the Transformation to Canonical (Phase-Variable) Form," IEEE Transactions on Automatic Control, Vol. AC-11, July 1966.
127. Rekasius, Z.V., "A General Performance Index for Analytical Design of Control Systems," IRE Trans. on Automatic Control, May 1961.
128. Tyler, J.S., Jr., and Tuteur, F.B., "The Use of a Quadratic Performance Index to Design Multivariable Control Systems," IEEE Trans. on Automatic Control, Vol. AC-11, No. 1, January 1966.
129. Stake, W.R., Cawood, C.V., Morris, G., "A Comparison of Aerodynamically Controlled Air-to-Ground Missile Configurations," LMSC-D052396, August 15, 1969, (AD 863220).
130. Anonymous, "Milan Production Based on Export Market," Aviation Week and Space Technology, March 16, 1970.
131. Lorenzetti, R.C., Nelson, G.L., Johnson, R.W., "Computerized Design of Optimal Direct Lift Controller," Journal of Aircraft, Vol. 6, No. 2, March-April 1969.
132. Cleveland, D., et.al., "Research and Development on Self-Organizing Control Systems for Air-Launched Missiles (U)," Final Technical Report, 17 March 1968, 16 November, 1969, Contract N00019-69-C-D106, Adaptronics, Inc., McLean, Virginia.
133. Stewart, E.C., "Application of Statistical Theory to Beam-Rider Guidance in the Presence of Noise," NACA RM A55E11, National Advisory Committee for Aeronautics.
134. Merrill, G., Editor, Principles of Guided Missile Design, D. Van Nostrand Co., Inc., 1955.
135. James, J.P., "Homing Guidance", A-62-1732.3-68, Aerospace Corporation, September 14, 1962.
136. Willems, G.C., "Optimal Controllers for Homing Missiles with Two Time Constants," Report No. RE-TR-69-20, 9 October 1969, (AD 862093).

137. Bryson, A.E., Jr., and Ho, Y.C., Applied Optimal Control, Blaisdell Publishing Co., Waltham, Massachusetts, 1969.
138. Jazwinski, A.H., Stochastic Processes and Filtering Theory, Academic Press, New York, 1970.
139. Luenberger, D.G., "Observers for Multivariable Systems," IEEE Transactions on Automatic Control, Vol. AC-11, No. 2, April 1966.
140. Dellon, F. and Sarachik, P.E., "Optimal Control of Unstable Linear Plants with Inaccessible States," IEEE Trans. on Automatic Control, Vol. AC-13, No. 5, October 1968.
141. Kalman, R.E., "Fundamental Study of Adaptive Control Systems," Technical Report No. ASD-TR-61-27, Vol. I, April 1962.
142. Levine, W.S. and Athans, M., "Average-Optimal Output-Feedback Controllers for Linear Time-Varying Systems," Paper ESL-P-377, February 1969, Electronic Systems Laboratory, Massachusetts Institute of Technology, Cambridge, Massachusetts.
143. Cassidy, J.F., Jr., "Optimal Control With Unavailable States," Final Report - Vol. III Contract No. NAS 8-21131, Rensselaer Polytechnic Institute, Troy, New York.
144. Wilkinson, J.A., The Algebraic Eigenvalue Problem, Clarendon Press, Oxford, England, 1964.
145. Hildebrand, F.B., Methods of Applied Mathematics, Prentice-Hall, Inc., New Jersey, 1952.
146. Gantmacher, F.R., The Theory of Matrices, Vol. 1, Chelsea Publishing Co., New York, 1959.
147. Potter, J.E., "A Matrix Equation Arising in Statistical Filter Theory," MIT Experimental Astronomy Laboratory, Report RE-9, February 1965.
148. Todd, J., Survey of Numerical Analysis, McGraw-Hill Book Co., Inc., 1962, New York, New York.



- 149. Blackburn, T.R., "Solution of the Algebraic Matrix Riccati Equation via Newton-Raphson Iteration," Joint Automatic Control Conference, University of Michigan, Ann Arbor, Michigan, 26-28 June 1968.
- 150. Freested, W.C., Webber, R.F., and Bass, R.W., "The 'Gasp' Computer Program-An Integrated Tool for Optimal Control and Filter Design," Joint Automatic Control Conference, University of Michigan, Ann Arbor, Michigan, 26-28 June 1968.
- 151. Fath, A.F., "Computational Aspects of the Linear Optimal Regulator Problem," Joint Automatic Control Conference, University of Colorado, Boulder, Colorado, 5-7 August 1969.
- 152. Kaufman, H. and DeRusso, P.M., "Stability Analysis of Predictive Control Systems," IEEE Trans. on Automatic Control, Vol. AC-11, No. 3, July, 1966.

UNCLASSIFIED

Security Classification

## DOCUMENT CONTROL DATA - R &amp; D

(Security classification of title, body of abstract and indexing annotation must be entered when the overall report is classified)

1. ORIGINATING ACTIVITY (Corporate author) The Analytic Sciences Corporation 6 Jacob Way Reading, Massachusetts		2a. REPORT SECURITY CLASSIFICATION Unclassified	
		2b. GROUP	
3. REPORT TITLE Adaptive Control and Guidance for Tactical Missiles Volume II: Parts III and IV, Adaptive Control Applications and Guidance			
4. DESCRIPTIVE NOTES (Type of report and inclusive dates) Technical Report			
5. AUTHOR(S) (First name, middle initial, last name) Charles F. Price			
6. REPORT DATE 30 June 1970		7a. TOTAL NO. OF PAGES 316	7b. NO. OF REFS 152
8a. CONTRACT OR GRANT NO. N00014-69-C-0391		9a. ORIGINATOR'S REPORT NUMBER(S) TR-170-1	
b. PROJECT NO.		9b. OTHER REPORT NO(S) (Any other numbers that may be assigned this report)	
c.			
d.			
10. DISTRIBUTION STATEMENT This document is subject to special export controls and each transmittal to foreign governments or foreign nationals may be made only with prior approval of the Office of Naval Research, Code 461.			
11. SUPPLEMENTARY NOTES		12. SPONSORING MILITARY ACTIVITY Office of Naval Research Department of the Navy Arlington, Virginia 22217	
13. ABSTRACT <p>The fields of adaptive control and guidance are searched for techniques that can be beneficially applied to the design of guidance systems for tactical missiles. A large number of existing adaptive control techniques are investigated and new methods which are suited to the needs of missile control systems, are proposed. The feasibility of promising autopilot design procedures is demonstrated through computer simulations, using realistic time-varying airframe dynamics. Guidance techniques for tactical missiles are also reviewed and a number of steering laws, derived from optimal control theory, are evaluated. Quantitative comparisons are made between different guidance laws on the basis of intercept accuracy and control effort expended.</p> <p>The report is published in two volumes containing four basic parts -- Introduction (which includes the summary and conclusions for the entire report), Adaptive Control Theory, Adaptive Control Applications, and Guidance. The first two parts constitute Volume I and the remainder together with several appendices compose Volume II.</p>			

DD FORM 1473

REPLACES DD FORM 1473, 1 JAN 64, WHICH IS OBSOLETE FOR ARMY USE.

UNCLASSIFIED

Security Classification

UNCLASSIFIED

Security Classification

14. KEY WORDS	LINK A		LINK B		LINK C	
	ROLE	WT	ROLE	WT	ROLE	WT
Adaptive Control Missile Guidance Autopilot Design Insensitive Control Systems Liapunov Synthesis Techniques Optimal Guidance Homing Guidance						

UNCLASSIFIED

Security Classification